Reflecting the Past in the Present: How Studying Living Crinoids Sheds Light on Their Fossil Record

by

Margaret A. Veitch

A dissertation submitted in partial fulfillment
of the requirements for the degree of
Doctor of Philosophy
(Earth and Environmental Sciences)
in the University of Michigan
2022

Doctoral Committee:

Professor Tomasz K. Baumiller, Chair
Professor Catharine Badgley
Professor Daniel C. Fisher
Associate Professor Matt Friedman
Professor Kyger C. Lohmann

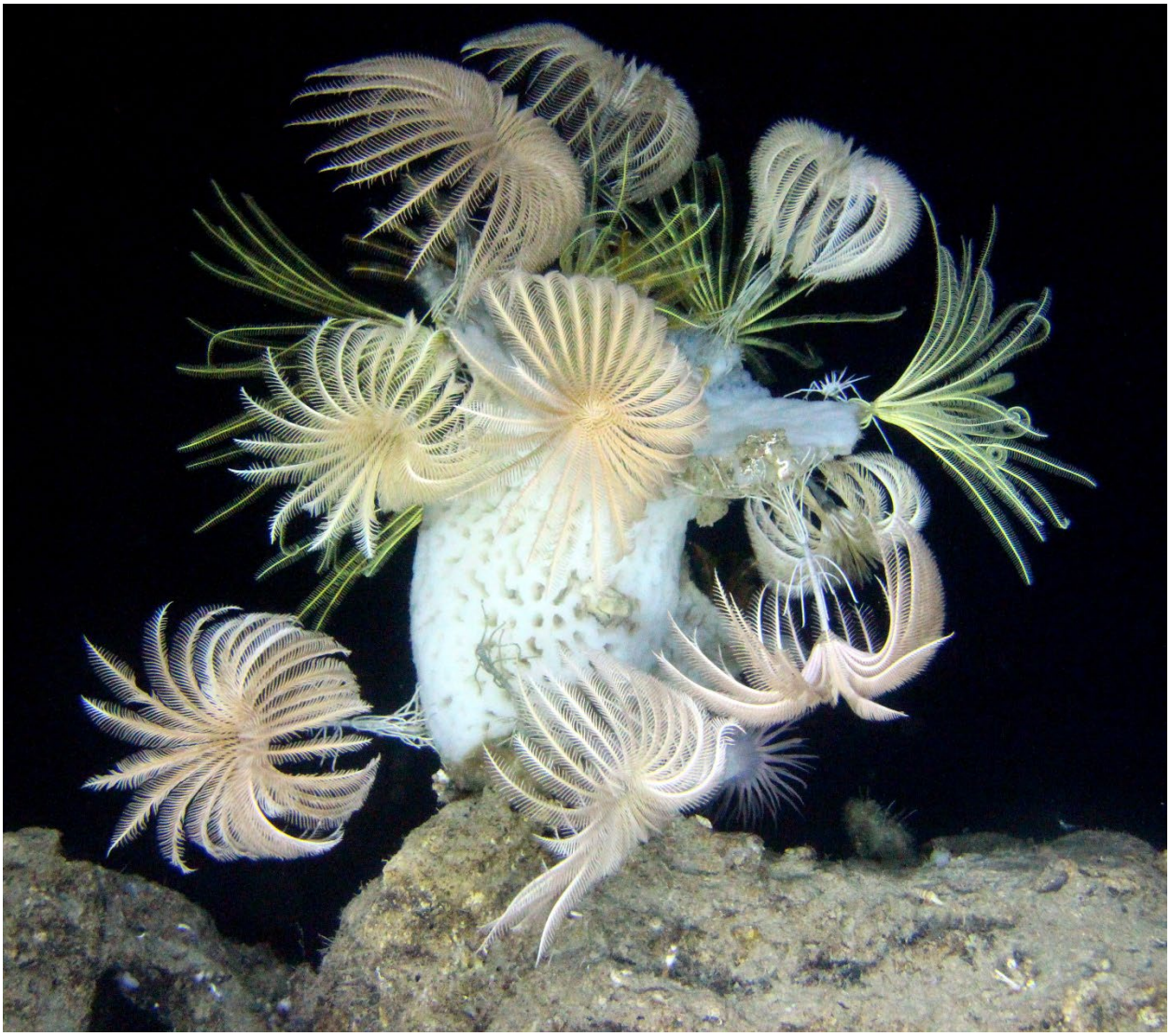

Margaret A. Veitch

maveitch@umich.edu

ORCID iD: 0000-0002-0555-8017

DEDICATION

This dissertation is dedicated to my grandparents, who each inspired me in different ways. And to all those that read this dissertation through to the very end.

ACKNOWLEDGMENTS

It is impossible for me to imagine undertaking the work presented in this dissertation without the aid from the many individuals who took part in some or all of this journey with me. From thoughtful discussions and feedback to direct contributions to projects, moral support and, in some cases literally keeping me on my feet (or on my chair) to work, I can only begin to express my immense gratitude for your presence since I began this work[*].

First and foremost, I thank my advisor Tom Baumiller, for all of his help and guidance throughout the course of this project. His breath of knowledge and depth of insight on crinoids, echinoderms and paleontology as a whole has been invaluable. He has never limited his mentorship to just research, and his support in developing my teaching and mentoring skills cannot be understated. And while tossing a graduate student into a submersible made in a garage may not have seemed like the safest idea when I first descended to those dark, deep, ocean depths, it changed how I viewed the world and I cannot be more grateful.

I would also like to thank my committee members, Catherine Badgley, Dan Fisher, Kyger Lohmann and Matt Friedman. Their support, comments, and suggestions over the course of this project have been invaluable. My research also benefitted from many discussions with my fellow Baumiller lab mates, especially Kris Purens, Val Syverson and Alex Janesvski, along with all of the people I am blessed to have spent time with in the paleo department, but especially John Fronimos, Katie Loughney, Molly Ng, Jen Bauer, Dan Miller, Rafa Rivero, Zack Quirk, Fabian Hardy and Bian Wang. To Bill Sanders and Carol Abraczinskas, you two expanded my knowledge far beyond what my research called for and kept me mostly sane during the pandemic with our virtual coffee mornings. Thank you to Linda Garcia, Naomi Levin and Anne Hudon, whom I was blessed not only with aid in navigating the university, but even better, friendship. I also thank the many people I have been lucky enough to teach with and be mentored by over the

[*] I do not thank: that tick that gave me Lyme disease, covid-19 nor that one barracuda. You know what you did, fish.

years, including Jamie Gleason, Jeroen Ritsema, Brian Arbic, Adam Simon, Selena Smith, Nathan Sheldon, Michela Arnaboldi and Greg Dick.

I would also like to thank the various foundations and programs that provided direct funding for my graduate studies and the research projects presented herein: The Paleontological Society Student Research Grants, Rackham Predoctoral Research Awards and the Department of Earth and Environmental Sciences Scott Turner Student Research Grant Award. Additionally I would like to thank Sadie Miller at the National Institute of Water and Atmospheric Research Ltd Invertebrate Collection, Adam Baldinger at the Museum of Comparative Zoology, Harvard University and Chuck Messing at Nova Southeastern University for providing specimens for this study. Thank you to Karl Stanley for piloting *Idabel* and excellent memory of site locations in Roatán, Honduras. And thank you to Tom Baumiller, Angela Stevenson, Chris Byrne and Andreas Kroh for all spending 6+ hours at a time with me in a tiny metal bubble in the ocean's depths.

There are many other people who have helped me at various stages of researching and writing this dissertation. To my colleagues and friends outside of Michigan: Angela Stevenson, Tadhg O'Conner, Andreas Kroh, Samuel Zamora, Chuck Messing and Dave Meyer; you provided joy and guidance in both the lab and the field and provided many a laugh for which I am grateful beyond words. Thank you to the many people who stood by me during the dark hours of my struggles and unexpected health issues, including my parents who are my original cheerleaders, Chris Byrne and Jim Veitch. Also my dear Pearl, with the most perfect purrs, as well as Becca Chelberge-Quirk, Neo Jing Ci, Juliana Mesa, Novia Wong, Todd Grant, Mara Page, Katie Rico, Erika Gleim, Meagan Yip, Chris Moody, Victoria Veitch, Vanessa Verden, Kara Feilich and Phyllis Gale. I also must thank Sensei John Burns, who let me punch him when I was four-year-old and has been encouraging me ever since.

I additionally thank my many students throughout the years, who taught me so many unexpected lessons. Additionally, I cannot miss thanking those that gave everything to this work: to the crinoids that died in service to my research, may your gift of life never be underestimated. And those crinoids who didn't die for my research and have to now live with the trauma of snipped arms, being captured and released, dislodged and/or being hit with sticks.

Thank you all, from the bottom of my heart.

TABLE OF CONTENTS

LIST OF TABLES

LIST OF FIGURES

LIST OF APPENDICES

ABSTRACT

Crinoids are one of the few clades on Earth that have both a well-documented fossil record and extant taxa with a similar morphology. Extant stalked crinoids are morphologically similar to fossil members from the Mesozoic onward, and provide an excellent study group for modern to fossil comparisons with the caveat that their deep bathymetric range left them relatively inaccessible until the last half century. With access to submersible technology, studies can now address questions from the fossil record, such as why stalked crinoids became restricted to depths greater than 100 meters, how largely sessile stalked crinoids orient themselves for feeding or protection, and what physical characteristics are useful to delineate stalked crinoid species.

Long-term *in situ* observations, field experiments, and morphological data from a large population of *Democrinus* (suborder Bourgueticrinina) off Roatán, Honduras, were used to explore the ecology, functional morphology, and taxonomy of this stalked crinoid genus. Major areas of interest in this thesis are assessing predation as a causal factor in the bathymetric restriction of stalked crinoids observed in the fossil record, mobility in stalked crinoid clades, and a general assessment of the taxonomy of modern *Democrinus.*

The post-Mesozoic bathymetric range restriction of stalked crinoids has long been attributed to an increase in predation intensity during the Mesozoic Marine Revolution. If predation was a determining cause, then we would expect to see that reflected in the intensity of predation on extant crinoids across bathymetric ranges. Stalked crinoids, limited to bathyal environments should encounter predators less frequently, and thus, face a lower predation

intensity than feather stars found in shallow water environments. Documentation of predation intensity in the Roatán *Democrinus* population revealed that individuals encounter predators nearly 60 times less often than reported previously for shallow-water feather stars, confirming that the predation intensity is much lower at greater depths.

Other stalked crinoids, i.e., isocrinids, are now known to be able to crawl and relocate, but this ability may be morphologically limited. Individuals from the population of *Democrinus* were dislodged, observed, and no individual was found to relocate from its original placement. However, all dislodged individuals regained a vertical upright posture, something previously thought impossible because of the absence of muscle in their stalk. Quantitative assessment of four biomechanical models showed that all were insufficient as the mechanism by which *Democrinus* might regain a vertical posture; it is likely instead that the tissues of the ligaments within the stalks have a contractile ability, even in the absence of muscle.

Examination of submersible-collected specimens from the Roatán *Democrinus* population and comparison to over 350 existing specimens, photographs, and drawings of known *Democrinus* species revealed significant differences in the Roatán population, which is designated a new species accordingly. This study also more precisely define certain features of the cup and brachials, and establishes that the attachment structure, is likely associated with environment rather than phylogeny. This assessment of defining characteristics was used to amend the diagnosis for the genus *Democrinus* and the species *D. rawsonii*, and has implications for the reassessment of other extant and fossil species.

Injury and regeneration rates cannot be determined from a static fossil, nor can fossil organisms' responses to challenges, such as changing currents, be observed. Thus, studying

extant crinoids to investigate aspects of their ecology, morphology and evolutionary history provides insights inaccessible from the fossil record.

CHAPTER I Introduction

Thought of by the broader public as almost exclusively working with fossils, paleontologists, in fact, often incorporate data from living organisms. Research on living organisms offers significant benefits when addressing questions that fossil data cannot answer fully, including aspects of soft tissues, functional morphology, ecology, behavior, and more. Scientists who study taxonomic groups with excellent fossil records and living analogs, such as some Crinoidea (Echinodermata), have a long tradition of combining modern and fossil data to answer such questions. However, that tradition has not come without challenges that we have begun to overcome only recently.

The stalked, flower-eques organisms abundant in the Paleozoic, remains the representation of crinoids envisioned commonly. Decimated during the Permian-Triassic extinction event, crinoids never reached the same level of abundance subsequently. However, the surviving lineage radiated, attained a comparable morphological diversity, expanded into new ecological niches, and is still thriving in today's oceans (Simms 1988, Foote 1999, Hess et al. 2011). Post-Paleozoic stalked crinoids, including the extant taxa, resemble their ancestors, with a crown raised above the bottom by a distinctive long, slender stalk composed of stacked columnals, which is attached at its distal end to the substrate with either an anchoring structure (Figure I.1 A) or flexible appendages referred to as cirri (Figure I.1 A). The crown itself consists of a sub-spherical theca (Figure I.2 B) and 5 feather-like rays that often branch multiple times and radiate outwards (Figure I.1 A, I.2 A). These rays (or arms) give the stalked crinoids their well-known flower-like appearance.

Although stalked crinoids are dominant as fossils and still extant, the crinoids seen most often today, the feather stars, lack the archetypal crinoid stalk (Figure I.1 B). Unlike stalked crinoids, feather stars shed their stalks as juveniles, become free-living, and often exhibit high levels of mobility. While feather stars appeared comparatively late in crinoid evolution (Late Triassic), they have become highly successful and represent approximately 85% of extant crinoid species (Hess et al. 2011). All feather stars can crawl, and some groups can even swim, behaviors credited with their evolutionary and ecological success (Meyer and Macurda 1977, Vermeij 1977, Meyer 1985, Roux 1987, Shaw and Fontaine 1990). Feather stars can be observed or collected easily by snorkeling, diving using a self-contained underwater breathing apparatus (SCUBA), and, in some cases, by standing in ankle-deep water (Clark 1915, Hess et al. 2011). In sharp contrast, stalked crinoids are less abundant, less diverse, and, importantly, found only at depths greater than 100 meters today (Meyer and Macurda 1977, Oji 1996). Consequently, extant crinoid studies have focused predominantly on feather stars.

A great deal has been learned about various aspects of crinoid biology from studies of extant feather stars, but given that they lack a stalk, using them as an analog for stalked crinoids, which represent the overwhelming majority of crinoids in the geological past, has significant limitations. The stalk is thought to play a critical role in various aspects of crinoid ecology, which may be the primary reason for the minimal attention that feather stars have received from paleontologists, particularly those who focused on paleoecology, until well into the 20th century (Meyer and Macurda 1977, Ausich and Kammer 2001). Although there are many living crinoids that retain their stalk as adults (orders Cyrtocrinida, Hyocrinida, Isocrinida, and suborder Bourgueticrinina) and the value of studying them to gain paleo-ecological insights has long been

clear, accessing stalked crinoids proved a major challenge to researchers. The will was there, but the mechanism was not.

For nearly two hundred years after they were first discovered, research on extant stalked crinoids was limited. As nearly all access was limited to dredging and trawling, a process that precludes observations that address ecology, functional morphology, growth, and interactions with other organisms, most of their studies focused on taxonomy, phylogeny, and biogeography. It was only when submersible technology became accessible to marine science in the late 1960s and early 1970s that researchers finally had the opportunity to investigate these animals by direct observation. Unsurprisingly, paleontologists were among the first to study stalked crinoids using submersibles, and their findings sparked a reevaluation of several long-held assumptions about stalked crinoid biology and ecology.

In 1972, Macurda and Meyer conducted an extended series of dives in the submersible *Neckton Gamma* and observed large populations of stalked crinoids off Jamaica. Their observations appeared rudimentary, simply a series of photographs that showed various feeding postures of stalked crinoids (Macurda and Meyer 1974). Nonetheless, these overturned nearly 100 years of suppositions about basic stalked crinoid ecology. They were not, as previously thought, rheophobic, waiting for food to fall as marine snow passively, with arms outstretched in a bowl-like fashion. Instead, they lived in current-dominated environments and manipulated their arms actively to form a "parabolic filtration fan" that maximized the flux water from which particulate nutrients could be extracted. This led paleontologists to reconsider the life modes of virtually all fossil crinoids, particularly with respect to feeding postures and the function of the stalk and the arms.

Submersible expeditions over the next several decades expanded on these initial observations and illustrated further the value of *in situ* studies of living stalked crinoids. Observations of a population of isocrinids off Jamaica and Grand Cayman showed evidence of relocation and reported active crawling on the part of one specimen (Messing et al. 1988), upending the long-held general opinion that all stalked crinoids were sessile. Later observations of isocrinids off Grand Bahama showed that the speed with which they crawl was rapid enough to allow escape from certain benthic predators, an advantage attributed previously only to feather stars (Baumiller and Messing 2007). Even more remarkable, the maximum recorded speed, ~10 mm/s, is faster than the maximum crawling speed reported for some shallow water feather stars (Clark 1915, Meyer et al. 1984). These findings spurred more consideration of the hypothesis that feather star mobility gave them an advantage in avoiding benthic predators and led to their continued presence in shallow waters above 100 m while stalked crinoids disappeared.

The hypothesis linking feather star mobility, predation, and their success in Recent oceans was itself influenced by deep-sea observations. Work on feather stars beginning in the 1960s had indicated already that the widely accepted idea that crinoids were distasteful and not subject to predation (Clark 1915) might need to be reconsidered (Fishelson 1966). This work contributed to the hypothesis that the disappearance of stalked crinoids above 100 m during the Cenozoic could be attributed to changes in predation intensity (Meyer and Macurda 1977). The newly begun submersible studies contributed significantly to the growing discussion on predation, particularly in the context of this hypothesis. Observations of direct fish predation on bathyal stalked crinoids (Conan et al. 1981) preceded documentation of such attacks on feather stars (Meyer et al. 1984). Studies of stalked crinoid arm injuries across a depth gradient (e.g., Oji 1996) showed decreasing frequencies of injuries with increasing depth, consistent with the

hypothesis that high predation intensity may determine the restriction of stalked crinoids to greater depths (Meyer and Macurda 1977, Roux 1987, Bottjer and Jablonski 1998, Oji 1996, Baumiller 2008).

Extant stalked crinoids also provided evidence that predation, rather than abiotic conditions, causes crinoid arm injuries most often, as collecting stalked crinoids by suction rarely resulted in crown or arm loss, even when this was done vigorously and crown first (Oji 1996, personal observations), indicating their robustness to physical perturbation. *In vitro* studies on collected isocrinids that demonstrated that grasping the arms with forceps did not induce arm autotomy, while simulating a fish nip using scissors did supported predation as the cause of injuries further (Oji and Okamato 1994). Experiments showed that certain extreme abiotic conditions lead to arm loss, but crinoids in natural settings are unlikely to experience such extremes (Baumiller 2003). Viewing arm injuries from this perspective led to the increasing use of regenerated arms as proxies for predation prevalence and incidence, both in living (see Oji 2015 for a recent review) and fossil crinoids (see Gahn and Baumiller 2010 for an overview).

Submersible research led to further advances in understanding benthic predator and crinoid interactions. Several studies recorded direct evidence of benthic predators feeding on stalked crinoids (Baumiller et al. 2000, Baumiller et al. 2008, Bowden et al. 2011), while evidence of predation on deep-water feather stars, although compelling, remains indirect (Stevenson et al. 2017) despite decades of more observation. Sediment samples from sites where interactions between stalked crinoids and sea urchins had been observed (Baumiller et al. 2008) and the remains of isocrinids fed to sea urchins in aquaria (Baumiller et al. 2010) revealed echinoid predation traces on crinoid skeletal elements; such traces were found subsequently to extend back as far as the Triassic (Baumiller et al. 2010, Gorzelak et al. 2012).

The full list of discoveries facilitated and their effect on our understanding of crinoids and their evolutionary history is too long to recount reasonably in detail for this dissertation. Direct observation and studies on undamaged specimens collected during submersible expeditions have expanded our understanding in such areas as taphonomy, biogeography, taxonomy, histology, and functional morphology, among others. Even more exciting is that these studies represent only the first steps in deep-sea crinoid research. While the early expeditions, in addition to the collection of specimens, involved observations carried out over very short periods of time, and provided only "snapshots" of the organisms (e.g., Macurda and Meyer 1974), over the past several decades, long-term, longitudinal studies began to be employed (Messing et al. 1988, David et al. 1998, Messing et al. 2007). The latter are logistically more difficult and, generally, much more expensive than single visits; thus, their use has been limited. The presence of a permanently based, manned submersible, the *Idabel* (Roatán Institute of Deepsea Exploration), with quick and convenient access to multiple stalked crinoid populations off Isla Roatán, Honduras, presented an excellent opportunity to carry out longitudinal, multi-year studies at a reasonable cost. In this dissertation, I report the results of several such studies of the stalked crinoids, *Democrinus* sp. (Perrier 1883) (Figure I.2). The results are based upon data collected over 2.5 years and 8 expeditions and the topics addressed include arm regeneration, biotic interactions, physiological responses to experimental manipulation, and taxonomy.

Chapter II explores crinoid predation. Predation intensity has been associated with several ecological changes in evolutionary history of crinoids, including the disappearance of stalked crinoids in depths above 100 m during the Cenozoic because of increased predation intensity associated with the radiation of predators during the Mesozoic Marine Revolution (MMR) (Vermeij 1977). Work conducted on stalked isocrinids off Japan demonstrated

decreasing frequencies of arm regeneration with increasing depth, adding credence to the hypothesis that crinoids at greater depths experience fewer encounters with predators than those found at shallower depths (Oji 1996). While Oji's study supported the MMR hypothesis, other studies reported that the prevalence of injuries in stalked crinoids (specifically the *Democrinus* sp. off Roatán) was of similar magnitude to that in several shallow water feather stars (Paschell and Water 2017).

These conflicting results are likely a consequence of the methodology used. Other than a single study by Syverson et al. (2014), previous work quantifying predation on stalked crinoids has been limited to documenting injury frequency (prevalence) based upon cross-sectional data collected during a single expedition. However, injury prevalence is an imperfect proxy for predation intensity, particularly for organisms like crinoids that sustain ephemeral arm injuries (Baumiller and Gahn 2013, Baumiller 2013b). In crinoids, the prevalence of injuries at any given moment is dictated by both the rate at which injuries are incurred in a population and the rate at which they disappear (by complete regeneration of an arm). To understand the predation intensity on crinoids fully, data across multiple visits, i.e., longitudinal data, are needed. By monitoring the population of *Democrinus* sp. off Roatán over several years, two longitudinal approaches were used to quantify predation intensity on the extant, deep-water, stalked crinoid, *Democrinus* sp.: (1) Absolute injuries, where injuries were estimated by counting individuals with decreased arm length between individuals, and (2) projected expected length, where injuries were estimated by counting the number of individuals with arms shorter than expected from the average rates of regeneration. The results indicated that the stalked *Democrinus* sp. does experience much lower predation intensity than crinoids living in shallow water and reinforces

the importance of considering time scales when investigating predation intensity in living crinoid populations.

Chapter III investigates the mobility potential of *Democrinus* sp. as a representative of the stalked Bourgueticrinidae (order Comatulida). As mentioned previously, submersible work over the past several decades has shown that stalked isocrinids (order Isocrinida) are not necessarily permanently sessile, as was long believed (Messing et al. 1988, Baumiller and Messing 2007). However, their active locomotion may be limited only to them because of their unique morphology, specifically the presence of cirri that allow them to return to an upright, feeding posture, articulations in the stalk specialized for autotomy, and the absence of a permanent holdfast that facilitates detachment from the substrate (Figure I.1 A). In contrast, stalked Bourgueticrinidae have a substantially different morphology, and they possess no obvious method to detach from the substrate. Their stalks terminate in a permanent holdfast of either several columnals with branching dendritic rootlets that anchor the animal in soft sediments (Figure I.2 A), or a disk cemented to the substrate. They also lack the specialized articulation for stalk autonomy, as they have columnal articulation characterized by a fulcral ridge along the longer diameter of the facet with deep ligamentary pits on either side (Figure I.2 C). In addition, if a Bourgueticrinidae could detach from the substrate, the lack of cirri along the stalk would leave them without a known method to reestablish an upright posture. Thus, Bourgueticrinidae morphology reinforces the general belief that *Democrinus* sp. is permanently sessile rather than mobile like feather stars and isocrinids.

Manipulations and experiments carried out on *Democrinus* sp. *in situ* were used to test this assumption. The behavior of experimentally dislodged *Democrinus* sp. observed supported the speculation that it does not locomote actively, as none of the specimens dislodged moved

from their original location over the course of the 2.5 years of study. However, unexpectedly, they did not remain prone on the substrate; instead, all dislodged individuals regained an upright posture. The mechanism by which this was accomplished presents a puzzle because, like all stalked crinoids, *Democrinus* sp. lack muscles in their stalk (Grimmer et al. 1984b). Chapter III outlines several potential mechanisms and biomechanical models used to interpret this behavior, including the crinoid using its crown as a kite to generate lift (Baumiller 1992) or engaging in rapid arm movement to generate thrust like swimming crinoids (Janevski and Baumiller 2010). Both the qualitative and quantitative data indicated that none of those mechanisms suffices to explain the behavior observed. We argue that the re-establishment of posture may involve active contraction of the Mutable Collagenous Tissue (MCT) found in all echinoderms and investigated previously in only a few laboratory studies (Birenheide and Motokawa 1996, Birenheide and Motokawa 1998, Birenheide et al. 2000).

In addition to the *in situ* studies described above, Chapter IV provides a review of the taxonomy of the genus *Democrinus*, with a special focus on specimens of *Democrinus* collected in Roatán. Analyses of museum specimens and the literature reveal that most of the *Democrinus* species were defined based upon specimens dredged or trawled in the early 1900s. Consequently, the original species descriptions relied on only a small number of specimens and often on incomplete specimens. This led to very imprecise, confusing, and often contradictory characteristic descriptions. A reassessment of the genus was initiated, but given the constraints COVID-19 imposed, it is not yet complete. What the review makes clear is that the *Democrinus* sp. off Roatán is a new species, *Democrinus newnamus*. In addition, Chapter IV makes several amendments to *D. rawsonii* and the genus overall.

Together, these studies expand our understanding of stalked crinoids in the areas of ecology, taxonomy, and functional morphology. Further, they highlight new approaches possible only recently accessible due to submersible research and represent only a few of the questions they can allow us to begin investigating.

References

Ausich WI, Kammer TW. 2001. The study of crinoids during the 10th century and the challenges of the 21st century. J Paleontol. 75(6): 1161–1173

Baumiller TK. 1992. Importance of Hydrodynamic lift to crinoid autecology, or, could crinoids function as kites? J Paleontol. 66(4):658–665

Baumiller TK. 2003. Experimental and biostratinomic disarticulation of crinoids: taphonomic implications. *In*: Fral JP, David B, editors. Echinoderm research 2001. Lisse: Balkema. p. 243–248

Baumiller TK. 2008. Crinoid ecological morphology. Annu Rev Earth Pl Sci. 36(1):221–249 https://doi.org/10.1146/annurev.earth.36.031207.124116

Baumiller TK. 2013b. Ephemeral injuries, regeneration frequencies, and intensity of the injury producing process. Mar Biol. 160:3233–3239. https://doi.org/10.1007/s00227–013–2302–9

Baumiller TK, Mooi R, Messing CG. 2000. Cidaroid-crinoid interactions as observed from a submersible. *In*: Barker M, editor. Echinoderms 2000. Lisse: Balkema. p. 3

Baumiller TK, Messing CG. 2007. Stalked crinoid locomotion, and its ecological and evolutionary implications. Paleontol. Electron. 10(1):1–10

Baumiller TK, Mooi R, Messing CG. 2008. Urchins in the meadow: paleobiological and evolutionary implications of cidaroid predation on crinoids. Paleobiology. 34(1):22–34. https:// doi.org/10.1666/07031.1

Baumiller TK, Salamon M, Gorzelak P, Mooi R, Messing CG, Gahn FJ. 2010. Benthic predation drove early Mesozoic crinoid radiation. PNAS 107(13):5893–5896

Baumiller TK, Gahn FJ. 2013. Reconstructing predation pressure on crinoids: estimating arm–loss rates from regenerating arms. Paleobiology. 39(1):40–51. https://doi.org/10.1666/0094–8373–39.1.40

Birenheide R, Motokawa T. 1996. Contractile connective tissue in crinoids. Biol Bull. 191:1–4

Birenheide R, Motokawa T. 1998. Crinoid ligaments: catch and contractility. *In*: Mooi R, Relford M, editors. Echinoderm: San Francisco. AA. Balkem, Rotterdam. p. 139–144

Birenheide R, Yokoyama K, Motokawa T. 2000. Cirri of the stalked crinoid *Metacrinus rotundus*: neural elements and the effect of cholinergic agonists on mechanical properties. Proc Biol Sci. 267(1438):7–16

Bottjer DJ, Jablonski D. 1988. Paleoenvironmental patterns in the evolution of post-Paleozoic benthic marine invertebrates. Palaios 3:540–60

Bowden DA, Schiaparelli S, Clark MR, Rickard GJ. 2011. A lost world? Archaic crinoid-dominated assemblages on an Antarctic seamount. Deep-Sea Res PtII. 58:119–127

Clark AH. 1915. A monograph of the existing crinoids. Bull U.S. Nat'l Mus. 82(1):1–406, 17 pls

Columna F. 1592. Phytobasanos, sive Plantarium Historia. Accessit Piscium aliquot Historia, Naples

Conan G, Roux M, Sibuet M. 1981. A photographic survey of a population of the stalked crinoid *Diplocrinus (Annacrinus) wyvillethomsoni* (Echinodermata) from the bathyal slope of the Bay of Biscay. Deep-Sea Res. 28:441–53

Foote M. 1999: Morphological diversity in the evolutionary radiation of Paleozoic and post-Paleozoic crinoids. Paleobiology 25:1–116

Gahn FJ, Baumiller TK. 2010. Evolutionary history of regeneration in crinoids (Echinodermata). Integr Comp Biol. 50(4):514–514 https://doi.org/10.1093/icb/icq155

Gorzelak P, Salamon MA, Baumiller TK. 2012. Predator–induced macroevolutionary trends in Mesozoic crinoids. Proc Natl Acad Sci USA. 109(18):7004–7007 https://doi.org/10.1073/pnas.1201573109

Grimmer JC, Holland ND, Messing CG. 1984b. Fine structure of the stalk of the bourgueticrinid sea lily *Democrinus conifer* (Echinodermata: Crinoidea). Mar Biol. 81:163–176

Hagdorn H, Campbell HJ. 1993. *Paracomatula triadica* sp. nov. an early comatulid crinoid from the otapirian (Late triassic) of new caledonia, Alcheringa. 17(1):1–17

Hess H, Messing CG, Ausich WI. 2011. Articulata. *In*: Hess H, Messing CG, Ausich WI, editors. Treatise on Invertebrate Paleontology. Part T. Echinodermata 2 Revised. Crinoidea. Vol. 3. Univ. of Kansas Press, Lawrence. p. 1–261

Janevski GA, Baumiller TK. 2010. Could a stalked crinoid swim? A biomechanical model and characteristics of swimming crinoids. Palaios. 25(9):588–596 https://doi.org/10.2110/palo.2009.p09–149r

Macurda JR, Meyer DL. 1974. Feeding posture of modem stalked crinoids. Nature. 247:394–396

Messing, CG, Rose-Smyth MC, Mailer SR, Miller JE. 1988. Relocation movement in a stalked crinoid (Echinodermata). Bull Mar Sci. 42:480–487

Meyer DL. 1985. Evolutionary implications of predation on Recent comatulid crinoids from the Great Barrier Reef. Paleobiology. 11(2):154–164 https://doi.org/10.1017/S0094837300011477

Meyer DL, Macurda DB. 1977. Adaptive radiation of the comatulid crinoids. Paleobiology. 3(1):74–82

Meyer DL, LaHaye CA, Holland ND, Arneson AC, Strickler JR. 1984. Time-lapse cinematography of feather stars (Echinodermata: Crinoidea) on the Great Barrier Reef, Australia: demonstrations of posture changes, locomotion, spawning and possible predation by fish. Mar Biol. 78:179–184

Oji T, Okamoto T. 1994. Arm autotomy and arm branching pattern as anti–predatory adaptations in stalked and stalkless crinoids. Paleobiology. 20(1):27–39 https://doi.org/10.1017/S0094837300011118

Oji T. 1996. Is predation intensity reduced with increasing depth? Evidence from the West Atlantic stalked crinoid *Endoxocrinus parrae* (Gervais) and implications for the Mesozoic marine revolution. Paleobiology. 22(3):339–351

Oji T. 2015. Regeneration, predatory-prey interaction, and evolutionary history of articulate criniods. Palaeoworld. 24(4):389–392

Paschall OC, Waters JA. 2017. Estimated predation rate of the stalked bourgueticrinid (Crinoidea) *Democrinus* from Roatán, Honduras. Geol J. 52(5):727–732 https://doi.org/10.1002/gj.28–31

Perrier E. 1883. Sur une nouveau Crinoide fixé, le *Democrinus parfaiti*, provenant des dragages du Travailleur. C. r. hebd. Séanc Acad Sci. Paris 96:450–452

Roux M. 1987. Evolutionary ecology and biogeography of recent stalked crinoids as a model for the fossil record. *In:* Balkema AA, editor. Echinoderm Studies. 2:1–53

Sars M. 1868. Memoires pour sevir a la connaissance des crinoides vivants. Programme de l'Universite royale de Norvege. Christiania. 1–65, 6 pls

Shaw GD, Fontaine AR. 1990. The locomotion of the comatulid *Florometra erraticism* (Echinodermata: Crinoidea) and its adaptive significance. Can J Zool. 68:942–950

Simms MJ. 1988. The phylogeny of post-Palaeozoic crinoids. *In*: Burke RD, Mladenov PV, Lambert P, Parsley RL., editors. Echinoderm Biology: Rotterdam, Balkema, p. 97–102

Stevenson A, Gahn FJ, Baumiller TK, Sevastopulo GD. 2017. Predation on feather stars by regular echinoids as evidenced by laboratory and field observations and its paleobiological implications. Paleobiology. 43(2):274–285 https://doi.org/10.1017/pab.2016.39

Syverson VJ, Messing CG, Stanley K, Baumiller TK. 2014. Growth, injury, and population dynamics in the extant cyrtocrinid *Holopus mikihe* (Crinoidea, Echinodermata) near Roatán, Honduras. Bull Marine Sci. 91(1):47–61 https://doi.org/10.5343/bms.2014.1061

Vermeij GJ. 1977. The Mesozoic marine revolution: evidence from snails, predators and grazers. Paleobiology. 3(3):245–258 https://doi.org/10.1017/S0094837300005352

Chapter I Figures

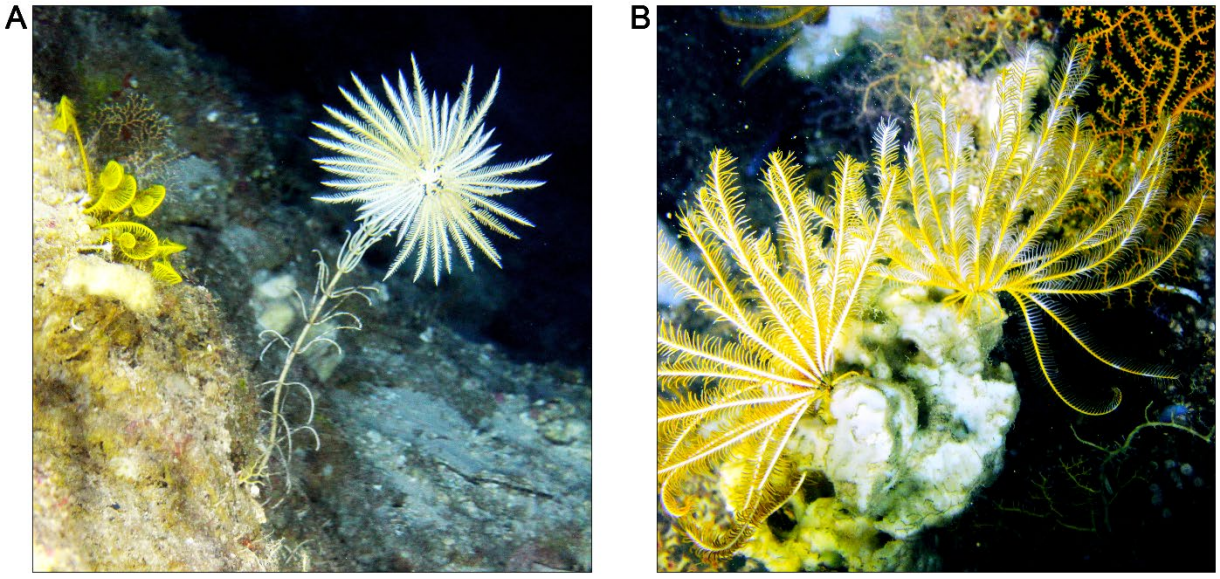

Figure I.1: A: A stalked isocrinid attached to a vertical rock face at ~160 m. The differing arm lengths visible are likely attributable to partial predation. The cirri along its stalk allow it to grasp the substrate at various points along the stalk. Isocrinids can move by either releasing the cirri or autotomizing the attached portion of the stalk and pulling its body along behind it with its arms. **B:** A pair of stalkless feather stars grasping a glass sponge using terminal cirri. Feather stars can move by releasing these cirri and using their arms to crawl or swim. Photo taken at ~450 m on May 12, 2016.

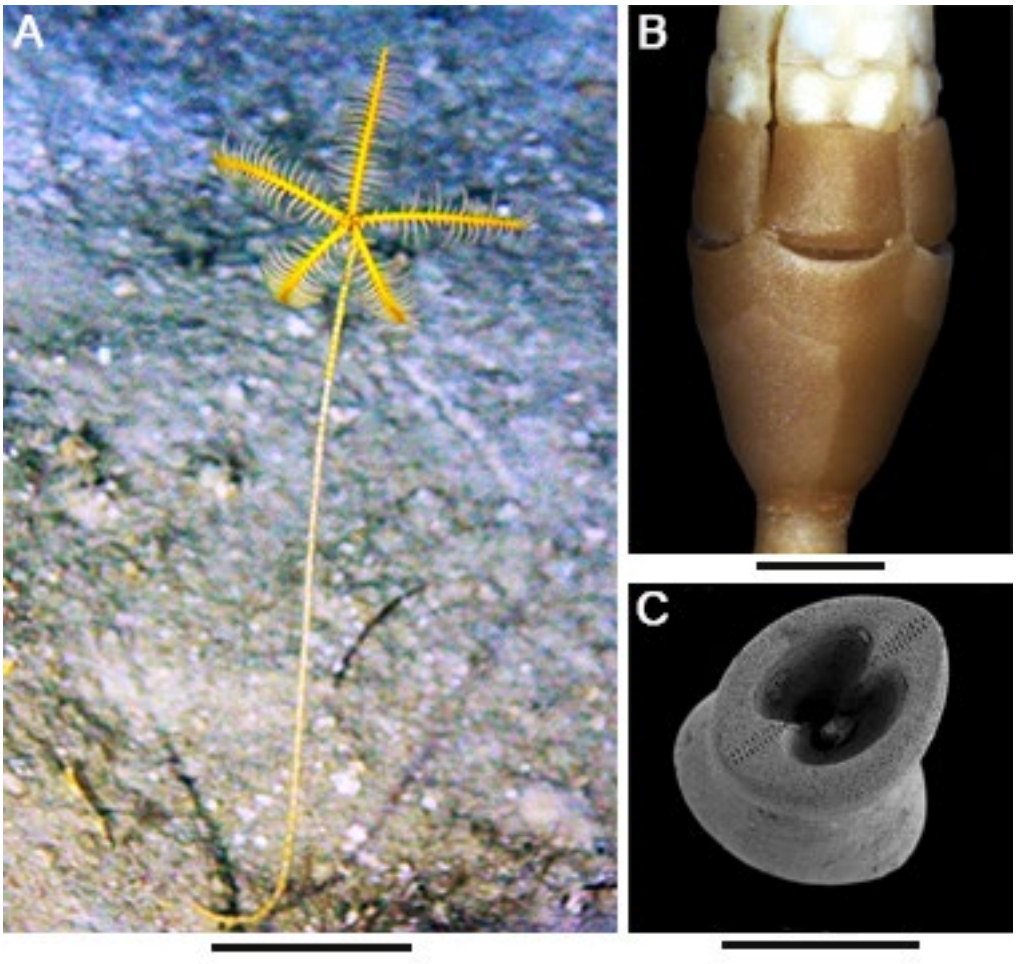

Figure I.2: A: Whole *Democrinus* sp. individual with five prominent arm rays. The individual is attached to loose sediment via a thin, hair-like radix. The stalk lacks any cirri. Scale is 5 cm. **B:** A close-up of a conical *Democrinus brevis cup* shows clear suture lines between the radial and basal plates. Arms remain attached in this specimen, and appear white, while the cup and first brachial are brown. Scale is 1 mm **C:** Synarthrial articulation facet of a bourgueticrinid stalk (*Democrinus* sp.). The fulcral ridge runs through the center of the facet, split by deep, figure-8 style ligament pits. Modified from Roux et al 2019. Scale is 1 mm.

CHAPTER II A "Deeper" Understanding: Low Predation Pressure on the Stalked Crinoid *Democrinus* sp. (Echinodermata), in Roatán, Honduras, Reveals Deep Water as Likely Predation Refuge [*]

ABSTRACT

Predation has been hypothesized to play a key role in the evolutionary and ecological history of crinoids. While evidence of predation on crinoids in the form of injuries is common, quantifying predation intensity, which is critical to test such hypotheses properly, has proven challenging. Two longitudinal approaches were used here to quantify predation intensity on the extant, deep-water, stalked crinoid, *Democrinus* sp.: (1) Absolute injuries, where injuries were estimated by counting individuals with decreased arm length between them, and (2) projected expected length, where injuries were estimated by counting the number of individuals that did not meet the amount of growth expected during the time between two successive observations. These quantitative estimates are based upon data collected from a manned submersible during expeditions conducted over a 2-year span. These results indicate that this deep-water crinoid is subject to much lower predation intensity than are those that live in shallow water, consistent with (1) an inverse relation between predation intensity and depth, and (2) the hypothesis that for stalked crinoids, which are unable to cope with high predation intensity, deep water is a refugium.

[*] Chapter 2 is published in *Bulletin of Marine Science.*: Veitch MA and Baumiller TK. 2021. "Low predation intensity on the stalked crinoid *Democrinus* sp. (Echinodermata), in Roatán, Honduras, reveals deep water as likely predation refuge". Bull Mar Sci. 97(1):107–128

INTRODUCTION

Predation is thought to have played a central role in the evolutionary and ecological history and it has been invoked as a determining factor in various morphological, physiological, and behavioral trends. Examples include changes in spinosity (Signor and Brett 1984, Syverson et al. 2018), calyx plate thickness (Signor and Brett 1984), predation–resistant arm branching patterns (Oji and Okamoto 1994, Syverson and Baumiller 2014), biochemical defenses (Meyer 1985, McClintock et al. 1999), gonad position (Lane 1984, Nichols 1994), reproductive strategy (Nichols 1994), and motility (Meyer and Macurda 1977, Seilacher and Hauff 2004, Baumiller et al. 2008, Janevski and Baumiller 2010, Gorzelak et al. 2012).

Two particularly well–established patterns, which are also thought to be predation–related, involve the recent and historical bathymetric distribution of crinoids. In today's marine environments, stalked crinoids are restricted to depths greater than 100 m, and only the free-living feather stars are found in shallower water. However, the distribution patterns found across the bathymetric gradient today were not always present in the past: The geologic record indicates that stalked crinoids were common and diverse in shallow-water environments during the Paleozoic and Mesozoic eras, and the current distribution pattern began to develop sometime in the Late Mesozoic and increased by the Early Cenozoic (Bottjer and Jablonski 1988, Whittle et al. 2018). A popular hypothesis associates today's distribution patterns with an increase in predation intensity that began with the Mesozoic Marine Revolution (MMR; Meyer and Macurda 1977, Vermeij 1977). According to this hypothesis, stalked crinoids were unable to cope with increased predation and became restricted over time to greater depths, a predation refugium (Meyer and Macurda 1977, Oji 1996). In contrast, high diversity and abundance of modern feather stars in shallow seas has been attributed to their resilience to predation (Oji 1996,

McClintock et al. 1999, Stanley 2008, Bowden et al. 2011, Gorzelak et al. 2012). Feather star mobility, behavior, and distastefulness are thought to be essential factors in avoiding fatal attacks by predators (Meyer and Macurda 1977, Stanley 1977, Vermeij 1977, Mladenov 1983, Meyer 1985, Schneider 1988, McClintock et al. 1999).

However compelling, the hypothesis above has proven challenging to test, in part because documenting and quantifying crinoid predation is difficult in modern settings and even more so in the fossil record. The evidence of predation on crinoids used most widely has been the presence of injuries, specifically arm injuries. In both extant and fossil crinoids, regenerating arms can represent such injuries. Although there are other causes of arm loss, including an ontogenetic process referred to as augmentative regeneration, in which arm number is increased by replacing a single shed arm with a pair (Breimer and Lane 1978, Ubaghs 1978), and stress from rapid environmental change (Roux 1976, Oji and Okamoto 1994, Baumiller 2003, Shibata and Oji 2003, Mizui and Kikuchi 2013), it is widely accepted that nonlethal predation represents the primary cause of arm loss (Meyer and Ausich 1983, Mladenov 1983, Meyer 1985, Schneider 1988, Nichols 1994, Baumiller 2008, Gahn and Baumiller 2010, Gorzelak et al. 2012, Syverson et al. 2014, Stevenson et al. 2017, Baumiller and Stevenson 2018). Predation–induced arm or pinnule loss has been observed in nature numerous times (Fishelson 1974, Conan et al. 1981, Meyer et al. 1984, Vail 1987, Schneider 1988, Nichols 1994, Oji 1996, Lawrence 2009, A. Stevenson, University of British Columbia, pers. Comm.), while environmentally–induced arm loss has been shown to occur only under extreme levels of stress produced during rare events of exceptional magnitude (Oji and Okamoto 1994, Baumiller 2003, Baumiller and Gahn 2003, Mizui and Kikuchi 2013). In addition to injuries to crinoid arms, loss and regeneration of the visceral mass have been observed (Smith et al. 1981, Meyer 1985, 1988). Injuries to the visceral

mass tend to be much more extensive and, in feather stars, the rate of regeneration has been shown to be species-specific (Dolmatov et al. 2020).

The general acceptance of arm injuries as predation–related has led researchers to employ such injuries as a surrogate to document and quantify predation on crinoids. For example, Oji (1996) found that the frequency (prevalence) of regenerated arms in *Endoxocrinus parrae*, an extant stalked crinoid common in the Caribbean, was lower in populations living above 500 m than those at greater depths, while Baumiller (2013a) showed that the frequency of injured arms in the extant feather star, *Florometra serratissima* (Clark 1907), decreased with depth. While these two examples used arm injuries to examine bathymetric trends in predation, Aronson et al. (1997) looked at spatiotemporal changes in predation intensity by comparing injuries in the Eocene stalked crinoid, *Metacrinus fossilis* (Rasmussen 1979), apparently associated with shallow, nearshore environments, to those in the extant deeper dwelling *Metacrinus rotundus* (Carpenter and Von Graff 1885), dredged off the coast of Japan. They found that the prevalence of injuries was significantly less in the former, a pattern the authors interpreted as a consequence of low predation levels associated with temperature and productivity changes in Antarctica at the time. However, the pattern can also be interpreted to be consistent with a temporal increase in predation initiated during the MMR and persisting into the Cenozoic.

One common feature of the studies cited above, and of nearly all other research that has focused on crinoid injuries as a predation proxy, is that they are cross-sectional, i.e., they use the frequency, or prevalence, of injuries in a subsample of individuals from a population as a proxy for predation intensity. For example, a population with a high prevalence of injuries is inferred to have been subject to greater predation intensity than one with a low prevalence of injuries. However, such an inference is not always justified. In instances in which interactions can be

either fatal or lead to injuries that remain detectable throughout life (i.e., scarring in nonfatal interactions), the prevalence of injuries is not a proxy for the incidence of predatory encounters (predation intensity), but rather of the probability that the encounter is fatal, also referred to as predator effectiveness (Schoener 1979). For crinoids, whose arm injuries are ephemeral, it has been shown theoretically and numerically that the prevalence of injuries represents a balance between two opposing processes, the rate at which injuries are added to the population (incidence of injuries) and the rate at which they are removed (regeneration rate; Baumiller 2013a,b, Baumiller and Gahn 2013). Consequently, for taxa with ephemeral injuries, data on both the prevalence of injuries and their rate of regeneration are needed to estimate predation intensity (incidences of injuries). Of course, if one assumes that the rate of regeneration does not vary across the populations that are being compared, the prevalence of injuries can be used to assess predation intensity qualitatively, but that assumption is rarely tested. Empirical (Baumiller and Stevenson 2018) and experimental (A. Stevenson, University of British Columbia, pers. comm.) data for crinoids suggest that while regeneration rates exhibit little variation at lower taxonomic levels, order of magnitude differences characterize higher taxa (Table 1). Thus, while cross-sectional data on injury prevalence alone can offer meaningful qualitative insights into predation intensity at lower taxonomic levels, such as in the three examples cited above (Oji 1996, Aronson et al. 1997, Baumiller 2013a), comparisons that rely on cross-sectional data at higher taxonomic levels require additional information on rates of regeneration.

Given the challenges above to quantifying predation intensity from injury prevalence in crinoids, a different approach is worth considering. Recently, a longitudinal study was conducted to quantify predation intensity on several species of feather stars off Negros Island in the Southern Philippines (Baumiller and Stevenson 2018). In that study, tagged individuals were

monitored periodically, which allowed the number of new injuries to be tracked over time, and the ratio injuries/time was used as a direct estimate of predation intensity (injuries/individuals*time^{-1}). A comparison of the longitudinally derived results to results those that combined injury prevalence and regeneration rates showed reasonable congruence (Baumiller and Stevenson 2018). Therefore, longitudinal studies allow for testing predation intensity across higher taxonomic levels, specifically between deep-water stalked crinoids and shallow-water feather stars, which is essential to test whether predation intensity is the cause of the recent bathymetric distribution of crinoids.

This dissertation used *Democrinus* sp. as the study organism because the taxonomy of the genus requires revision. The species examined likely belongs to one of two species currently recognized: *D. rawsonii* (Pourtalès, 1874) or *D. conifer* (Clark, 1909). However, it is currently unclear whether several synonymized names, including *D. rawsonii*, represent valid species or not.

METHODS

Between May 2012 and December 2017, eight expeditions were conducted in the manned submersible *Idabel* (Roatán Institute of Deepsea Exploration) to explore the deep-water crinoid fauna off Isla Roatán, Honduras. The fauna include members of Comatulida (both feather stars and stalked Rhizocrinidae), Isocrinida, and Cyrtocrinida. Thousands of small (1520 cm tall) *Democrinus* sp. are found on sediment-covered slopes between 200 and 350 m. Here, densities can approach 9 ind m^2. Features of *Democrinus* sp. relevant to this study include: (1) it is permanently sessile, anchored in soft sediments by branched radices covering the distal-most part of its stalk; (2) adults possess five undivided rays, so it does not undergo ontogenetic autotomy and augmentative regeneration; and (3) numerous specimens of *Democrinus* sp. off

Isla Roatán have been observed missing arms entirely or with extremely short arms, indicative of predatory injuries (Veitch et al. 2016, Paschall and Waters 2017).

Idabel can accommodate a pilot and two observers, the latter in an observation compartment with a 76 cm diameter viewport. The two observers used interior digital video and SLR cameras with synchronized exterior strobes to capture images of *Democrinus* sp. with scale provided by a pair of externally fixed lasers set 10 cm apart, and a laserbox with three lasers each set 2 cm apart, mounted inside the sub on its flat, bottom port. Images with scale were used to measure arm length and stalk diameter of *Democrinus* sp. using Adobe Photoshop C6 with vectors calibrated to laser scales. The use of lasers for scale requires that they be projected onto an individual's crown and that all parts of each arm are positioned in the same plane. This is a difficult task, given that *Democrinus* sp. only has five short arms that sometimes curl inwards or outwards at the tips (depending upon feeding position). In most of the *Democrinus* sp. imaged, the lasers appear not on the crown, but on the sediment-covered bottom some distance away, preventing using the lasers as an accurate scale for those individuals. To increase the sample size of individuals measured accurately, we developed a scale by measuring stalk diameters of several collected *Democrinus* sp. specimens with digital calipers in the lab. These measurements revealed little variability in the diameter of the stalk [mean diameter 0.18 cm (SD 0.03), n = 7], even for individuals with different stalk and arm lengths. The mean diameters measured in the lab were statistically indistinguishable from the laser–calibrated measurements [mean diameter 0.19 cm (SD 0.04), n = 53]. Thus, we used the stalk diameter as a proxy to obtain arm length when laser scales could not be used reliably.

Measurements of *Democrinus* sp. stalk lengths from videos and photos were also obtained using the same approach described above. However, all stalk measurements

underrepresent true stalk lengths, as *Democrinus* sp. lives with the radix bearing, distal-most part of its stalk rooted in soft sediment, so a portion of the stalk is often buried in the sediment (Figure II.1). Consequently, for many specimens, the only part of the stalk that can be measured from videos and photos is the exposed length from the substrate to the base of the crown. Even this visible portion is difficult to measure accurately because it is generally arcing and rarely equidistant/coplanar with the picture plane. These constraints prevented uniformly accurate measurements of stalk lengths.

This longitudinal study was conducted at a semi-permanent, well-marked site at a depth of 240 m, where deployed float markers and natural landmarks facilitated the detailed mapping of the position of 63 *Democrinus* sp. individuals (Figures II.3 and II.4). The site was visited and the specimens were censused four times: November 2015; May 2016; December 2016, and December 2017. During each census visit, photos and videos were taken of the area delimited by the markers (Figures II.3 and II.4), and each individual's arms lengths were measured as described above. Because image quality was not sufficiently high in some instances, we acquired accurate measurements of only 39 individuals (n = 24 individuals measured across all four census visits and n = 15 across either two or three visits).

The bottom temperature was recorded every 30 min from May 2016 to December 2017 using a Hobo Tidbit v2 Temperature Data Logger (0.2 C accuracy), and the data were downloaded using HoboWare software. Detecting injuries in *Democrinus* sp. required a different approach than is used with feather stars and isocrinids. In the latter two taxa, an injury affects only one or several arms per event and rarely the entire length of an individual's arm. In these taxa, injuries are recognized by either discontinuity in the size (diameter) of adjacent plates on one arm or by the anomalously shorter length of the injured arm(s) relative to the individual's

other arms. In feather stars and isocrinids, this difference in length persists until the injured arm is regenerated fully and no longer recognizable. On the other hand, in *Democrinus* sp., injuries lead to the loss of all five arms. The underlying mechanism of why Democrinus sp. lose all five of their arms rather than just one or two is not understood, but in all but a single instance of *Democrinus* sp. with missing or regenerating arms, all arms were lost. Moreover, nearly the entire length of each arm is lost, with only the five first brachials (Br1) remaining (Figure II.5). This is likely a consequence of the fact that *Democrinus* sp. has short arms (approximately 2.6 cm vs. >10 cm for feather stars and isocrinids) with an autotomy-specialized articulation between brachials 1 and 2 (Br1 and 2; Figure II.5 A, C), while in the generally many–armed feather stars and isocrinids, each arm can have multiple autotomy articulations. In the latter two taxa, predatory encounters rarely involve the loss of the entire crown; usually, only a single arm, or a subset of adjoining arms, is lost, shed at an autotomy articulation near the point of injury (Oji and Okamoto 1994, A. Stevenson, University of British Columbia, pers. comm.). The mode of arm loss in *Democrinus* sp. makes it difficult to identify injured individuals accurately, as all five arms are of the same size (Figure II.5 A, B). Although extreme close-ups reveal a discontinuity in the size (diameter) of brachial 1 (Br1) and brachial 2 (Br2; Figure II.5 B) in injured individuals, such photographs are rarely available. Another approach involves identifying individuals with anomalously short arms as those that have been injured. The decision about what constitutes anomalously short arms is arbitrary, ranging from individuals missing all arms entirely (Veitch et al. 2016) to using a cut–off ratio of arm length to stalk length >1/6 (Paschall and Waters 2017). The first of these underestimates the number of injured individuals, as it can includes none with partially regenerated arms, while the use of arm length to stalk length ratios is unreliable because even if the visible portion of the stalk could be measured accurately from

videos or photos, for many individuals, the sediment obscures an unknown length. Similarly, the ratio of arm length to calyx height was not useful, as the latter varied widely among the specimens collected (1/3–1/9).

The difficulties in detecting injuries in *Democrinus* sp. above demonstrate that the accuracy of estimates of their prevalence derived from cross-sectional studies, which rely on single snapshots of a population, must be questioned. This is much less of a problem in feather stars and isocrinids, where injuries can be detected until the injured arms regenerate fully. Unlike cross-sectional studies, longitudinal studies employ a temporal sequence of multiple snapshots of the same individual. This allows any changes in arm lengths over time to be detected. An individual with arms that decreased in length between consecutive observations is classified as having been injured during the interval. Thus, the longitudinal approach is suited particularly well to studying predation on *Democrinus* sp., as it avoids the problems associated with injury detection from a single snapshot.

Injuries counted by taking only arm lengths that decreased between observations were used as a conservative approach to estimate the total number of injuries. The decrease in length approach estimated individual predation intensity (i, injuries d $^{-1}$) using the following equation:

$$i = \mathrm{N} / \sum_{ind=1}^{ind=39} \sum_{v=1}^{v=4} (t_{ind,v} - t_{ind,v-1}) \qquad \text{(II.1)}$$

in which N is the number of injuries, and the denominator represents the number of days between the dates of two successive census visits summed over all sampled individuals, and where t is the date of the visit (e.g., $t_{1,2}$ is the value recorded for individual 1 during census 2). To illustrate, the time span for individual 1 in Table II is 752 d ($t_{1,2}$ $t_{1,1}$ = 175, $t_{1,3}$ $t_{1,2}$ = 213, $t_{1,4}$ $t_{1,3}$ = 364), while for individual 14, it is 577 d ($t_{14,2}$ $t_{14,1}$= 0, $t_{14,3}$ $t_{14,2}$ = 213, $t_{14,4}$ $t_{14,3}$ = 364); the 0 d value results from the absence of arm length data for individual 14 during census visit 1.

Although absolute decreases in arm length provide a conservative assessment of injuries, this approach can underestimate injuries if the monitoring frequency is too low. In such a case, some injured arms may regenerate sufficiently so that no decrease in length, or even an increase in length, will be observed. To account for this, we employed a second method: projected expected length. The estimate of *Democrinus* sp. regeneration rate obtained by monitoring arm length over time, can be used to predict the amount of growth expected during the time between two successive observations. For a given individual, if the observed increase in length between observations is less than expected, then an injury is inferred to have taken place between census visits.

To estimate intrinsic arm regeneration rate of *Democrinus* sp., the rate of change in arm length was calculated for each individual between successive visits using the following equation:

$$rr_{ind,v-1\ to\ v} = \left(\frac{Lobs_{ind,v} - Lobs_{ind,v-1}}{t_{ind,v} - t_{ind,v-1}}\right) \quad \text{(II.2)}$$

in which *rr* is the regeneration rate, *Lobs* is the measured arm length on a given visit, and *t* is the date of the visit, with the subscripts as in Equation II.1. Using the arm lengths recorded during each census visit (Table II.2), regeneration rates were calculated from changes in arm length over time spans from 6 to 12 months. Note that negative rates correspond to arms that decreased in length between successive census visits, which indicate injured individuals identified using the previous approach. Because the intrinsic regeneration rate is positive by definition, including these negative rates in its estimate would bias the rate downwards. Therefore, only non-negative rates were used to estimate the mean regeneration rate in this population.

The mean regeneration rate for *Democrinus* sp. was then used to calculate the projected expected arm length for each of the monitored individuals on the latter date of two successive visits. This was accomplished by setting the initial arm length equal to the arm length observed

on the day of the earlier of the two visits ($Lobs_{\mathrm{ind,v\text{-}1}}$; Table 2.2), and adding to that the expected change in arm length attributable to regeneration during the time interval to the current visit v:

$$Lexp_{\mathrm{ind,v}} = Lexp_{\mathrm{ind,v-1}} + (rr_{avg})(t_{\mathrm{ind,v}} - t_{\mathrm{ind,v-1}}) \quad (2.3)$$

The expected arm length, $Lexp_{\mathrm{ind,v}}$, on the second of the two successive visits was compared to the length observed on that visit and instances in which the latter was shorter than expected were categorized as having suffered an injury sometime between visits v–1 and v.

In addition to the longitudinal data gathered at the 240 m site, cross-sectional data of *Democrinus* sp. populations were obtained from photos and videos during the expeditions mentioned above and four earlier ones (June 2012, June 2013, July 2014, May 2015). All photos and videos were taken as the submersible moved several meters off the bottom either parallel or perpendicular to the 180, 200, 230, and 245 m isobaths. These transects primarily provide information on the presence/absence of *Democrinus* sp. crowns. However, in instances when the images included a clear scale, either via lasers or stalk diameter, arm lengths were measured. These cross-sectional data were available for 205 individuals. The data were both temporally (5 yr. span) and bathymetrically (180–245 m range) heterogeneous. Nevertheless, they provide a sample of the areas of the *Democrinus* sp. population that can be compared to the longitudinally gathered data at the 240 m site.

RESULTS

The census data are presented in Table II.2. The pooled mean arm length across all census visits was 2.6 cm (SD 1.5; n = 135). As each individual's arms may decrease or increase in length because of injury or regeneration between any two successive visits, each observation of the same individual was treated as an independent datum in calculating the pooled average. Mean

arm lengths for each of the four census visits ordered chronologically were 2.1 cm (SD 1.3; n = 35), 2.6 cm (SD 1.5; n = 34), 3.1 cm (SD 1.7; n = 36), and 2.3 cm (SD 1.2; n = 30).

These means showed no obvious trend over time. A closer look at the data indicated that what underlies this observation is a dynamic quasi-equilibrium, with length increases attributable to growth balanced roughly by decreases attributable to injury. Comparing the length of an individual's arms from one visit to the next revealed that the arms lengthened in 52 and shortened in 39 of the 91 observations (Table 2.2). Using the decrease in length approach, the estimate of per individual predation intensity on *Democrinus* sp. was $i = 0.0016$ injuries d^{-1}. A more intuitive measure of predation intensity is the average waiting time between injuries, obtained by taking the reciprocal of *i*. This conservative method estimated that an individual *Democrinus* sp. loses arms every 613 d on average (Table II.3).

As discussed earlier, the decrease in length approach is conservative and provides only a minimum estimate of injuries. The more realistic estimate uses projected expected length, the calculated mean regeneration rate for *Democrinus* sp. [0.008 cm d^{-1} (SE 0.0009; n = 52); Figure II.6]. Table III shows the injuries inferred and the corresponding predation intensities obtained using the mean (SE) regeneration rate from Equation 2.2. As the injury count obtained using the mean regeneration rate must exceed the count based solely upon decreases in length, and given that the denominator in Equation 2.1 remains the same in both approaches, the expected length approach results in a higher estimate of predation intensity and consequently shorter waiting times between arm loss events than the decrease in length approach (Table II.3).

The cross-sectional data for *Democrinus* sp. populations gathered (n = 205) were statistically indistinguishable ($p = 0.88$, KS test; Figure II.7) from the longitudinal data at the 240 m site (n = 135).

DISCUSSION

The primary goal of this study was to quantify predation intensity on the deep-water, stalked, sessile crinoid, *Democrinus* sp., by focusing on injuries to its arms. Because crinoid arm injuries are ephemeral and disappear following some interval of regeneration, the prevalence of injuries, *P*, in a population represents a balance between the incidence of injuries, *i*, and the rate at which they are eliminated through regeneration, *rr*. Thus, while the prevalence of injuries may be obtained cross-sectionally from a single snapshot at an instant in time, estimating injury incidence and regeneration rates requires individuals to be monitored over time via a longitudinal approach. In this study, 39 individuals of *Democrinus* sp. observed at a depth of 240 m near Isla Roatán, Honduras, were surveyed periodically over a 2-year period. The surveys revealed that, at this site, *Democrinus* sp. regenerates its arms at an average rate of 0.008 cm d^{-1} and suffers injuries with an incidence of approximately 0.0033 d^{-1}, equivalent to a waiting time between injuries of approximately 303 d. Because arm injuries in crinoids are interpreted generally to be attributable to nonlethal (partial) predation (Meyer and Ausich 1983, Mladenov 1983, Meyer 1985, Schneider 1988, Nichols 1994, Baumiller 2008, Gahn and Baumiller 2010, Syverson et al. 2014, Stevenson et al. 2017, Baumiller and Stevenson 2018), other possible causes of injuries should be considered before accepting the approximate 0.0033 d^{-1} incidence of injuries as a measure of predation intensity, particularly because, unlike in feather stars (Fishelson 1974, Conan et al. 1981, Meyer et al. 1984, Vail 1987, Schneider 1988, Nichols 1994, Oji 1996, Lawrence 2009, A. Stevenson, University of British Columbia, pers. comm.), predation–related arm loss in *Democrinus* sp. has not been observed directly.

Augmentative regeneration (one arm replaced by two or more) does not occur in the five–armed *Democrinus* sp., so ontogenetic arm loss cannot explain the data observed. Other plausible

causes include temperature excursions or high current velocities that could result in trauma and arm loss. Temperature data were collected every 30 min at the 240 m site from May 2016 to December 2017 (Figure II.8) and an average temperature of 16.4 °C was recorded with an approximate 4 °C range. Daily fluctuations of 12 °C were surprisingly common, suggesting that *Democrinus* sp. is habituated to, and not traumatized by, such variations. Although no comparable temporal sequence of near-bottom current velocity data is available for the 240 m site, semi-quantitative estimates based upon the movement of suspended particles, as well as the submersible's velocity moving against the current under full throttle, allowed rough estimates of current velocities. Generally, the bottom currents, reflected by movements of suspended particles at the *Democrinus* sp. localities, were well below 5 cm s^{-1}, with stronger currents up to 15 cm s^{-1} rarely observed. However, no evidence of arm loss or other injuries was observed during or immediately following even the strongest currents observed. To test the effect of stress/trauma attributable to strong currents further, a 5 cm PVC pipe was attached to the submersible, powered by its thrusters, and pointed directly at the crown of *Democrinus* sp. (Figure II.9). As the thrusters were turned on, their posture changed abruptly from the normal roughly parabolic feeding posture, with arms extended perpendicular to the current, aboral–side upstream and arm tips flexed into the current, to a low–drag posture, with all arms aligned parallel to the flow and tips facing down–current. A similar postural response has been described previously in other stalked crinoids subjected to high currents (Baumiller et al. 2008). Importantly, this thruster-produced flow did not lead to arm loss or any other type of injury. Similarly, when the thrusters were reversed, which created a suction force strong enough for the crown to be pulled into the PVC pipe, no arms were injured.

Given the observations above, it is unlikely that thermal and/or current stress of the magnitudes observed caused the arm injuries seen in *Democrinus* sp. Still, because the temperature sensor was deployed for only part of the study (May 2016, December 2017) and current velocities were estimated during only a few hours on several days, episodic events characterized by more extreme environmental fluctuations may have occurred. If such extreme, episodic events did cause arm loss, and assuming that similar tolerance to stress characterizes all individuals of a species, such injuries would likely be clustered in time and occur simultaneously in most individuals. Arm lengths under such a scenario should show a narrow range of values centered on one or several modes. On the other hand, predatory attacks are unlikely to occur at the same instant on all prey in a population, so arm loss in the population should be distributed more or less randomly over time, and arm lengths should show a flat distribution. Computer simulations (R v. 3.5.3; R Core Team 2019) parameterized with values based upon results from the 240 m site were used as a heuristic to explore these two scenarios. In each of 1000 simulations, a population of 39 individuals with 2.5 cm long arms was subjected to arm loss events and arm growth for 10,000 time steps, equivalent to 10,000 days. In each time step, each individual could lose the entire length of all of its arms with an average probability of 0.0033, as observed at the 240 m site; injured and uninjured arms grew at the empirically derived rate of 0.008 cm/time step^{-1}. At the end of each simulation, one time step was selected at random from among the last of the 2000 steps (8001 to 10,000), and the distribution of arm lengths in the 39 individuals in that time step was compared to the arm lengths observed at the 240 m site using the F–test of equality of variance. For the time-homogeneous scenario (predation), the probability of injury was stochastically constant (0.0033) in each time step, while for the time–

inhomogeneous scenario (extreme/rare events), probabilities were modeled after Foote (1994) using the following expression:

$$F(i) = e^{k}[\ln(x)], 0 < x = 1 \quad \text{(II.4)}$$

in which F(i) is the probability that the risk of injury is less than or equal to x and k = 0.0033/(1–0.0033). The latter expression was chosen because it produces the temporally clustered distribution of injuries intended and has the same mean probability of injury per time step, 0.0033, as used in the time-homogeneous scenario. In the 1000 time-homogeneous (predation) simulations, 90% of the distributions were statistically indistinguishable from the data observed (F–test, p >0.05). In 1000 of the time–inhomogeneous (extreme/rare events) simulations, 89% of the simulated distributions differed statistically from the data observed (F–test, p <0.05). While inconclusive, these results favor predation as the cause of *Democrinus* sp. arm injuries.

The arguments above support the inference that the incidence of arm loss, i, reported above is equivalent to predation intensity on *Democrinus* sp. at the 240 m site. If predation intensity is a driving cause of bathymetric restriction of stalked crinoids, as the MMR suggests, it is critical to compare these results with shallow-water predation intensity. However, while data on injury prevalence (number of injuries/total population) in crinoids are relatively common, data on predation intensity (injuries time^{-1}) are rare. To the best of our knowledge, Baumiller and Stevenson (2018) provided the only longitudinal study of predation intensity on shallow water crinoids and demonstrated that for the tropical feather stars, *Capillaster multiradiatus* (Linnaeus 1758) and *Clarkcomanthus mirabilis* (Rowe et al. 1986), the average waiting time between injuries is 45-62 d (i = 0.016-0.022 d^{-1}) in nearshore environments (depth 530 m) of Negros Oriental, The Philippines. This is a dramatically higher incidence of injuries than in *Democrinus* sp. at 240 m, and is consistent with the existence of a bathymetric gradient in predation pressure

on crinoids. Of course, drawing more robust conclusions about the generality of this pattern requires more data on predation intensity. These can be obtained using an approach described in detail by Baumiller (2013a,b), Baumiller and Gahn (2013), and Baumiller and Stevenson (2018) that combines cross-sectional data on injury prevalence (P) with data on regeneration rates (*rr*) and length of arm lost per event (L_{avg}), which is summarized by the following equation:

$$i = -\ln(1-P)\left(\frac{rr}{\propto L_{avg}}\right) \quad \text{(II.5)}$$

Relevant data for calculating predation intensity using Equation 5 are available for only three taxa: the feather star, *F. serratissima*, collected at 1734 m in Barkley Sound, British Columbia, Canada (p = 0.8; L_{avg} = 14 cm, *rr* = 0.05 cm d^{-1}, Mladenov 1983); the isocrinid, *M. rotundus*, dredged from depths of 100160 m off the coast of Japan (p = 0.89, Meyer and Oji 1993; L_{avg} = 13 cm, Carpenter and Von Graff 1885; *rr* = 0.017 cm d^{-1}, Amemiya and Oji 1992) and the cyrtocrinid, *Holopus mikihe*, from 430 to 640 m off Isla Roatán, Honduras (p = 0.18; L_{avg} = 4 cm, *rr* = 0.002 cm d^{-1}, Syverson et al. 2014). Figure II.10 summarizes the predation intensities derived longitudinally as well as those for the three taxa listed above using Equation II.5 with α equal to 0.5 (1/2 of the average arm length lost per incident). The results reveal a pronounced bathymetric trend, with increasing crinoid depth correlated with a reduced incidence of arm injuries (longer waiting time; Figure II.10). Some of this signal may be because different prey taxa have different levels of predation resistance. For example, *H. mikihe* responds to a tactile stimulus by closing its 10, heavily–calcified arms very quickly into a protective fist–like posture that might reduce the incidence of injuries (Syverson et al. 2014), and isocrinids can crawl, perhaps as a way to escape benthic predators (Baumiller and Messing 2007).

Any direct comparison of predation must acknowledge the potential that different predators prey on shallow-water feather stars and deep-sea stalked crinoids. Certainly, fishes are

known to prey on shallow-water feather stars (Fishelson 1974, Conan et al. 1981, Meyer et al. 1984, Lawrence 2009, A. Stevenson, University of British Columbia, pers. comm.) and on stalked isocrinids (Conan et al. 1981). No active predation on *Democrinus* sp. has been observed, but injuries involve the crown, not the stalk, which favors nektonic rather than benthic predators. Either way, there is no evidence currently to suggest that, given an opportunity, predators that cause injuries to shallow-water feather stars would not do the same to stalked crinoids. In fact, tests of preference between feather star and isocrinid food pellets presented to fishes showed no difference (McClintock et al. 1999), although presenting entire isocrinids elicited no aggressive feeding behavior. Further, the biology of most deep-water stalked crinoids shows little evidence of strategies that would reduce the incidence of arm injuries attributable to predation. However, the shallow-water feather stars exhibit such strategies instead (e.g., mobility, behavior, and distastefulness). Moreover, the interpretation of the gradient as attributable to predators rather than differences in the prey's biology is supported by two studies that focused on populations of a single species, which eliminates the influence of biological differences among taxa as causal to the incidence of injuries. Both the isocrinid, *E. parrae* (Oji 1996), and the feather star, *F. serratissima* (Baumiller 2013a), showed a decrease in predation intensity with depth. Thus, while more data will surely reveal the pattern better, the bathymetric trend for crinoids appears general and robust and is consistent with the hypothesis that predators determine the restriction of stalked crinoids to deep water.

Finally, it is worth considering the consequences that changes in the incidence of non-lethal predation on crinoids may have on certain ecologically important traits, such as arm length. The mean arm length (dimension L) is the ratio of the process that leads to an increase in its length (regeneration rate, *rr*, dimension $L\ t^{-1}$) and can be expressed by the process that reduces

its length (incidence of injuries, *i*, dimension t^{-1}). For example, in current bathyal environment of *Democrinus* sp., the mean arm length based upon this ratio is 2.4 cm (0.008 cm d^{-1} / 0.0033 d^{-1}; Table II.3), virtually identical to the mean arm length observed. Hypothetically, if this population of *Democrinus* sp. was transplanted to shallow water and experienced predation intensity comparable to the levels feather stars experience in that environment (*I* = approximately 0.019 d^{-1}), while all else remained the same, the mean arm length in the transplanted population would decrease by a factor of approximately 5, from 2.4 cm to approximately 0.4 cm. Thus, the most direct effect of increasing nonfatal predation intensity would be shorter arms, assuming no major ecological or environmental differences other than predation. In the context of the present-day bathymetric predation gradient, the exclusion of certain taxa of crinoids from shallow depths where predation intensity is highest may be attributable to not only their lack of escape, biochemical, or morphological anti-predatory traits, but also because of their intrinsically low regeneration rates that would result in arm lengths too short to capture sufficient nutrients.

CHAPTER SUMMARY

Our longitudinal study of the deep-water stalked crinoid, *Democrinus* sp., revealed that individuals lose arms to injuries once every 303 days and regenerated lost arms at a rate of 0.008 cm d^{-1}. Several lines of evidence, including *in situ* observations and experiments, high–resolution temperature records, and population-level distribution of arm lengths, suggest that predation (rather than abiotic factors) is the main cause of these injuries in *Democrinus* sp. Comparison of the incidence of injuries obtained from this study to longitudinally–derived estimates in shallow–water feather stars indicates that predation is 57 times more intense in shallow water than at greater depths. Estimates of predation intensity from cross-sectional studies also reinforce the claim that an inverse relation characterizes predation intensity on crinoids relative to depth and is

consistent with the hypothesis that the deep sea serves as a refugium for crinoids unable to cope with intense predation. The results of this study add crinoids to the list of taxa [mollusks (Kropp 1992) and rhynchonelliform brachiopods (Harper and Peck 2016)] for which predation intensity decreases with depth, suggesting that this pattern may be quite general.

Acknowledgments

Funding was provided by NSF grant 10366393 (TKB), National Geographic Society CRE Research Grant 9283–13 (TKB), the Paleontological Society Student Research Grants, and Rackham Predoctoral Research Awards. The authors thank CG Messing for reading and commenting on an early version of the manuscript, K Stanley for piloting *Idabel* and excellent memory of site locations, C Abraczinskas for help with figures, P Etnoyer for the loan of lasers, and two anonymous reviewers for comments. The authors also thank C Byrne, B Hays, Dr. A Kroh, Dr. A Stevenson, and Dr. J Veitch for shore support across various visits and for extreme tolerance during long cramped hours of submersible rides and camera usage critiques.

References

Amemiya S, Oji T. 1992. Regeneration in sea lilies. Nature. 357:546–547. https://doi.org/10.1038/357546a0

Aronson RB, Blake DB, Oji T. 1997. Retrograde community structure in the late Eocene of Antarctica. Geology. 25:903–906. https://doi.org/10.1130/0091–7613(1997)025¡0903:RCSITL>2.3.CO;2

Baumiller TK. 2003. Experimental and biostratinomic disarticulation of crinoids: taphonomic implications. In: Fral JP, David B, editors. Echinoderm research 2001. Lisse: Balkema. p. 243–248.

Baumiller TK. 2008. Crinoid ecological morphology. Annu Rev Earth Planet Sci. 36(1):221–249.

Baumiller TK. 2013a. Arm regeneration frequencies in Florometra serratissima (Crinoidea, Echinodermata): impact of depth of habitat on rates of arm loss. Cah Biol Mar. 54:571–576.

Baumiller TK. 2013b. Ephemeral injuries, regeneration frequencies, and intensity of the injury producing process. Mar Biol. 160:3233–3239. https://doi.org/10.1007/s00227–013–2302–9

Baumiller TK, Gahn FJ. 2003. Predation on crinoids. In: Kelley PH, Kowalewski M, Hansen TA, editors. Predator–prey interactions in the fossil record. Topics in Geobiology. 20th ed. New York: Springer. p. 263–278.

Baumiller TK, Messing CG. 2007. Stalked crinoid locomotion, and its ecological and evolutionary implications. Palaeontol Electronica. 10(1):1–10.

Baumiller TK, Mooi R, Messing CG. 2008. Urchins in the meadow: paleobiological and evolutionary implications of cidaroid predation on crinoids. Paleobiology. 34(1):22–34. https:// doi.org/10.1666/07031.1

Baumiller TK, Gahn FJ. 2013. Reconstructing predation pressure on crinoids: estimating arm–loss rates from regenerating arms. Paleobiology. 39(1):40–51. https://doi. org/10.1666/0094–8373–39.1.40

Baumiller TK, Stevenson A. 2018. Reconstructing predation intensity on crinoids using longitudinal and cross–sectional approaches. Swiss J Palaeontol. 137(2):189–196. https://doi. org/10.1007/s13358–018–0169–6

Bottjer DJ, Jablonski D. 1988. Paleoenvironmental patterns in the evolution of post–Paleozoic benthic marine invertebrates. Palaios. 3:540–560.

Bowden DA, Schiaparelli S, Clark MR, Rickard GJ. 2011. A lost world? Archaic crinoid–dominated assemblages on an Antarctic seamount. Deep Sea Res Part II Top Stud Oceanogr. 58(12):119–127.

Breimer A, Lane NG. 1978. Paleoecology. In: Moore RC, Teichert C, editors. Treatise on invertebrate paleontology, Part T, Echinodermata 2 (1). New York and Lawrence: Geological Society of America and University of Kansas Press. p. T316–T347.

Ciampaglio CN, Donovan SK, Weaver PG. 2007. A new bourgueticrinid (Crinoidea) from the Castle Hayne Formation (Eocene) of southeastern North Carolina, USA. Swiss J Geosci. 100(2):243–249 https://doi.org/10.1007/s00015–007–1221–5

Clark AH. 1909. Four new species of the crinoid genus Rhizocrinus. Proc U S Natl Mus. 36(1693):673–676 https://doi.org/10.5479/si.00963801.36–1693.673

Conan G, Roux M, Sibuet M. 1981. A photographic survey of a population of the stalked crinoid Diplocrinus (Annacrinus) wyvillethomsoni (Echinodermata) from the bathyal slope of the Bay of Biscay. Deep–Sea Res. 28(5):441–453 https://doi.org/10.1016/0198–0149(81)90136–9

Dolmatov IY, Kalacheva NV, Mekhova ES, Frolova LT. 2020. Autotomy and regeneration of the visceral mass in feather stars. Zoomorphology. 139:171–187 https://doi.org/10.1007/s00435–020–00483–4

Donovan SK, Veltkamp CJ. 2001. The Antillean Tertiary crinoid fauna. J Paleontol. 75(3):721–731 https://doi.org/10.1017/S0022336000039755

Fishelson L. 1974. Ecology of northern Red Sea crinoids and their epi–and endozoic fauna. Mar Biol. 26:183–192 https://doi.org/10.1007/BF00388888

Foote M. 1994. Morphological disparity in Ordovician–Devonian crinoids and the early saturation of morphological space. Paleobiology. 20(3):320–344 https://doi.org/10.1017/S009483730001280X

Gahn FJ, Baumiller TK. 2010. Evolutionary history of regeneration in crinoids (Echinodermata). Integr Comp Biol. 50(4):514–514 https://doi.org/10.1093/icb/icq155

Gorzelak P, Salamon MA, Baumiller TK. 2012. Predator–induced macroevolutionary trends in Mesozoic crinoids. Proc Natl Acad Sci USA. 109(18):7004–7007 https://doi.org/10.1073/pnas.1201573109

Håkansson E, Thomsen E. 1999. Benthic extinction and recovery patterns at the K/T boundary in shallow water carbonates, Denmark. Palaeogeogr Palaeoclimatol Palaeoecol. 154(1 2):67–85 https://doi.org/10.1016/S0031–0182(99)00087–5

Harper EM, Peck LS. 2016. Latitudinal and depth gradients in marine predation pressure. Glob Ecol Biogeogr. 25:670–678 https://doi.org/10.1111/geb.12444

Jagt JWM. 1999. Late Cretaceous and Paleogene echinoderms, pt. 2. Crinoids. Scripta Geol. 166:59–255

Janevski GA, Baumiller TK. 2010. Could a stalked crinoid swim? A biomechanical model and characteristics of swimming crinoids. Palaios. 25(9):588–596 https://doi.org/10.2110/palo.2009.p09–149r

Kjaer CR, Thomsen E. 1999. Heterochrony in bourgueticrinid sea–lilies at the Cretaceous/ Tertiary boundary. Paleobiology. 25(1):29–40

Klikushin VG. 1982. Cretaceous and Paleogene Bourgueticrinina (Echinodermata, Crinoidea) of the USSR. Geobios. 15(6):811–843 https://doi.org/10.1016/S0016–6995(82)80034–X

Kropp RK. 1992. Repaired shell damage among soft–bottom mollusks on the continental shelf and upper slope north of Point Conception, California. Veliger. 35:36–51

Lane NG. 1984. Predation and survival among inadunate crinoids. Paleobiology. 10:453–458 https://doi.org/10.1017/S0094837300008459

Lawrence JM. 2009. Arm loss and regeneration in stellate echinoderms: an organismal view. In: Johnson C, editor. Echinoderms in a changing world: Proceedings of the 13th International Echinoderm Conference. Hobart, Tasmania. p. 53–66

McClintock JB, Baker BJ, Baumiller TK, Messing CG. 1999. Lack of chemical defense in two species of stalked crinoids: support for the predation hypothesis for Mesozoic bathymetric restriction. J Exp Mar Biol Ecol. 232(1):1–7. https://doi.org/10.1016/S0022–0981(98)00003–3

Meyer DL. 1985. Evolutionary implications of predation on Recent comatulid crinoids from the Great Barrier Reef. Paleobiology. 11(2):154–164 https://doi.org/10.1017/S0094837300011477

Meyer DL. 1988. Crinoids as renewable resources: rapid regeneration of the visceral mass in a tropical reef–dwelling crinoid from Australia. In: Burke RD, Mladenov PV, Lambert P, Parsley RL, editors. Echinoderm biology: proceedings of the sixth International Echinoderm Conference. Rotterdam: Balkema. p. 519–522

Meyer DL, Macurda DB Jr. 1977. Adaptive radiation of the comatulid crinoids. Paleo- biology. 3(1):74–82. https://doi.org/10.1017/S0094837300005121

Meyer DL, Ausich WI. 1983. Biotic interactions among recent and among fossil crinoids. In: Tevesz MJS, McCall PL, editors. Biotic interactions in recent and fossil benthic communities. Topics in Geobiology. 3rd ed. Plenum, New York. p. 377–427

Meyer DL, LaHaye CA, Holland ND, Arneson AC, Strickler JR. 1984. Time–lapse cinematography of feather stars (Echinodermata: Crinoidea) on the Great Barrier Reef, Australia: demonstrations of posture changes, locomotion, spawning and possible predation by fish. Mar Biol. 78(2):179–184. https://doi.org/10.1007/BF00394698

Meyer DL, Oji T. 1993. Eocene crinoids from Seymour Island, Antarctic Peninsula: paleobiogeographic and paleoecologic implications. J Paleontol. 67:250–257 https://doi.org/10.1017/S0022336000032170

Mizui R, Kikuchi T. 2013. Arm damage and regeneration of Tropiometra afra macrodis- cus (Echinodermata: Crinoidea) in Sagami Bay, Central Japan. In: Johnson C, editor. Echinoderms in a changing world. London: Taylor and Francis Group. p. 119–124

Mladenov PV. 1983. Rate of arm regeneration and potential causes of arm loss in the feather star Florometra serratissima (Echinodermata: Crinoidea). Can J Zool. 61(12):2873–2879 https://doi.org/10.1139/z83–375

Moore RC. 1967. Unique stalked crinoids from the Upper Cretaceous of Mississippi. Paleontolocial Contributions, University of Kansas. 17:1–43

Nichols D. 1994. Reproductive seasonality in the comatulid crinoid Antedon bifida (Pennant) from the English Channel. Philos Trans R Soc B. 343(1304):113–134 https://doi.org/10.1098/rstb.1994.0015

Oji T. 1996. Is predation intensity reduced with increasing depth? Evidence from the West Atlantic stalked crinoid Endoxocrinus parrae (Gervais) and implications for the Mesozoic marine revolution. Paleobiology. 22(3):339–351 https://doi.org/10.1017/S0094837300016328

Oji T, Okamoto T. 1994. Arm autotomy and arm branching pattern as anti–predatory adaptations in stalked and stalkless crinoids. Paleobiology. 20(1):27–39 https://doi.org/10.1017/S0094837300011118

Paschall OC, Waters JA. 2017. Estimated predation rate of the stalked bourgueticrinid (Crinoidea) Democrinus from Roatán, Honduras. Geol J. 52(5):727–732 https://doi.org/10.1002/gj.28–31

R Core Team. 2017. R: A language and environment for statistical computing. Vienna, Austria: R Foundation for Statistical Computing. URL https://www.R–project.org/

Roux M. 1976. Aspect de la variabilit et de la croissance au sein dune population de la pentacrine actuelle: Annacrinus wyvillethomsoni Jeffreys (Crinoidea). Thalass Jugosl. 12:307–320

Roux M, Eleaume M, Amziane N. 2019. A revision of the genus Conocrinus d'Orbigny, 1850 (Echinodermata, Crinoidea, Rhizocrinidae) and its place among extant and fossil crinoids with a xenomorphic stalk. Zootaxa. 4560(1):51–84 https://doi.org/10.11646/zootaxa.4560.1.3

Schneider JA. 1988. Frequency of arm regeneration of feather star crinoids in relation to life habit. In: Burke RD, Mladenov PV, Lambert P, Parsley RL, editors. Echinoderm biology: proceedings of the sixth International Echinoderm Conference. Rotterdam: Balkema. p. 531–538

Schoener TW. 1979. Inferring the properties of predation and other injury–producing agents from injury frequencies. Ecology. 60(6):1110–1115 https://doi.org/10.2307/1936958

Seilacher A, Hauff RB. 2004. Constructional morphology of pelagic crinoids. Palaios. 19:3–16

Shibata TF, Oji T. 2003. Autotomy and arm number increase in Oxycomanthus japonicus (Echinodermata, Crinoidea). Invertebr Biol. 122(4):375–379 https://doi.org/10.1111/j.17447410.200

Signor PW, Brett CE. 1984. The mid–Paleozoic precursor to the Mesozoic marine revolution. Paleobiology. 10(2):229–245 https://doi.org/10.1017/S0094837300008174

Smith DF, Meyer DL, Horner SMJ. 1981. Amino acid uptake by the comatulid crinoid Cenometra bella (Echinodermata) following evisceration. Mar Biol. 61:207–213 https://doi.org/10.1007/BF00386661

Stanley SM. 1977. Trends, rates, and patterns of evolution in the Bivalvia. In: Hallam A, editor. Patterns of evolution as illustrated by the fossil record. Developments in palaeontology and stratigraphy. Vol 5. Amsterdam: Elsevier. p. 209–250

Stanley SM. 2008. Predation defeats competition on the seafloor. Paleobiology. 34(1):1–21 https://doi.org/10.1666/07026.1

Stevenson A, Gahn FJ, Baumiller TK, Sevastopulo GD. 2017. Predation on feather stars by regular echinoids as evidenced by laboratory and field observations and its paleobiological implications. Paleobiology. 43(2):274–285 https://doi.org/10.1017/pab.2016.39

Syverson VJ, Baumiller TK. 2014. Temporal trends of predation resistance in Paleozoic crinoid arm branching morphologies. Paleobiology. 40(3):417–427 https://doi.org/10.1666/13063

Syverson VJ, Messing CG, Stanley K, Baumiller TK. 2014. Growth, injury, and population dynamics in the extant cyrtocrinid Holopus mikihe (Crinoidea, Echinodermata) near Roatán, Honduras. Bull Marine Sci. 91(1):47–61 https://doi.org/10.5343/bms.2014.1061

Syverson VJ, Brett CE, Gahn FJ, Baumiller TK. 2018. Spinosity, regeneration, and targeting among Paleozoic crinoids and their predators. Paleobiology. 44(2):290–305 https://doi.org/10.1017/pab.2017.38

Ubaghs G. 1978. Skeletal morphology of fossil crinoids. In: Moore RC, Teichert C, editors. Treatise on invertebrate paleontology, Part T, Echinodermata 2 (1). New York and Lawrence: Geological Society of America and University of Kansas Press. p. T58–T216

Vail L. 1987. Diel patterns of emergence of crinoids (Echinodermata) from within a reef at Lizard Island, Great Barrier Reef, Australia. Mar Biol. 93:551–560 https://doi.org/10.1007/BF00392793

Veitch MA, Messing CG, Baumiller TK. 2016. Escape to the deep? Assessing predation intensity on bathyal stalked crinoids using injury frequencies and rates of arm regeneration. GSA Abstracts with Programs. 48(7):197 https://doi.org/10.1130/abs/2016AM–286379

Vermeij GJ. 1977. The Mesozoic marine revolution: evidence from snails, predators and grazers. Paleobiology. 3(3):245–258 https://doi.org/10.1017/S0094837300005352

Whittle RJ, Hunter AW, Cantrill DJ, McNamara KJ. 2018. Globally discordant Isocrinida (Crinoidea) migration confirms asynchronous Marine Mesozoic Revolution. Commun Biol. 1(46):1–10 https://doi.org/10.1130/abs/2018AM–316163

Zamora S, Aurell M, Veitch MA, Saulsbury J, Lpez–Horgue M, Fernando F, Arz JA, Baumiller T. 2018. Environmental distribution of post–Palaeozoic crinoids from the Iberian and south–Pyrenean basins (NE Spain). Acta Palaeontol Pol. 63(4):779–794 https://doi.org/10.4202/app.00520.2018

Chapter II TABLES

Table II.1: Regeneration rates across higher crinoid taxa.

Order	Species	Source	Regeneration rate (cm d^{-1})
Comatulida	Capillaster multiradiatus	Baumiller and Stevenson (2018)	0.055
	Cenometra bella	Baumiller and Gahn (2013)	0.035 –0.05
	Clarkcomanthus mirabilis	Baumiller and Stevenson (2018)	0.063
	Florometra serratissima	Mladenov (1983)	0.05
Cyrtocrinida	Holopus mikihe	Syverson et al. (2014)	0.002
Isocrinida	Metacrinus rotundus	Amemiya and Oji (1992)	0.017

Table II.2: Arm lengths of 39 *Democrinus* sp. measured during longitudinal study at the 240 m site off Isla Roatán, Honduras. Individuals 1—39: individuals mapped at the site. Zeros correspond to individuals missing all arms on the day of the visit. Blank cells are individuals that were present, but for which accurate measurements could not be obtained.

	Arm Lengths, *Lobs* per ind, v (cm)			
	Visit 1 (26 Nov, 2015)	Visit 2 (18 May, 2016)	Visit 3 (17 Dec, 2016)	Visit 4 (15 Dec, 2017)
Ind. 1	0.8	4.0	5.4	1.9
Ind. 2	2.7	4.8	2.7	2.5
Ind. 3	4.3	4.4	6.4	1.6
Ind. 4	0.5	4.0	2.7	5.6
Ind. 5	1.0	3.0	4.0	0.2
Ind. 6	1.9	5.2	3.8	4.3
Ind. 7	0.4	2.0	3.4	2.4
Ind. 8	4.3	0.0	4.1	1.6
Ind. 9	1.2	3.6	3.5	1.7
Ind. 10	1.7	3.4	1.0	2.7
Ind. 11	2.1	1.6	1.3	—
Ind. 12	3.2	2.5	5.3	3.0
Ind. 13	2.0	2.4	0.0	2.2
Ind. 14	—	0.0	3.4	2.8
Ind. 15	3.2	—	0.4	—
Ind. 16	0.8	—	2.3	—
Ind. 17	0.0	3.9	3.9	—
Ind. 18	3.0	3.2	1.1	—
Ind. 19	0.0	—	—	2.1
Ind. 20	2.2	—	—	3.1
Ind. 21	1.3	2.7	2.6	2.1
Ind. 22	4.1	2.0	4.5	2.0
Ind. 23	4.3	3.5	3.7	3.5
Ind. 24	—	2.1	4.4	0.6
Ind. 25	2.2	3.3	3.4	—
Ind. 26	1.8	0.0	2.2	2.3
Ind. 27	2.7	2.8	4.3	2.7
Ind. 28	1.4	3.7	0.0	0.8
Ind. 29	0.0	2.5	3.7	—
Ind. 30	2.8	0.0	4.6	—
Ind. 31	1.6	—	—	3.4
Ind. 32	—	0.7	0.0	2.4
Ind. 33	0.8	1.1	4.6	—
Ind. 34	3.0	3.2	5.4	1.0
Ind. 35	3.2	4.0	4.8	4.2
Ind. 36	1.7	4.1	4.9	2.2
Ind. 37	3.3	3.1	4.2	1.8
Ind. 38	—	0.0	1.5	3.3
Ind. 39	4.7	0.3	1.4	0.0
Mean arm length (cm)	2.1	2.6	3.1	2.3
Standard deviation of arm length (cm)	1.3	1.5	1.7	1.2
# individuals per visit	35	34	36	30

Table II.3: Injury incidence, *i*, in *Democrinus* sp. population at the 240 m site off Isla Roatán, Honduras. Two methods were employed to count injuries and thus calculate *i*: (1) the conservative method, the decrease in length approach, which considers injuries only if an individual shows a decrease in arm length between two successive visits (negative *rr*); (2) expected length approach, where individuals with lower than expected increases in arm length were presumed injured. Expected increases in arm length were calculated as the product of mean regeneration rate [0.008 cm d^{-1} (SE 0.0009)] and elapsed time between two successive visits. *i* = (# injuries d^{-1}), waiting time = 1/*i*, *rr* = regeneration rate.

	Expected Length			Decrease in length
	rr SE lower	*rr* avg	*rr* SE upper	Negative *rr*
Study duration (d)	23,913	23,913	23,913	23,913
# injuries	76	79	79	39
i (# injuries d^{-1})	0.0032	0.0033	0.0033	0.0016
Waiting time (d)	315	303	303	613

Chapter II FIGURES

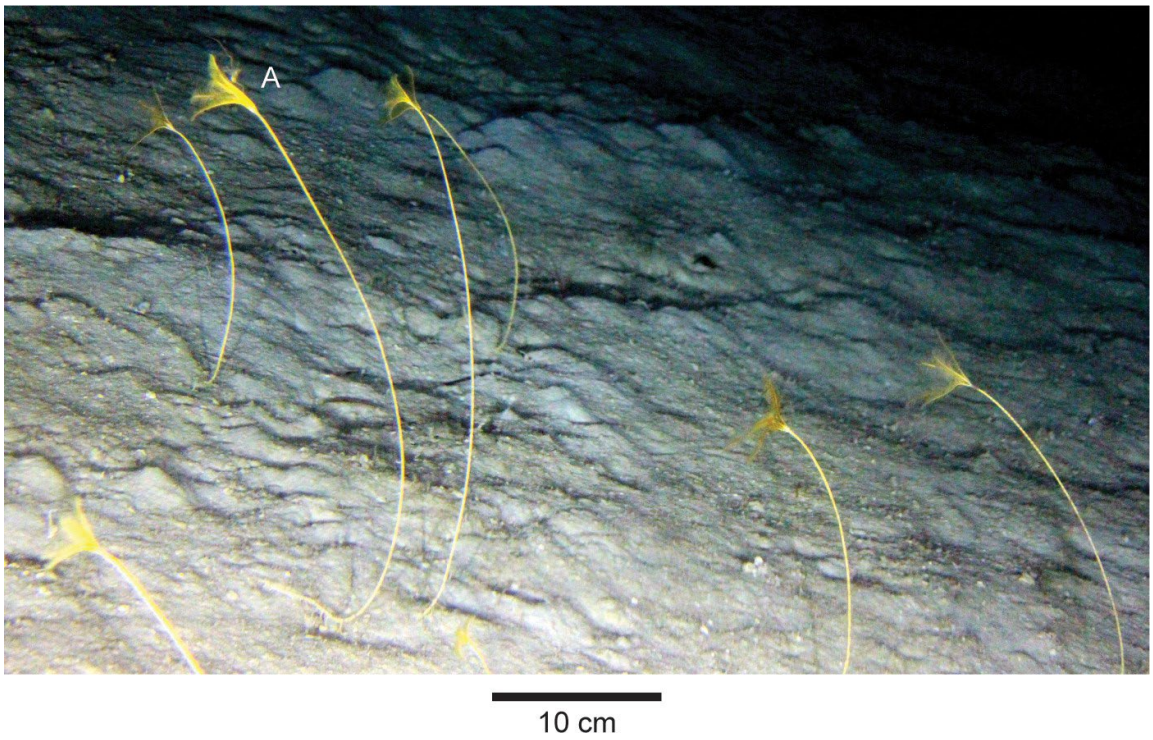

Figure II.1: Several individuals of *Democrinus* sp. at the 240 m site off Isla Roatán, Honduras. All individuals are rooted in soft, fine-grained sediment. Part of the stalk of Individual A lies along the sediment with an elongated distal, radix–bearing root portion of the stalk visible. Photo was taken during the May 2015 census from submersible, *Idabel*, using a mounted SLR camera.

		Deep	Shallow
Quaternary	Holocene	×	O
	Pleistocene	×	–
Neogene	Pliocene	×	–
	Miocene	×	–
Paleogene	Oligocene	–	–
	Eocene	×	×
	Paleocene	×	×
K	Upper	×	×

× Present
O Absent
– No record

Figure II.2: Presence/absence of rhizocrinids (bourgueticrinids) in shallow–and deep-water environments. Shallow–and deep-water definitions are based upon source descriptions of the fossil-bearing formations: Moore (1967), Klikushin (1982), Håkansson and Thomsen (1999), Jagt (1999), Kjaer and Thomsen (1999), Donovan and Veltkamp (2001), Ciampaglio et al. (2007), Zamora et al. (2018), and the Oceanic Biogeographic Information System (https://obis.org/).

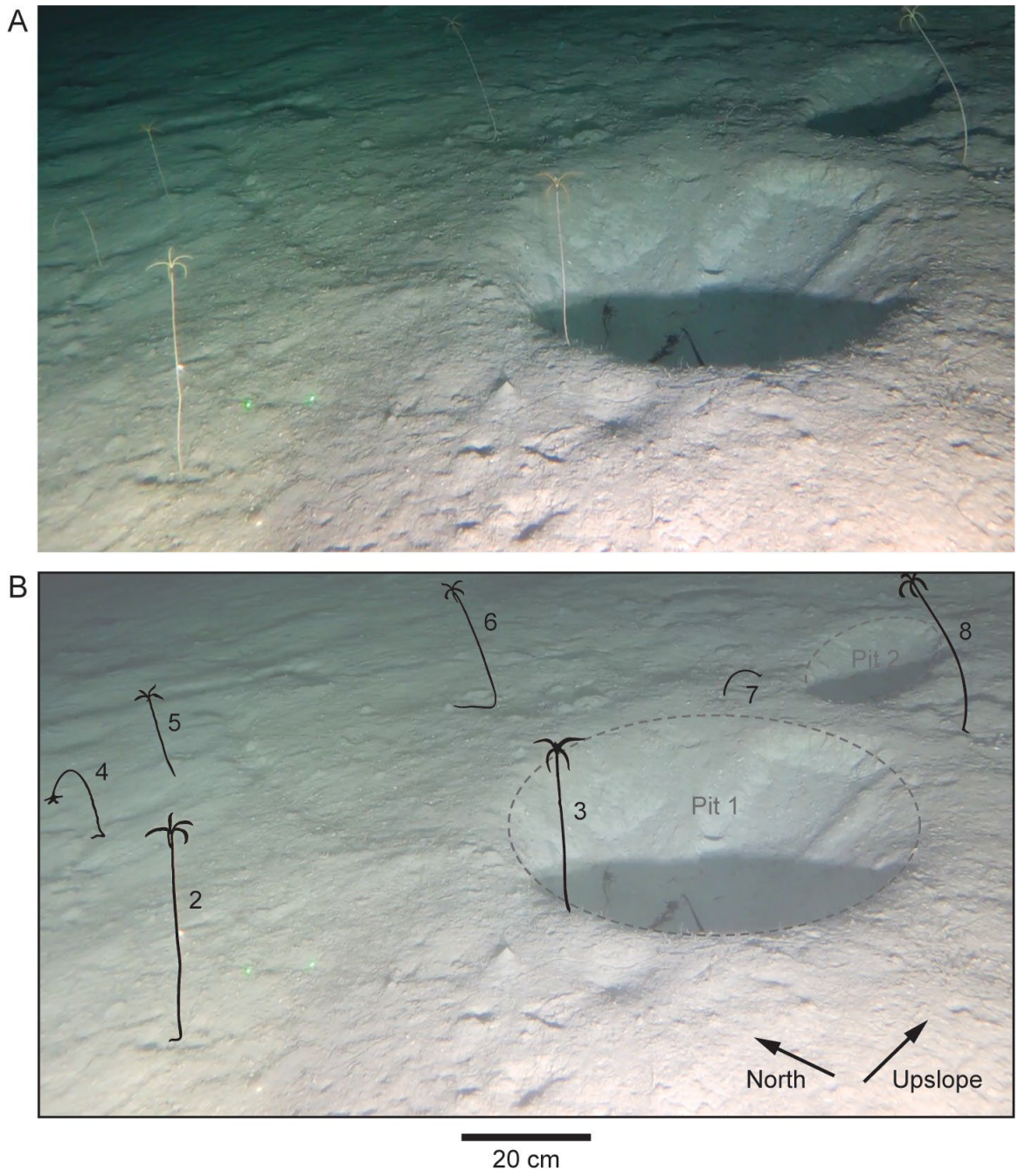

Figure II.3: *Democrinus* sp. individuals 2–8 in the northwest corner of the mapped site at 240 m, November 2015. **A:** West–facing photograph of individuals. **B:** Outlines of individuals and key sedimentary features (Pit 1 and Pit 2) in A for clarity. Individuals 4 and 6 show extended stalk laying on the sediment; individual 7 lacks its crown. Pit 1 and Pit 2 are natural landmarks used to relocate individuals seen in the image.

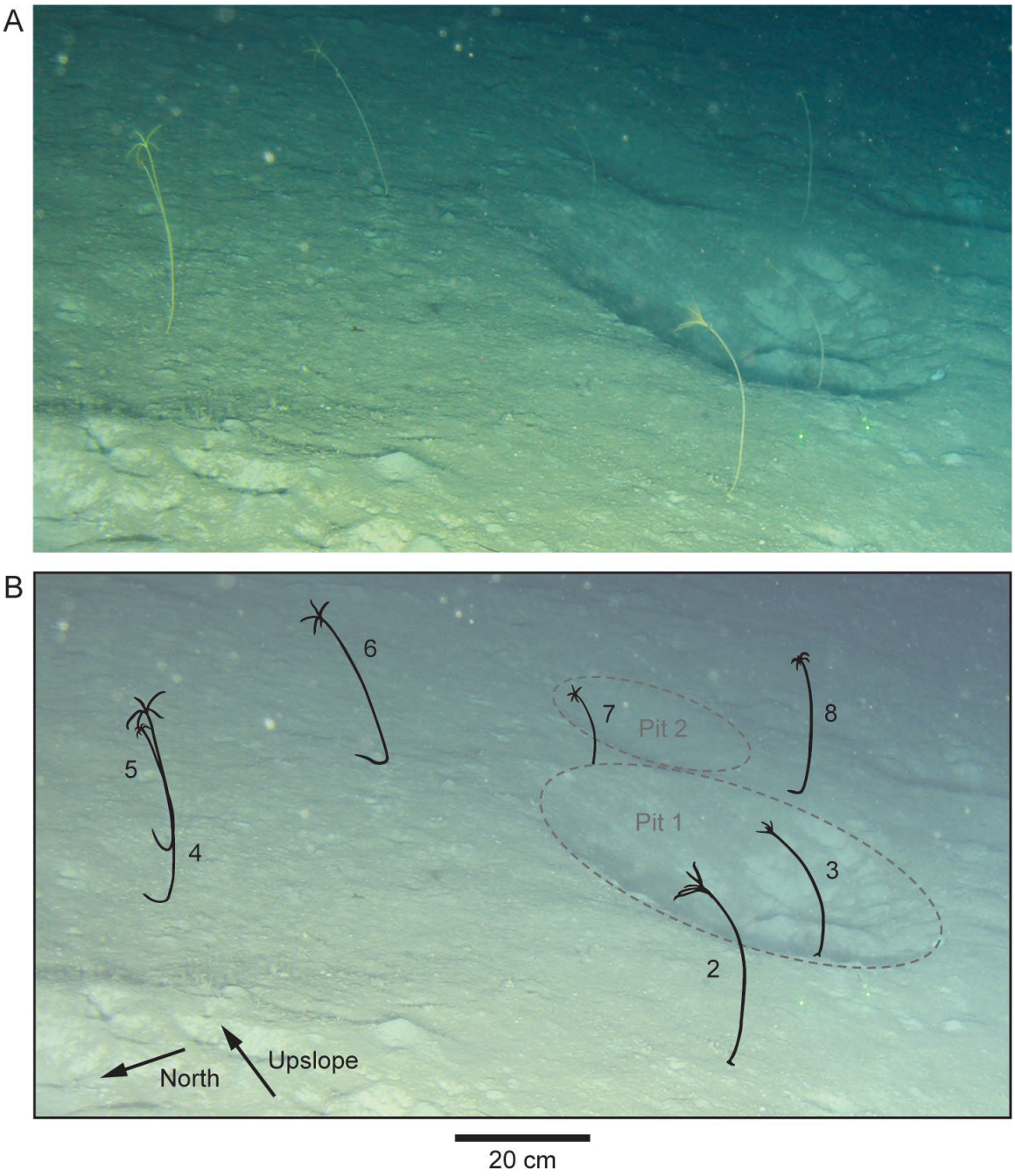

Figure II.4: *Democrinus* sp. individuals 2–8 in the northwest corner of the mapped site at 240 m, December 2017. **A:** East–facing photograph of individuals. **B:** Outlines of individuals and key sedimentary features (Pit 1 and Pit 2) for clarity. Individual 7 has regenerated its crown.

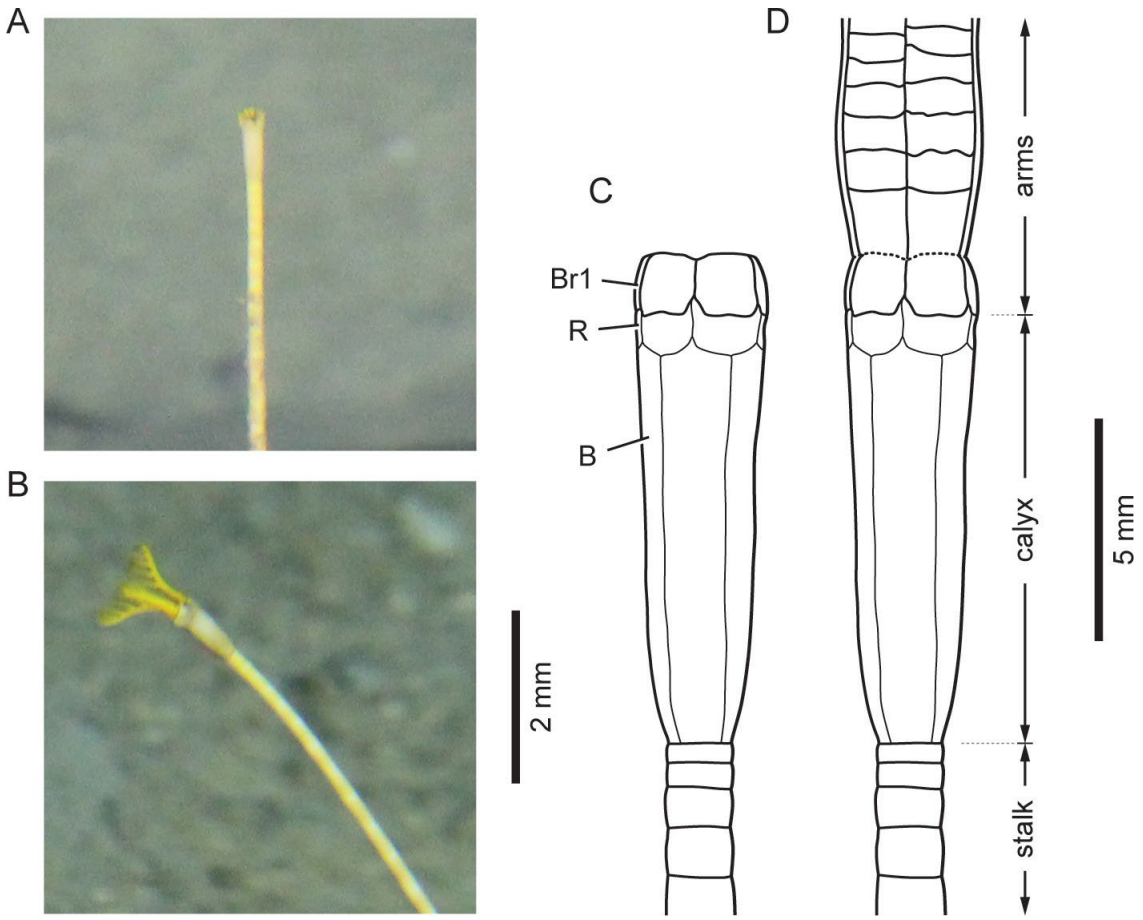

Figure II.5: Overview of *Democrinus* sp. morphology. **A and B:** Close-ups of *Democrinus* sp. specimens (outside census area): ***(A)*** specimen missing all five arms distal to the first brachial (Br1), and ***(B)*** different specimen with partially regenerated arms. All arms are the same length indicating a constant rate of regeneration (*rr*). Scale for A and B is 2 cm. **C and D:** Schematics of proximal stalk, cup, and proximal arms of *Democrinus* sp.: ***(C)*** without arms, emphasizing usual autotomy location at the ligamentary articulation between the first and second brachial, and ***(D)*** with arms. Basals = B, radial = R, first brachial = Br1, dotted line between Br1 and Br2 = ligamentary articulation. Scale for C and D is 0.5 cm.

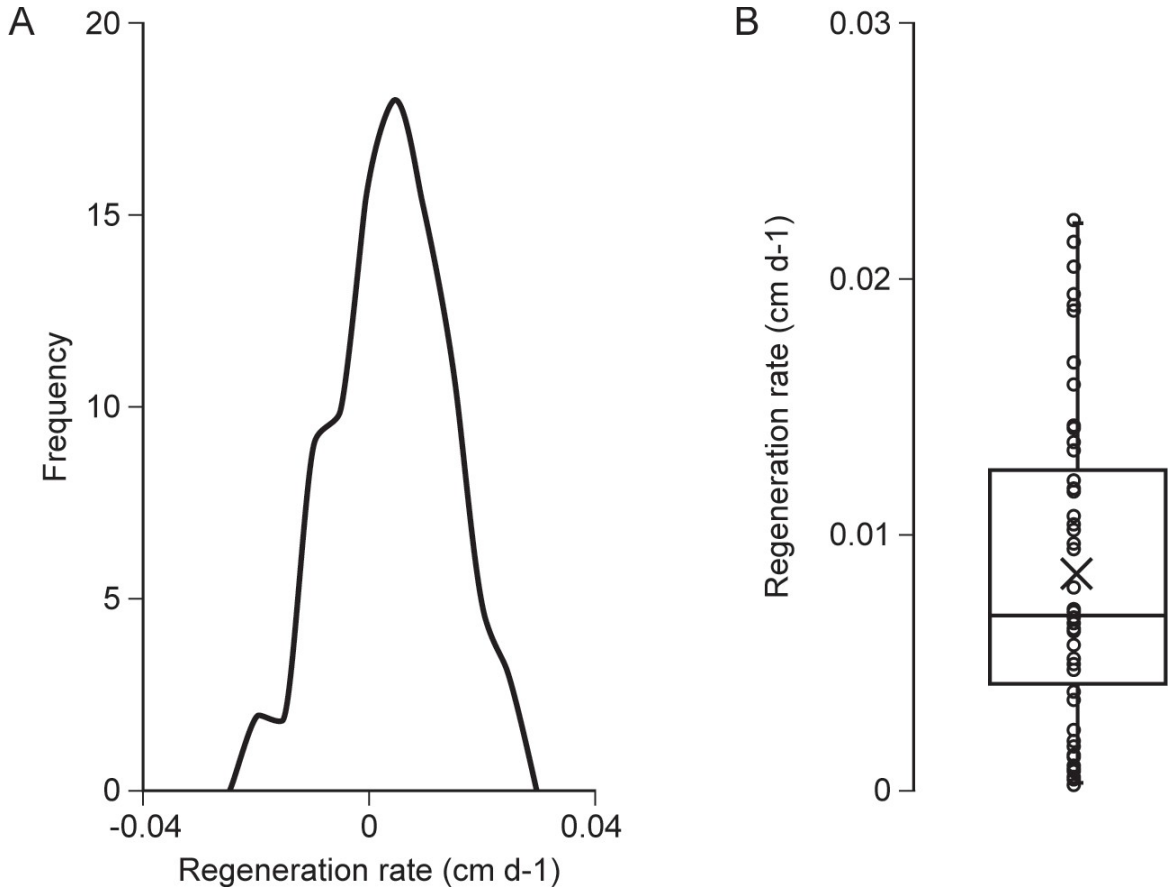

Figure II.6: A: Frequency distribution of calculated regeneration rates in *Democrinus* sp. from the 240 m site (n = 91). Regeneration rates = change in individual's arm length on successive census visits to site/time between visits. **B:** Box and whisker plot of positive regeneration rates only (open circles) with mean rate (0.008 ± 0.0009 cm d^{-1}, n = 52).

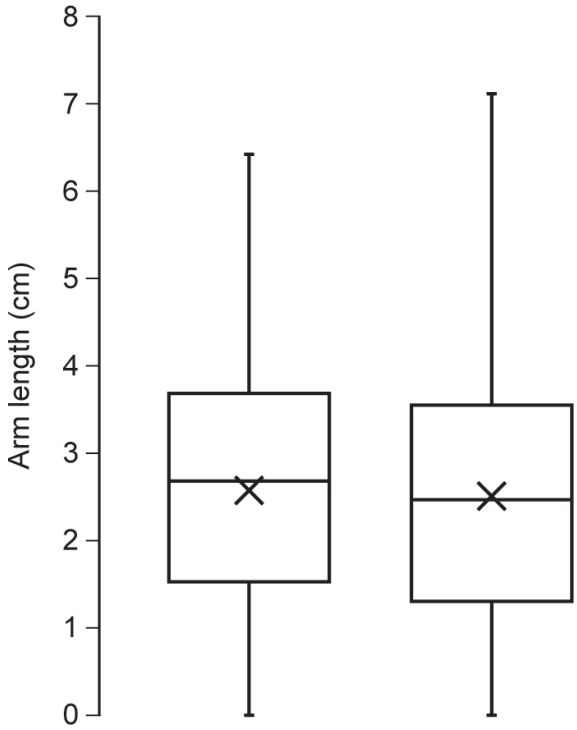

Figure II.7: Box and whisker plots of arm lengths in *Democrinus* sp. for data from the 240 m site. **Left:** multiple measurements of the same individuals on 4 different dates (mean: = 2.6 ± 1.5 cm, n = 135). **Right:** cross-sectional data gathered at various sites between June 2012 and December 2017 (Mean: = 2.5 ± 1.6 cm, n = 205). The two distributions are statistically indistinguishable (p = 0.88; KS–test).

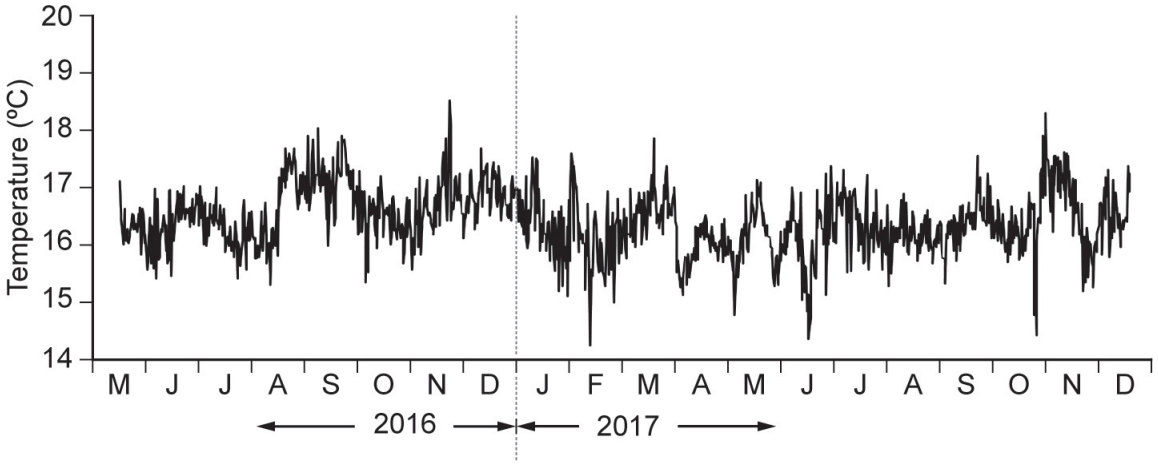

Figure II.8: Temperature at the 240 m site from May 2016 to December 2017. Data in the figure were subsampled every 12 hrs from the 30 min record to enhance clarity.

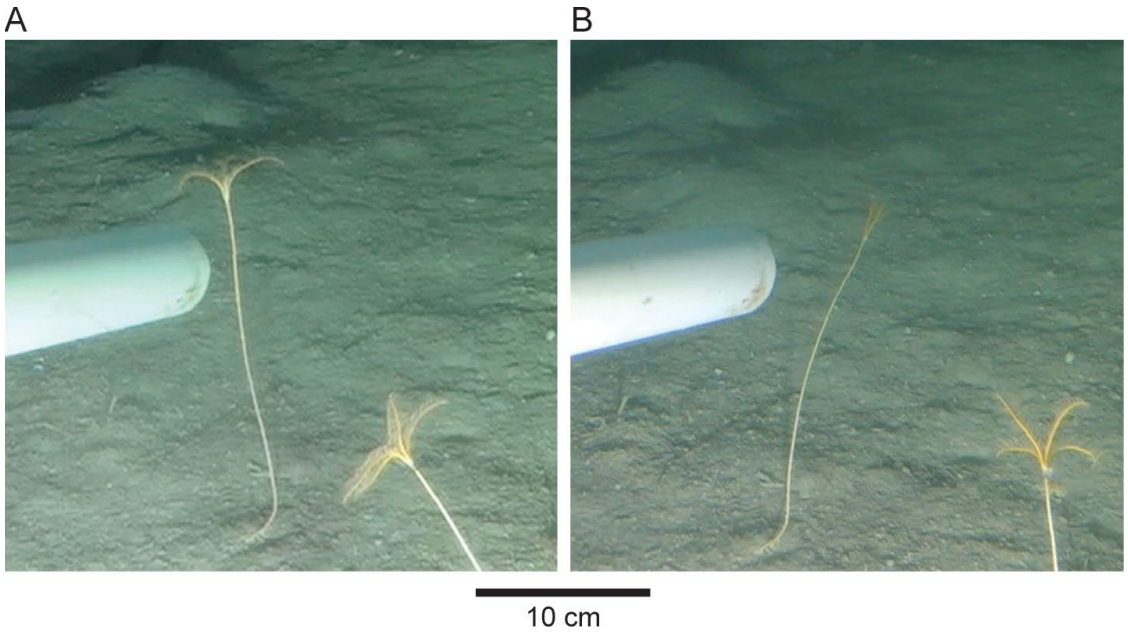

Figure II.9: *Democrinus* sp. under stimulated flow **A:** *Democrinus* sp. individual just prior to initiating a thruster–produced flow. The stalk is upright; the crown is in feeding position. **B:** Same individual 45 sec after thrusters were turned on. Note collapsed crown and bent stalk. The increased flow was maintained for approximately 1 min, and did not result in injury (arm shedding).

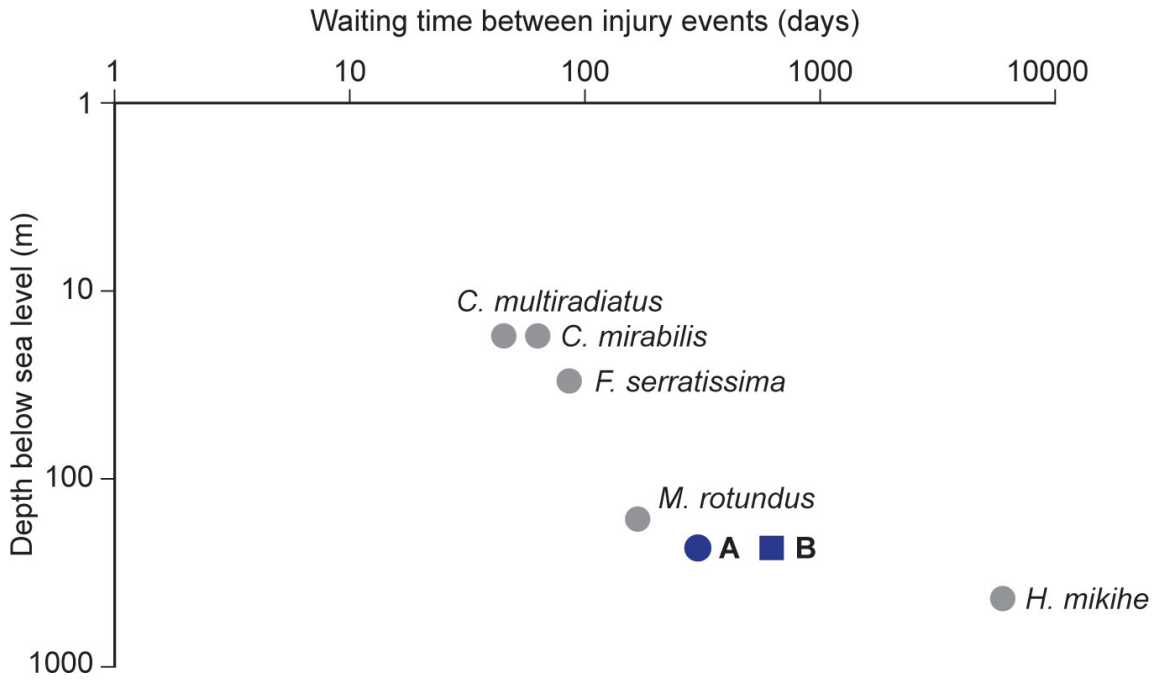

Figure II.10: Waiting time between injuries as a function of depth for six crinoid taxa. A and B represent *Democrinus* sp. waiting times obtained using the expected length (A, circle) and the decrease in length (B, square) approaches. For *Florometra serratissima, Metacrinus rotundus*, and *Holopus mikihe*, waiting time was calculated using Equation 2.5 and cross-sectional data on injury prevalence and regeneration rates. For *Capillaster multiradiatus*, *Clarkcomanthus mirabilis*, and *Democrinus* sp., waiting time was obtained from longitudinal data. Both axes are logarithmic scales.

CHAPTER III "Keep Your Crown Up": Evidence of Ligament Contractility from *In situ* Submersible Experiments and Observations of a Stalked Crinoid, *Democrinus* sp.

ABSTRACT

The stalked crinoids in family Bourgueticrinina have previously been thought to be sessile and unable to move actively in their environment in the absence of any external force. Experiments and observations conducted from a submersible at a depth of 240 m near Isla Roatán, Honduras, revealed that the stalked crinoid, *Democrinus* sp., while unable to crawl like isocrinids, can regain an upright posture following dislodgement. Quantitative evaluation of the plausible mechanisms, parametrized with morphological data, revealed that the righting behavior observed in *Democrinus* sp. must involve the active contraction of tissues in its stalk. Because *Democrinus* sp. lacks muscle in its stalk, it is the contraction of ligaments on opposite sides of the fulcrum on columnal articulations that bends the stalk, and allows an upright feeding posture to be re-established. The implications of ligament contractility for crinoids include a) active stalk bending necessary for righting and postural control; b) the active flexion of cirri crawling stalked crinoids (isocrinids) need to attach, reattach, and right the stalk, and c) active arm movement in crinoids that lack muscular arm articulations, which includes the majority of Paleozoic taxa, and thus provides them the ability to adjust their feeding posture and cope better with predation.

INTRODUCTION

Crinoid mobility remains one of the most notable behavioral changes in crinoid evolution. Attributed to the evolution of muscular arms that distinguish all post-Paleozoic crinoids, these arms engage in a broad repertoire of motions that allowed some crinoids to depart from the completely sessile lifestyle of Paleozoic crinoids (Macurda and Meyer 1983, Mladenov 1983, Meyer et al. 1984, Shaw and Fontaine 1990, Meyer and Macurda 1977, Baumiller and Messing 2007, Janevski and Baumiller 2010). The long-standing assumption of permanent sessility in all stalked crinoids and their relative inaccessibility because of their restriction to depths greater than 100 m in modern oceans has limited our understanding of the role mobility may play in their behavior and ecology. Most previous studies on crinoid mobility focused on crinoids that lack stalks, such as the feather stars, and left questions about stalked crinoid mobility, particularly in groups outside of Isocrinida, an area in need of further study.

The historical focus on feather stars is understandable. Feather stars best represent the extent of crinoid mobility, as all are able to crawl and many to swim. Diverging morphologically from the classical stalked bauplan, adult feather stars discard their stalks as juveniles in favor of a cirri-bearing skeletal element referred to as the centrodorsal. These flexible cirri enable feather stars to grasp or release substrates actively, allowing them to exploit a free-living existence (Hess 2014). In modern oceans, feather stars dominate extant crinoid diversity, where they outnumber all other crinoid species by an order of magnitude (Messing 1997, Hess 2014); this is in stark contrast to the overwhelming prevalence of stalked taxa in the fossil record. They stand out further as the only crinoids that still live at depths shallower than 100 m, with all stalked articulates restricted to depths greater than 100 m (Bottjer and Jablonski 1988, Messing 1997, Oji 1996).

As such, a rich body of data exists for living shallow-water feather stars and their mobility, but data are sparse for the more inaccessible stalked crinoids. Dredging practices during the 19th and 20th-century allowed some insights into stalked crinoid physiology, but little information about their ecology beyond the substrate they lived on. In the last half-century, the advent of submersibles and remotely operated vehicles allowed for *in situ* studies that have shed new light on the similarities and differences between stalked and stalkless crinoids. Recent observations of stalked isocrinids found active locomotion, contradicting the long-standing assumption that all stalked crinoids are permanently sessile. Isocrinids can crawl: they use their arms to pull themselves along the substrate, drag their stalk behind, and subsequently re-anchor and re-establish an upright feeding posture (Messing et al. 1988, Baumiller 1997, Baumiller and Messing 2007). The isocrinid motility observed suggests that the breadth of behaviors of stalked crinoids may be much greater than assumed previously. Further, the crawling ability of isocrinids forces a reassessment of motility in stalked crinoids, the timing of its appearance, and its original biological role (Baumiller and Hagdorn 1995, Baumiller et al. 2010, de Carvalho et al. 2016).

Whether the isocrinid behavior and function observed may apply to other stalked articulates is unclear, as distinct morphological features found in isocrinids are critical to their observed mobility. As with feather stars, isocrinids lack any specialized terminal rooting structure (except for the Proisocrinidae). Instead, the active flexing and grasping of cirri spaced at whorls in regular intervals along the stalk, serve to anchor the animal to the substrate, much as in feather stars (Figure III.1 A) (Baumiller et al. 1991, Birenheide and Motokawa 1994). Conversely, the stalked crinoids in the suborder Bourgueticrinina (order Comatulida) lack any cirri and their stalk terminates in an anchoring structure (Figure III.1 B). An equally substantial difference between the isocrinids and bourgueticrinids is the columnal articulations in the stalk.

In isocrinids, each columnal articulation facet is either symplexial (Figure III.1 C, D), with interlocking ridges on adjacent columnals that allow for some stalk flexibility at each columnal facet, or synostosial, which is flat, featureless, and stiff, but critical for stalk autotomy (Donovan 1990, Wilkie et al. 1994, Baumiller 1997, Wilkie 2001). Bourgueticrinid stalks contain neither symplexial nor synostosial articulation. Instead, bourgueticrinid stalk columnal articulations are synarthrial: Each facet possesses a fulcral ridge along the longest diameter, with deep ligamentary pits on either side (Figure III.1 E, F). The orientation of the ridge changes between proximal and distal facets and produces the notable twisted outline of the stalk.

The differing stalk morphologies of bourgueticrinids and isocrinids suggest substantially different functions. The attachment by cirri in isocrinids is suited well for motility; the animal frees itself by either shedding the anchoring portion of its stalk or releasing the cirri that grip the substrate (Baumiller et al. 1991). Bourgueticrinids' terminal attachment structures point to the converse: a permanently sessile life. Neither the disk nor the root-like structure permits active detachment, and the absence of synostosial articulations prevents shedding these anchoring structures. The synarthrial articulations in Bourgueticrinids synarthrial articulations contrast further with the absence of a fulcral ridge on columnal articulations, suggesting that the mechanism behind the stalk bending in these groups may differ.

Insights into the function of bourgueticrinid stalks can serve to clarify the role of these morphological differences and expand our understanding of the role of synarthrial articulations in crinoid stalks. Thousands of bourgueticrinids, *Democrinus* sp. (family Rhizocrinidae, Roux et al. 2019), live on the sediment-covered slopes off Roatán, Honduras. Submersible dives conducted in the area previously have noted several specimens lying prone on the substrate naturally (Figure III.2). Such a prone position may potentially indicate active motility. As

mentioned previously, isocrinids pull themselves along the ocean floor using their arms. While *Democrinus* sp. has the necessary muscular arms, the morphology of its stalk does not allow it to either shed its stalk or detach actively from the sediment. Consequently, a dislodgment event would be necessary to free the root structure and permit movement. If this were to occur, a second problem with *Democrinus* sp. crawling is the mechanism by which it would regain an upright posture. In isocrinids, the cirri distributed along their stalk may help lift their stalk and crown off the substrate (Baumiller et al. 1991). However, as *Democrinus* sp., like other bourgueticrinids, lacks cirri, it would require another, as yet unknown mechanism to regain an upright posture.

It is the paradoxical presence of prone individuals of *Democrinus* sp. and the absence of any obvious means by which these individuals could right themselves that led us to conduct *in situ* experimental manipulations on this taxon in Roatán, Honduras. The experiments and manipulations involved 1) dislodging specimens of *Democrinus* sp., 2) observing these specimens over time for changes in posture, and 3) interpreting their postural, kinematic changes, in terms of forces (dynamics).

METHODS

Long–term in situ study

Isla Roatán, the largest of Honduras' Bay Islands, is located in the western Caribbean Sea near the southern edge of the Mesoamerican Reef. The islands lie just south of the west end of the Cayman Trough, part of the tectonic boundary between the Caribbean and North American plates (Rosencrantz and Mann 1991). Isla Roatán's northern margin is characterized by a variety of geologic features, including numerous slump blocks and a range of substrates, rock faces free

of sediment, and extensive areas of unconsolidated sediment. Thousands of small *Democrinus* sp. live rooted in sediment slopes at 200-275 m off the island's west edge at 200-275 m, with population densities that approach 9 individuals per m^2. *Democrinus* sp. is characterized by (1) a branched holdfast that anchors it in soft sediments; (2) a crown that consists of five undivided rays, and (3) a relatively small stature, with stalks rarely over 30 cm in length (Figure III.1 B).

We conducted eight expeditions to the sediment slopes between May 2012 and December 2017 with the submersible *Idabel*, owned and piloted by Karl Stanley and based at the Roatán Institute for Deepsea Exploration, West End, Roatán, Honduras (see Acknowledgments), the *Idabel* has been used to study deep-sea crinoids previously (e.g., Syverson et al. 2014, Veitch and Baumiller 2021). The submersible was equipped with two sets of lasers: A scaling pair, 10 cm apart, mounted externally on the forward rail, and a laser box mounted internally on the flat bottom port with three fixed lasers 2 cm apart. In addition, either a 4.3 m pole ending in a metal hook was mounted on *Idabel*'s port-side rail, or a 5 cm PVC pipe was attached at one end to the submersible's thrusters. The latter either produced suction (negative pressure) or flow (positive pressure) by reversing the thrusters. Digital video and SLR cameras synchronized with external strobes captured images via the 76 cm diameter viewport. Weighted plastic bags with attached neon-yellow floats demarcated the two study sites at 240 m and 260 m depth.

During three expeditions, May 2015, November 2015, and May 2016, we dislodged four specimens of *Democrinus* sp. from an upright position and left them prone on the substrate. Other individuals were hooked and dragged free of the substrate using the pole mounted on *Idabel* or pulled out of the substrate via suction from the attached PVC pipe and dropped (Table III.1). Individuals were photographed and video-recorded before and after dislodgment (Figures III.3, III.4, III.5). We revisited and photographed the individuals manipulated in May 2015 and

November 2015 within 48 hours of dislodgement. Unfortunately, the weather conditions deteriorated after the May 2016 individuals were dislodged, which prevented a return visit during that month's expedition. However, the individuals dislodged in November 2015 and May 2016 were revisited and photographed on subsequent expeditions in December 2016 and December 2017. The photos imported into Adobe Photoshop C6 with vectors calibrated to the laser scales, allowed the position and dimensions of the specimens dislodged at each visit to be calculated.

Biomechanical Models

As stalked crinoids are believed to be unable to engage in stalk movement without an external force because they lack muscular tissues in the stalk (Grimmer et al. 1984b, Donovan 1988, Baumiller et al. 1991, Baumiller 1992, Baumiller and LaBarbera 1993, Donovan 1989b, Donovan 1997, Baumiller 1997, Kitazawa and Oji 2014, Donovan 2016) we employed several biomechanical models to assess the stalk movement observed in the field. The models were parameterized using morphological data obtained in the lab from *Democrinus* specimens (stalks n = 8, crowns n = 2) collected with the suction device. These morphological data included: (1) linear dimensions measured using digital calipers; (2) weight in air (WIA, dyn) via a Mettler balance (Mettler P160; 0.01 g precision); (3) weight in water (WIW, dyn), obtained by suspending each specimen from a hanging postal scale (precision 0.01 g) in a large beaker filled with fresh water. To account for the higher density of saltwater increasing buoyancy, WIW was divided by 1.024 (WIW_{sw}; Tables III.2, III.3). For each of the stalks and arm sets collected, the WIW_{sw} was normalized to the length of the stalk (L_{Stalk}) or arms (L_{Arm}). The normalized WIW_{sw} were averaged to estimate the WIW per 1 cm of stalk (WIW_{Stalk}) and the WIW per 1 cm of arms (WIW_{Arm}) estimate for *Democrinus* sp. (Table 3.2).

We did not collect the dislodged *Democrinus* sp. and measured their stalk lengths (L_{Stalk}) and arm lengths (L_{Arm}) from photos and videos instead. The values measured combined with the length-normalized, averaged WIW_{Stalk} and WIW_{Arm} from the specimens collected allowed each of the dislodged specimens' weight in water (WIW_{Esw}) to be estimated (Table III.4) using the following equation:

$$WIW_{Esw} = WIW_{Stalk}L_{Stalk} + 5\ x\ WIW_{Arm}L_{Arm} \qquad \text{(III.1)}$$

To calculate the volume (V) for each specimen collected, we used a modified Archimedes' principle: The difference between WIA and WIW, ΔW, corresponds to the weight of water displaced by the sample (see Baumiller 1992). The mass of water, M_w, displaced by the sample is its weight divided by the acceleration attributable to gravity (980 cm/s^2) and as mass is the product of volume and density, the volume of the displaced water, and hence, the sample's volume, is:

$$V = \frac{M_w}{\rho_w} \qquad . \qquad \text{(III.2)}$$

The ratio of each sample's dry mass to its volume, V, was used to estimate the density of the sample, ρ (Table III.2).

We tested two biomechanical models to assess the potential for *Democrinus* sp. to regain an upright posture: hydrodynamic lift, the "kite" model, and hydrodynamic drag, the "swimming" model.

Hydrodynamic Lift, the Kite Model

For the crinoid to move under the kite model, a lift force must be generated by an external current that interacts with the crown (e.g., Breimer and Webster 1975, Rasmussen 1978, Breimer 1978). The most extreme version of this hypothesis proposes that a crinoid could generate sufficient upward lift to act as a kite, beginning prone on the substrate to raise the crown

and proximal stalk off the substrate, with the attachment structure acting as a tether. The magnitude of the downward (gravitational) and the upward (lift) forces required for the kite model depends upon the shape, size, and density of the crinoid, and the velocity of the current that affects it (see Baumiller 1992 and Appendix A, Part I for more details on the model's development).

The kite model follows the assumption that the lift force (F_L) generated must be greater or equal to the downward gravitational force (WIW_{sw}) acting on the crinoid (Figure III.6). This threshold must be met for the crinoid to succeed in elevating itself off the substrate. Thus, the given crinoid's WIW_{sw} is the gravitational force that F_L must overcome and is governed by a standard lift equation:

$$F_L = \frac{1}{2} C_L 5 SA_{Arm} \rho_{fluid} {U_C}^2 \qquad \text{(III.3)}$$

in which F_L = hydrodynamic lift, ρ_{fluid} = density of the fluid, SA_{Arm} is the total solid portion of a single arm, C_L = coefficient of lift, and U_C = current velocity (Vogel 1994). C_L, SA_{Arm}, and ρ_{fluid} were derived empirically for each dislodged specimen (see Appendix A, Part I). SA_{Arm}, ρ_{fluid}, and C_L act as constants for the given crinoid. Thus, the current velocity (U_C) is the determining factor in generating a force great enough to lift the crinoid. Equation (3.3) was applied to a range of current velocities from U_C = 0 cm/s through U_C = 60 cm/s and compared to the WIW_{Esw} calculated for each of the four dislodged individuals (CI 95%).

Hydrodynamic Drag, the Swimming Model

The swimming model examines the ability of a crinoid to generate thrust via rapid arm movement to adjust its position in the water, much like the way feather stars swim. Documentation of several different swimming strokes exists (Clark 1915, Macurda and Meyer 1983, Shaw and Fontaine 1990), but the most detailed swimming analysis published is for

Florometra serratissima (Shaw and Fontaine 1990). *F. serratissima* swims using a drag–based mechanism. During the power stroke, the orally extended arm with outstretched pinnules generates drag by pivoting aborally through a certain angle (dependent upon stroke length) with a certain angular velocity (dependent upon stroke speed). During the recovery stroke, the now enfolded arm pivots orally and returns to its original position. Adjacent arms alternate in their power–recovery strokes, and only half of the arms produce thrust at any given moment. The muscular arm articulations in *Democrinus* sp. allow it to bend its arms effectively, and while in a normal upright posture, it exhibits rapid arm–bending behavior occasionally (maximum observed approximately 1.1 seconds subtending an angle of ~80°). Thus, it is worth considering whether such rapid arm strokes could produce a sufficient upward thrust to serve as the mechanism to lift the crown and proximal stalk off the substrate following dislodgement.

We applied a modified version of a simplified swimming model (Janevski and Baumiller 2010; see Appendix A, Part II for more details) to the dislodged *Democrinus* sp. to test this hypothesis. The original model calculates vertical thrust via drag using empirically–derived parameters based upon the behavior and morphology of *F. serratissima* (Shaw and Fontaine 1990) and a standard equation for hydrodynamic drag (Vogel 1994). To achieve lift, the vertical drag, D_V, the arms produce must be equal to or greater than the given WIW. The magnitude of D_V changes as the arm pivots across an angle, θ, during the drag-producing power stroke (Figure III.7). To determine the mean instantaneous upward thrust, $\bar{D}_V$, one needs to solve for D_V and divide by the period of the arm, t_p (sec):

$$\overline{D_V} = \frac{D_T}{t_p}\left(\frac{1}{\omega}\right)(\cos(\alpha) - \cos(\alpha + \theta)) \qquad \text{(III.4)}$$

in which ω is the arm's angular velocity (radians/sec) with a maximum value 1.1 s, α = 30° and θ = 80° representing the maximum observed distance for *Democrinus* sp. arm movements, and D_T

is the drag force an arm stroke produces overall (see Appendix A, Part II, Janevski and Baumiller 2010, for details of deriving and calculating D_T and D_V). Two variables drive the $\bar{D}_V$ generated in a stroke: arm length and time to complete a power stroke, t_p. Therefore, for each individual, we calculated $\bar{D}_V$ twice: first for a range of arm lengths, holding angular velocity constant at the maximum time observed for a power stroke (t_p = 1.1 s), and second, for a range of power stroke speeds, with arm length held constant at D1 = 3.11 cm.

In addition, we also considered: muscle–bearing arms pushing the crown off the substrate, the "push–up" model, and (2) neutral or positive buoyancy caused by low density, or the "balloon" model.

RESULTS

Table III.1 summarizes the timeline and each dislodged individual's status (posture and arm number) across four visits to the field site. Table III.2 shows the collected specimens' stalk data, and Table III.3, the arm data. The calculated WIW_{sw} per 1 cm estimates for *Democrinus* sp.'s stalk and arms were 27.47 ± 3.62 dyn and 13.35 ± 0.12 dyn, respectively (Tables III.2 and III.3). Table III.4 presents the WIW calculations and measurements for dislodged *Democrinus* sp. collected at the 240 m depth site.

Figures III.8 and III.9 summarize the results from the quantitative evaluation of *Democrinus* sp. using the kite model. Appendix A, Part I details the quantitative evaluation of *Democrinus* sp. overall and additional results using the hydrodynamic lift or kite model. Figure III.10 and Appendix A, Part II summarize the quantitative evaluation of *Democrinus* sp. using the hydrodynamic drag or swimming model.

All four *Democrinus* sp. individuals survived the experimental trauma of our dislodgment. However, none of the experimentally dislodged *Democrinus* sp. exhibited any

evidence of locomotion; all remained in the same place that they were left (Figures III.3, III.4, and III.5). However, despite lacking any cirri, the four *Democrinus* sp. did not remain prone on the substrate.

Subsequent visits to the study sites showed that all four dislodged individuals of *Democrinus* sp. reestablished an upright posture, with the stalk held sub–vertically and the crown several arm lengths above the substrate. The posture change timing varied among individuals (Table III.1), with the shortest estimate at four days, as D1 was only half upright on day 2, and the longest greater than 4 and fewer than 175 days (D3). While D3 and D4 were dislodged together on May 19, the weather conditions deteriorated and prohibited another visit during the May 2016 expedition. However, both individuals were upright by the next visit on December 15, 2016.

We monitored D2, D3, and D4 for >12 months and, as far as we could tell, all were thriving more than a year after dislodgement. D2 lost its arms sometime after it was dislodged on November 22, 2015, and the next expedition, May 17, 2016, but its stalk was upright—a sign of recovery (Table III.1). While we cannot be certain whether D2 reestablished an upright posture before or after arm loss, given the known regeneration rates of *Democrinus* sp. (Veitch and Baumiller 2021), the loss of arms must have occurred a short time before the visit, no more than approximately 30 days, which would indicate that arm loss occurred approximately 145 days after dislodgement, probably from a predation attempt, and most likely after it was already upright, as the regeneration rate for *Democrinus* sp. is approximately 0.008 cm d^{-1} and arm injuries are effectively undetectable after arm lengths reach over 3 cm (Veitch and Baumiller 2021). Even individual D4, which was missing its arms when dislodged, survived the event and

was upright with five regenerated arms when seen next on December 14, 2016, 213 days later (Table III.1).

The fact that *Democrinus* sp. can achieve this unexpected posture change demonstrates that bourgueticrinids may be capable of greater motility than suspected previously. Nonetheless, the *in situ* observations of posture change did not reveal directly the mechanism by which *Democrinus* sp. reestablishes an upright posture. Below, we explore four plausible mechanisms that may explain this unexpected behavior.

The Push-up Model

When in a normal upright posture, the muscular arm articulations in *Democrinus* sp. have been observed to allow occasional rapid arm–bending behavior (maximum approximately 1.1 seconds to cross an angle of ~80°). The arm flexibility and range of movements of *Democrinus* sp. suggest that it may be capable of a "push-up" of sorts: the crinoid may lift the crown by placing the tips of several arms on the substrate and extending the arms such that their long axes are straight and perpendicular to the substrate. This push-up would elevate the cup above the bottom. However, its elevation would be limited to the length of the longest arm and all individuals dislodged experimentally reestablished an upright posture with their crowns elevated much higher than the maximum length of their arms (Figures III.3, III.4, and III.5).

Buoyancy, the Balloon Model

Several authors have proposed that some crinoids may be neutrally or positively buoyant (Breimer 1978, Grimmer et al. 1984b, Haude 1992). A detailed transmission electron microscopy (TEM) study of one bourgueticrinid, *Democrinus conifer*, identified lipid-rich organelles in its stalk and cup (Grimmer et al. 1984b). The authors postulated that these might lower the density

sufficiently to allow the crown and a portion of the stalk to float above the seafloor while the distal-most stalk and attachment structure anchored *Democrinus conifer* to the bottom, functioning much like a balloon. However, the balloon mechanism hypothesized has remained untested.

Our study provided two lines of evidence against the balloon hypothesis. Although we could not confirm whether lipids are present in *Democrinus* sp., and if so, how much they may reduce density, it was evident from *in situ* observations and laboratory measurements that these crinoids are negatively buoyant. *In situ*, negative buoyancy was illustrated clearly by the fact that when dislodged, all four individuals fell to the bottom and lay prone, the stalk and crown in contact with the substrate. Had they been positively buoyant, one would expect that even with a dense, sediment-covered attachment structure, the crown and proximal stalk would rise off the bottom immediately after dislodgement. Negative buoyancy was also confirmed by laboratory measurements: the crown and stalk of *Democrinus* sp. are substantially denser than seawater (Table III.3).

The negative buoyancy of *Democrinus* sp. was consistent with data on densities of other crinoids, including feather stars and isocrinids (Messing et al. 1988, Baumiller 1992, Baumiller 1993, Baumiller 1997, Baumiller and Janevski 2010). In fact, no single example of a neutrally or positively buoyant extant crinoid has been reported in the literature. Thus, positive or neutral buoyancy appears unlikely in any extant crinoid. Further, even hypothesized cases of positive buoyancy in some extinct taxa (Haude 1992) have been challenged recently (Gorzelak et al. 2020). Therefore, the balloon model must be rejected at this time.

Hydrodynamic Lift, the Kite Model

As with other crinoids evaluated under the kite model (Baumiller 1992), *Democrinus* sp. is unlikely to employ this mechanism to elevate its crown off the substrate. To be able to do so would require (1) maintaining an optimal arm posture to generate lift and (2) a minimum current of 35 cm/s (Figures III.8 and III.9, Appendix A, Part II). Observations of *Democrinus* sp. revealed that it undergoes a dramatic posture change at velocities between 7 and 15 cm/s. While below 7 cm/s, *Democrinus* sp. holds its crown as a parabolic fan, with arms splayed out, long axes perpendicular to the current, and tips recurved into the current, at higher velocities, the long axes of the arms align parallel to the flow and the tips face down–current (Figure III.11, top). The latter posture ("cone") exposes a much lower surface area to the current than the parabolic fan posture, and reduces drag and lift thereby. Even if the crinoid generates some lift in this posture, its magnitude would be much lower than the *Democrinus* sp. modeled with arms extended (Figures III.1 A, III.5 A, III.10 B). It is unknown whether this postural change in *Democrinus* sp. represents an active response or whether the arms collapse passively once drag exceeds the strength needed to maintain aboral flexure. Regardless, the response decreases drag, as postulated for other taxa with this behavior, including other bourgueticrinids (Tunnicliff et al. 2016) at similar current velocities and isocrinids (Baumiller et al. 2008) and feather stars (Meyer 1973, Meyer et al. 2021) at higher velocities.

Assuming the four dislodged *Democrinus* sp. were able to maintain a parabolic fan posture above the threshold velocities, the kite model could not provide the mechanism for them to become upright because there is no evidence of currents of the appropriate magnitude. We drew this conclusion based upon sedimentological and biological criteria. The sediment cover at the dislodgement site is silt-sized and it would take current velocities ~ 20 cm/s to mobilize such particles (McCave et al. 1995, McCave 2008, McCave et al. 2017, Grifoll et al. 2019). Current

velocities that approach the threshold (above 35 cm/s) would suspend and winnow substantial volumes of sediment, but there was no evidence of this at the site. For example, a partially buried beer can at the demarcated site showed no change in the buried proportion during its observation period (November 2015–December 2017). Moreover, the attachment structures of *Democrinus* make them particularly susceptible to being dislodged and transported by currents that approach the threshold velocity. Such velocities would create substantial volumes of suspended sediment that would lead to (1) mass dislodgement of the dense populations of *Democrinus* sp.; (2) transport of the dislodged individuals in suspension, and (3) burial when the current subsided. Yet there was no evidence of this: The four individuals were not transported, exhumed, or buried; they remained at the site of dislodgement with little or no sediment covered their attachment structures or distal stalks throughout the duration of the study. Therefore, hydrodynamic lift was rejected as a sufficient mechanism.

Hydrodynamic Drag, the Swimming Model

A complete power stroke involves the arm rotating through 80°, or $\theta = \sim 1.4$ radians. Under the simplified swimming model, when considering a range of arm lengths, no dislodged specimen had an arm length sufficient to produce thrust to overcome its WIW_{Esw}. The maximum arm length observed for any *Democrinus* sp. was less than 8 cm. Even assuming a *Democrinus* sp. with 10 cm long arms, the thrust generated fails to reach the estimated threshold needed for lift (Figure III.10 A).

Figure III.10 B shows the thrust generated as a function of time to complete the power stroke, considering a range of angular velocities from 0.28 rad/s to near infinity with arm length held constant. In addition, the model assumes that *Democrinus* sp. moves all of its arms simultaneously, rather than in an alternating fashion as observed in feather stars, which

maximizes potential lift (from 5 to ~0 s). At the angular velocity observed, demarked by a circle in Figure III.10 A, even if all five arms moved in unison, the instantaneous thrust generated, ~ 10 dynes, would be roughly 1.5 orders of magnitude lower than WIW_{Esw}. For *Democrinus* sp. to generate the thrust required, it would have to flap its arms at 10 Hz, approximately the frequency with which the giant hummingbird flaps its wings when it hovers (13 Hz, Fernandez 2010).

DISCUSSION

Thousands of individuals of *Democrinus* sp. were observed, photographed, and videoed during the eight multi–dive expeditions that spanned five years (2012–2017), but uprooting/dislodgement was never observed directly. However, as mentioned earlier, several specimens were observed lying prone on the substrate, some with crowns fully intact, suggesting that such events do occur, potentially related to faunal "bulldozing" (Figure III.12). Regardless of the cause, given the results of the dislodgement experiments, such events are survivable and *Democrinus* sp. can regain an upright position.

Our analyses indicated that the mechanism by which *Democrinus* sp. rights itself cannot result from the push–up, balloon, kite, or swimming models. Their arm lengths are too short for the push-up model to be the cause and we found no evidence of positive buoyancy necessary for the balloon model. Although the kite and swimming models are theoretically appealing and plausible on biomechanical grounds, they failed to account for the behavior observed. *Democrinus* sp. modifies its posture at currents half of what the kite model requires. Assuming *Democrinus* sp. could maintain an optimal fan posture in currents faster than 15 cm/s, the threshold current velocity modeled is higher than currents at this site. Similarly, *Democrinus* sp. could not generate sufficient thrust by moving its arms to re-establish its upright posture

following dislodgement, even under the most generous scenarios, and the swimming model failed.

Contractility of the stalk ligament in **Democrinus** *sp.*

One final mechanism to consider is the active flexure of the stalk, analogous to the active flexing of muscular arms of extant crinoids. However, although the columnal facets in *Democrinus* sp. have a central fulcrum that would be compatible with active bending, their stalk has no muscular tissues (Grimmer et al. 1984b). Other non–muscular tissues hypothesized to produce contraction, such as the bundles of filaments in the coelomic epithelium of feather star cirri (Holland and Grimmer 1981a), are also absent in the stalk of *Democrinus conifer* (Grimmer et al. 1984b). Assuming that *D. conifer* is a reasonable representative of the genus, the only tissue that connects adjacent columnals in *Democrinus* is ligamentary, which is also true for all other extant stalked crinoids (Grimmer et al. 1984a,b, Grimmer and Holland 1985, Holland et al. 1991).

Historically, crinoid scholars have interpreted the absence of stalk muscles as an indication that stalked crinoids are unable to flex their stalks actively (Grimmer et al. 1984b, Donovan 1988, Baumiller et al. 1991, Baumiller 1992, Donovan 1989b, Donovan 1997, Baumiller 1997, Kitazawa and Oji 2014, Donovan 2016). Field observations of isocrinids and feather stars supported this interpretation, with the possible exception of the stalks of larval feather stars (see Grimmer et al. 1984a for a review). In the absence of active flexure, the best biomechanical model used to discuss crinoid stalks is a multi-element cantilever beam passively undergoing deflection because of external forces, e.g., gravitational, hydrodynamic, or those generated by arms or cirri (Baumiller and LaBarbera 1993). The multi-element cantilever model accounts not only for the fact that crinoid stalks are segmented, but also for the fact that their ligaments are mutable (Baumiller 1992).

As in other echinoderms, the crinoid ligament consists of actively mutable collagenous tissues, or MCT. These unique tissues allow the animal to stiffen and de-stiffen ligaments over several orders of magnitude within a short time (Smith et al. 1981, Wilkie 1983, Motokawa 1984, Wilkie et al. 1994, Birenheide and Motokawa 1994, Wilkie et al. 1994, Wilkie 2001, Motokawa et al. 2004, Wilkie 2005, Ribeiro et al. 2011, Barbaglio et al. 2015, Mo et al. 2016). Certain echinoderms use MCT in conjunction with muscle extremely effectively (Motokawa and Fuchigami 2015). However, the variability in the mechanical properties of MCT is entirely independent of muscle and has been noted in its absence (Wilkie 2001, 2005). It has been suggested that the changes in the mechanical properties result from modulation of the ligament fiber matrix that switches from a stiff "catched" state to a soft, stretchable "slide" state (Smith et al. 1981, Wilkie et al. 1994, Motokawa et al. 2004, Ribeiro et al. 2011, Barbaglio et al. 2015, Mo et al. 2016). Thus, a stalk with MCT functions as a cantilever beam with variable and controllable stiffness. While in the "slide" state, crinoids can adjust their feeding posture passively using external forces such as varying current conditions. In the "stiff" state, crinoids maintain their posture at little energetic cost, and some taxa can autotomize the stalk (Baumiller and Labarbera 1993, Birenheide and Motokawa 1996, Baumiller 1997, Wilkie 2001, 2005, Takemae et al. 2009, Motokawa et al. 2012, Kitazawa and Oji 2014). Yet, despite its importance to echinoderms' ability to function, the variable properties of ligament associated with MCT cannot explain active stalk flexure, as that requires contractility.

Early in the 20th century, the idea that echinoderm ligaments could contract had several proponents (e.g., Reichensperger 1912, Gislén 1924). However, several physiological experiments designed to detect it failed, and the idea fell out of favor (see summaries in Takahashi 1967b, Wilkie 1979, 1983, and Motokawa 1982). It gained attention again in the mid–

1990s when several laboratory studies reported active contractility in response to chemical stimuli in the ligaments of crinoid arms and cirri (Birenheide and Motokawa 1996, 1998, Birenheide et al. 2000). These studies suggested that the crinoid ligament is not simply mutable (MCT), but that it is contractile also (Contractile Connective Tissue, CCT). CCT contraction was shown subsequently to be an order of magnitude slower than muscular contraction but, like stiffness, to be under nervous control (Motokawa et al. 2004). However, the phenomenon has remained somewhat conjectural, as none of the studies has elucidated the molecular mechanism of ligament contractility. Moreover, experiments on contractility have involved the use of dissected or fragmented crinoid segments in a controlled setting. The righting behavior of *Democrinus* sp. reported in this study offers additional and complementary evidence for the contractile properties of the crinoid ligament in a natural setting and suggests strongly that it is under nervous system control.

If crinoid ligaments are contractile, as this study and previous laboratory results suggest (Birenheide and Motokawa 1996, 1998, Birenheide et al. 2000), the functional implications are profound and extend beyond the righting behavior of *Democrinus* sp. observed. First, synarthrial stalk articulations such as those in the stalk of the *Democrinus* sp. are also found among other extant crinoids. For example, they occur in all stalked members of Bourgueticrinina (Hess and Messing 2011), juvenile feather stars (Haig and Rouse 2008), and juvenile isocrinids (Amemiya et al. 2016). While active movement has been proposed previously for several of them (see Grimmer et al. 1984a for discussion of this phenomenon in the larval stalk of feather stars), it has been rejected generally because of the absence of muscles associated with synarthries (Grimmer et al. 1984a,b, Grimmer and Holland 1985, Holland et al. 1991); however, in light of the results of this study, active movement in all of those synarthries must be considered highly plausible.

Synarthrial stalk articulations are known among fossil crinoids (see Donovan 1988 for a summary), although the nature of soft tissues in fossil crinoids is difficult to discern and generally involves the use of skeletal or taphonomic proxies (e.g., Lane and Macurda 1975, Donovan 1989b, Baumiller and Ausich 1993, Ausich and Baumiller 1993, Baumiller and Hagdorn 1995, Boháty 2011, Gorzelak et al. 2014). In most fossil crinoids, the microstructure of synarthrial stereom is galleried and, based upon analogy with extant crinoids, these synarthries are thought to have been ligamentary (Donovan 1988). However, it has been argued recently that in at least one fossil crinoid, the Devonian *Ammonicrinus*, the stalk was muscular and capable of active movement (Boháty 2011, Gorzelak et al. 2014, Gorzelak and Zamora 2016). The inference of muscles in the stalk of *Ammonicrinus* was based upon the presence of labyrinthic stereom (Gorzelak et al. 2014, Gorzelak and Zamora 2016), a proxy used widely, but not foolproof: In at least one extant crinoid, *Calamocrinus diomedae*, the labyrinthic stereom is associated with ligament, not muscle (Holland et al. 1991). Regardless, based upon the results presented here, *Ammonicrinus* need not have relied on muscles to bend its stalk; contractile ligaments would have sufficed.

The functional implications of ligament contractility for non-synarthrial columnal articulations are not as obvious. As discussed previously, two common types of stalk articulations are synostoses and symplexies (Figure III.1 C - F). In isocrinids, stalk flexibility is associated with changes in the stiffness of ligaments at symplexies, while synostoses are specialized for autotomy, and MCT's central role in both of these functions is recognized well (Wilkie and Emson 1988, Wilkie et al. 1994, Baumiller and Hagdorn 1995, Baumiller 1997, Birenheide et al. 2000, Wilkie 2001, Baumiller 2008). However, ligament contraction at symplexies or synostosis would not result in seesawing (rotation) of adjacent columnals relative

to each other. Rather, contraction would cause adjacent columnals to press more firmly against each other. Thus, in a stalk that is already straight, rather than bending the stalk, contracting ligaments would make it more resistant to bending (Baumiller 2008). However, a stalk that had been bent by some external forces, such as gravity or hydrodynamic drag, could be "unbent" (straightened) by ligament contraction; i.e., a crinoid stalk in a curved posture could return to a straight, upright posture without a new external force to provide a drag force on the crown. In other animals, such unbending is assumed generally to result from the elastic recoil of the stretched ligaments. However, MCT ligaments are visco-elastic and are known to regain only about half of the displacement lost (Wilke et al. 1994). Thus, they may be unable to recover their original length fully when the external load is removed.

Ligament contractility may also play an indirect role in the bending of stalks with non-synarthrial articulations through its effect on the active bending of stalk cirri. Cirri have long been known to be actively motile (e.g., Agassiz 1888). In feather stars, cirral bending is interpreted to involve the contraction of filaments located away from the central fulcrum of the cirral joint in the wall of the coelomic canal (Holland and Grimmer 1981a). However, in the cirri of isocrinids, such as *Metacrinus rotundus*, the central canal and the associated filaments run through the center of the fulcrum (Birenheide et al. 2000). Thus, contraction of the canal tissue, as suggested for feather stars, would bring the two adjacent ossicles closer to each other rather than allowing rotation around the fulcrum, while contraction of ligaments on one side of the cirral fulcrum could produce rotation and account for active cirral bending (Birenheide et al. 2000).

Further, ligament contraction has significant consequences for early Paleozoic crinoids. Together with its role in the fossil crinoid stalk discussed previously, the presence of CCT would

alter the way we interpret early crinoid arms. The skeletal morphology of arm facets in some Paleozoic eucladids is notably similar to that in articulate crinoid arms. A transverse ridge separates the facet into aboral and adoral sides, which suggests that these crinoids had muscular arms, a hypothesis that the arm articulation microstructure (Lane and Macurda 1975) and the mode of preservation (Ausich and Baumiller 1993) supports further. Traditionally, other Paleozoic crinoids are regarded as having only ligamentary articulations between their arm plates, which are generally inferred to be capable of only passive movement via external forces. However, ligament contraction may have allowed some of these crinoids, for example, calceocrinids and some disparids that have ridges analogous to those found in muscular articulations, to bend actively to a limited extent (Ubaghs 1978). Moreover, as discussed above for non-synarthrial stalk articulations, contractile ligaments in arms that lack a fulcrum entirely could allow active "unbending" of arms bent by external forces. This could affect filter-feeding by allowing a certain degree of arm adjustment in environments with variable currents (Meyer and Macurda 1977, Meyer 1979, Baumiller 1993, Kitazawa et al. 2007).

CONCLUSIONS

1. Field observations of dislodged individuals of *Democrinus* sp. demonstrated that they are able to regain an upright posture within a relatively short timescales (48 hours).

2. Quantitative evaluation of four mechanisms of the phenomenon above, including the use of arms to push the crown off the bottom (push-up model), buoyancy (balloon model), hydrodynamic lift (kite model), and thrust generated through hydrodynamic drag by aboral flexure of the arms (swimming model), revealed that none is adequate.

3. Having excluded the mechanisms above, we concluded that the righting behavior observed in *Democrinus* sp. involves the active contraction of tissues on either side of a fulcral

ridge that characterizes its synarthrial columnal articulations. Contraction of the ligament on one side of the fulcrum causes flexion at the joint and active stalk bending.

4. This study corroborates a previous hypothesis that the connective tissue of the crinoid ligament is contractile (Birenheide and Motokawa 1996).

5. The implications of ligament contractility for crinoids include: (1) active stalk bending is necessary for righting and postural control of *Democrinus* sp. and other crinoids with synarthrial stalk articulations; (2) active flexure of cirri is necessary for the animal to attach and reattach to the substrate, and, possibly, to right the stalks that lack synarthrial articulations; (3) active arm movement occurs in crinoids that lack muscular arm articulations, which includes the majority of Paleozoic taxa. Ligament contractility would allow adjustments of the feeding posture and possibly anti-predatory behaviors.

References

Agassiz, A. 1888. Three cruises of the United States Coast and Geodetic Survey steamer "Blake" in the Gulf of Mexico, in the Caribbean Sea, and along the Atlantic coast of the United States, from 1877 to 1880 (Vol. II). Bull Mus Comp Zool. Harvard Univ. 15:1–220

Amemiya S, Omori A, Tsurugaya T, Hibino T, Yamaguchi M, Kuraishi R, Kiyomoto M, Motokawa T. 2016. Early stalked stages in ontogeny of the living isocrinid sea lily *Metacrinus rotundus*. Acta Zool -Stockholm. 97(1):102–116

Ausich WI, Baumiller TK. 1993. Taphonomic method for determining muscular articulations in fossil crinoids. Palaios. 8:477–484

Barbaglio A, Tricarico S, Ribeiro AR, Benedetto CD, Barbato M, Dessì D, Fugnanesi V, Magni S, Mosca F, Sugni M, Bonasoro F, Barbosa MA, Wilkie IC, Candia Carnevali MD. 2015. Ultrastructural and biochemical characterization of mechanically adaptable collagenous structures in the edible sea urchin *Paracentrotus lividus*. Zoology. 118:147–160

Baumiller TK, LaBarbera M, Woodley JD. 1991. Ecology and functional morphology of the isocrinid *Cenocrinus asterius* (Linnaeus) (Echinodermata: Crinoidea): *in situ* and laboratory experiments and observations. Bull Mar Sci. 48(3):731–748

Baumiller TK. 1992. Importance of hydrodynamic lift to crinoid autecology, or, could crinoids function as kites? J Paleontol. 66(4):658–665

Baumiller TK, Ausich WI. 1992. The broken-stick model as a null hypothesis for crinoid stalk taphonomy and as a guide to the distribution of connective tissue in fossils. Paleobiology. 18 (3):288–298

Baumiller TK. 1993. Survivorship analysis of Paleozoic Crinoidea: effect of filter morphology on evolutionary rates. Paleobiology. 19(3):304–321

Baumiller TK, LaBarbera M. 1993. Mechanical properties of the stalk and cirri of the sea lily *Cenocrinus asterius*. Comp Biochem Phys A. 106(1):91–95

Baumiller, TK, Hagdorn H. 1995. Taphonomy as a guide to functional morphology of *Holocrinus*, the first post-Paleozoic crinoid. Lethaia. 28:221–228

Baumiller TK, Ausich WI. 1996. Crinoid stalk flexibility: theoretical predictions and fossil stalk postures. Lethaia. 29(1):47–59

Baumiller TK. 1997. Crinoid functional morphology. Paleontological Society Papers. 3:45–68

Baumiller TK, Messing CG. 2007. Stalked crinoid locomotion, and its ecological and evolutionary implications. Paleontol Electron. 10(1):1–10

Baumiller TK. 2008. Crinoid ecological morphology. Annu Rev Earth Pl Sci. 36(1):221–249

Baumiller TK, Mooi R, Messing CG. 2008. Urchins in the meadow: paleobiological and evolutionary implications of cidaroid predation on crinoids. Paleobiology. 34(1):22– 34

Baumiller TK, Salamon M, Gorzelak P, Mooi R, Messing CG, Gahn FJ. 2010. Benthic predation drove early Mesozoic crinoid radiation. PNAS 107(13):5893–5896

Birenheide R, Motokawa T. 1994. Morphological basis and mechanics of arm movement in the stalked crinoid *Metacrinus rotundus* (Echinodermata, Crinoidea). Mar Biol. 121:273–283

Birenheide R, Motokawa T. 1996. Contractile connective tissue in crinoids. Biol Bull. 191:1–4

Birenheide R, Motokawa T. 1998. Crinoid ligaments: catch and contractility. *In*: Mooi R, Telford M. editors. Echinoderm: San Francisco. AA. Balkema, Rotterdam

Birenheide R, Yokoyama K, Motokawa T. 2000. Cirri of the stalked crinoid *Metacrinus rotundus*: Neural elements and the effect of cholinergic agonists on mechanical properties. Proc Biol Sci. 267(1438):7–16

Boháty J. 2011. Revision of the flexible crinoid genus *Ammonicrinus* and a new hypothesis on its life mode. Acta Palaeontol Pol. 56:615–639

Bottjer DJ, Jablonski D. 1988. Paleoenvironmental patterns in the evolution of post-Paleozoic benthic marine invertebrates. Palaios 3:540–60

Breimer A, Webster GD. 1975. A further contribution to the paleoecology of fossil stalked crinoids. Proc K Ned Akad Wet C. 80:149–67

Breimer A. 1978. Ecology of recent crinoids. *In:* Moore RC, Teichert C. editors. Treatise on Invertebrate Paleontology, Part T1, Echinodermata. Geo Soc Am. Univ Kansas Press, Boulder, Lawrence. T316–30

de Carvalho CN, Pereira BC, Klompmaker AA, Baucon A, Moita JA, Pereira P, Machado S, Belo J, Carvalho J, Mergulhão L. 2016. Running crabs, walking crinoids, grazing gastropods: behavioral diversity and evolutionary implications in the Cabeço da Ladeira lagerstätte (Middle Jurassic, Portugal). Comunicações Geológicas Especial 103(1):39–54

Clark HL. 1915. The comatulids of Torres Strait: with special reference to their habits and reactions. Pap Dep Mar Biol Carnegie Instn Wash. 8:67–125

Cohen BL, Pisera A. 2016. Crinoid phylogeny: new interpretation of the main Permo-Triassic divergence, comparisons with echinoids and brachiopods, and EvoDevo interpretations of major morphological variations. Biol J Linn Soc. 120(1):38–53

Donovan SK. 1984. Stem morphology of the Recent crinoid *Chladocrinus* (*Neocrinus*) *decorus*. Palaeontology. 27:825–41

Donovan SK. 1988. Functional morphology of synarthrial articulations in the crinoid stem. Lethaia. 21:169–175

Donovan SK. 1989b. The improbability of a muscular crinoid column. Lethaia. 22(3):307–315

Donovan SK. 1997. Comparative morphology of the stems of the extant bathycrinid *Democrinus perrier* and the Upper Paleozoic platycrinids (Echinodermata, Crinoidea). Bulletin of the Mizunami Fossil Museum. 23:1–27

Donovan SK. 1990. Functional morphology of synostosial articulation in the crinoid column. Lethaia. 23: 291–296

Donovan SK. 2016. Problematic aspects of the form and function of the stem in Palaeozoic crinoids. Earth-Science Reviews 154:174–182.

Fernandez MJ. 2010. Flight Performance and Comparative Energetics of the Giant Andean Hummingbird (*Patagona gigas*). PhD diss., University of California, Berkeley

Gorzelak P, Głuchowski E, Salamon MA. 2014. Reassessing the improbability of a muscular crinoid stem. Sci Rep-UK. 4(6049):1–8

Gorzelak P, Zamora S. 2016. Understanding form and function of the stem in early flattened echinoderms (pleurocystitids) using a microstructural approach. PeerJ. 4:18–20

Gorzelak P, Kołbuk D, Salamon MA, Łukowiak M, Ausich WI, Baumiller TK. 2020. Bringing planktonic crinoids back to the bottom: Reassessment of the functional role of scyphocrinoid loboliths. Paleobiology. 46:104–122

Gislén T. 1924 Echinoderm studies. Zoologiska Bidrag fran Uppsala. 9:1–316

Grifoll M, Cerralbo P, Guillén J, Espino M, Hansen LB, Sánchez-Arcilla A. 2019. Characterization of bottom sediment resuspension events observed in a micro-tidal bay. Ocean Sci. 15(2):307–319

Grimmer JC, Holland ND, Kubota H. 1984a. The fine structure of the stalk of the pentacrinoid larva of a feather star, *Comanthus japonica* (Echinodermata: Crinoidea). Acta Zool. 65(1):41–58

Grimmer JC, Holland ND, Messing CG. 1984b. Fine structure of the stalk of the bourgueticrinid sea lily *Democrinus conifer* (Echinodermata: Crinoidea). Mar Biol. 81:163– 176

Grimmer JC, Holland ND, Hayami I. 1985. Fine structure of the stalk of an isocrinid sea lily (*Metacrinus rotundus*) (Echinodermata, Crinoidea). Zoomorphology. 105(1):39–50

Haig JA, Rouse GW. 2008. Larval development of the feather star *Aporometra wilsoni* (Echinodermata: Crinoidea). Invertebr Biol. 127(4):460–469

Hess H. 2014. Origin and radiation of the comatulids (Crinoidea) in the Jurassic. Swiss J Palaeontol. 133:23–34

Hidaka M, Takahashi K. 1983. Fine structure and mechanical properties of the catch apparatus of the sea-urchin spine, a collagenous connective tissue with muscle-like holding capacity. J Exp Biol. 103(1):1–14

Holland ND, Grimmer JC. 1981a. Fine structure of the cirri and a possible mechanism for their motility in stalkless crinoids (Echinodermata). Cell Tissue Res. 214:207–217

Holland ND, Grimmer JC, Wiegmann K. 1991. The structure of the sea lily *Calamocrinus diomedae*, with special reference to the articulations, skeletal microstructure, symbiotic bacteria, axial organs, and stalk tissues (Crinoida, Millericrinida). Zoomorphology, 110(3):115–132 doi: 10.1007/bf01632868

Janevski GA, Baumiller TK. 2010. Could a stalked crinoid swim? A biomechanical model and characteristics of swimming crinoids. Palaios. 25(9):588–596 doi: 10.2110/palo.2009.p09-149r.

Kitazawa K, Oji T. 2014. Active feeding behavior of and current modification by the sea lily *Metacrinus rotundus* (Echinodermata: Crinoidea). J Exp Mar Biol. Ecol. 453:13–21

Lane NG, Macurda DB Jr. 1975. New evidence for muscular articulations in Paleozoic crinoids. Paleobiology. 1:59–62

Macurda DB Jr, Meyer DL. 1974. Feeding posture of modern stalked crinoids. Nature. 247:394–396

Macurda DB Jr, Meyer DL. 1983. Sea lilies and feather stars. Am Sci. 71(4):354–365

McCave IN, Manighetti B, Robinson SG. 1995. Sortable silt and fine sediment size/composition slicing: Parameters for palaeocurrent speed and palaeoceanography. Paleoceanography. 10(3):593–610

McCave IN. 2008. Size sorting during transport and deposition of fine sediments: sortable silt and flow speed. Dev Sedimentol. 60:121–143

McCave IN, Thornalley DJR, Hall IR. 2017. Relation of sortable silt grain-size to deep-sea current speeds: Calibration of the 'Mud Current Meter'. Deep-Sea Res Pt I. 127:1–12

Messing, CG, Rose-Smyth MC, Mailer SR, Miller JE. 1988. Relocation movement in a stalked crinoid (Echinodermata). Bull Mar Sci. 42:480–487

Messing CG. 1997. Living comatulids. Paleontological Society Papers. 3:3–30

Meyer DL. 1973. Feeding behavior and ecology of shallow-water unstalked crinoids (Echinodermata) in the Caribbean Sea. Mar Biol. 22:105–129

Meyer DL, Macurda DB Jr. 1977. Adaptive radiation of the comatulid crinoids. Paleobiology. 3(1):74–82

Meyer DL, LaHaye CA, Holland ND, Arneson AC, Strickler JR. 1984. Time-lapse cinematography of feather stars (Echinodermata: Crinoidea) on the Great Barrier Reef, Australia: demonstrations of posture changes, locomotion, spawning and possible predation by fish. Mar Biol. 78:179–184

Miller MC, McCave IN, Komar PD. 1977. Threshold of sediment motion under unidirectional currents. Sedimentology. 24:507–527

Mladenov PV. 1983. Rate of arm regeneration and potential causes of arm loss in the feather star *Florometra serratissima* (Echinodermata: Crinoidea). Can J Zool. 61(12):2873–2879

Mo J, Prévost SF, Blowes LM, Egertov M, Terrill NJ, Wang W, Elphick MR, Gupta HS. 2016. Inter-fibrillar stiffening of echinoderm mutable collagenous tissue demonstrated at the nanoscale. Proc Natl Acad Sci USA. 113(42):6362–6371

Motokawa T. 1982. Factors regulating the mechanical properties of holothurian dermis. J Exp Biol. 99:29–41

Motokawa T. 1984. Connective tissue catch in echinoderms. Biol Rev. 59(2):255–270

Motokawa T, Shintani O, Birenheide R. 2004. Contraction and stiffness changes in collagenous arm ligaments of the stalked crinoid *Metacrinus rotundus* (Echinodermata). Biol Bull. 206(1):

Motokawa T, Fuchigami Y. 2015. Coordination between catch connective tissue and muscles through nerves in the spine joint of the sea urchin *Diadema setosum*. J Exp Biol. 218(5):703–710

Motokawa T, Sato E, Umeyama K. 2012. Energy expenditure associated with softening and stiffening of echinoderm connective tissue. Biol Bull. 222(2):150–157

Oji T. 1996. Is predation intensity reduced with increasing depth? Evidence from the West Atlantic stalked crinoid *Endoxocrinus parrae* (Gervais) and implications for the Mesozoic marine revolution. Paleobiology. 22(3):339–351

Pourtalès LF de. 1884. Zoological results of the Hassler expedition: crinoids and corals. *In*: Agassiz A. Editors. Echini, crinoids, and corals. Museum of Comparative Zoology. Cambridge. 8(12):27–33

Rasmussen HW, Sieverts-Doreck H. 1978. Articulata Classification. *In:* Moore RC, Teichert, C. Editors. Treatise on invertebrate paleontology, Part T, Echinodermata 2, vol. 3. Geo Soc Am. Univ Kansas Press, Boulder and Lawrence. 813–927

Ribeiro AR, Barbaglio A, Di Benedetto C, Ribeiro CC, Wilkie IC, Candia Carnevali MD, Barbosa MA. 2011. New insights into mutable collagenous tissue: Correlations between the microstructure and mechanical state of a sea-urchin ligament. Mitraki A, editor. PLoS ONE. 6(9):24–82

Rouse GW, Jermiin LS, Wilson NG, Eeckhaut I, Lanterbecq D, Oji T, Young CM, Browning T, Cisternas P, Helgen LE, Stuckey M, Messing CG. 2013. Fixed, free, and fixed: the fickle phylogeny of extant Crinoidea (Echinodermata) and their Permian-Triassic origin. Mol Phylogenet Evol. 66(1):161–181

Roux M, Eléaume M, Améziane N. 2019. A revision of the genus *Conocrinus* d'Orbigny, 1850 (Echinodermata, Crinoidea, Rhizocrinidae) and its place among extant and fossil crinoids with a xenomorphic stalk. Zootaxa. 4560(1):51–84

Sars, M. 1868. Memoires pour servir a la connaissance des crinoïdes vivants. I. Du *Rhizocrinus lofotensis* M. Sars, nouveau genre vivant des crinoïdes pedicelles, dits lis de mer. Brøgger and Christie, Christiania, 46 pp. + plates I-IV

Shaw GD, Fontaine AR. 1990. The locomotion of the comatulid *Florometra serratissima* (Echinodermata: Crinoidea) and its adaptive significance. Can J Zool. 68: 942–950

Simms MJ. 1989. Columnal ontogeny in articulate crinoids and its implications for their phylogeny. Lethaia. 22(1):61–68

Smith DS, Wainwright SA, Baker J, Cayer ML.1981. Structural features associated with movement and catch of sea-urchin spines. Tissue Cell. 13:299–320

Syverson VJ, Baumiller TK. 2014. Temporal trends of predation resistance in Paleozoic crinoid arm branching morphologies. Paleobiology. 40(3):417–427

Takahashi 1967b. The catch apparatus of the sea-urchin spine. II. Responses to stimuli. J Fac Sci Univ Tokyo Sec. IV. 11: 121-130 Univ. Tokyo Sec. IV11, 121–130

Takemae N, Nakaya F, Motokawa T. 2009. Low oxygen consumption and high body content of catch connective tissue contribute to low metabolic rate of sea cucumbers. Biol Bull. 216(1):45–54

Trotter JA. 1996. Stiparin: a glycoprotein from sea cucumber dermis that aggregates collagen fibrils. Matrix Biol. 15(2):99–110

Tunnicliffe V, Roux M, Eléaume M, Schornagel D. 2016. The stalked crinoid fauna (Echinodermata) of the Molucca and Celebes Seas, Indonesia: taxonomic diversity and observations from remotely operated vehicle imagery. Mar Biodiv. 46(2):365–388

Ubaghs G. 1978. Skeletal morphology of fossil crinoids. *In*: Moore RC, Teichert C, editors. Treatise on Invertebrate Paleontology, Part T, Echinodermata 2 (1). Geological Society of America and University of Kansas Press, New York and Lawrence. p. T58–T216

Veitch MA, Baumiller TK. 2021. Low predation intensity on the stalked crinoid *Democrinus* sp. (Echinodermata), in Roatán, Honduras, reveals deep water as likely predation refuge. Bull Mar Sci. 97(1):107–128

Vogel S. 1994. Life in Moving Fluids: Princeton University Press, Princeton, New Jersey.

Wilkie IC. 1979. The juxtaligamental cells of *Ophiocomina nigra* (Abildgaard) (Echinodermata: Ophiuroidea) and their possible role in mechano-effector function of collagenous tissue. Cell Tiss Res. 197: 515–530

Wilkie IC. 1983. Nervously mediated change in the mechanical properties of the cirral ligaments of a crinoid. Mar Behav Physiol. 9:229–48

Wilkie IC. 1984. Variable tensility in echinoderm collagenous tissues - a review. Mar Behav Physiol. 11(1):1–34

Wilkie IC, Emson RH. 1988. Mutable collagenous tissues and their significance for echinoderm palaeontology and phylogeny. *In*: Paul CRC, Smith AB, editors. Echinoderm Phylogeny and Evolutionary Biology. Clarendon Press, Oxford. p. 312–330

Wilkie IC, Emson RH, Young CM. 1994. Variable tensility of the ligaments in the stalk of a sea-lily. Comp Biochem Phys Part A. Phys. 109(3):633–641.

Wilkie IC. 2001. Autotomy as a prelude to regeneration in echinoderms. Microsc Res Tech. 55(6):369–396

Wilkie IC. 2005. Mutable collagenous tissue: overview and biotechnological perspective. *In:* R. Burke et al.: Matranga V, editor. Echinodermata. Progress in molecular and sub-cellular biology 39. Subseries, Marine molecular biotechnology. Berlin: Springer-Verlag. 219–248

Chapter III TABLES

Table III.1: Record of dislodged individuals of *Democrinus* sp. visited during the study. All individuals were seen over multiple visits, and their relative positions on the sediment were noted. Unless specified otherwise, individuals had complete crowns. The method of dislodgement varied only for D2, which was dislodged via suction rather than hooking. D1 was not seen after May 2015, nor were any individuals mapped on May 2015 (see discussion section for more detail).

	D1	D2	D3	D4
Visit date	Dislodgment: hooked and dragged	Dislodgment: Suction and dropped	Dislodgment: hooked and dragged	Dislodgment: hooked and dragged
5/4/2015	Dislodged	—	—	—
5/6/2015	15.5 cm curving off sediment. Crown raised 7 cm, 3 cm of stalk still on sediment.	—	—	—
11/24/2015	Missing	Dislodged	—	—
11/26/2015	Missing	prone on sediment	—	—
5/17/2016	Missing	Upright, only attachment structure on sediment. No arms.	—	—
5/19/2016	Missing	Upright, only attachment structure on sediment	Dislodged	Dislodged, No arms
12/15/2016	Missing	Upright, only attachment structure on sediment	Upright, no visible stalk on sediment (attachment structure likely under sediment)	Upright, no visible stalk on sediment (attachment structure likely under sediment)
12/14/2017	Missing	Upright, only attachment structure on sediment	Upright, no visible stalk on sediment (attachment structure likely under sediment)	Upright, no visible stalk on sediment (attachment structure likely under sediment)

Table III.2: Lab measurements of stalk dimensions and masses of eight collected individuals. Arm and crown measurements are not included, as only the May 2015 A specimen had any crown attached. Calculating WIWsw via WIW measured has an additional step, as the values were gathered in fresh water. WIW was divided by 1.024 to account for the higher density of salt water, which increases buoyancy, and was represented as a force value in dynes (x 980 cm/s). The last column is WIWsw per 1 cm of stalk (dynes/cm). Density ρ = WIA/V.

Specimen	L_{Stalk} (cm)	WIA (dyn)	V (cm^3)	ρ (g/cm^3)	WIW_{sw} (dyne)	WIW_{Stalk} (dyne/cm)
May 2015 A	20.21	960.40	0.51	1.91	516.80	25.57
May 2016 A	17.57	911.40	0.46	2.01	449.80	25.60
May 2016 B	25.23	1185.80	0.64	1.88	526.37	20.86
December 2016 A	36.58	1871.80	0.94	2.03	909.18	24.85
December 2016 B	37.27	2273.60	0.95	2.45	1291.99	34.67
December 2016 C	27.63	1881.60	0.71	2.70	1148.44	41.56
December 2016 D	19.50	686.00	0.49	1.43	181.84	9.33
Stalk Segment	15.39	989.80	0.41	2.44	574.22	37.31
Average					699.83	27.47
StDev					379.08	10.24
StError					143.28	3.62

Table III.3: Lab measurements for the two arms of specimen May 2015 A and a detached crown. Density calculated by mass/volume. WIW_{sw} was calculated by dividing the measured WIW 1.024 to account for the density of salt water.

Specimen	L_{Arm} (cm)	Arm number	Arm_{radius} (cm)	WIA (dyn)	WIW (dyn)	V (cm^3)	ρ (g/cm^3)	WIW_{sw} (dyne)	WIW_{Arm} (dyne/cm)
May 2015 A	2.00	2	0.08	107.80	58.80	0.08	1.78	54.23	13.26
Detached Crown	1.58	5	0.08	254.80	107.80	0.15	1.46	105.27	13.56
Average									13.44
StDev									0.16
StError									0.12

Table III.4: WIW_{sw} values calculated for dislodged individuals. Arm and stalk length varied across individuals, but all had 5 arms. Stalk length (L_{Stalk}) and arm length (L_{Arm}), were calculated using dimensions from photos and videos. WIW_{Esw} was found by multiplying mean WIW_{Arm} (13.44 dynes/cm) and mean WIW_{Stalk} (27.47 dynes/cm) by the dislodged specimens' dimensions. 95% confidence intervals were calculated by simulating 1000 WIW_{Esw} from the calculated WIW_{Esw} values and their error.

	L_{Stalk} (cm)	L_{Arm} (cm)	WIW_{Esw} (dynes)	WIW_{Esw} Error (dynes)	95% CI [LL,UL]
D1	15.10	3.11	623.95	56.53	[508.70, 742.03]
D2	25.07	5.13	1033.67	93.83	[848.03, 1217.38]
D3	27.45	5.75	1140.74	102.82	[932.60, 1354.02]
D4	24.00	4.20	941.73	941.73	[766.72, 1122.26]

Chapter III FIGURES

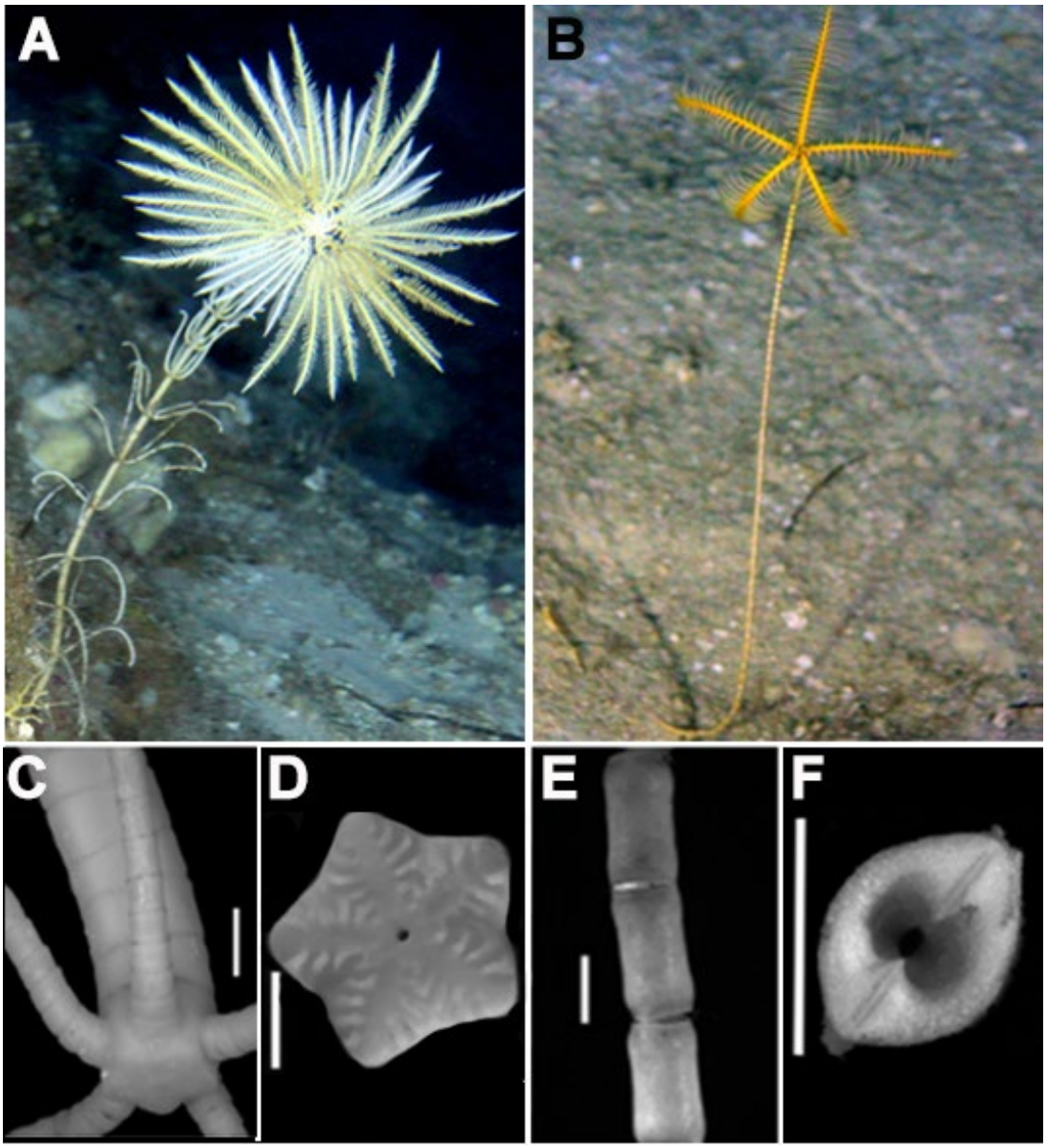

Figure III.1: Overview of stalk morphology for a stalked isocrinid and stalked bourgueticrinid. **Top: (*left)*** A stalked isocrinid, *Cenocrinus asterius*, and (***right***) a stalked bourgueticrinid, *Democrinus* sp., *in situ* off Roatán, Honduras. *C. asterius* uses cirri to cling to a vertical wall (~150 m), while *Democrinus* sp. is rooted in sediment. **Bottom, left to right: (A)** Lateral view of an isocrinid stalk (*Endoxocrinus*) terminating at a synostosis. Five cirri are present just above the characteristic flat surface of the articulation. **(B)** A close-up of a symplexial articulation facet (*Endoxocrinus*). The central canal is small and the articulation is marked with distinct ridges in a flower-like pattern. The ridges interlock with adjacent ones on the next columnal. **(C)** Lateral view of a bourgueticrinid stalk (*Democrinus* sp.). At the synarthrial articulation facets, adjacent columnals connect along a central fulcral ridge. A gap between adjacent columnals is visible on either side of this fulcral ridge. The ridge rotates approximately 65—70 degrees on each successive facet. **(D)** Synarthrial articulation facet of a bourgueticrinid stalk (*Democrinus*

sp.). The fulcral ridge runs through the center of the facet, split by deep ligament pits. All scales at 0.2 cm.

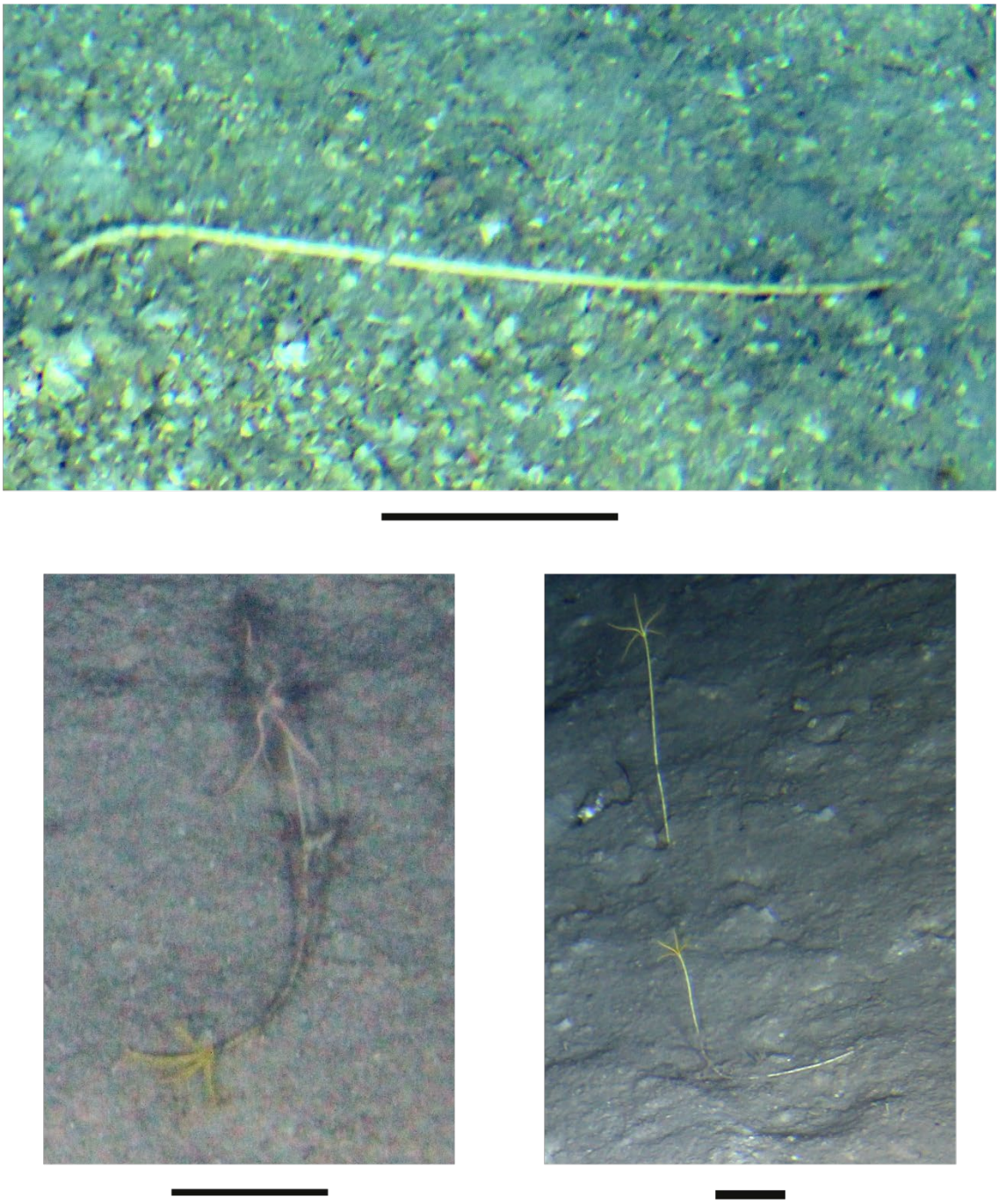

Figure III.2: Images of several prone *Democrinus* sp. **Top:** An individual at the 260 m site on May 4, 2015. The individual is lying prone on sediment and lacks a crown. **Bottom: (*Left*)** An individual with a brittle star at the stalk base, lying prone on the sediment (December 16, 2016). **(*Right)*** An individual with more than half its stalk prone on the sediment (December 15, 2017). Scale bars set at 5 cm.

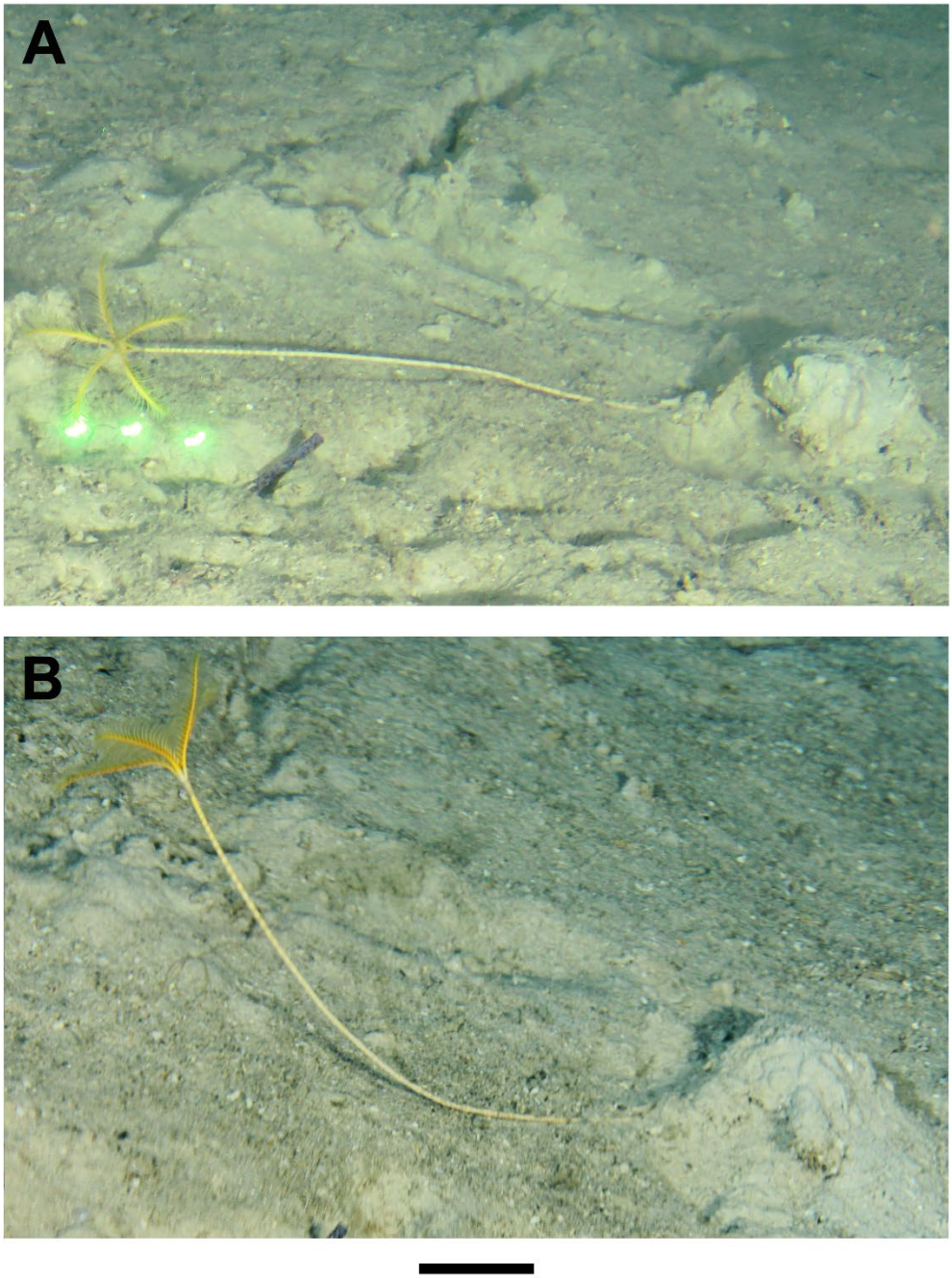

Figure III.3: Dislodged *Democrinus* sp. individual D1 at the 240-meter site off Isla Roatán, Honduras. **A:** On May 4, 2015 between 3 and 5 pm, a wooden board ending in a hook attached to the front of the submersible was used to catch the attachment structure and pull individual D1 until it uprooted. Then, it was left lying on the sediment. **B:** Two days later, on May 6, 2015 around 4 pm, D1 was observed in a partially vertical position (crown raised approximately 7 cm, 15.5 cm of the stalk off the sediment). Although the angle of the two photos differs slightly, and thus not all of the scarring in the sediment is visible, the deep drag depression the hook made during dislodgement on May 4 is visible in both photos directly behind individual D1. Scale 4 cm.

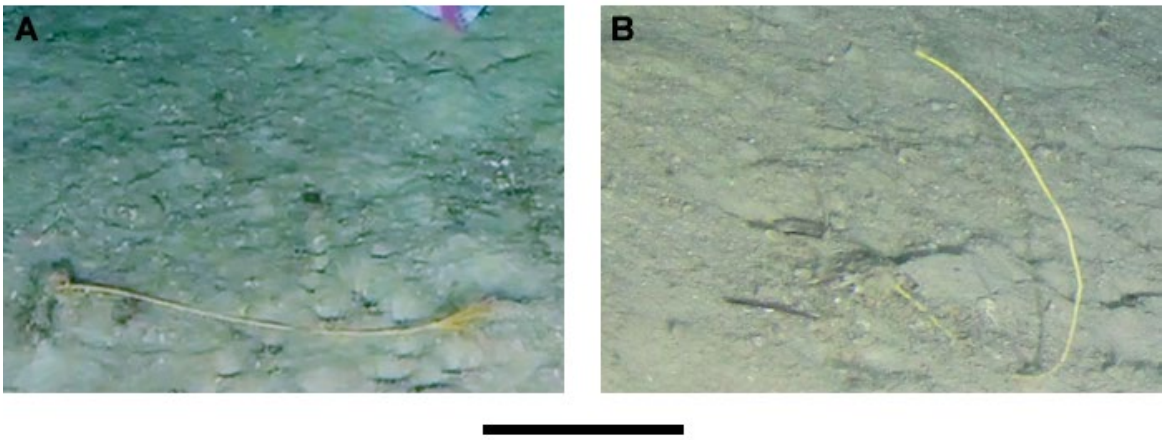

Figure III.4: Dislodged individual D2. **A:** Initially dislodged via suction and dropped in front of marker M2 on November 22, 2015. No changes in posture were observed on November 24 (not shown). **B:** By the next visit on May 17, 2016, D2 had lost its crown (likely predation-related), but had reestablished an upright posture.

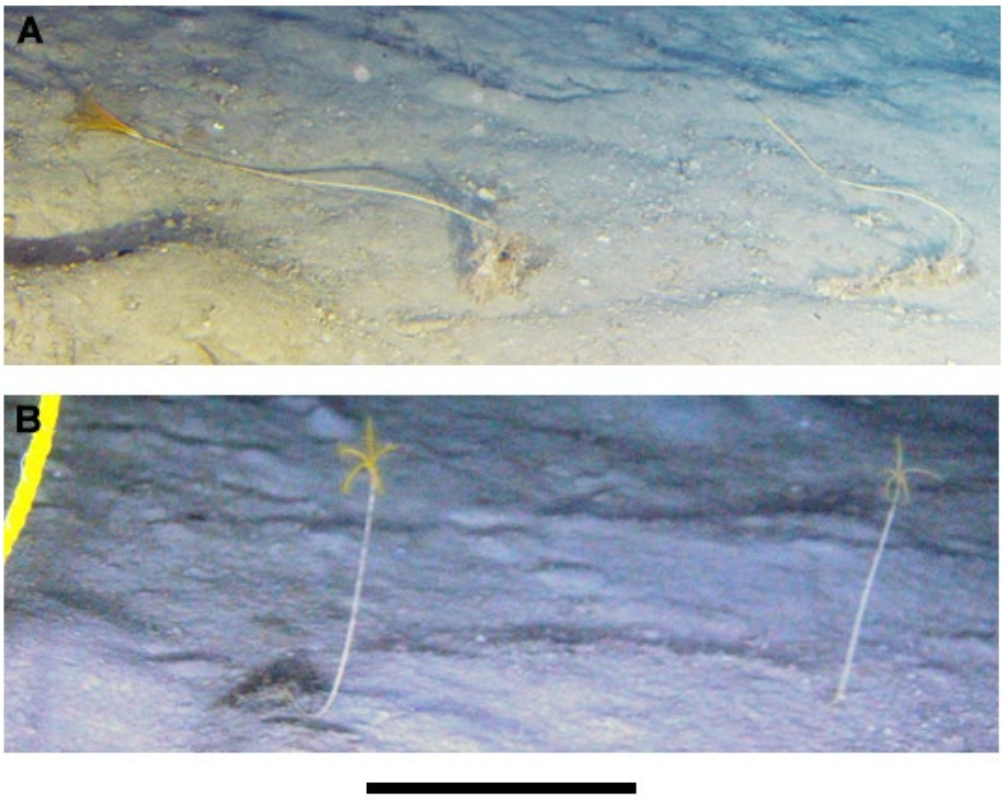

Figure III.5: Dislodged individuals D3 and D4. **A:** On May 19, 2016, the mounted board and hook on the submersible front dislodged individuals D3 (left) and D4 (right). D4 was chosen because it had no crown to see whether this might influence regaining an upright posture. Unfortunately, extreme weather conditions prevented a return visit during the May 2016 expedition. **B:** By December 15, 2016 both individuals were upright, and D4 had regrown its crown. Scale bar set at 10 cm.

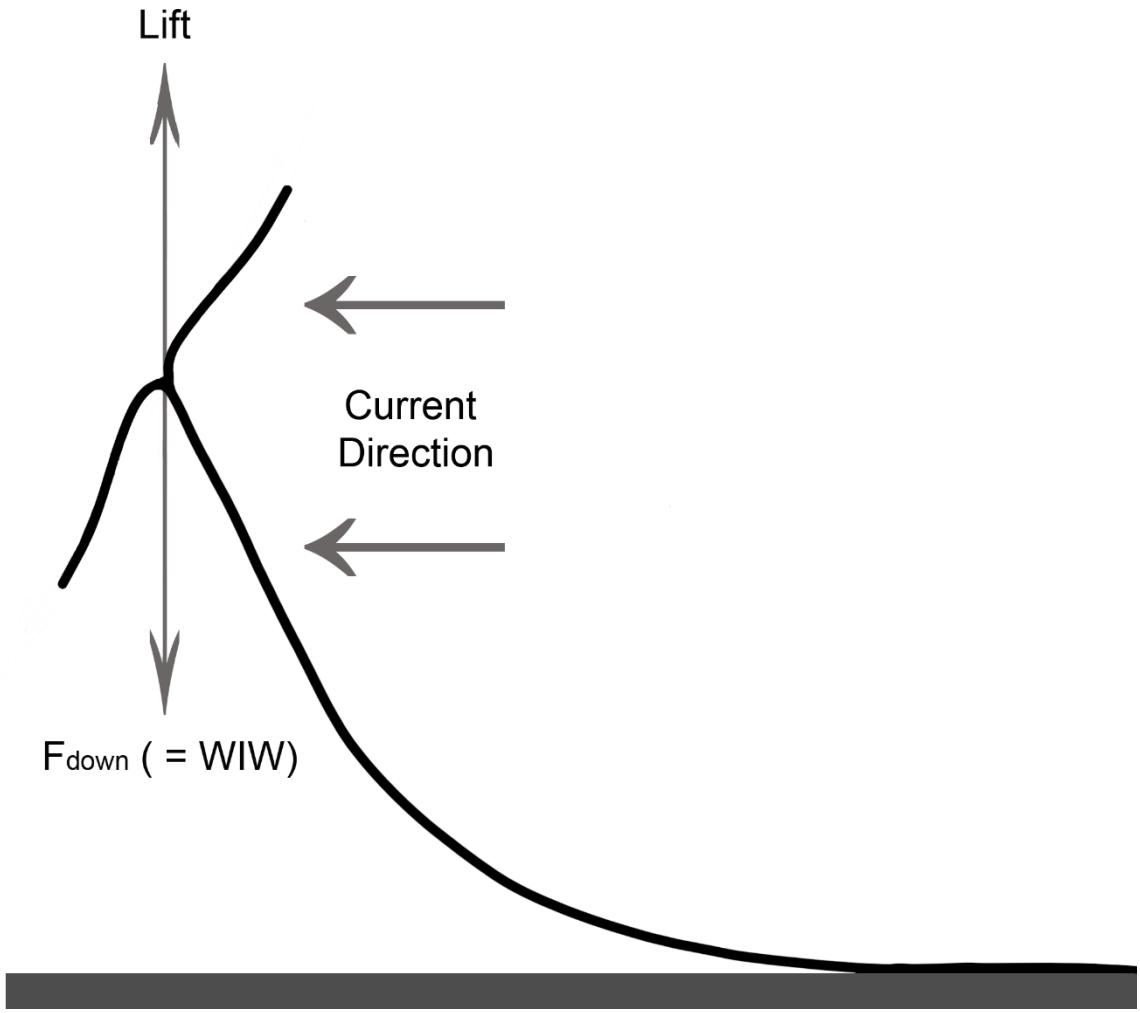

Figure III.6: Forces on a stalked crinoid using the current to generate lift with the distal portion of stalk laying along the sediment. In this model, lift must be greater than the downward force (F_{down}), which is equal to the weight of the prone individual in water (WIW). The current velocity necessary for a given WIW is calculated with Equation III.3, and is based upon an individual's WIW, crown surface area ($5*SA_{Arm}$), and the coefficient of lift, C_L, which is a function of the crown's solidity (SA_{Arm}/ SA_R). The WIW that lift must overcome varies based upon how much stalk is off the sediment.

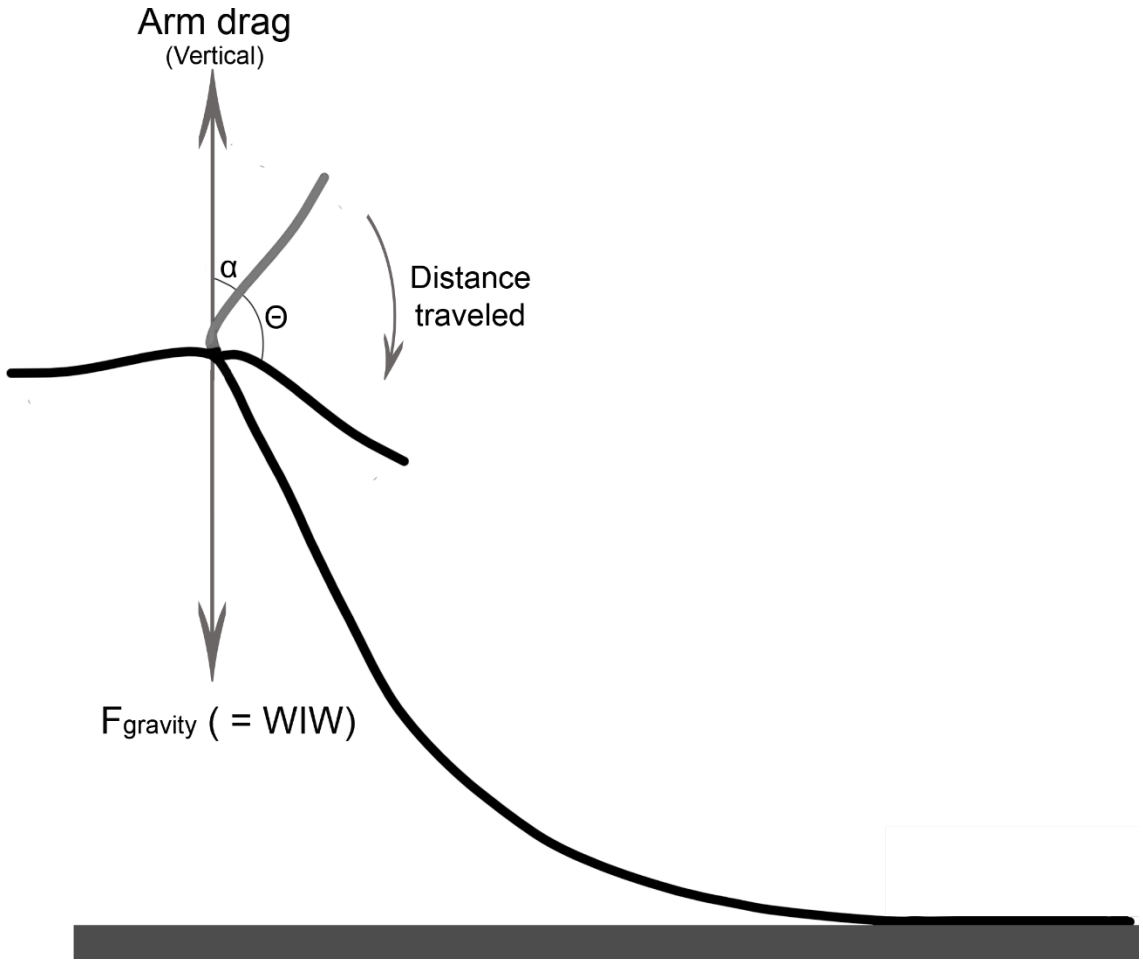

Figure III.7: Simplified model of crinoid with the distal portion of stalk laying along the sediment and the crown generating thrust via vertical drag through arm movement, the swimming model. The power stroke of the arm (right) is illustrated in starting position (grey arm) relative to vertical (α) and at the end of the power stroke (black arm), after it has rotated through θ. Using the period of the power stroke, t_p, the linear velocity of the arm tip, $U_L = (L_{Arm} * \theta)/t_p$, as well as the arm's angular velocity ($\omega = \theta/t_p$), can be calculated. Total drag force represents the force generated during a single arm stroke (D_T), detailed in Appendix A, Part II, and is used to calculate the mean instantaneous vertical drag force ($\bar{D}_V$) (Equation III.4). $\bar{D}_V$ must be equal to or greater than the crinoid's weight in water (WIW) to raise the crown and stalk off the sediment.

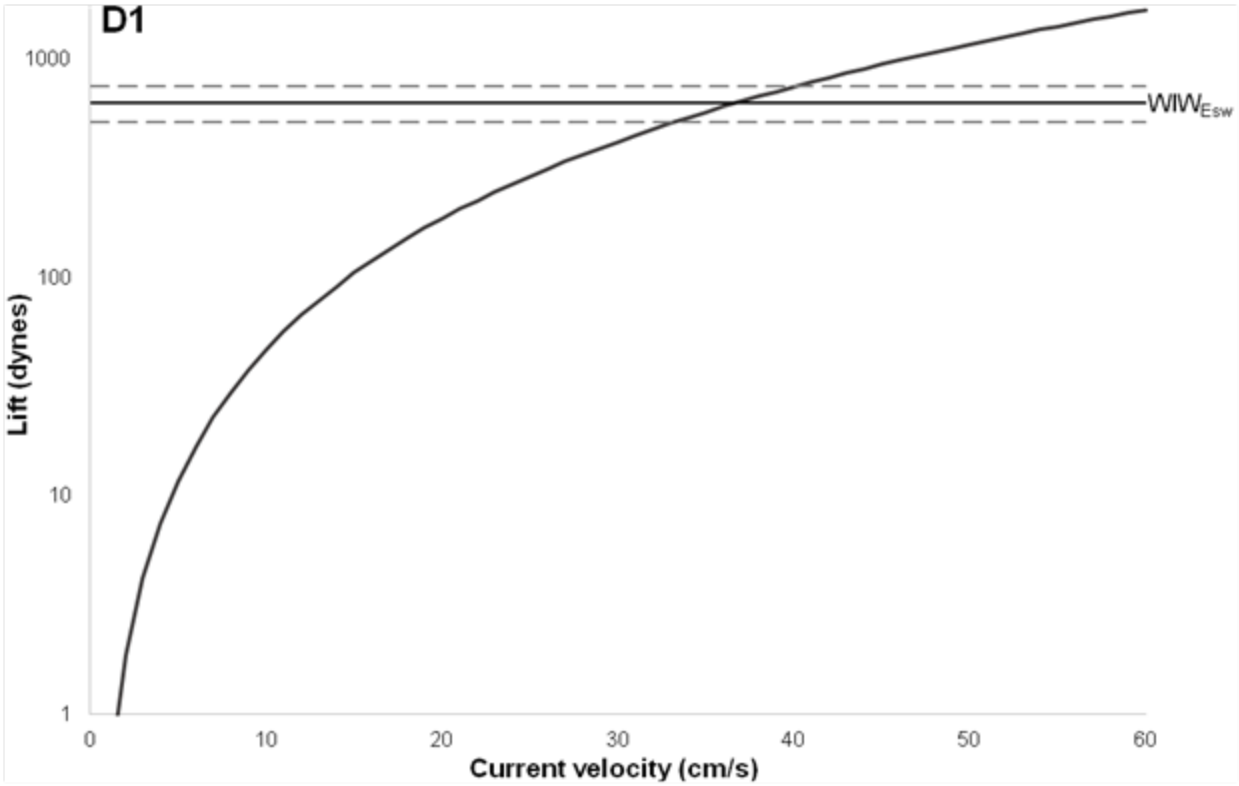

Figure III.8: Lift generated by D1 under the kite model plotted as log. Under the kite model, the crinoid's morphology (surface area of outstretched arms, arm number *SA_{Arm}), the coefficient of lift (constant, based upon the solidity of the crown, C_L), and the density (constant) and the fluid's velocity all influence lift (See Equation III.3 for constants and details). Lift was calculated for a range of current velocities, from 0 to 60 cm/s, with SA_{Arm} based upon the dimensions of individual D1. To achieve an upright posture, lift must be greater than or equal to a given crinoid's weight in water (WIW). The value of WIW_{Esw} for D1 (thin black horizontal line) is shown here with its 95% CI (light grey dashed lines).

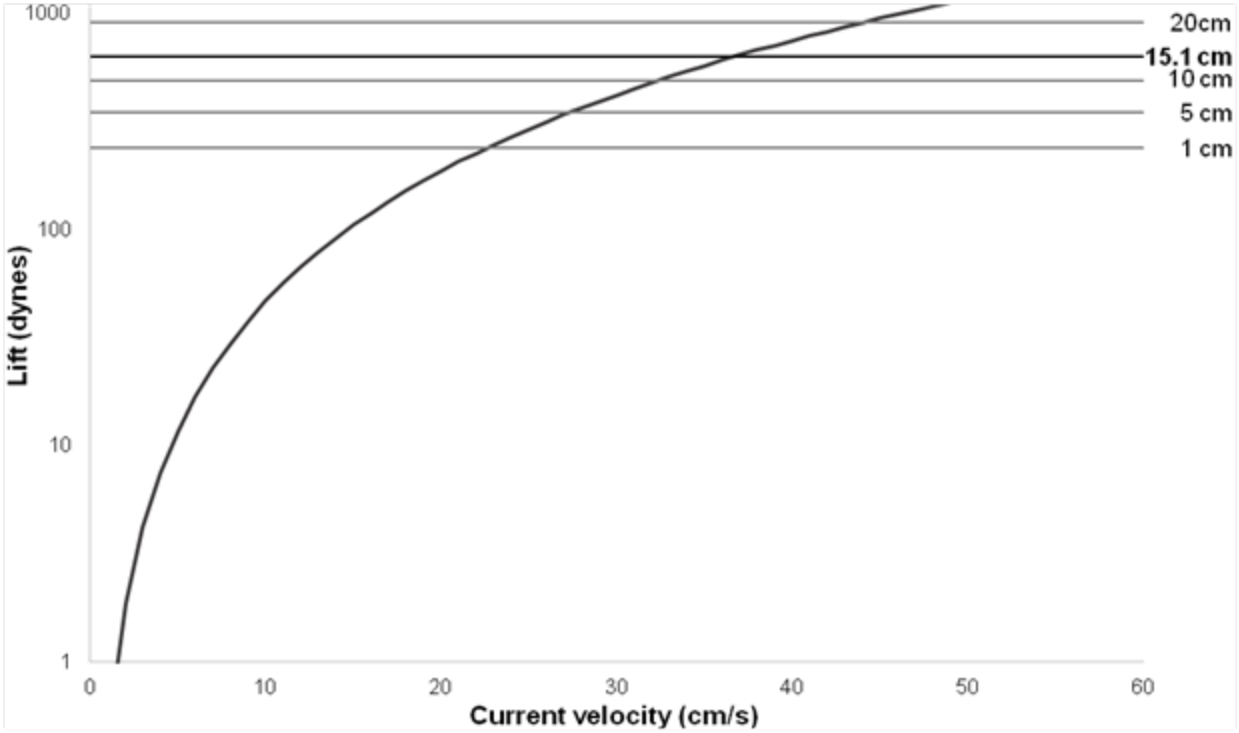

Figure III.9: Lift force generated for a range of current velocities, from UC = 0 to 60 cm/s, with SA_{Arm} based upon the dimensions of individual D1. The WIW_{Esw} to lift 1, 5, 10, and 20 cm of stalk are shown as horizontal gray lines. The WIW_{Esw} to lift 15.1 cm of stalk, the length of D1's stalk, had lifted by the return visit, is represented by a horizontal black line. Current velocities in excess of 30 cm/s would be necessary to produce sufficient lift for any stalk length over ~5 cm, and in excess of 20 cm/s for even 1 cm of stalk. Lift is plotted as log.

Figure III.10: Thrust force produced for D1 as calculated via the swimming model. Under the swimming model, thrust force (F_T) is equivalent to the vertical drag, D_V, produced during power stroke of the crinoid's arms, and the average $\bar{D}_V$ must be equal to or greater than the given individual's weight in water (WIW). The size of the paddle influences the thrust force (SA_{Arm}, and the coefficient of drag C_D, based upon arm solidity) while performing the power stroke (SA_{Arm}, and the coefficient of drag C_D, based upon arm solidity) and how rapidly the crinoid completes the stroke. Estimates of C_D were based upon measurements of the arm's filter and experimental results (Baumiller 1993), set at 0.22. Arm movements of *Democrinus* sp. were observed and recorded on numerous occasions, and while the reason for this behavior is unknown, they provide data to estimate the start angle, α (~30°) relative to vertical and the angle subtended during the movement, θ (~80°) (See Equation III.4, Appendix A, Part 2 for expanded details on obtaining $\bar{D}_V$). The values of WIW_{Esw} for D1 isare shown with its 95% CI (light grey dashed lines). The model assumes that all five arms move together, behavior not seen in any living crinoid (feather stars move approximately half of their arms up and half down at any given time). F_T is plotted on a log axis.

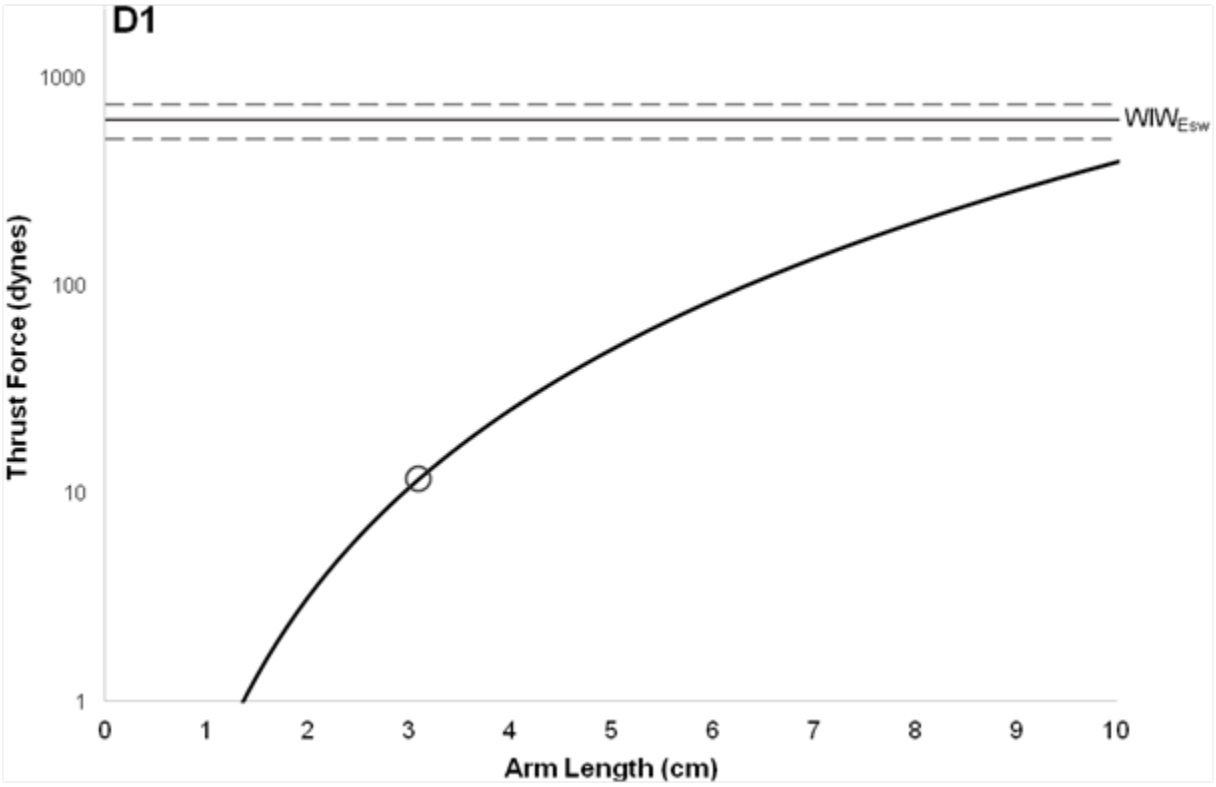

Figure III.10 A: Thrust force plotted against arm length. Assuming the fastest observed speed for a complete power stroke, 1.1 seconds, F_T was calculated for arm lengths between 0.01 cm and 10 cm. A circle (o) denotes the smallest arm length measured (individual D1), and where it falls on both the SA_{Arm} range. WIW_{Esw} is for D1. The thrust the arms produced was far below that necessary for the crinoid to achieve an upright posture. Note, no *Democrinus* sp. with an arm length greater than 8 cm was measured.

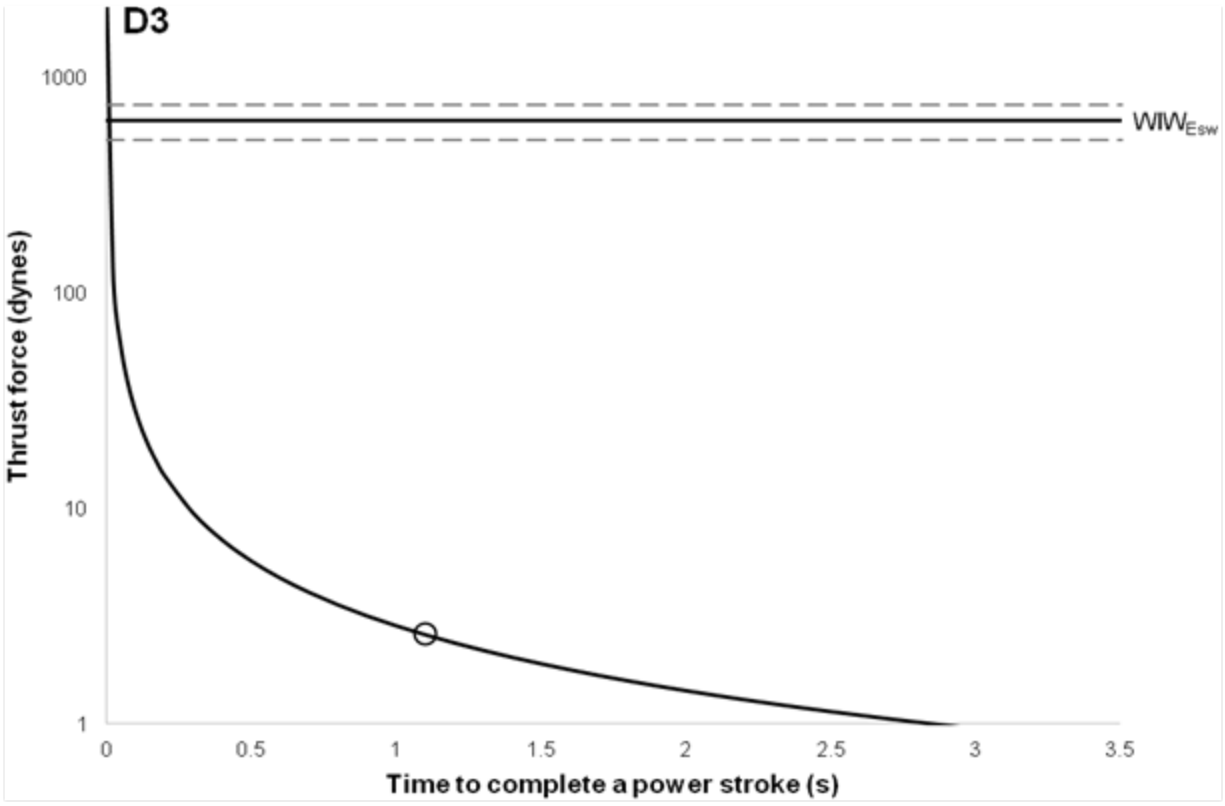

Figure III.10 B: Thrust force plotted against period of power stroke (time to subtend the 80°). Assuming the maximum arm length measured (D3), F_T was calculated for a range of periods, from 0.01 seconds (fastest) to 5 seconds (slowest). The period observed for *Democrinus* sp., 1.1 seconds, is marked by an open circle. The slowest stroke period that would generate sufficient thrust to overcome the crinoid's weight in water is approximately 0.05 seconds.

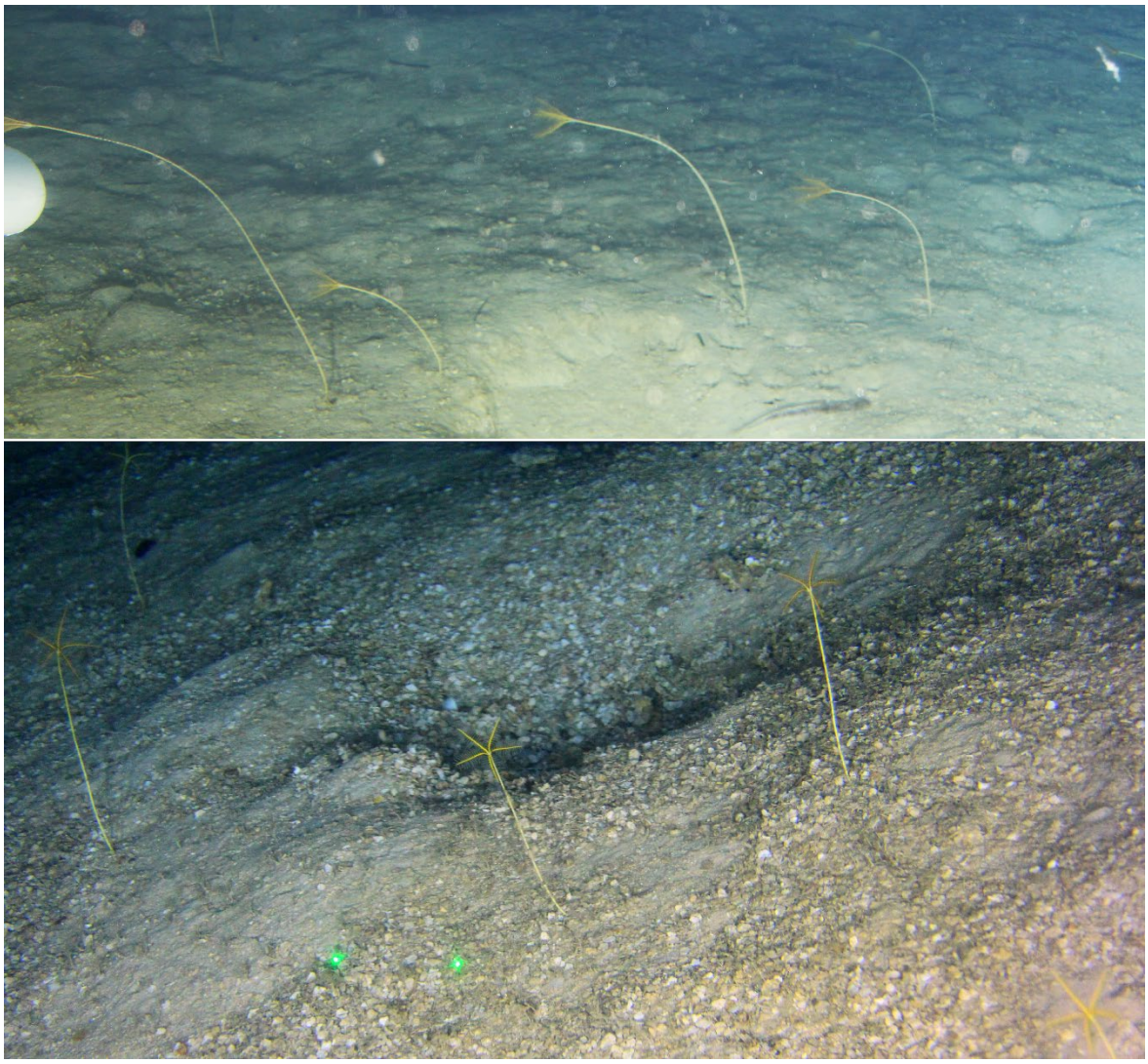

Figure III.11: *Democrinus* sp. in various current speeds. **Top:** May 19, 2016. Five *Democrinus* sp. with crowns in the low-drag postures, with tips facing down-current. Suspended particles of the substrate are visible in the upper portion of the photo. All of the *Democrinus* sp. stalks are bent down-current. The flow speed calculated using suspended particles was approximately 11 cm/s, with current direction approximately right to left. **Bottom:** December 15, 2016. *Democrinus* sp. in less than 2 cm/s current. The arms are outstretched, the long axes perpendicular to the current, and stalks are vertical. The current direction is approximately perpendicular to the plane of the photograph. Scale lasers are 10 cm apart.

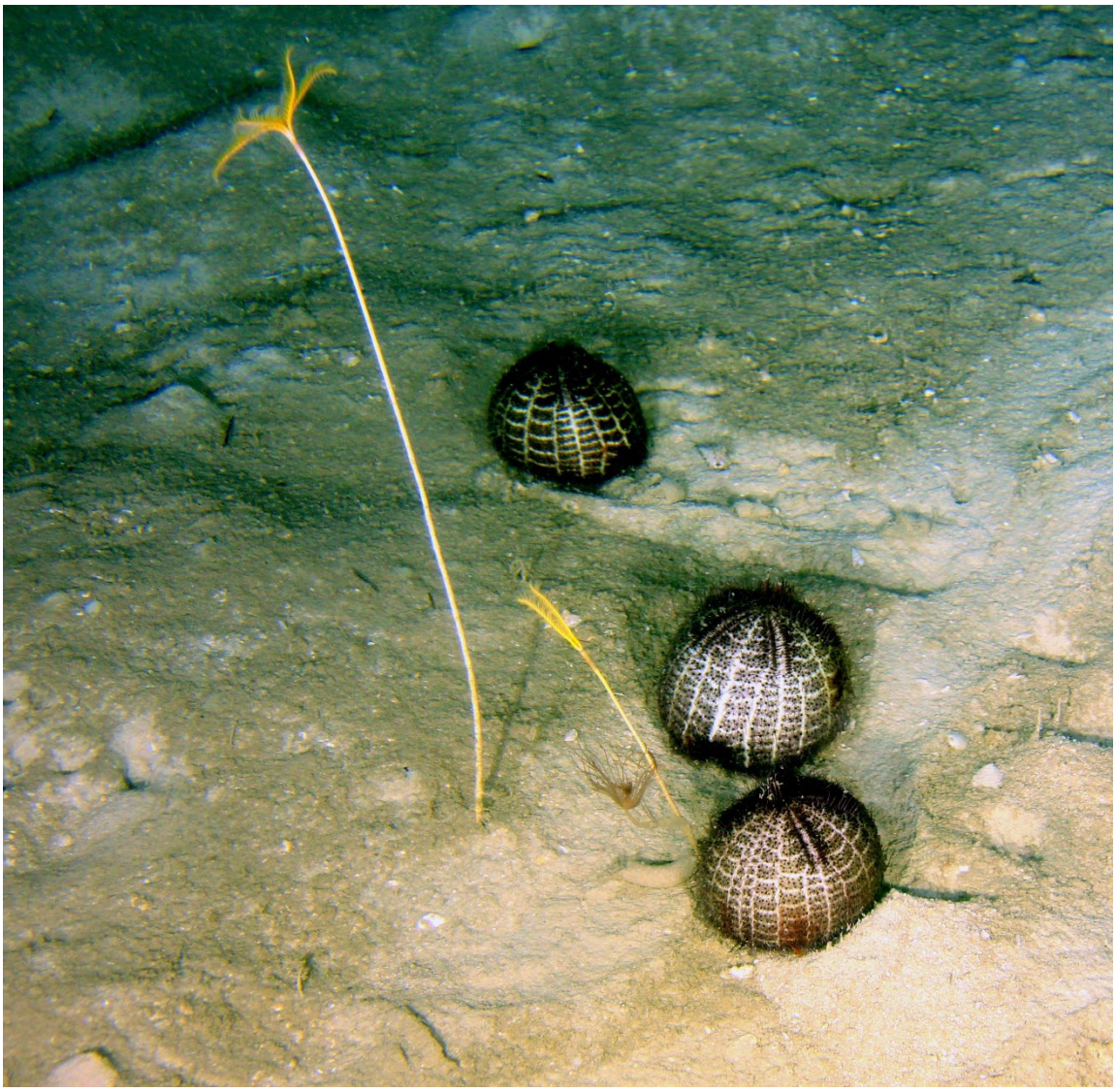

Figure III.12: Interaction between the echinoid, *Paleopneustes cristatus* (Agassiz, 1873), and *Democrinus* sp. (December 14, 2017). The echinoid appears to be pushing slightly against the visible stalk base, causing the individual to lean. However, no actual dislodgement was observed. Echinoids are approximately 10 cm in diameter.

CHAPTER IV *Democrinus newnamus*, a New Species of Stalked Crinoid (Crinoidea, Comatulida, Rhizocrinidae) from the Southern Caribbean Sea

ABSTRACT

Democrinus newnamus, a new species collected during submersible dives at depths of 230–300 m off the northwestern end of Isla Roatán, Honduras, is described. The new species is placed in the five-armed genus *Democrinus*, family Rhizocrinidae Jaekel, 1894, and is most similar to *Democrinus rawsonii*. It differs in: (1) having a significantly smaller ratio of the diameter of the central depression to cup diameter overall; (2) greater maximum size; (3) greater maximum width across the radial plates; (4) greater ratio of basal height to width, and (5) the first pinnule on Br7–Br9 rather than on Br5–Br7. A review of other species of *Democrinus* resulted in several amendments to the description of *D. rawsonii* and the genus as a whole.

INTRODUCTION

Previously, the xenomorphic stalk united all crinoids within the suborder Bourgueticrinina Sieverts-Doreck in Ubaghs, 1953. Molecular and morphological work over the past two decades has shown that this feature is a paedomorphic homoplasy (Cohen et al. 2004, Hemery et al. 2011, Rouse et al. 2012, Hemery et al. 2013, Roux et al. 2013), which prompted a reassessment of the clade at higher taxonomic levels (i.e., family and above). This reassessment placed genus *Democrinus* Perrier, 1883 (Figure IV.1) in the recently resurrected family Rhizocrinidae Jaekel, 1894 (Roux et al. 2019, WoRMS Editorial Board 2022).

The change above is only the latest in the complex history of the genus *Democrinus*. The genus was synonymized initially with *Rhizocrinus* Sars, 1868 (Carpenter 1884) within a year of its original description (Perrier 1883), and was not reestablished for more than 20 years (A. H. Clark 1909). All *Democrinus* have xenomorphic stalks characterized by synarthrial articulations, five undivided arms (occasionally four or six), and conical or elongated and sub-cylindrical cups (Figure IV.1). As with many crinoids, arm characteristic are often key features in identifying species, but many *Democrinus* species are defined poorly in this respect. Individual *Democrinus* are delicate and fully articulated specimens in museum collections are rare: Most fossil *Democrinus* are represented only by cups and columnals, while living specimens collected by dredging are often few in number, damaged, and have arms that are broken or missing entirely.

Diagnosing species of *Democrinus* primarily using cup characters is complicated, as no single characteristic is unique to any of the species assigned to the genus. Instead, each species is identified by a suite of cup characters (Figure IV.1) that often vary widely within a species, as exemplified by *D. chuni* (A. M. Clark 1972); arm and stalk features are used rarely. A

consequence of the paucity of complete, undamaged specimens is that nearly every living *Democrinus* species has been synonymized and split at least once, sometimes more (see A. M. Clark 1972 for an overview of these issues, as well as A. H. Clark 1909, Gislén 1938, Gislén 1947, A. M. Clark 1977).

Currently, 12 living (Figure IV.2) (WoRMS Editorial Board 2022) and 4 fossil species (Hess 2011, Roux et al. 2019) are recognized within *Democrinus*. The use of Remote Operated Vehicles (ROVs) and submersibles in the last half-century has provided new collection methods that limit the damage dredging causes and has led to an increase in the number of specimens collected. While only a few species have been reassessed, the resulting data now allow more accurate taxonomic descriptions and detailed comparisons across species. These descriptions address several the taxonomic problems that arose from historical collection methods. Further, the diagnostic characters of five undivided arms and of synarthrial stalk articulations (Figure IV.1), are now thought to be convergent (Roux et al. 2013). Future studies are likely to lead to further rearrangement of species assigned to *Democrinus,* particularly if features such as the knobby processes on the arms (Mironov and Pawson 2014, Roux et al. 2019) are shown to hold phylogenetic value.

This chapter details recent work on a population of *Democrinus* studied off Roatán, Honduras via submersible (Figures IV.3, IV.4). Examination of submersible-collected specimens demonstrated that these *Democrinus* represent a new species, the first new species since 1973 (McKnight). This brings the number of extant species of *Democrinus* to 13. Here, I describe this new species and in addition, provide amended diagnoses for *D. rawsonii* and the genus *Democrinus*. I also show that several features used historically to diagnose species of *Democrinus* are problematic.

Physical and Biological Setting

Located ~60 km north of mainland Honduras, Isla Roatán is the largest island of Islas de la Bahia. Uplifted only recently (early Oligocene, Pindell and Barret 1990), Roatán is the surface-reaching part of the East-Northeast trending submarine Bonacca Ridge. The Ridge runs parallel to a major left-lateral transform fault system at the southern margin of the Cayman Trough (Figure IV.3 A, Holcombe et al. 1973, Pindell and Barret 1990, Rosencrantz and Mann 1991, Avé Lallemant and Gordon 1999). The location and formation of Roatán led to several unique features. Key among these is a northwestern oceanic barrier reef and a substantial drop-off that reaches depths greater than 500 meters quickly (Kornicker and Bryant 1967, Mehrtens et al. 2001).

The northwestern drop-off's topography is highly varied between 100–700 m. Near-vertical rock faces dominate the shallower sections before bottoming out to extensive slopes with unconsolidated sediment, rock faces, and slump blocks. Both feather stars and stalked crinoids live in environments below ~150 m. The study area is a sediment slope that extends from 185–300 m dominated by a population of the new species of *Democrinus* (Figure IV.3 B) that numbers in the thousands. The sediment consists primarily of silt-sized particles and sedimentation rates are low, while flow events greater than 15 cm/s are rare (see Chapter III discussion section for more details). The study area lacks any other notable populations of either epifaunal or pelagic organisms, other than scattered unidentified anemones, small (< 3 cm long) spider crabs found on many of the *Democrinus,* and small (< 20) roving groups of the echinoid *Paleopneustes cristatus* Agassiz, 1873.

Democrinus is found widely across the sediment slope from 200–300 m, with the largest densities of up to 9 individuals per m^2 between 215–260 m. As one approaches the edges of the

depth range, individuals become more scattered. *Democrinus* typically holds its stalk vertical or slightly bent; rare individuals appear lying prone on the substrate. Under current velocities < 7 cm/s, most individuals extend their arms in the characteristic feeding posture of stalked crinoids, a parabolic fan with arms splayed out, long axes perpendicular to, and tips recurved into the current (Figure IV.4). At higher current velocities, individuals begin to collapse their arms parallel to the flow, with tips oriented down-current. Regenerating arms are frequent (~ 18% of individuals), most likely attributable to injuries from predators (Veitch and Baumiller 2021).

METHODS

We accessed this study area using the submersible *Idabel,* owned and piloted by Karl Stanley and based at the Roatán Institute of Deepsea Exploration, West End, Roatán, Honduras. We conducted eight expeditions over five years (2012–2017), with 16 separate dives spanning different seasons (May–June, October–December). We documented each visit using digital video and SLR cameras synchronized with external strobes via *Idabel*'s 76 cm diameter viewport. Lasers mounted externally (two placed 10 cm apart) and internally (3, each placed 2 cm apart) on a flat viewport provided scale in the media collected. In May 2015, we marked a site at 240 m and another at 260 m in depth, using weighted bags equipped with neon-yellow floats, and revisited them on the four following expeditions.

We attached a 5 cm PVC pipe provided with suction from *Idabel*'s thrusters to collect nine *Democrinus* individuals on four separate occasions (Table IV.1). Collection depths were approximated for six of the nine individuals, as the sampling sometimes involved several individuals collected at slightly different depths. We recovered three complete crowns (unattached to a cup) and two arms (up to the 12^{th} and 15^{th} brachials); the remainder of the material collected consisted of cups with the stalk attached and portions of the rooting structures.

The *Democrinus* collected were examined in the lab using a binocular microscope and compared with known species of *Democrinus*. Table IV.2, and Figures IV.5 and IV.6 show the characters used for this study, while Figure IV.7 shows other *Democrinus* cup features mentioned in this study.

Additional material examined included published descriptions, photographs and diagrams, photographs of specimens provided by colleagues and by the National Institute of Water and Atmospheric Research (NIWA), specimens from C. G. Messing's personal collection at Nova Southeastern University (abbreviated herein as NSU-CGM), and specimens on loan from the Harvard Museum of Comparative Zoology (MCZ). Appendix B summarizes the details of the additional material examined, including the collection site and date, accession number, institution where housed, and any additional notes. An overview of that material is as follows:

Democrinus aoteanus McKnight, 1973: 21 specimen photographs from NIWA that V. Sadie Mills, NIWA invertebrate collection manager, took under a dissecting scope by. Holotype description and photograph from McKnight 1973.

Democrinus brevis A. H. Clark, 1909: 221 specimens from NSU-CGM; 1 photograph of the holotype C. G. Messing took in 2012.

Democrinus cabiochi Roux, 1976: 1 photograph of the holotype, available online from the Muséum national d'Histoire naturelle (MNHN-IE-2013-10100); original description from Roux, 1976.

Democrinus chuni Döderlein, 1907: 1 specimen from MCZ; plates of 13 individuals in Döderlein, 1912; photographs of 3 specimens (Gislén 1937), and diagrams of 3 specimens from A. M. Clark, 1972.

Democrinus conifer A. H. Clark, 1909: 35 specimens from NSU-CGM; 1 photograph of the holotype C. G. Messing took in 2019; the latter synonymized *Rhizocrinus robustus* (Gislén 1938) original description's measurements from A. H. Clark 1909.

Democrinus japonicus Gislén, 1927: 2 specimens from MCZ; 4 diagrams, including one of the holotype and 25 descriptions/measurements from Gislén 1927.

Democrinus nodipes Döderlein 1907: 1 diagram and 2 individuals from plates and measurements from Döderlein 1907.

Democrinus parfaiti Perrier, 1883: 1 specimen from MCZ; holotype description from Perrier, 1883; diagrams of 2 individuals from Carpenter, 1884 and 2 from A. M. Clark, 1977.

Democrinus rawsonii Pourtalès, 1874: 4 syntypes and 17 specimens from MCZ; 4 specimens from NSU-CGM; diagrams of 1 individual from Pourtalès, 1874, and 1 from A. H. Clark, 1915; the original descriptions' measurements from A. H. Clark, 1909 for one of the syntypes and the later synonymized *R. sabae*.

Democrinus weberi Döderlein, 1907: plates and measurements of 8 individuals from Döderlein 1907.

Neither *D. globularis* Gislén, 1925 nor *D. poculum* Döderlein, 1907 were examined quantitatively, as the placement of both species in *Democrinus* is in doubt. Both were moved to *Conocrinus* (Roux 2002, Roux et al. 2019), but are still listed as *Democrinus* as of this paper (WoRMS Editorial Board, 2022).

Ontogenetic shape differences are reported in two species of *Democrinus*: *D. chuni* (Gislén 1938) and *D. japonicus* (Gislén 1927). Burnaby (1966) proposed a method of multivariate analysis that removes the effect of isometric growth, referred to as Burnaby's Back Projection Method (BBPM). BBPM provides accurate and unbiased estimates of between-group

differences, even when groups have many overlapping variables (Klingenberg 1996b, McCoy et al. 2006, Klingenberg 2016). Species with multiple similar variables and differing maximum heights, such as *D. newnamus* **n. sp.** and *D. rawsonii*, were compared using Principal Component Analysis (PCA) after BBPM was applied to the dataset. All analyses were carried out in R (R Core Team 2020).

RESULTS

Suborder Bourgueticrinina Sieverts-Doreck, 1953

Family Rhizocrinidae Jaekel, 1894

Genus *Democrinus* Perrier, 1883

Type species: *Democrinus parfaiti* Perrier, 1883.

Synonymy:

Democrinus Perrier, 1883: 450; A.H. Clark, 1917: 392; Gislén, 1938: 25; A.M. Clark 1977: 167–168; Rasmussen, 1978: T844; Hess, 2011: 149–151.

Rhizocrinus pars Carpenter, 1884: 245, A.H. Clark, 1909: 673–676.

Rhizocrinus (Bythocrinus) Döderlein, 1912: 11–14.

Bythocrinus A.H. Clark, 1917: 392.

Species Included:

Bourgueticrinus londinensis Forbes, 1852 (Ypresian), *Conocrinus elongatus* Roux, 1978a (Bartonian), *Democrinus simmsi* Ciampaglio, Donovan, and Weaver, 2007 (Middle-Upper Eocene), *Democrinus* sp. Roux et al. 2019 (Danian). Extant species: *D. aoteanus* McKnight, 1973; *D. brevis* A. H. Clark, 1909; *D. cabiochi* Roux, 1976; *D. chuni* Döderlein, 1907; *D. conifer* A. H. Clark, 1909; *D. globularis* Gislén, 1925; *D. japonicus* (Gislén 1927; *D.*

nodipes Döderlein, 1907; *D. parfaiti* Perrier, 1883; *D. poculum* Döderlein, 1907; *D. rawsonii* Pourtalès, 1874, and *D. weberi* Döderlein, 1907. See also Figure IV.2.

Emended diagnosis: Crinoids with xenomorphic stalks as adults characterized with synarthrial articulations, conical or elongated and sub-cylindrical cups, and five undivided arms (occasionally four or six) (see Figure IV.1 for example *Democrinus* overview). Stalk columnals distal to the 4–8 proximal columnals show *Conocrinus*-type synarthries (Roux et al. 2019), with the figure-8 ligament depression (Figure IV.1 B) that increases in size more distally along the stalk, and extends often over two-thirds or more of the articular facet before the attachment structure. The synarthries on proximal and distal facets of each columnal rotate between 60° to 90° relative to each other (mean angle of rotation appears to be species dependent) (Figure IV.1 A). Sutures between basal and radial plates vary from highly visible to inconspicuous. The height of the basal circlet constitutes the majority of the cup height (Figure IV.1). The distal face of the radial circlet has muscular fossae with conspicuous upward curves that extend often over the inner portion of the interradial crest (Figure IV.7 A). The articular facets are as large as the distal radial width and lack any interradial process or thorn (Figure IV.7 A). The ratio of the central depression to the distal radial circlet diameter ranges from 0.20–0.60. Beginning with the first syzygy between Br1 and Br2, all brachials have articulations with a distinct trifascial pattern (Figure IV.7 B). When present, knobby processes appear at least by the upper portion of IBr2 (Roux et al. 2019). Tapering of the arms begins by Br5 (Figure IV.1), and the first pinnule is usually between Br4 and Br12.

Remarks: In *D. newnamus* **n. sp.**, the ratio of the diameter of the central depression to the cup diameter (CD:R_d) falls short of the expected 30–40% specified previously as diagnostic for the genus *Democrinus.* Instead, the ratio matches that of *Pseudoconocrinus* (Roux et al. 2019);

however, *D. newnamus* **n. sp.** lacks the conspicuous interradial crests and ten arms found in *Pseudoconocrinus*. Examination of this feature in several other living *Democrinus* species suggests that the CD:R_d range is larger than documented previously, as several specimens of *D. brevis*, *D. rawsonii*, and *D. japonicus* fall between 25–30%.

Roux et al. (2002) removed both *D. poculum* Döderlein, 1907 and *D. globularis* Gislén, 1925 from *Democrinus* and placed them within the genus *Conocrinus.* No justification was offered for reassigning *D. poculum*, but *D. globularis* was reassigned based upon the fact that it is known only from one specimen with extremely constricted proximal stalk columnals compared to the cup base (Figure IV.8 A) (Roux et al. 2019). If other specimens of *D. globularis* were found, and all had this feature, it would be reasonable to remove it from *Democrinus.* However, the presence of constricted proximal columnals compared to the cup base is found in several specimens of *D. brevis* and *D. chuni* (Figure IV.8). Abnormalities in cup shape are documented well in *D. chuni*, possibly due to different growth patterns (Döderlein 1912, A. M. Clark 1972), and this study found similar abnormalities in *D. brevis* (Figure IV.8 C). It may be that the constricted proximal columnals are merely another such abnormality; without additional specimens or additional features to distinguish *D. globularis* from other *Democrinus*, removing the species from *Democrinus* seems premature.

The position of the first pinnule is adjusted from Br4–Br8 to Br4–Br12. Döderlein (1912) originally reported *D. chuni* has the first pinnule on the 5th or 6th pair of brachials (i.e., on Br9/Br10 and Br11/12) on page 15: “Vom 5. oder 6. Armgliederpaar ab sind Pinnulä vorhanden,” and *D. baueri*, later synonymized with *D. chuni* (Gislen 1938), as the 8th brachial pair (i.e., Br16). Gislén (1938) later reported a single specimen of *D. chuni* he dredged off S.

Africa that had the first pinnule on Br8. A. M. Clark (1972) reported that two specimens collected during a voyage of the *Anton Bruun* had the first pinnule on Br8 and Br12.

Democrinus newnamus **n. sp.**

Etymology: It is currently a placeholder.

Holotype: The specimen is uncatalogued, current designation is November 2015 (Figure IV.9).

Diagnosis: Sub-cylindrical aboral cup, with 150–180% increase in width from the cup base to the widest point across the radial circlet (Figure IV.9 A). Radial height is 40–70% of the radial width and 50–80% of the Br1 height. The ratio of the diameter of the central depression to the cup diameter 20–30%. Br1 is rectangular in shape, with a height that usually reaches between 80–100% of its width. Four of the nine individuals had intact or partially intact arms, with the first pinnule between Br7 to Br9. No arms displayed either knobby processes or any tapering along the arm (Figure IV.9 B).

Characters and measurements for all nine specimens are listed in Table IV.3.

Description: The cups of the nine specimen collected ranged in height from 3.6–9.1 mm. In seven of the nine, the cups increase in width continuously from the base to the distal edge of the radial circlet. In specimens Dec 2016C and Dec 2016D, there is a slight hollowing or inward slope across the middle of the radials (Figure IV.10 A); however, it is not sufficiently abrupt to be considered a constriction (Figure IV.11; see also Discussion for the definition of a constriction in *Democrinus*). May 2014A appears to have a minimally extruding ring approximately 1/3 of the way up the basal plates; a similar feature has been noted in other species and is interpreted as representing healed breakage (Gislén 1927, Gislén 1947).

Unbroken arms of *in situ* specimens (n = 192) rarely exceeded 5 cm, although lengths of up to 7.2 cm have been recorded. The brachials are taller than wide until approximately Br5/Br6, where the trend reverses (Figure IV.9 B). Of 17 arms (3 complete crowns and 2 arms), one has the first pinnule on Br7, 13 on Br8, and four on Br9. The first pinnule appears to occur equally on the left or right arm side. The pinnules average 0.5 mm long and 0.1 mm wide, with the shortest at the base and tip of an arm, and the longest in the middle. Arm brachials after Br1 and Br2 are alternatingly joined by syzygy (such as between Br3 and Br4) and separated by muscular synarthries (Br4 and Br5).

Stalk length, including those in individuals *in situ* (n = 197), averaged approximately 17 cm; the longest stalk was 40 cm. The stalks of specimens collected averaged approximately 22 cm, possibly because many *in situ D. newnamus* **n. sp.** have sections of distal stalk laying along the sediment where they are not easily visible, which leads to an underestimate of the stalk length. The proximal columnals of the collected individuals had smaller diameters (1.3–1.6 mm), but for the majority of the stalk, ~85%, the diameters averaged 1.8 mm (Figures IV.4, IV.9 C). This is consistent with measurements of diameters taken from field photos where the laser scales were at the base of the stalk (n = 11, mean 2.0 ± 0.2 mm). The proximal columnals are shorter than wide until approximately the 4th or 5th columnal. The columnals reached a maximum height of 3.0 mm in the distal stalk, just proximal of the columnals before the attachment structure. The columnals are largely rectangular in shape when viewed in profile, and assume a faint hourglass shape only near the attachment structure, where the width at the center of the columnal is only 90% of the maximum width at the articulations (Figure IV.9 C). The fulcral ridges of the proximal and distal facets of each columnal are offset by ~60° (Figure IV.1 A). The attachment structure is a series of thin radices growing parallel at each articulation joint along a distal

portion of the stem, usually 2–6 cm long (Figure IV.9 D). These radices appear to branch only a few times, although the distal-most tips were not been observed as they broke off during collection.

Color: The arms are a bright yellow *in situ*, while the cup appears a more muted brown-yellow (Figures IV.3, IV.9, IV.10). The stalk is creamy to off-white (Figures IV.4, IV.9 C). After several years of storage in 70% ethanol, the arms fade to a color similar to the stalk.

Distribution: *D. newnamus* **n. sp.** is currently known only from depths of 200–300 m off the northwestern side of Isla Roatán, Honduras.

Remarks: *D. newnamus* **n. sp.** differs from other *Democrinus* most notably in a smaller ratio of the distal radial diameter to the width of the central depression (CD:R_d). Most other *Democrinus* have CD:R_d of 30–40%, with only a few specimens in any species less than 30% or more than 40%. All nine specimens of *D. newnamus* **n. sp.** examined had a ratio of 20–30%.

D. newnamus **n. sp.** resembles *D. rawsonii* most closely. Both species possess an elongated, sub-cylindrical cup (Figures IV.10, IV.12), a rectangular Br1 that is usually taller than wide, distal stalk columnals with a minimal hourglass shape, and arms which do not tapered (Figures IV.9, IV.13). As with other species of *Democrinus*, many characters overlap between the two species and diagnosis requires the use of several characters. Taken together, the following five characters distinguish *D. newnamus* **n. sp.** from *D. rawsonii***: (1)** the height to width of the radial plates of *D. newnamus* **n. sp.** never exceeds ~70%, while *D. rawsonii* ranges from 44% to 120%); (2) the location of the widest point of the cups (across the basal-radial suture or radial plates in *D. newnamus* **n. sp.**, across the basal plates in *D. rawsonii*); (3) location of the first pinnule (Br7 or higher in *D. newnamus* **n. sp.**, Br5 or Br6 and rarely Br7 in *D. rawsonii*); (4) the ratio of the CD:R_d (between 20–30% in *D. newnamus* **n. sp.**, approximately

30% in *D. rawsonii*); (5) Br1 height always greater than radial height in *D. newnamus* **n. sp.**, while it is between 0.8–1.7x as high in *D. rawsonii* (Table IV.4). Taken together, these characters are diagnostic.

Given the similarities, the overlap of diagnostic characters, and height differences (*D. rawsonii* maximum recorded as 7.1 mm and *D. newnamus* **n. sp.** reaching upward of 9 mm) the possibility that the differences observed represent different ontogenetic stages of a single species must be considered. Principal Component Analysis was used to evaluate the continuous characters of the species after the BBPM was applied (Burnaby 1966). The analysis showed separation between *D. newnamus* **n. sp.** and *D. rawsonii* (Figure IV.14). Further, while the sample size of the *D. newnamus* **n. sp.** collected was small (n = 9), all individuals with cup heights smaller than the maximum known cup height of *D. rawsonii* (< 7.1 mm) have their widest point across the radial circlet, while in all *D. rawsonii*, the widest point is across the basal circlet. In addition, the first pinnule on *D. newnamus* **n. sp.** appears typically on or distal to the Br7, while in *D. rawsonii*, it is never above Br6.

Additional biological notes: *D. newnamus* **n. sp.** often shows shortened or missing arms in the field (~18% of the population) that are attributed to predation (Veitch and Baumiller 2021). However, no signs of drilling or scratches, as seen in other extant and fossil *Democrinus* (Döderlein 1912, Gislén 1927, Jagt 1999), were found on any of the cups of the individuals collected.

Democrinus rawsonii Pourtalès, 1874

Synonymy: *Rhizocrinus sabae*: A. H. Clark 1909: 673–676.

Syntypes: MCZ 147. Four specimens, here referred to as MCZ 147 A, B, C, and D, were collected in 1871 off Barbados, at 13.151944 N, 59.6694 W, and a depth 146–220 m (Pourtalès 1874).

Emended diagnosis: The aboral cup is elongated and sub-cylindrical, with the widest point across the basal circlet, usually just below the basal-radial suture. Overall width of the cup increases < 30% from the width at the base of the cup. Radial plates are always wider than tall, Br1 is equal or greater in height than width (Figure IV.12). The central cup depression width to the distal radial circlet width is between 0.29–0.31 (n = 5). The arms lack knobby processes or tapering, and the first pinnule appears most often on Br5 and Br6, rarely on Br7.

Descriptions: Cup heights for *D. rawsonii* range from 3.0–7.1 mm (n = 20), with a mean height of approximately 4.3 mm. As with all *Democrinus*, the basal plates constitute most of the cup height, ~80%. In all specimens, the widest point of the cup is across the basal circlet. Some cups display a slight hollowing on the aboral side of the widest point that has been mischaracterized as a constriction (Döderlein 1912, Gislén 1938, 1947) (see discussion below on the definition of a constriction in *Democrinus*). In the most extreme examples of cups with this hollowing, the cup takes on a bulging rather than cylindrical shape (Figure IV.12 B, D).

Columnals are wider than high for the proximal 4–6 columnals, while more distal columnals are 1.5–2x higher than wide. The columnal height increases to reach nearly 4 mm at the distal end of the stalk just proximal to the attachment structure. The columnal diameter is relatively constant, with proximal columnals averaging 1.5 mm and those of the mesistele and dististele reaching 1.7 mm. The fulcral ridge rotates ~70° between the proximal and distal articular facets of each columnal. Individuals with both the *Knotted*-type and *Disk*-type attachment structures are present. (Figure IV.15).

Color: The cups are a light beige to dark brown (Figure IV.12), and the stalks are off-white, as are the arms (Figure IV.13). The latter may be attributable to fading as seen in the arms of other *Democrinus* stored in alcohol.

Distribution: Known to be from the Leeward Islands in the Eastern Caribbean, the Bahamas, and the northeastern Gulf of Mexico.

Remarks: Almost immediately after Pourtalès described *D. rawsonii* in 1874, Carpenter synonymized the species with *D. parfaiti* (1884). Apparently, in doing so, Carpenter did not examine the specimens Pourtalès collected and relied only on specimens collected during the *Challenger* expedition from nearby areas in the Caribbean. However, later examination revealed that Carpenter's specimens were *D. brevis* (A. H. Clark 1909), meaning that what Carpenter perceived to be *D. parfaiti* included three different species: *D. parfaiti*, *D. rawsonii,* and *D. brevis.* Although A. H. Clark split *D. brevis* and *D. rawsonii* from *D. parfaiti* once again in 1909, Carpenter's grouping affected the species assignment for *Democrinus* throughout the last century.

Since 1900, all "*D. rawsonii"* collected in northwest Africa and the Bay of Biscay have been reassigned to *D. parfaiti* (Gislén 1938, Roux 1977). A. M. Clark (1977), who examined specimens in the National History Museum in London (NHM) and assigned them previously to *D. rawsonii,* reassigned them all to either *D. brevis* or *D. parfaiti*. In fact, two specimens that currently appear in the NHM catalog and are listed as *D. rawsonii* are actually the designated holotype and paratype of *D. brevis.* Reassessment of the material examined in this study led me to conclude that 3 of the 22 bourgueticrinids labeled *D. rawsonii* (NSU-CGM: JSL2-3684, CRI-529, CRI-524) and 1 labeled *D. parfaiti* (MCZ: CRI-142) are more appropriately assigned to *D.*

brevis, as a comparison of these three species revealed significant differences between *D. rawsonii*, *D. brevis*, and *D. parfaiti*.

Both *D. rawsonii* and *D. parfaiti* possess cups of similar height and width (Perrier 1883, Pourtalès 1874, Gislén 1947). However, the sutures between the basals and radials are distinct in all specimens of *D. rawsonii* (Pourtalès 1874, Koehler 1909, Gislén 1938, Gislén 1947), while *D. parfaiti* undergoes a fusion of the basiradial sutures in all but the smallest specimens, as well as of the interradial sutures in the largest specimens (Gislén 1947). In addition, the ratio of the cup height to maximum cup width and the ratio of the maximum cup width to minimum cup width differs significantly between the two species (p-value = 0.0015 and 0.0043, respectively). Finally, while previous studies (Gislén 1938, 1947) have described a constriction in the basiradials or radials, none of the 22 *D. rawsonii* that I examined, including the 4 syntypes, had a constriction in the cup (Figure IV.11, see also Discussion for the definition of a constriction in *Democrinus* used here), while *D. parfaiti* always does.

D. rawsonii differs more obviously from *D. brevis* than *D. parfaiti* (see A. M. Clark 1977 for an extensive review, as well as A. H. Clark 1909, 1915, Gislén 1938, 1947). The most obvious difference is in the cup's shape: sub-cylindrical in *D. rawsonii*, conical in *D. brevis* (Figure IV.2). This is shown quantitatively in the difference between the ratio of cup height to maximum width (Ch:CWmx) for the two species. The cup of *D. rawsonii* has a Ch:CWmx never less than 1.6, which results in the sub-cylindrical shape, while in *D. brevis* that ratio is always less than 1.5, and some specimens even have cups wider than high (Ch:CWmx <1).

In addition, both *D. brevis* and *D. parfaiti* most commonly have their maximum cup width across the radial plates, while in *D. rawsonii*, it lies across the basal plates. *D.*

rawsonii also lacks the tapered arms found in both *D. brevis* and *D. parfaiti.* The former also has its first pinnule between Br5 and Br7, while the latter two have their first pinnules between Br7 and Br12.

In the original description of *D. rawsonii*, Pourtalès (1874) refers to the first and second brachial, Br1 and Br2, as the second and third radial, a nomenclature not used currently (Hess et al. 2011). This would place the location of the first pinnule on Br6 according to the original description, not Br4. Later authors continue to list *D. rawsonii* has the first pinnule on Br4, as Pourtalès (1874) indicated, without adjusting for the change in nomenclature. A review of four arms associated with the syntypes (MCZ 147 A, B, C, and D) found one first pinnule on Br5 and three on Br6, consistent with Pourtalès original description adjusted for the change in nomenclature for Br1 and Br2. Additional specimens reviewed (one crown and two detached arms) showed the first pinnule on Br6, and one case of an arm with the first pinnule on Br7.

Additional biological notes: No cup showed signs of healed breakage (Gislén 1927, Gislén 1947), drilling, or scratches, as seen in other extant and fossil *Democrinus* (Döderlein 1912, Gislén 1927, Jagt 1999). MCZ: CRI 148 has an unidentified epizoan on the distal portion of its stalk.

DISCUSSION

Cup constriction As a Diagnostic Characteristic in Democrinus

The presence of a constriction on the cup of *Democrinus* has historically been a defining character for several species (Perrier 1883, A. H. Clark 1909, 1915, Döderlein 1907, 1912, Gislén 1927, 1938, 1947, A. M. Clark 1977). However, the use of the character is problematic because different authors have defined this feature differently. For example, some authors have

considered a slight decrease in cup width followed by a gentle widening, as seen in the radial plates of *D. rawsonii* syntypes (Figures IV.11 C, 12 A), a constriction (Carpenter 1884, Döderlein 1912, Gislén 1938). Others, including Pourtalès (1883), A. H. Clark (1909), and A.M. Clark (1977), restrict the term to an abrupt wedge-shaped narrowing in the cup (Figure IV.11 B). I followed the latter definition in this study, and restricted the term to the wedge-shaped narrowing.

Additional problems related to using the cup constriction as a taxonomic character in *Democrinus* relate to its intraspecific variability. For example, Döderlein (1912) indicated that *D. chuni* has a cup constriction, although many of the specimens he assigned to the species that I re-examined lack it entirely; other studies also noted this (Gislén 1938, A. M. Clark 1972). The same is true for *D. conifer*, where a cup constriction is a diagnostic character, although some specimens lack the feature (A. H. Clark 1909, Gislén 1938). The location of the constriction on the cup, which has also been used as a diagnostic feature, is similarly variable. In *D. parfaiti*, the constriction can be found across the radials (Perrier 1883, Carpenter 1884, A. M. Clark 1977) or at the basiradial suture (Carpenter 1884, Döderlein 1912, Gislén 1947). Similarly, *D. chuni* is known to have the constriction across the radials (Döderlein 1912, A. M. Clark 1972), but in at least one specimen described, it is across the basals (A. M. Clark 1972). *D. conifer* was described from two specimens, one with the constriction across the radials, and the other at the basiradial suture; *Rhizocrinus robustus*, later synonymized with *D. conifer*, has the constriction in either the radials or basals (A. H. Clark 1909). Thus, the definition, presence, and location of a cup constriction requires further investigation to clarify its utility as a diagnostic trait in *Democrinus* species.

Attachment Structures in Democrinus

Although some species' descriptions use attachment type as a diagnostic character, in this study the evidence showed that the attachment type is highly variable and reflects the environment rather than phylogeny. *Democrinus* has three basic attachment types: a terminal Disk-type, a Knotted-type akin to the classic look of tree roots, and an extended series of Thread-type radices that grow out of the joints at each columnal where the articulation facets meet, in the distal-most few cm of stalk (Figure IV.15). Although several species are known only to exhibit a single type of attachment, these species have been described only from sites with similar substrate characteristics. Species collected at several sites with a range of substrates, such as *D. aoteanus, D. brevis*, *D. parfaiti,* and *D. rawsonii*, exhibit more than one attachment type, and *D. rawsonii* and *D. brevis* have representatives of all three (Figures IV.16, IV.17).

The Knotted-type and the Thread-type attachments are both known in *Democrinus* that live on soft-sediment substrates. For example, 36 individuals of *D. brevis* collected by the R/V *Bellows* off Elliott Key (NSU-CGM: Bellows) from soft-substrate sediments contained 8 intact attachment types: 6 had the Thread-type, and 2 the Knotted-type (Figure IV.17 A, B). An additional 11 specimens of *D. brevis* collected in the northern Gulf of Mexico in 1984 (NSU-CGM: CRI-553) included only 2 with intact attachment structures: a specimen with a *Disk*-type attachment and another with a Knotted-type that appeared to be partially cemented (Figure IV.17 C, D); however, the substrate where they were collected is not listed. Some fossils have reported the Knotted-type as a cementing holdfast associated with hard surfaces (Jagt and Donovan 2012), much like the Disk-type. No collections from a single locality containing both a Disk-type and a Thread-type have been reported, consistent with the former being associated only with hard substrates and the latter with loose sediments.

SUMMARY

Democrinus newnamus **n. sp.** from Roatán, Honduras, increases the number of known extant species of *Democrinus* to 13. *D. newnamus* **n. sp.** differs from other species of *Democrinus* by having: a ratio of the diameter of the central depression to overall cup diameter < 0.3; (2) the maximum cup width across the radial circlet; (3) radial plates wider than high; (4) Br1 height greater than radial height, and (5) the first pinnule on Br7–Br9.

Thus, the genus *Democrinus* is emended to include greater variation in the ratio of the central depression's diameter to cup diameter. The description for *D. rawsonii* is amended with the following: (1) the location of the widest point of the cup lays across the basal plates; (2) the width of the cup from the base to the widest point increases by < 30%; (3) the correct placement of the first pinnule is on Br5, Br6, or rarely Br7, and (4) the Disk-type attachment structure is not diagnostic for the species.

The constriction in the cups of *Democrinus* was discussed and restricting its use to "an abrupt wedge-shaped narrowing in the cup" is proposed. In addition, *Democrinus* attachment structures appear to be influenced environmentally and thus have little taxonomic use. Both the Thread-type and Knotted-type structures are associated with loose, soft sediments, while the Knotted-type and the Disk-type with hard substrates.

Acknowledgments

Specimens images and data for *Democrinus aoteanus* were provided by the National Institute of Water and Atmospheric Research Ltd (NIWA) Invertebrate Collection and were collected on various NZOI expeditions, voyage TAN0707 as part of Ocean Survey 20/20 Chatham/Challenger Biodiversity and Seabed Habitat Project, jointly funded by the former New Zealand Ministry of Fisheries, Land Information New Zealand, NIWA, and New Zealand Department of Conservation, and voyage TAN1308, a West Coast South Island fishing trawl survey conducted by NIWA and funded by the New Zealand Ministry for Primary Industries. Additionally, thank you to Sadie Mills from NIWA for photographing all the *D. aoteanus* used in this study.

Thank you to Adam Baldinger at the Museum of Comparative Zoology, Harvard University for the loan of 22 specimens of *D. rawsonii,* along with several *D. brevis*, and a *D. chuni.* All photographs of *D. rawsonii* presented in this chapter are ©President and Fellows of Harvard College.

Finally, a large thank you to Charles Messing, who provided over 300 specimens for this study from his own collections.

References

Agassiz A. 1888. Three cruises of the United States Coast and Geodetic Survey steamer ”Blake” in the Gulf of Mexico, in the Caribbean Sea, and along the Atlantic coast of the United States, from 1877 to 1880 (Vol. II). Bull Mus comp Zool Harvard Univ. 15:1–220

Amemiya S, Omori A, Tsurugaya T, Hibino T, Yamaguchi M, Kuraishi R, Kiyomoto M, Minokawa T. 2016. Early stalked stages in ontogeny of the living isocrinid sea lily *Metacrinus rotundus*. Acta Zool. 97(1):102–116

Avé Lallemant HG, Gordon M. 1999. Deformation History of Roatán Island: implications for the origin of the Tela Basin (Honduras). *In*: Mann P, editor. Caribbean basins. Sedimentary basins of the world, vol. 4. Elsevier Science, Netherlands. P. 197–218

Bather FA. 1899. A phylogenetic classification of the Pelmatozoa. Brit Assoc Advanc Sci. Report 1899:916–923

Burnaby TP. 1966. Growth-invariant discriminant functions and generalized distances. Biometrics. 22:96–110

Carpenter PH. 1884. Report upon the Crinoidea collected during the voyage of H.M.S. CHALLENGER during the years 1873–1876. Part I, General morphology with descriptions of the stalked crinoids. Rep. Sci. Results Explor. Voyage H.M.S. CHALLANGER. Zool. 11(32):1–442, 62 pls

Ciampaglio CN, Donovan SK, Weaver PG. 2007. A new bourgueticrinid (Crinoidea) from the Castle Hayne Formation (Eocene) of southeastern North Carolina, USA. Swiss J Geosci. 100(2):243–249 https://doi.org/10.1007/s00015–007–1221–5

Clark AH. 1909. Four new species of the genus *Rhizocrinus*. Proc U.S. Nat Mus. 36:673–676 https://doi.org/10.5479/si.00963801.36-1693.673

Clark AH. 1915. A monograph of the existing crinoids. Bull U.S. Nat'l Mus. 82(1):1–406, 17 pls

Clark AH. 1917. A revision of the recent genera of the crinoid family Bourgueticrinidae with the description of a new genus. J Wash Acad Sci. 7:388–392

Clark AM. 1973. Some new taxa of Recent stalked Crinoidea. Bull Brit Mus (nat Hist) Zool. 25 (7):267–288

Clark AM. 1977. Notes on deep-water Atlantic Crinoidea. Bull Brit Mus (nat His) Zool. 31(4):159–186

Cohen LC, Pisera A. 2016. Crinoid phylogeny: new interpretation of the main Permo-Triassic divergence, comparisons with echinoids and brachiopods, and EvoDevo interpretations of major morphological variations. Biol J Lin Soc. 120(1):38–53 https://doi.org/10.1111/bij.12868

Döderlein L. 1907. Die gestielten Crinoiden der Siboga-Expedition. Siboga Expeditie: uitkomsten op zoologisch, botanisch, oceanographisch en geologisch gebied, verzameld in Nederlandsch Oost-Indië (1899–1900). Leiden. 42:1–54, 23 pls.

Döderlein L. 1912. Die gestielten Crinoiden der deutschen Tiefsee-Expedition. Wissenschaftliche Ergebnisse der Deutschen Tiefsee Expedition auf dem Dampfer "Valdivia" 1898–1899. 17(1):1–34, 12 pls. G. Fischer, Jena

Forbes E. 1852. Monograph of the Echinodermata of the British Tertiaries. Palaeontographical Soc. London. 36

Gislén T. 1927. Japanese crinoids. Papers from Dr. Th. Mortensen's Pacific Expedition 1914-16. Videnskabelige Meddelelser fra det Dansk naturhistorisk Forening. 83(37):1–69

Gislén T. 1938. A revision of the Recent Bathycrinidae with a study of their phylogeny and geographical distribution. Lunds Universitets Årsskrift, Neue Folge. 34(10):1–30

Gislén T. 1947. The echinoderms collected by the “Skagerak” expedition in the eastern Atlantic 1946: Part 2 Crinoidea. Meddelanden Från Göteborgs Musei Zoologiska Avdelning. 117(10): 4–22

Haig JA, Rouse GW. 2008. Larval development of the feather star *Aporometra wilsoni* (Echinodermata: Crinoidea). Invertebr Biol. 127(4):460–469

Hemery LG, Roux M, Améziane N, Eléaume M. 2013. High-resolution crinoid phyletic inter-relationships derived from molecular data. Cah Biol Mar. 54:511–523

Hess H. 2011. Bourgueticrinina. *In*: Hess H, Messing CG, Ausich WI, editors. Treatise on Invertebrate Paleontology. Part T. Echinodermata 2 Revised. Crinoidea. Vol. 3. Univ. of Kansas Press, Lawrence. 146–158

Holcombe TL, Vogt PR, Matthews JE, Murchinson RR. 1973. Evidence for sea-floor spreading in the Cayman Trough. Earth Pl Sci Lett. 20: 357–371

Jaekel O. 1894. Entwurf einer Morphogenie und Phylogenie der Crinoiden. Sitzungsberichte der Gesellschaft Naturforschender Freunde zu Berlin. 101–121.

Jagt JWM. 1999. Late Cretaceous and Paleogene echinoderms, pt. 2. Crinoids. Scripta Geol. 166:59–255

Jagt JWM, Donovan SK, Deckers MM. 2012. Clustered bourgueticrinid crinoid holdfasts on late Maastrichtian echinoids from northeast Belgium and southeast Netherlands. *In*: Kroh A, Reich M, editors. Echinoderm Research 2010: Proceedings of the Seventh European Conference on Echinoderms. Göttingen, Germany. Zoosymposia. 7:81 – 90

Kjaer CR, Thomsen E. 1999. Heterochrony in bourgueticrinid sea–lilies at the Cretaceous/ Tertiary boundary. Paleobio. 25(1):29–40

Klingenberg CP. 1996b. Multivariate allometry. *In*: Marcus LF, Corti M, Loy A, Naylor GJP, Slice DE, editors. Advances in morphometrics. Plenum, New York. 284:23–49

Klingenberg CP. 2016. Size, shape, and form: concepts of allometry in geometric morphometrics. Dev Genes Evol. 226:113 –137

Koehler R, Bather FA. 1902. Gephyrocrinus grimaldii, crinoide nouveau provenant des campagnes de la PRINCESSE ALICE. Mém Soc Zool. France. 15:68–79

Kornicker L, Bryant W. 1967. Sedimentation on continental Shelf of Guatemala and Honduras. *In*: McBirney A, editor. Tectonic relationship of Northern Central America and the Western Caribbean, The Bonacca Expedition. Amer Assoc Petr Geol Mem. 11:244–257

Loriol P de. 1882. Description of a new species of *Bourgueticrinus*. J Cincinnati Soc. of Nat. Hist. 118(5)

McCoy MW, Bolker BM, Osenberg CW, Miner BG, Vonesh JR. 2006. Size correction: comparing morphological traits among populations and environments. Oecologia. 148:547–554

McKnight DG. 1973. Stalked crinoids from the New Zealand region. N. Z. O. I. Rec., Wellington. 1(14):199–210

Mironov AN and Pawson DL. 2014. A new species of Western Atlantic sea lily in the family Bathycrinidae (Echinodermata: Crinoidea), with a discussion of relationships between crinoids with xenomorphic stalks. Zootaxa. 3873(3):259–274

Mehrtens CJ, Rosenheim B, Modley M, Young RS. 2001. Reef morphology and sediment attributes, Roatán, Bay Islands, Honduras. Carbonates and Evaporites. 16:131–140

Pindell J, Barret S. 1990. Geological Evolution of the Caribbean Region: A plate-tectonic perspective. *In*: Dengo G, Case JE, editors. The Caribbean region: Geol Soc Am Geol N Amer. 405–432

Perrier E. 1883. Sur une nouveau Crinoide fixé, le *Democrinus parfaiti*, provenant des dragages du Travailleur. C. r. hebd. Séanc Acad Sci. Paris 96:450–452

Pourtalès LF de. 1874. On a new species of *Rhizocrinus* from Barbados. Mem Mus Comp Zool. Harvard 4(8):27–31, 5 pls.

Simms MJ. 1989. Columnal ontogeny in articulate crinoids and its implications for their phylogeny. Lethaia. 22(1):61–68

R Core Team. 2020. R: A language and environment for statistical computing. Vienna, Austria: R Foundation for Statistical Computing. URL https://www.R–project.org/

Rasmussen HW. 1978. Articulata. *In*: Moore RC, Teichert C, editors. Treatise on Invertebrate Paleontology. Part T. Echinodermata 2. Crinoidea. Geol. Soc. of Amer. Boulder, and the Univ. of Kansas, Lawrence. p. T58–T216

Rouse GW, Jermiin LS, Wilson NG, Eeckhaut I, Lanterbecq D, Oji T, Young C., Browning T, Cisternas P, Helgen LE, Stuckey M, Messing CG. 2013. Fixed, free, and fixed: the fickle phylogeny of extant Crinoidea (Echinodermata) and their Permian-Triassic origin. Mol. Phylogenet Evol. 66 (1):161–181 https://doi.org/10.1016/j.ympev.2012.09.018

Roux M. 1976. Découverte dans le Golfe de Gascogne de deux espèces actuelles du genre cénozoïque *Conocrinus*. C R Acad Sci. Paris. 283:757–760

Roux M. 1977. Les Bourgueticrinina (Crinoidea) recueillis par la Thalassa dans le Golfe de Gascogne : anatomie compare des pédoncules et systématique. Bull Mus Natn Hist nat Zool. 296:25–83

Roux M. 1978a. Les crinoïdes pédonculés (Echinodermes) du genre *Conocrinus* provenant de l'Eocène des environs de Biarritz. C R Acad Sci. Paris. 286:265–268

Roux M., Messing CG, Améziane N. 2002. Artificial keys to the genera of living stalked crinoids (Echinodermata). Bull Mar Sci. 70(3):799–830

Roux M, Eléaume M, Hemery LG, Améziane N. 2013. When morphology meets molecular data in crinoid phylogeny: a challenge. Cah Biol.Mar. 54:541–548

Roux M, Eléaume M, Améziane N. 2019. A revision of the genus *Conocrinus* d'Orbigny, 1850 (Echinodermata, Crinoidea, Rhizocrinidae) and its place among extant and fossil crinoids with a xenomorphic stalk. Zootaxa. 4560(1):51–84

Sieverts-Doreck H. 1953. Sous-Classe 4. Articulata J.S. Miller 1821. *In*: Ubaghs G, editor. Traité de Paléontologie, Classe des Crinoïdes. Masson, Paris. 3:756–765.

Tunnicliffe V, Roux M, Eléaume M, Schornagel D. 2016. The stalked crinoid fauna (Echinodermata) of the Molucca and Celebes Seas, Indonesia: taxonomic diversity and observations from remotely operated vehicle imagery. Mar Biodiv. 46:365–388 https://doi.org/10.1007/s12526-015-0369-x

Veitch MA, Baumiller TK. 2021. Low predation intensity on the stalked crinoid *Democrinus* sp. (Echinodermata), in Roatán, Honduras, reveals deep water as likely predation refuge. Bull Mar Sci. 97(1):107–128

WoRMS Editorial Board (2022). World Register of Marine Species. Available from https://www.marinespecies.org at VLIZ. Accessed 2022-03-02. doi:10.14284/170

Chapter IV TABLES

Table IV.1: Record of individuals of *Democrinus newnamus* **n. sp.** collected from Isla Roatán, Honduras. All individuals were collected via suction using a 5 cm PVC pipe attached to the *Idabel*'s thrusters. As the individuals could not be sorted before reaching the surface, in the case of detached crowns and multiple individuals, which individual the crown may have belonged to is unknown.

Number of collected individuals	Collection date (YYYY/MM/DD)	Collection method	Collection Depth (m)	Notes
2	2014/05/07	Suction	One at 230 One at 260	2 crowns collected, not attached
1	2015/11/22	Suction	~230	Two arms still attached when collected
2	2016/05/09	Suction	~230	No crowns collected
4	2017/12/16	Suction	245 - 260	One crown collected, not attached

Table IV.2: List of ratios used based upon characters measured. Location of measurement points shown in Figures 5 and 6.

Ratios	Abbreviation
Cup height:Cup width (max)	Ch:CWmx
Cup width (max):Cup width (min)	CWmx:CWmin
Basal height:Cup height	Bh:Ch
Basal height:Basal width (max)	Bh:BWmx
Basal width (max):Basal width (min)	BWmx:BWmin
Radial height:Radial width	Rh:RW
Basal width:Radial width	BW:RW
Basal height:Radial height	Bh:Rh
Cup width (max):Radial width	CWmx:RW
Primibrachial height:Primibrachial width	Brh:BrW
Primibrachial height:Radial height	Brh:Rh
Cup height:Primibrachial height	Ch:Brh
Central depression:Distal radial circlet diameter	CD:Rd
Distal columnal articulation facet diameter:Columnal midpoint width	ColAd:ColMW
Distal columnal height:Distal columnal width	Colh:ColMW

Table IV.3: Quantitative and discrete characters for the nine individuals of *D. newnamus* **n. sp.** collected from Roatán, Honduras during 4 separate visits. Abbreviations: RR = Radial plates, Rec = Rectangular, NP = Not present, N/A = Data not available.

Character	Dec 2017A	Dec 2017B	Dec 2017C	Dec 2017D	May 2016A	May 2016B	May 2014A	May 2014B	Nov 2015A
Location of Constriction (if present)	NP	NP	NP	NP	NP	NP	NP	NP	NP
Location of Cup max width	RR	RR	RR	RR	RR	RR	RR	RR	RR
Location of first pinnule	N/A	N/A	Br7*	N/A	N/A	N/A	Br8	Br8	Br7
Location of arm taper (if present)	NP	NP	NP	NP	NP	NP	NP	NP	NP
Shape of Br1	Rec	Rec	Rec	Rec	Rec	Rec	Rec	Rec	Rec
Cup height (mm)	7.9	9.1	6.3	8.8	5.6	6.6	7.4	3.6	4.3
Cup max width (mm)	2.4	2.6	2.6	2.1	2.3	2.5	2.4	2.2	1.7
Cup minimal width (mm)	1.5	1.4	1.7	1.3	1.4	1.6	1.4	1.3	1.3
Basal height (mm)	7.3	8.2	6.0	7.9	5.3	5.8	6.7	3.1	3.9
Basal max width (mm)	1.1	1.2	1.4	1.2	1.2	1.5	1.2	1.1	0.7
Basal minimal width (mm)	0.9	0.8	0.8	0.7	0.8	0.8	0.9	0.7	0.6
Radial height (mm)	0.7	0.9	0.6	0.8	0.7	0.9	0.9	0.7	0.6
Radial width (mm)	1.3	1.7	1.5	1.4	1.4	1.3	1.5	1.2	1.00
Br1 Height (mm)	1.4	1.2	1.2	1.1	1.2	1.2	1.1	1.0	0.9
Br1 width (mm)	1.5	1.3	1.4	1.2	1.4	1.4	1.3	1.2	1.0

Ratio of Cup max width to minimal width	1.7	1.8	1.6	1.7	1.6	1.5	1.7	1.3	1.4
Ratio of Cup height to cup max width	3.3	3.5	2.4	4.1	2.5	2.7	3.1	1.7	2.5
Ratio of Basal max width to minimal width	1.3	1.6	1.7	1.7	1.6	1.8	1.4	1.4	1.1
Ratio of Cup height to basal height	1.1	1.1	1.1	1.1	1.1	1.1	1.1	1.2	1.1
Ratio of Basal height to width	6.5	6.8	4.3	6.6	4.3	4.0	5.8	3.0	5.7
Ratio of Radial height to width	0.6	0.5	0.4	0.6	0.5	0.7	0.6	0.6	0.6
Ratio of Basal width to Radial width	0.9	0.7	0.9	0.9	0.9	1.1	0.8	0.9	0.7
Ratio of Basal height to Radial height	10.2	9.7	9.5	9.7	7.4	6.5	7.8	4.6	6.4
Ratio of Cup max width to Radial width	1.9	1.6	1.8	1.5	1.6	1.9	1.6	1.8	1.7
Ratio of Cup height to Br1 height	5.5	7.5	5.4	8.4	4.6	5.5	6.7	3.5	5.1
Ratio of Br1 height to Radial height	2.0	1.4	1.9	1.3	1.7	1.3	1.3	1.5	1.4
Ratio of Br1 height to Br1 width	0.9	0.9	0.8	0.8	0.9	0.8	0.8	0.8	0.8
Ratio of central depression width to Radial circlet width	N/A	0.2	0.3	0.3	0.3	0.2	N/A	N/A	0.2
Ratio of distal Columnal edge to center width	1.1	1.1	1.1	1.1	1.1	1.1	1.1	1.1	1.1
Ratio of distal Columnal height to width	2.1	2.0	2.0	2.1	1.9	1.7	2.1	1.6	2.0

*Only one crown of the four individuals collected in December 2017 survived collection. However this crown was detached, so was assigned arbitrarily to Dec 2017 C.

Table IV.4: Character measurements range from the minimum to the maximum value for *D. newnamus* **n. sp.** and *D. rawsonii*. *p*-values shown were calculated using an unpaired *t*-test and * indicates *p*-values < 0.05. *p*-values were not applied to discrete characters. Abbreviations: RR = Radial plates, BB = Basal plates, NP = Not present, N/A = Data not available.

Characters	*D. newnamus* (n = 9)	*D. rawsonii* (n = 18)	*p*-value
Location of Constriction (if present)	NP	NP	
Location of Cup max width	RR	BB	
Location of first pinnule	Br 7–9	Br 5–7	
Location of arm taper (if present)	NP	NP	
Shape of Br1	Rectangular	Rectangular	
Proximal columnals with width ≥ height	3–4	4–5	
Cup height (mm)	3.6–9.1	3.0–7.2	0.0011*
Cup max width (mm)	1.7–2.6	1.5–2.8	0.73
Cup minimal width (mm)	1.3–1.7	1.1–2.1	0.0071*
Basal height (mm)	3.1–8.2	1.1–2.1	0.00058*
Basal max width (mm)	0.7–1.5	0.7–1.6	0.15
Basal minimal width (mm)	0.6–0.9	0.5–1.3	0.0097*
Radial height (mm)	0.6–0.9	0.4–1.1	0.53
Radial width (mm)	1.0–1.7	0.7–1.4	0.14
Br1 height (mm)	0.9–1.4	0.5–1.3	0.049
Br1 width (mm)	1.0–1.5	0.7–1.3	0.034
Ratio of Cup height to cup max width	1.7–4.3	1.7–2.6	0.062
Ratio of Cup max width to min width	1.4–1.8	1.2–1.8	0.98
Ratio of Basal max width to min width	1.1–1.8	0.7–1.8	0.47
Ratio of Cup height to basal height	1.1–1.2	0.9–1.2	0.0009*
Ratio of Basal height to width	3.0–6.8	3.0–4.5	0.013*
Ratio of Radial height to width	0.4–0.7	0.4–1.2	0.0097*
Ratio of Basal height to Radial height	4.6–10.2	3.2–9.9	0.34
Ratio of Basal width to Radial width	0.7–1.1	0.8–1.7	0.0043*
Ratio of Cup max width to Radial width	1.5–1.9	1.6–3.9	0.000038*
Ratio of Br1 height to Radial height	0.8–0.9	0.6–1.1	0.085
Ratio of Br1 height to Br1 width	0.8–0.9	0.8–1.7	0.069
Ratio of Cup height to Br1 height	3.5–8.4	3.8–7.9	1
Ratio of central depression to distal Radial circlet diameter	0.2–0.3	0.3	0.0043*
Ratio of distal Columnal height to width	1.6–2.1	1.5–2.0	0.087

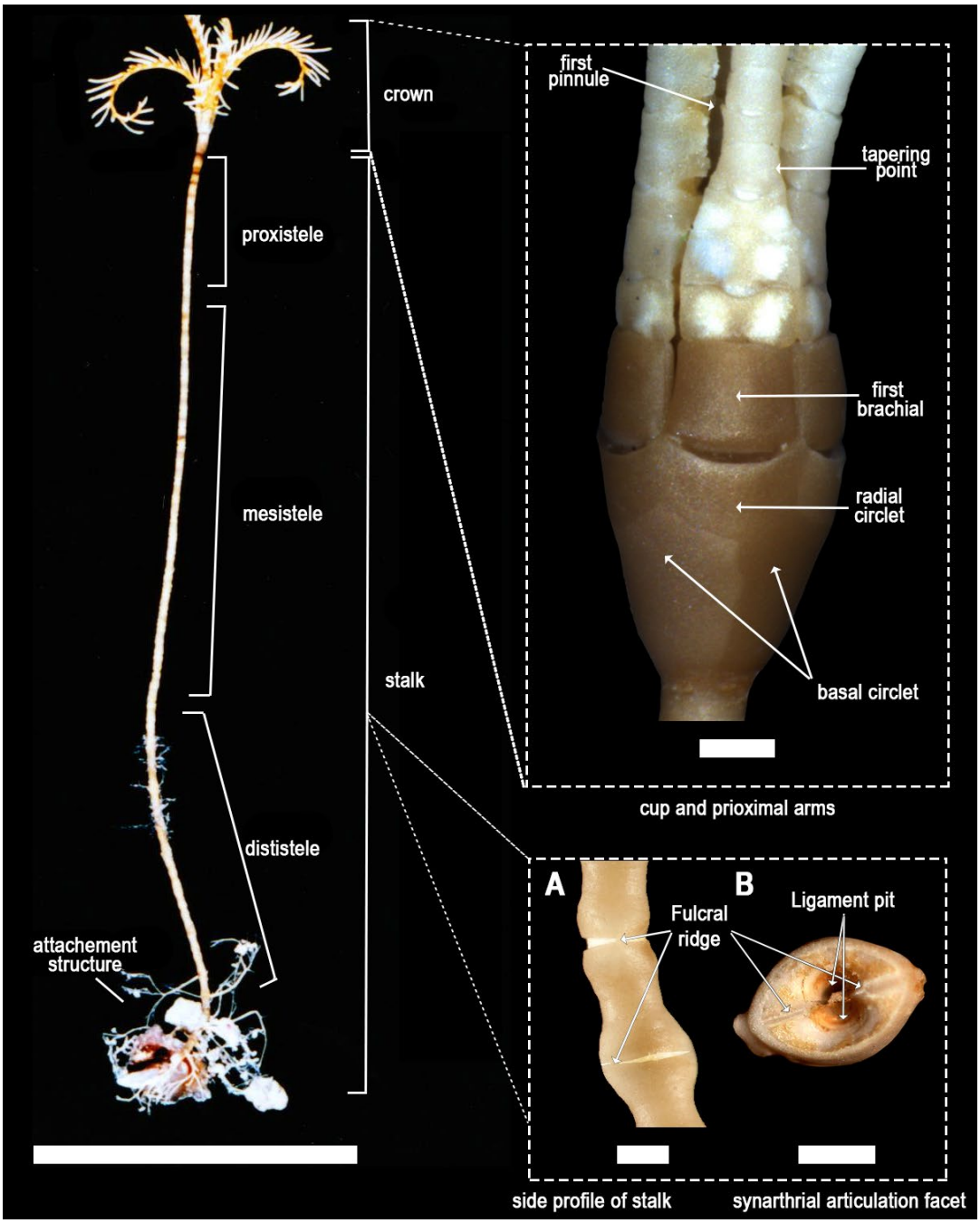

Figure IV.1: General overview of the features and terms used to describe the bourgueticrinid genus *Democrinus*. **Left:** Overview of an entire *D. brevis* (NSU-CGM: CRI-556) specimen showing crown, stalk and attachment structure. Scale bar: 5 cm. **Right:** ***(Top)*** Close up of a cup from *D. brevis*, showing cup details. Scale bar: 1 mm. ***(Bottom)*** **A:** Close up of a side profile of several stalk columnals from *D. brevis.* Note fulcral ridge ordination change between the proximal and distal synarthrial facets in the middle columnal. **B:** Close up of a synarthrial articulation facet from a *Democrinus newnamus* **n. sp.** (Dec 2016D) Scale bars: 0.1 mm.

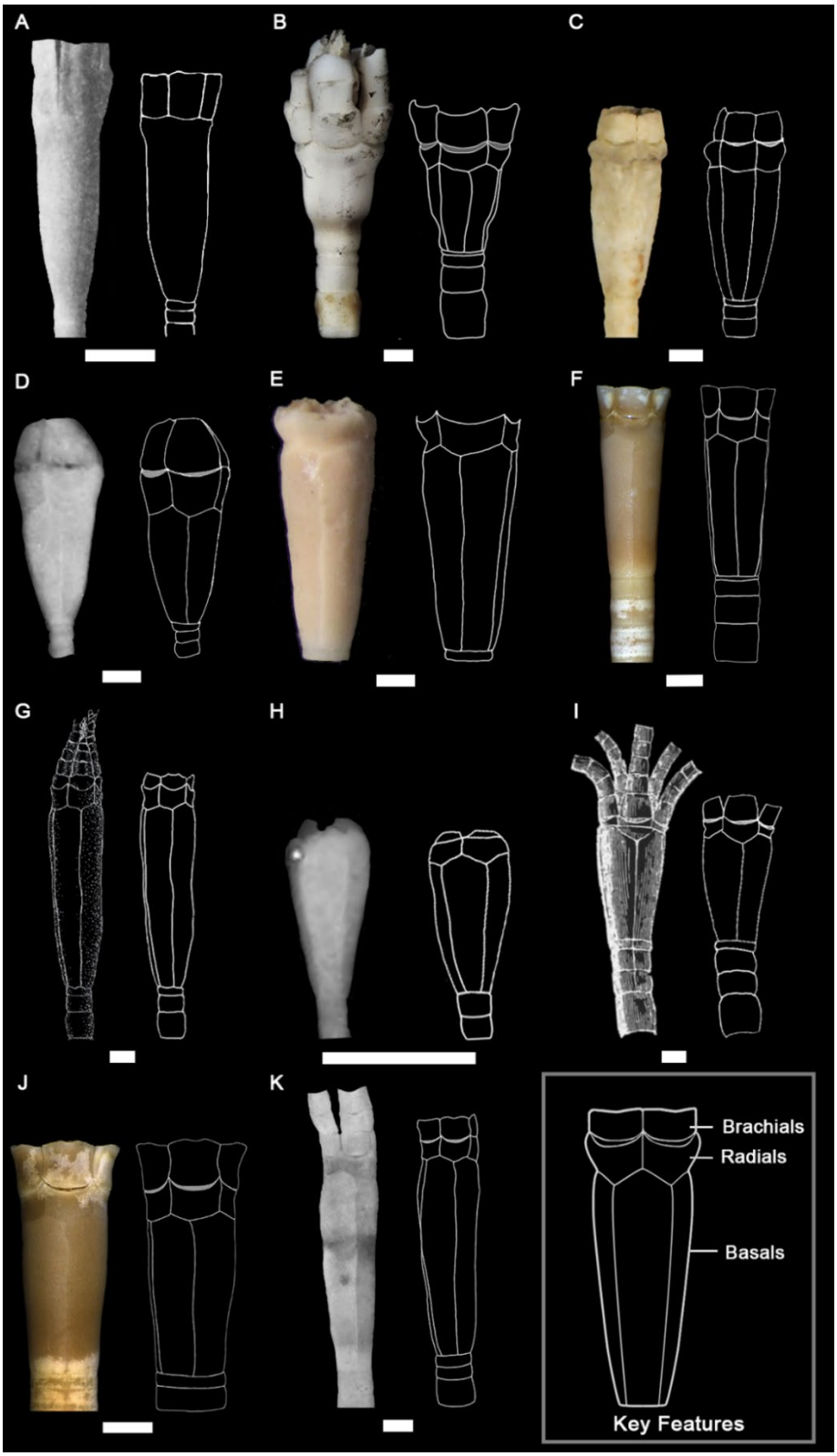

Figure IV.2: Collection of photographs and diagrams of the original holotypes (or syntype) for species in genus *Democrinus* and a schematic rendition for each. *D. poculum* Döderlein 1907 and *D. globularis* Gislén 1925 are excluded as there is uncertainty about their current placement within *Democrinus* (see Roux 2002, Roux et al. 2019). Diagrams and grayed photos are taken from the respective publication of

the holotype (i.e., *D. aoteanus* is from McKnight 1973). **A:** *D. aoteanus* McKnight, 1973. **B:** *D. brevis* Clark, 1909 (BMNH-846208), **C:** *D. cabiochi* Roux, 1976, **D:** *D. chuni* Döderlein, 1912, **E:** *D. conifer* Clark, 1909 (USNM 22679), **F:** *D. newnamus* **n. sp.** (November 2015), **G:** *D. japonicus* Gislén, 1927, **H:** *D. nodipes* Döderlein, 1907, **I:** *D. parfaiti* Perrier, 1883, **J:** *D. rawsonii* Pourtalès, 1874 (MCZ: CRI-147 D), **K:** *D. weberi* Döderlein, 1907. A key of the schematic characters drawn for each holotype is found in the bottom right. Scale bars: 1 mm.

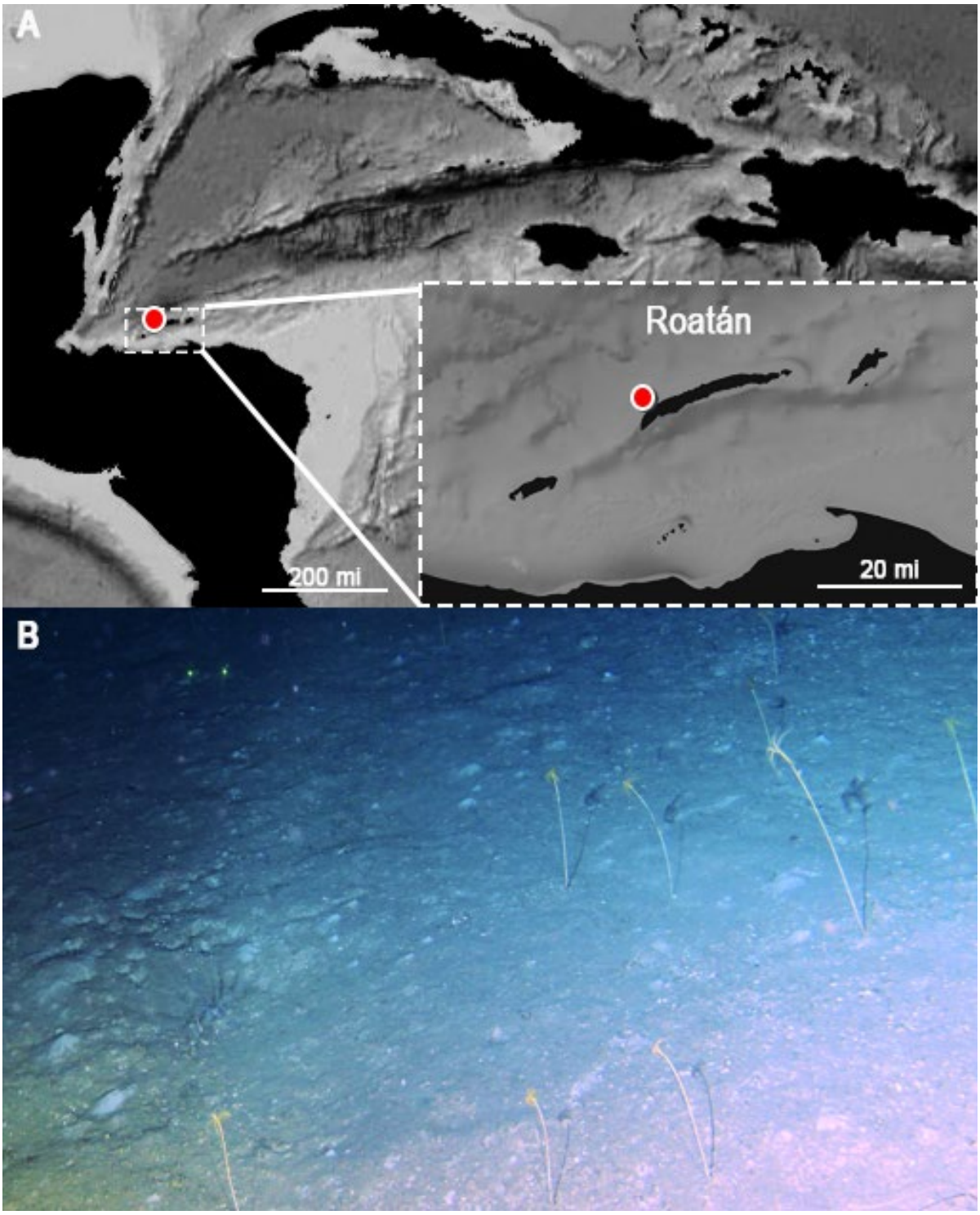

Figure IV.3: Type locality. **A:** Map of Roatán within the greater Caribbean Basin. A red dot represents the approximate location of the sediment slope off Roatán's West end. **B:** Habitat where *D. newnamus* **n. sp.** is found. The bourgueticrinids occupy the slope at depths between ~200–275 m and are found in densities up to 9 individuals per m^2. Green lasers are 10 cm apart.

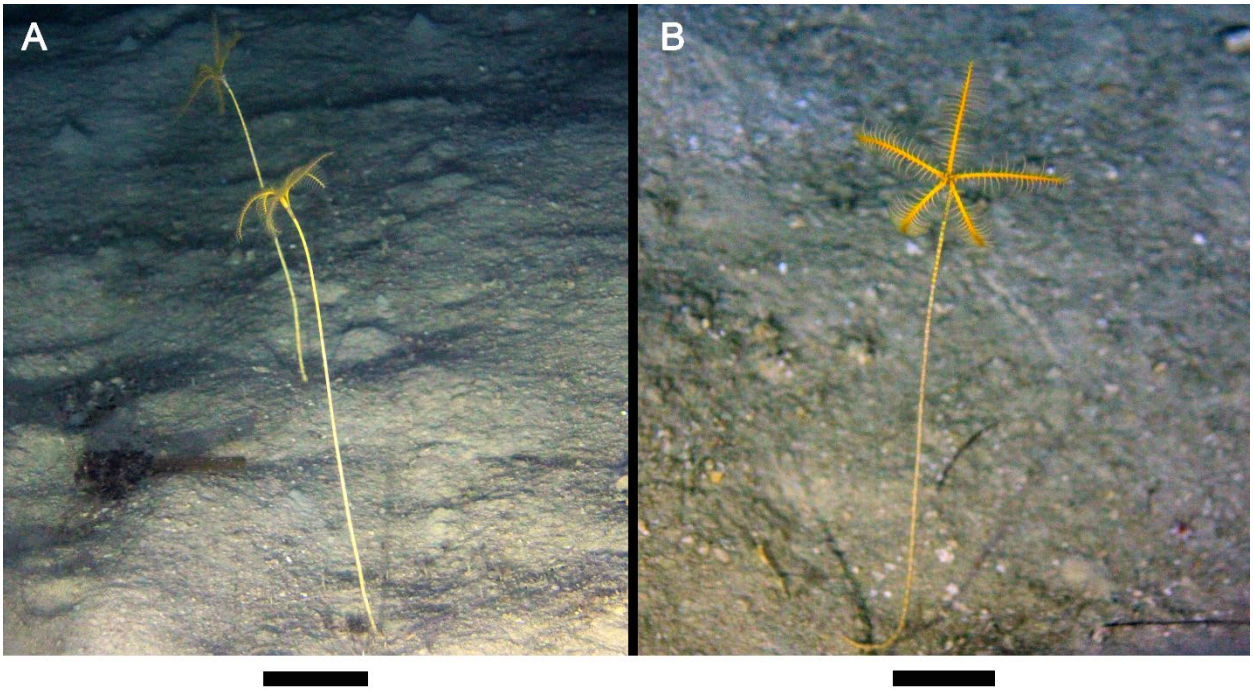

Figure IV.4: *In situ D. newnamus* **n. sp.** off Isla Roatán, Honduras. **A**: Side profile of two individuals, crowns held in a parabolic fan. **B**: Front profile of an individual. Note slightly recurved arms, with pinnules outstretched. Approximately 7 cm of the stalk is partially visible along the substrate where terminal radices root the crinoid in the sediment. Scale bars: 5 cm.

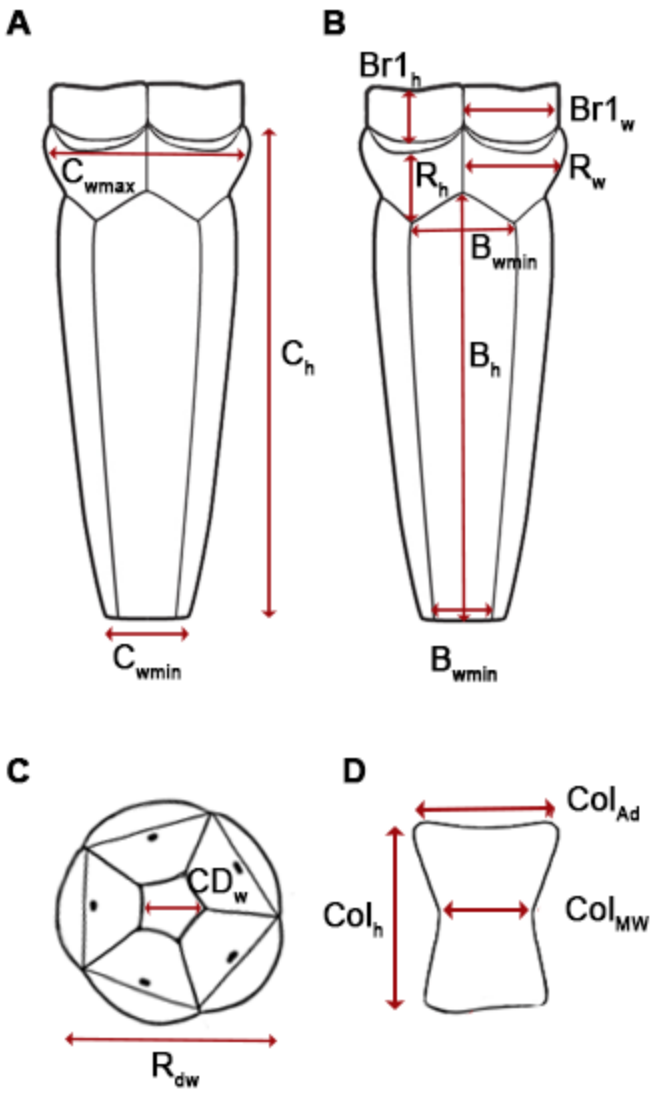

Figure IV.5: Schematics detailing the characters measured in this study. **A:** Cup measurements, including the height overall (C_h), maximum and minimum widths (C_{wmax}, C_{wmin}). **B:** basal measurements (B_h, B_{wmax}, B_{wmin}), radial measurements (R_h, R_w), and first brachial measurements (Br_h, Br_w). **C:** Overhead view of the distal radial circlet facet showing the central depression (CD) and radial circlet diameter (R_d). **D:** Measurements for distal columnal, including the height (Col_h), midpoint width (Col_{MW}), and articulation facet diameter (Col_{Ad}).

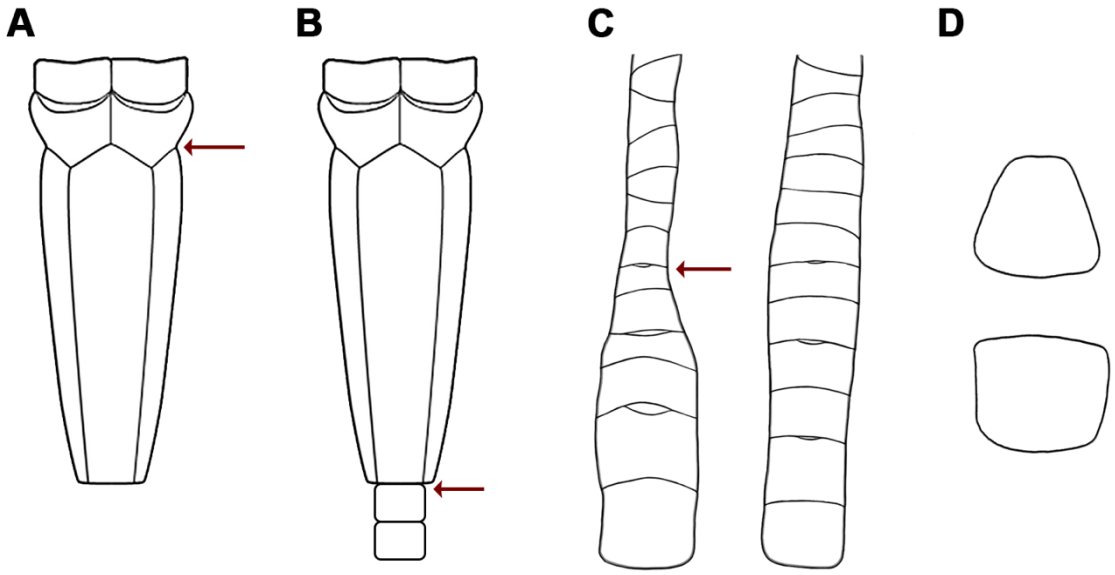

Figure IV.6: Schematics of discrete characters used in this study. **A:** *Democrinus* cup with a constriction. **B:** *Democrinus* cup with proximal columnals that exhibit a notably smaller width than the base of the cup. **C: (*Left)*** *D. brevis* arm diagram showing tapering beginning at Br5/Br6. Although all arms taper eventually, the rapid decrease in width by nearly 40% defines "tapering" as a character. **(*Right*)** *D. rawsonii* arm diagram showing no tapering. **D: (*Top*)** *D. chuni* Br1 diagram showing trapezoidal shape. **(*Bottom*)** *D. rawsonii* Br1 diagram showing rectangular shape.

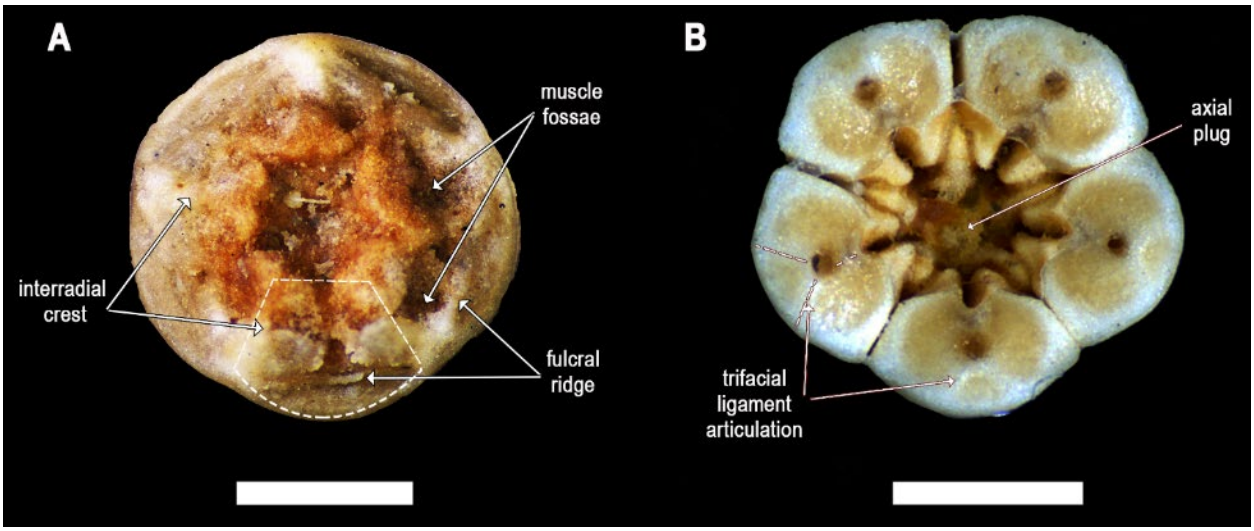

Figure IV.7: Characters on the distal surface of the aboral cup. **A:** Distal view of the aboral cup of *Democrinus rawsonii* (MCZ 147B). A single articulation facet is outlined; the fulcral ridge involved in arm movement, the muscle fossae, and the interradial crest are noted. **B:** Distal view of the aboral cup of *D. newnamus* **n. sp.** (November 2015, holotype) with Br1 still attached. The trifascial ligament articulation on the distal end of each Br1 that distinguishes genus *Democrinus* from *Rhizocrinus* is noted. Scale bars: 1 mm.

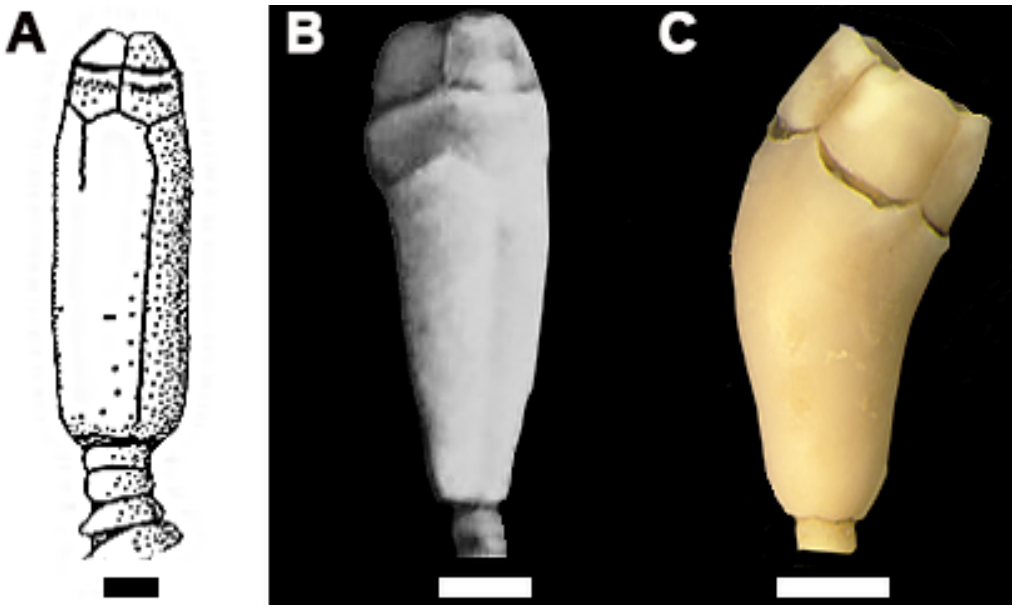

Figure IV.8: Individuals of *Democrinus* that exhibit extremely constricted proximal stalk columnals compared to the cup base. **A:** Diagram of *D. globularis* from Gislén 1925. **B:** *D. chuni* from Döderlein 1912 (plate 5, specimen 2). **C:** *D. brevis* that shows deformation and constricted proximal stalk (NSU-CGM: CRI-538). Scale bars: 1 mm.

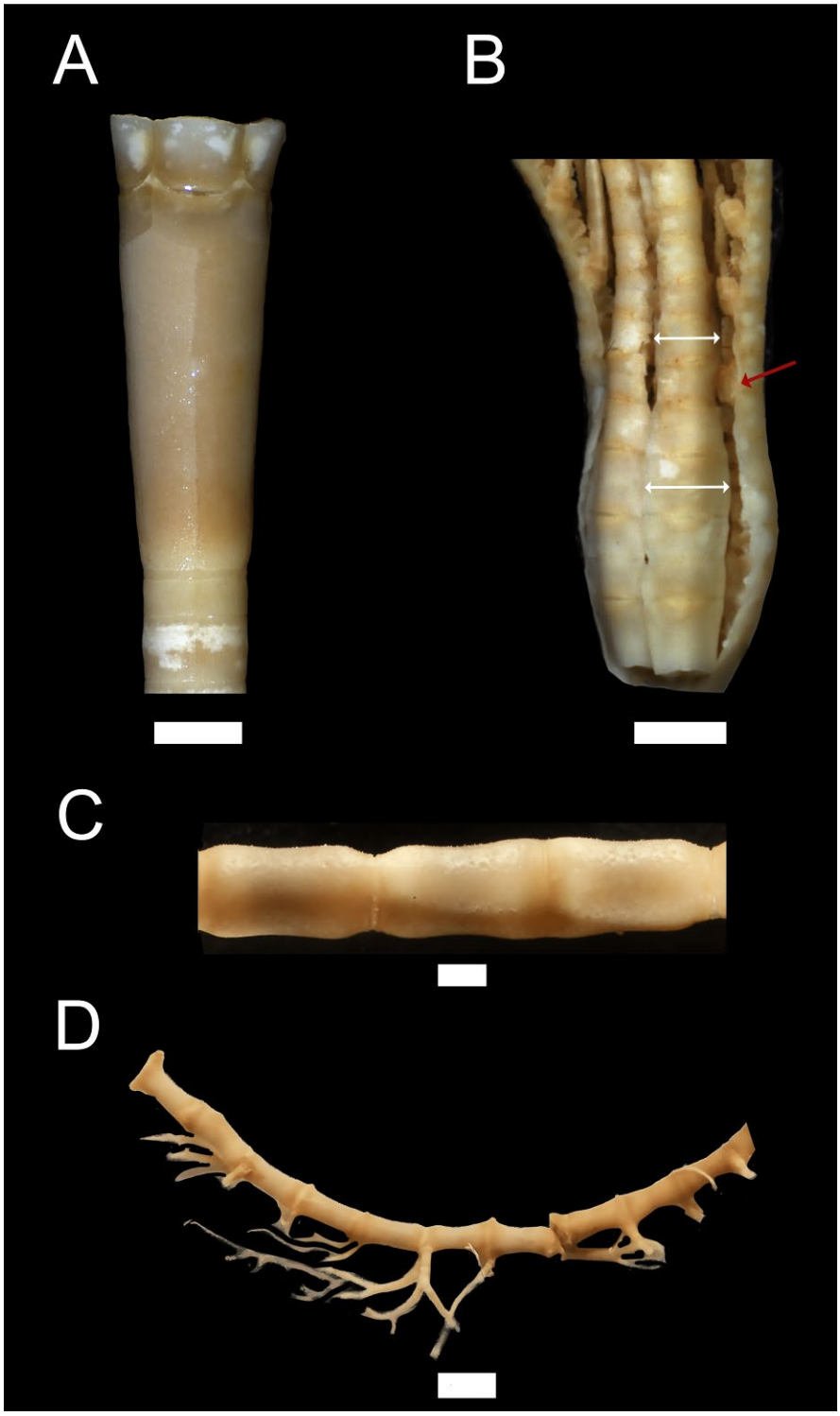

Figure IV.9: *D. newnamus* **n. sp.** overview. **A:** Aboral cup collected in November 2015 (holotype). **B:** Detached crown from December 2016. Red arrow shows the first pinnule on Br8. White arrows show point of slight decrease of approximately 20% in arm width, not enough to be considered a taper. **C:** Distal stem that shows slight hourglass shape. **D:** Attachment structure that shows thread-like radices. Scale bars **A–C**, 1 mm; **D**, 2 mm.

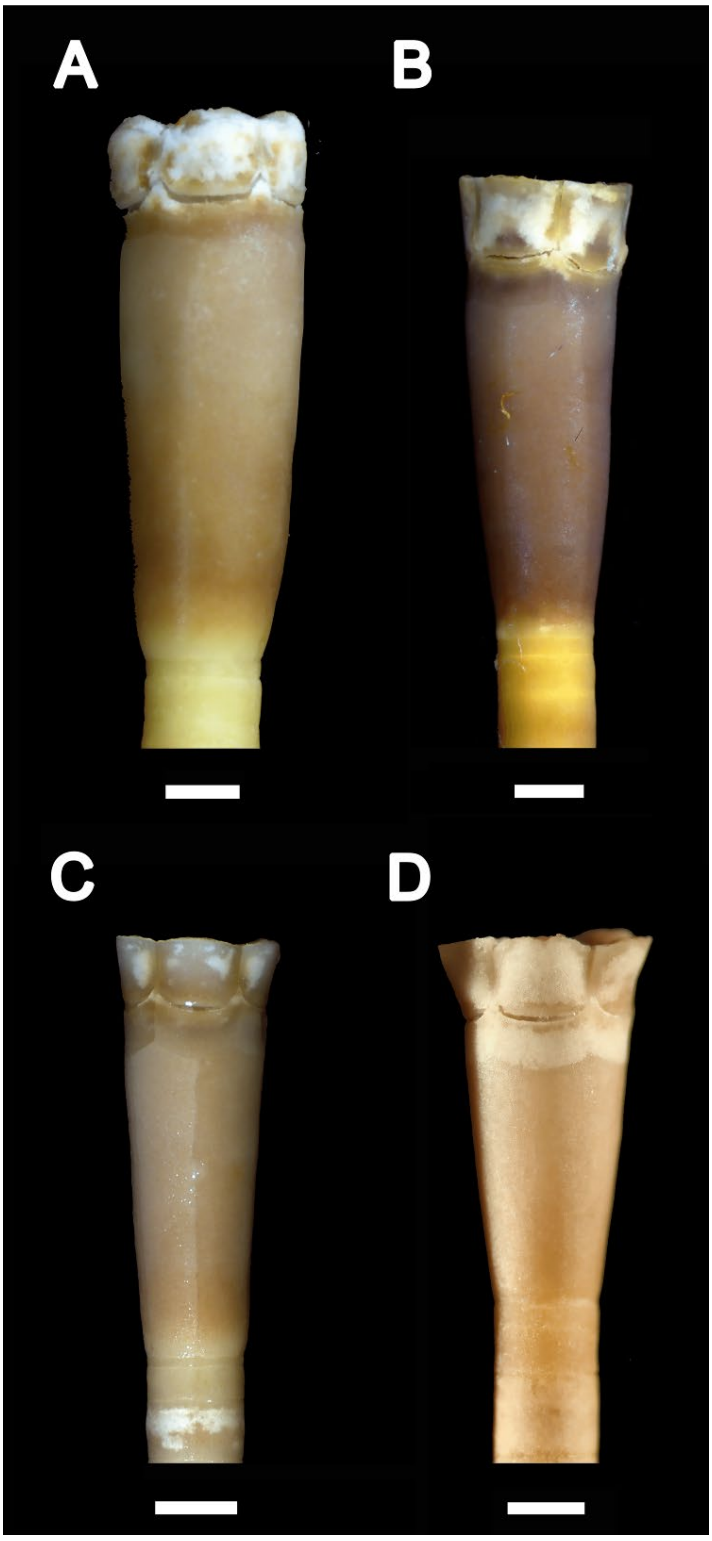

Figure IV.10: Four cups of *Democrinus newnamus* **n. sp.**, selected to demonstrate variation between individuals. **A:** December 2016 C, the single specimen that shows a slight decrease in width across the radial circlet compared to the basal circlet. **B:** May 2016 A showing the darkest brown the cup color reaches. **C:** November 2015 (Designated holotype). **D:** May 2014 B, the smallest specimen collected (3.62 mm) that displays a slightly conical shape. Scale bars: 1 mm.

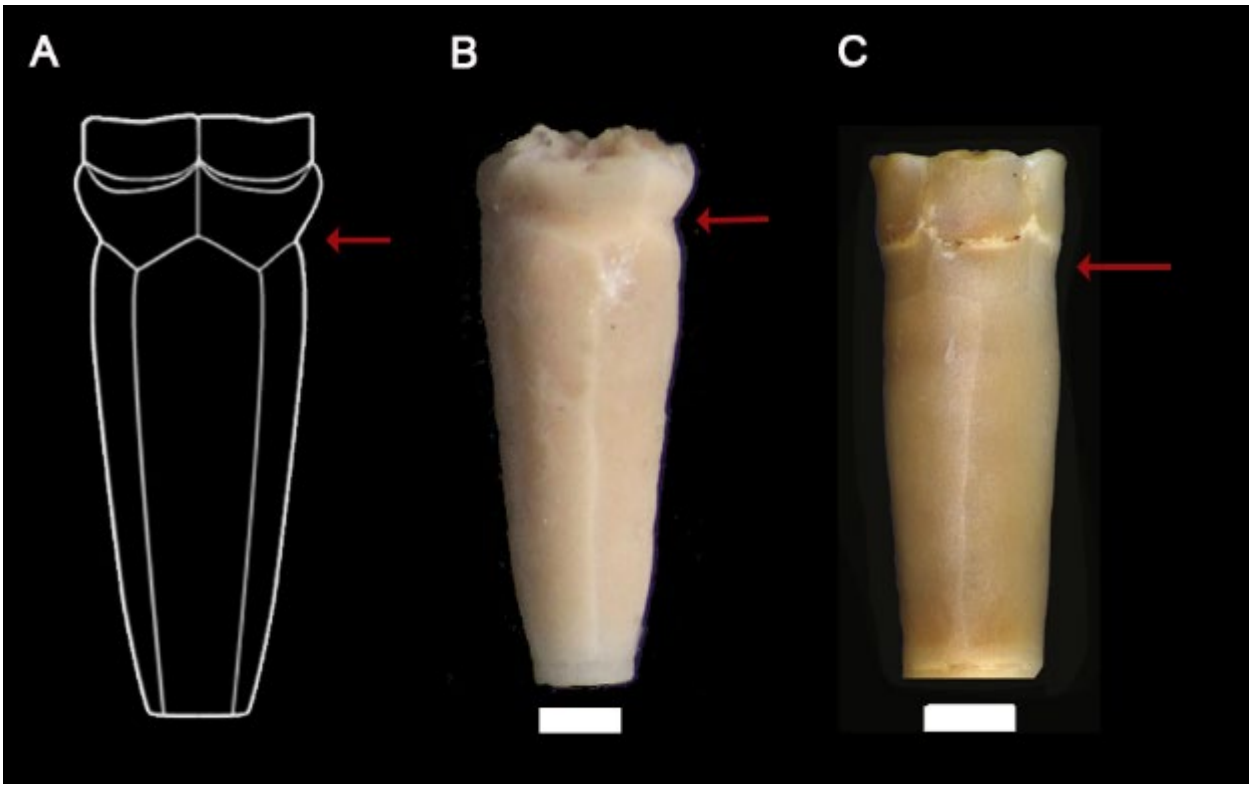

Figure IV.11: Constriction in *Democrinus*. **A:** Diagram of a bourgueticrinid cup showing the sharp pinch that denotes a constriction. It is pictured here at the basiradial suture, but can appear anywhere on a cup. The constriction usually creates a triangular indent in what would otherwise be a straight profile of the cup. **B:** Holotype of *D. conifer* showing a constriction (USNM 22679). **C:** Syntype MCZ 147D showing the slow, sloping decrease in the cup's width that 19th century authors did not consider a constriction, but some 20th century scientists mischaracterized as such. Such an indent creates a very shallow curve in the cup's profile, rather than a triangle. Scale bars: 1 mm.

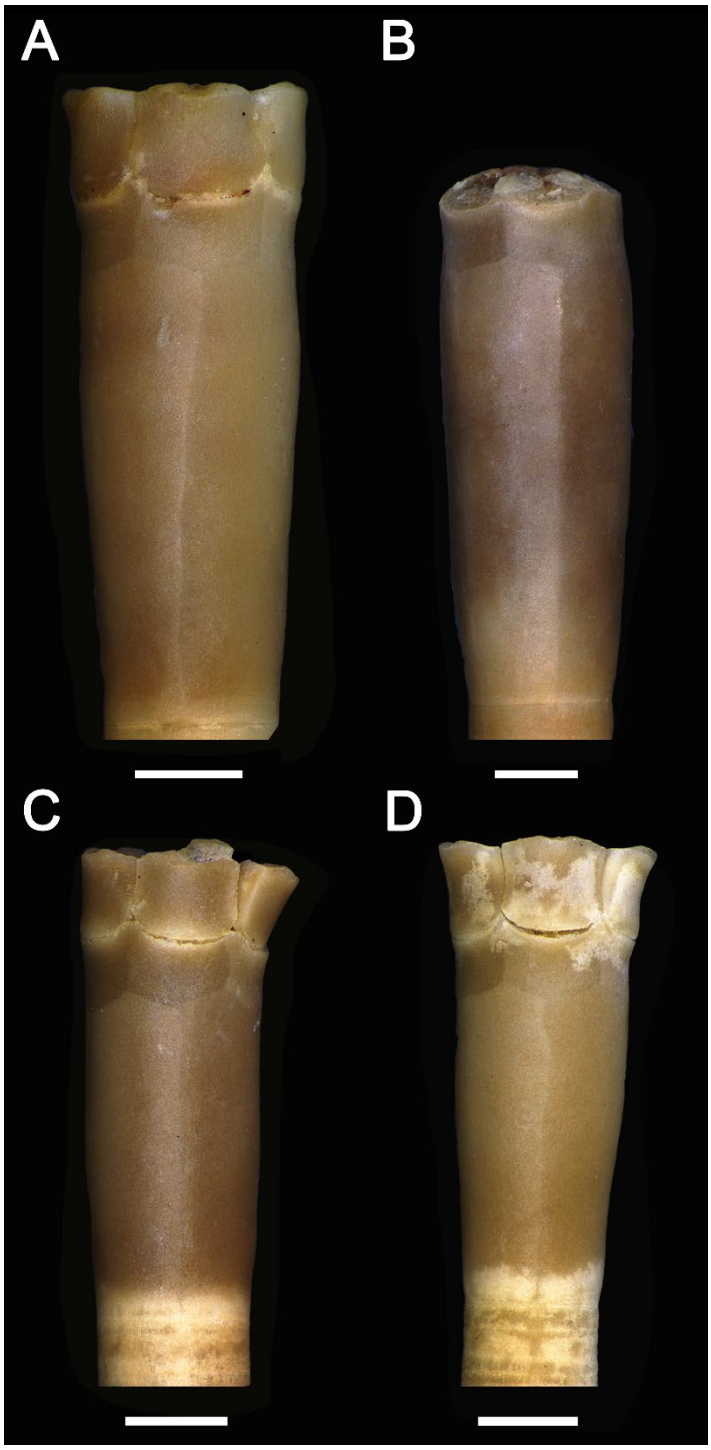

Figure IV.12: Syntypes of *D. rawsonii* housed at the Harvard Museum of Comparative Zoology, accession #147. Collected in 1871 at 13.151944, -59.6694, west side of Barbados, depth: 146–220 m. A and D show best the slight, sloping decrease in cup width in the radials that is not sufficiently sharp to constitute a constriction. **A:** MCZ 147A, **B:** MCZ 147B, **C:** MCZ 147C, and **D**: MCZ 147D. Scale bars: 1 mm.

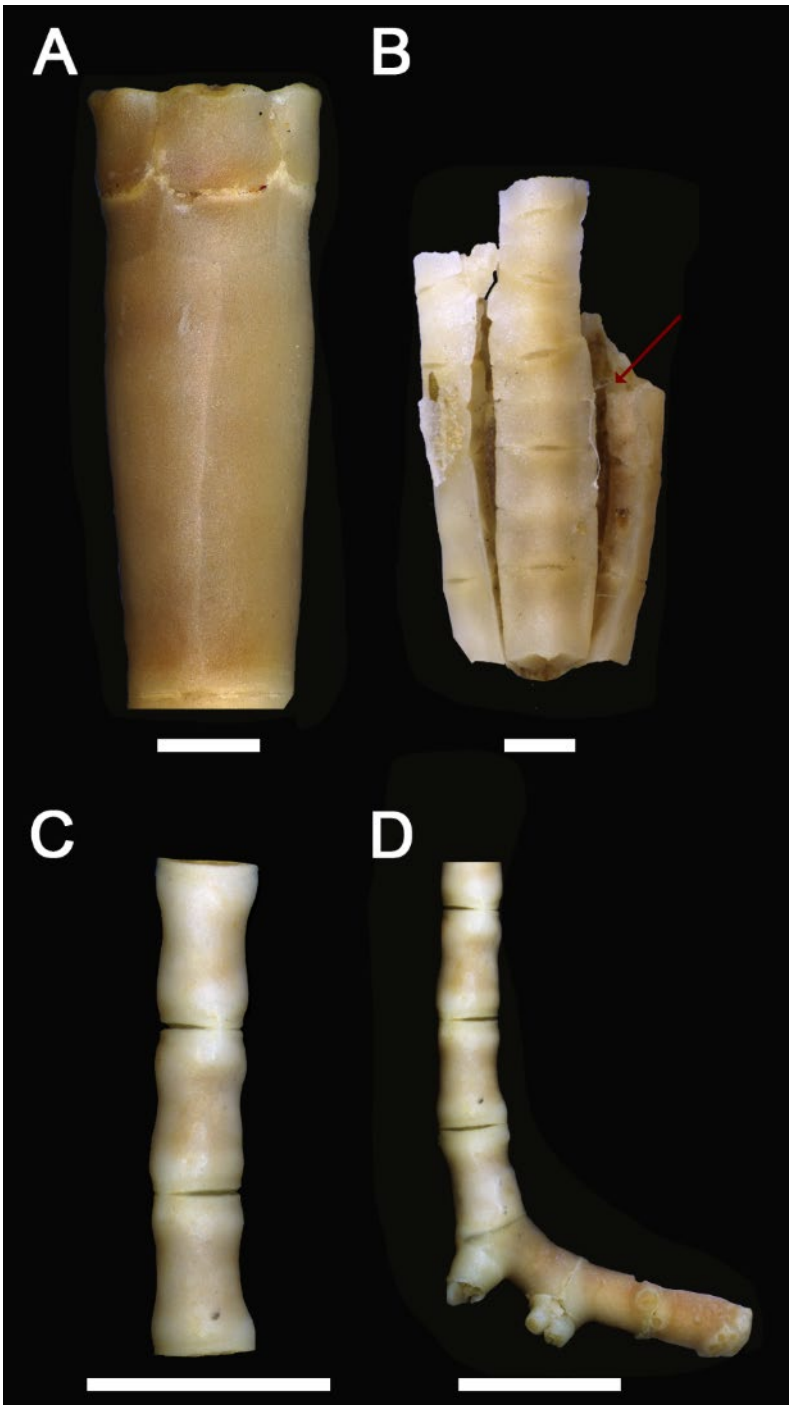

Figure IV.13: *D. rawsonii* syntype MCZ 147A. **A:** Aboral cup. **B:** Three detached arms of likely HMCZ 147A, based upon measurement of the Br1 distal facet on the cup and the potentially corresponding Br2 proximal facet on the arms. Red arrow shows the first pinnule on the arms on the far side of Br5. **C:** Distal stem of one of the syntypes shows a slight hourglass shape. **D:** Broken attachment structure, the only one from the 4 specimens collected. Scale bars: **A–B,** 1 mm; **C–D**, 1 cm.

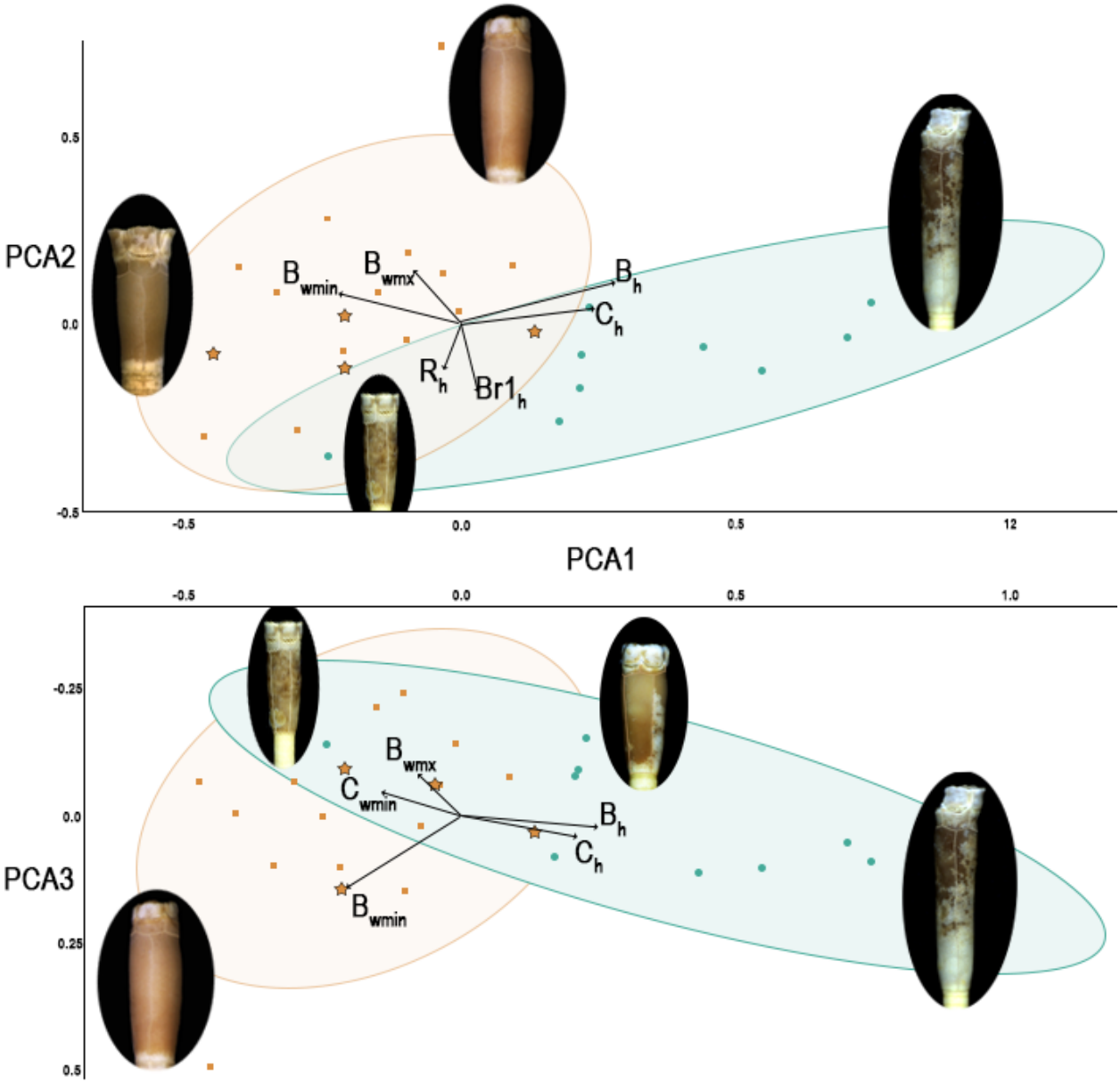

Figure IV.14: Principal Component Analysis on the continuous characters for *D. newnamus* **n. sp.** and *D. rawsonii* after performing BBPM to remove any potential isometric size effect in the clustering. *D. newnamus* is shown in blue with round markers. *D. rawsonii* is shown in orange, with syntypes starred and other individuals are marked with squares. Only the highest contributing characters for the loadings in the PCA (> 50%) are shown. Ellipses represent the 95% confidence interval.

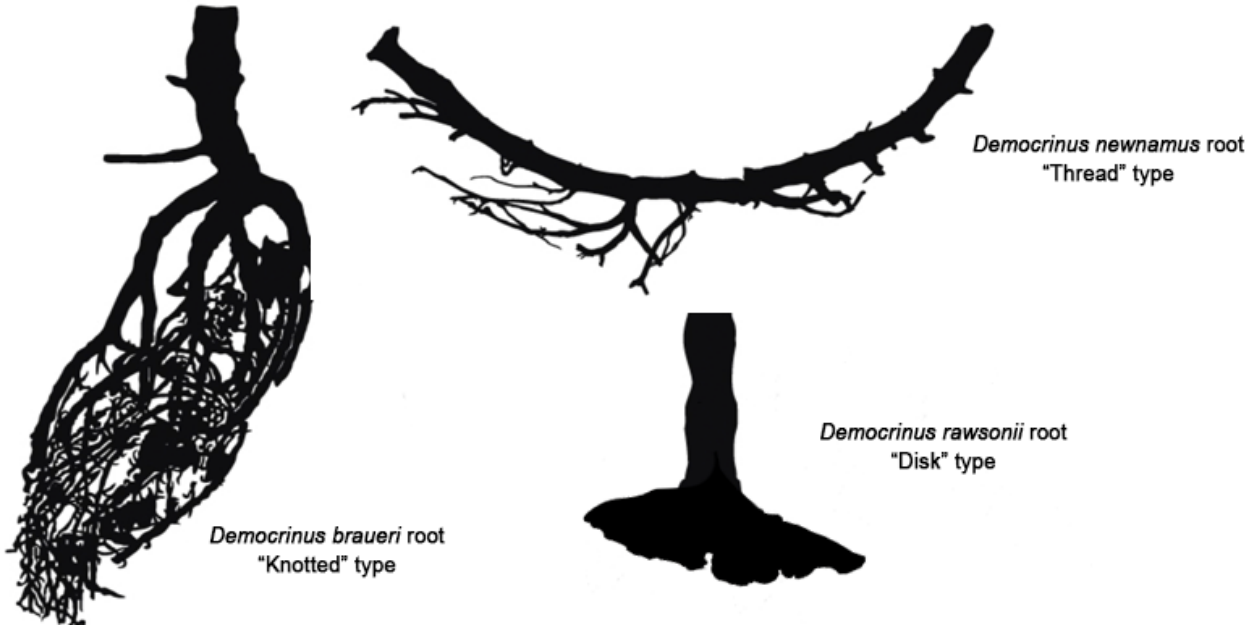

Figure IV.15: Examples of the three attachment structures found in *Democrinus*. The "Knotted-type" and the "Thread-type" have both been found associated with soft substrates and have been found together in large groups of individuals. The "Disk-type" is known to be associated with hard substrates in both extant and fossil species; the "Knotted-type" has been found on hard substrates as well in the latter.

Figure IV.16: Examples of the three attachment types found in *Democrinus*. All three specimens are individuals of *D. rawsonii*. **A:** Broken "Knotted" type structure, showing the beginning of the major branches (MCZ: CRI-150). **B:** "Thread" type structure, with the parallel thread-like radix at each articulation joint (MCZ: CRI-148 B). **C:** "Disk" type attachment structure (MCZ: CRI-149). Scale bars: 1 mm.

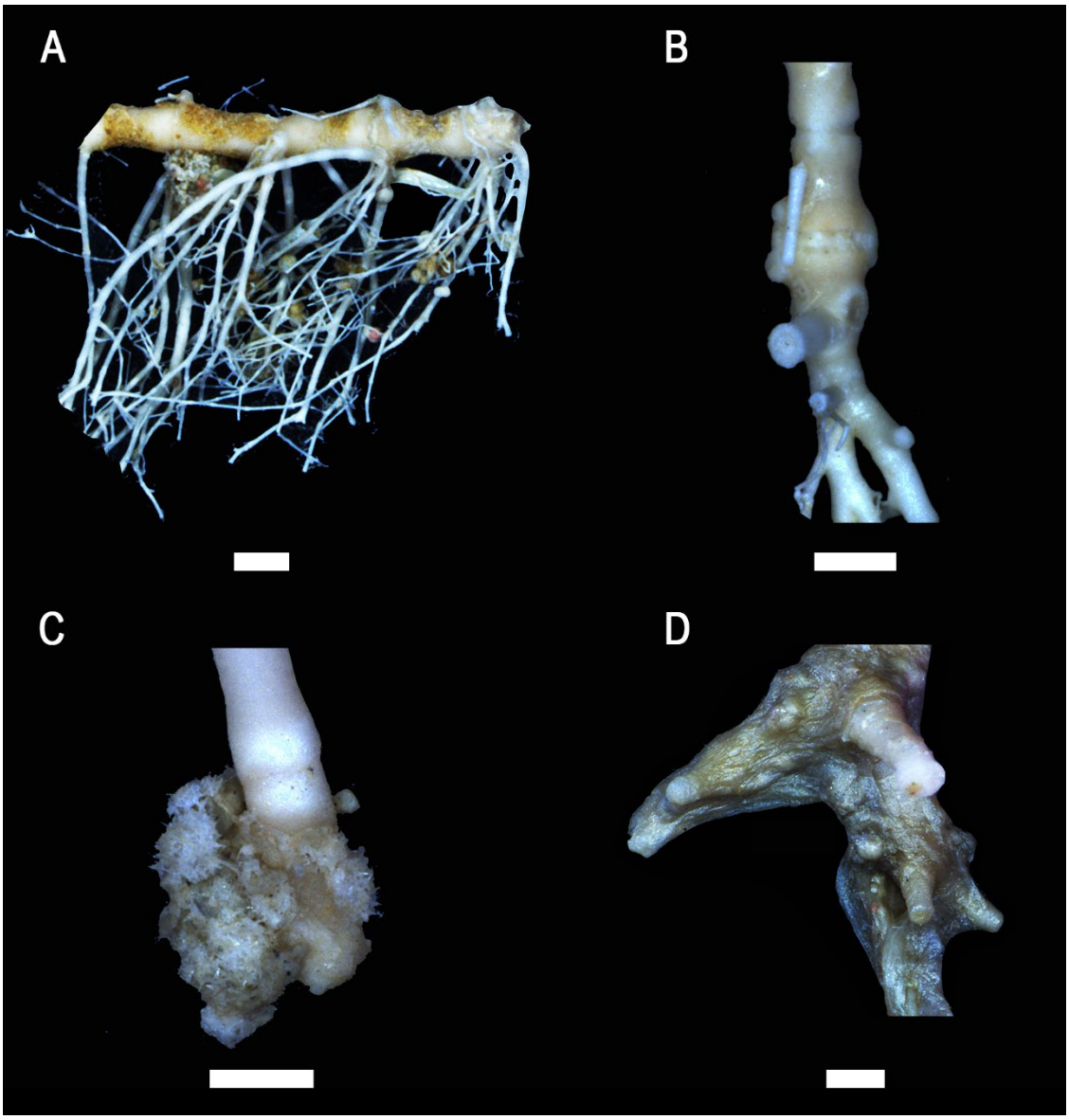

Figure IV.17: *D. brevis* attachment structures. **Top:** Two attachment structures from individuals collected in 2004 off Elliott Key by R/V *Bellows*. These *D. brevis* lived in soft sediment and displayed two different types of attachment structures. (*A*) "Thread" type attachment structure (NSU-CGM: *Bellows* #8) and (*B*) "Knotted" type attachment structure (NSU-CGM: *Bellows* #30). **Bottom:** Two attachment structures from an unknown substrate collected in 1984 in the northeastern Gulf of Mexico. (*C*) The typical "Disk" type attachment structure (NSU-CGM: CRI-553 #6) and (*D*) a "Knotted" type attachment structure that appears to be cemented in part (NSU-CGM: CRI-553 #2). Scale bars: 1 mm.

CHAPTER V Conclusions

A paleontologist's work necessarily entails piecing together an understanding of organisms, their ecologies, and landscapes we can never observe directly; our inferences come with the knowledge that even our best work will always provide an incomplete picture. The nature of this work requires the paleontologist to be a "jack-of-all-scientists", as interdisciplinary studies are foundational to a meaningful reconstruction of Earth's history. For crinoid paleontologists, the expansion of modern deep-sea research will likely continue to influence all studies of the clade.

Access to living bathyal stalked crinoids allows us to test hypotheses about patterns in the fossil record, as discussed in Chapter II. When considering whether increasing predation made conditions unsustainable for stalked crinoids in shallow waters, as predicted by the Mesozoic Marine Revolution hypothesis (MMR), we expect to find an inverse relation between predation intensity and depth. Indeed, we found this to be true for *Democrinus newnamus,* which experiences arm-loss events nearly 60 times less often than stalkless shallow-water feather stars. However, while this result supports the MMR hypothesis, it is moot why stalked crinoids could not withstand the higher predation pressure that characterizes shallow water. One possible answer is that crinoid mobility may be key, as bourgueticrinids, which are attached permanently to the seafloor, are unable to escape predators. Yet, mobility cannot be the complete answer, as other stalked crinoids that are mobile, the isocrinids, are also restricted to depths greater than 100 m in today's oceans.

An alternative hypothesis may involve high regeneration rates as the deciding factor in being able to withstand increasing predation intensity. Recent work on feather stars suggests that

the regeneration rate may be related to swimming ability, in which greater mobility necessitates a higher rate (Stevenson et al. 2022). As a higher regeneration rate would allow feather stars to recover faster from injury, they likely can withstand more frequent injuries. Studying the way regeneration rates change across different clades of stalked crinoids and whether or not they vary across large depth gradients within species are potential areas of future research that could illuminate the potential role of regeneration within the context of the MMR hypothesis. Studying regeneration rates could also shed light on the evolutionary history of feather stars—which came first, faster regeneration or greater mobility? The former could indicate that there is a phylogenetic signal to be found in regeneration rates, the latter that functional morphology may influence the rates to a greater extent.

Chapter III focused on crinoid mobility, or more accurately, on the presumed passivity of crinoid stalks. While the individuals of *D. newnamus* do not engage in crawling and relocating as isocrinids do, they exhibit unexpected behavior: they regain an upright posture when knocked over *in situ*. Four possible mechanisms for this behavior were assessed: that the crinoid could (1) use its arms to push itself up; (2) generate lift by holding its crown in a kite-like position; (3) 'flap' its arms to create an upward thrust akin to swimming behavior in feather stars, or (4) rely on positive buoyancy in the crown. None proved sufficient to explain their righting behavior, which led us to conclude that active contraction of the ligaments found in the stalk must be involved. This interpretation is consistent with *in vito* studies of crinoid arms and cirri that have argued for ligament contraction by the so-called "Contractile Connective Tissue" (Birenheide and Motokawa 1996, Birenheide and Motokawa 1998, Birenheide et al. 2000).

Active contraction of crinoid ligaments provides an alternative to the generally held assumption that the stalk and arms must either have muscle or no active contraction at all. Thus,

it has important consequences for the functional morphology of Paleozoic crinoids, most of which had muscle-less stalks and arms. While the mechanism of ligament contraction and its functional implications are yet to be explored fully, one obvious consequence of contraction relates to the active flexure of stalks with synarthrial articulations, as in *D. newnamus*. Yet synarthrial articulations are comparatively rare in both extinct and extant crinoids, perhaps because they are less able to resist torque (Donovan 1988). Accordingly, further exploration is needed.

Finally, Chapter IV describes a new species of extant *Democrinus, D. newnamus.* Moreover, it provides a review of the genus based upon morphological data from 285 physical specimens, diagrams, plates, and descriptions of 65 specimens from the literature, and photographs of 23 specimens. A discussion of several morphological features in the context of taxonomy is included. Among other things, it argues that the attachment structure, a diagnostic character used previously for *Democrinus*, is likely associated with the environment rather than phylogeny. In this case, the presence of a constriction on the cup, and a constriction of the proximal columnals below the stalk base, have diagnostic value only when consistently defined. Thus, it is warranted to conduct a more thorough reassessment of *Democrinus*, with more precise character definitions and a better understanding of variation.

Further, Chapter IV touches on several other taxonomic problems in the Bourgueticrinina. Fossil bourgueticrinids are rarely intact, which makes it difficult or impossible to assess the features used to distinguish extant members, such as pinnule location. As more extant *Democrinus* are collected with methods that limit damage, more data will become available on characteristics that are useful to diagnose extant and fossil crinoids. Further, larger samples of undamaged extant bourgueticrinids will allow a better assessment of intraspecific

variation. Critically, such morphological work should be performed in conjunction with molecular studies, as several features that unite the clade currently are likely non-homologous (Rouse et al. 2013, 2019). Thus far, molecular work has focused at the level of family or higher; to help resolve the extant and fossil relationships better, in the future, it will important to apply this at lower taxonomic levels and combine it with comprehensive morphological details.

This dissertation addressed organisms living in the deep-sea. The data were collected *in situ* and relied on technologies that have been available only since the latter half of the 20th century. Although relatively new, these approaches have provided new perspectives and unique insights into the biology, ecology, and ultimately, the evolutionary history of deep-sea organisms. May this dissertation serve as only one in a long line of such endeavors.

References

Amemiya S, Omori A, Tsurugaya T, Hibino T, Yamaguchi M, Kuraishi R, Kiyomoto M, Minokawa T. 2016. Early stalked stages in ontogeny of the living isocrinid sea lily *Metacrinus rotundus*. Acta Zool. 97(1):102–116

Birenheide R, Motokawa T. 1996. Contractile connective tissue in crinoids. Biol Bull. 191:1–4

Birenheide R, Motokawa T. 1998. Crinoid ligaments: catch and contractility. *In*: Mooi R, Relford M. editors. Echinoderm: San Francisco. AA. Balkema, Rotterdam

Birenheide R, Yokoyama K, Motokawa T. 2000. Cirri of the stalked crinoid *Metacrinus rotundus*: Neural elements and the effect of cholinergic agonists on mechanical properties. Proc Biol Sci. 267(1438):7–16Bottjer DJ, Jablonski D. 1988. Paleoenvironmental patterns in the evolution of post-Paleozoic benthic marine invertebrates. Palaios 3:540–60

Donovan SK. 1988. Functional morphology of synarthrial articulations in the crinoid stem. Lethaia. 21:169–175

Meyer DL, Macurda DB. 1977. Adaptive radiation of the comatulid crinoids. Paleobiology. 3(1):74–82

Rouse GW, Jermiin LS, Wilson NG, Eeckhaut I, Lanterbecq D, Oji T, Young C., Browning T, Cisternas P, Helgen LE, Stuckey M, Messing CG. 2013. Fixed, free, and fixed: the fickle phylogeny of extant Crinoidea (Echinodermata) and their Permian-Triassic origin. Mol Phylogenet Evol. 66 (1):161–181 https://doi.org/10.1016/j.ympev.2012.09.018

Roux M, Eléaume M, Améziane N. 2019. A revision of the genus *Conocrinus* d'Orbigny, 1850 (Echinodermata, Crinoidea, Rhizocrinidae) and its place among extant and fossil crinoids with a xenomorphic stalk. Zootaxa. 4560(1):51–84 https://doi.org/10.11646/zootaxa.4560.1.3

Stevenson A, Ó Corcora TC, Harley CDG, Baumiller TK. 2022. Ability to swim (not morphology or environment) explains interspecific differences in crinoid arm regrowth. Mar Sci. 13:1-10

APPENDIX A Details on the Hydrodynamic Models and List of Abbreviations Used in Chapter III

Part I: Hydrodynamic lift, the kite model

For the kite Model to serve as the mechanism by which *Democrinus* sp. elevates itself off sediment after being dislodged, the generated lift force (F_L) on the crown must be greater than the downward gravitational force acting on the crinoid. In this case, the gravitational force equals the given crinoid's estimated weight in water, WIW_{Esw} (Figure III.5). Therefore, we calculated F_L using a standard lift equation (equation III.3 in text), where F_L = WIW, C_L = coefficient of lift, ρ_{fluid} = density of the fluid, U_C = current velocity, and SA_R is the total area of the arm as a solid rectangle (Vogel 1994). As *Democrinus* sp. has five arms, $5*SA_{Arm}$ is the surface area of the entire filter, the *Democrinus* sp. crown. C_L of a filter is a function of the angle of attack relative to the fluid and its solidity (ratio of the exact surface area of solid filter elements, SA_{Arm}, to the total area of arm as a solid rectangle, SA_R). Each arm is effectively rectangular (Figure A.1); thus, SA_R is calculated by:

$$SA_R = (L_{Arm}(d_A + 2L_{pin})) \quad \text{(A.I.1)}$$

SA_{Arm} is calculated as:

$$SA_{Arm} = L_{Arm}d_A + L_{pin}d_{pin}P_{num} \quad \text{(A.I.2)}$$

In which L_{Arm}= arm length, d_A = arm diameter, L_{pin} = pinnule length, d_{pin} = pinnule diameter, and P_{num} = the number of pinnules on the arm of the given crinoid (Figure A.1). L_{pin} and d_{pin} values were averaged from measurements on 98 pinnules and set at L_{pin} = 0.49 and d_{pin} = 0.05.

Baumiller (1992) obtained values of lift and C_L experimentally for a range of circular filters composed of orthogonally oriented fibers of different dimensions and spacing for a range of current velocities and angles of attack. The filter formed by the arms and pinnules of *Democrinus* sp. has a solidity (SA_{Arm} / SA_R, Table A.I.1) ~0.31. This most closely approximates "Filter A" in Baumiller, 1992 (Table 2, Fig. 10), with C_L = 0.05 assuming the crown is held at the optimal angle.

SA_{Arm}, ρ_{fluid} and C_L are constants for any dislodged individual; whether or not the crinoid gains enough force for lift is determined by current speed (U_C). Rearranging equation III.3 calculates U_C as follows:

$$U_C = \sqrt{\frac{2*F_L}{C_L*5SA_{Arm}*\rho_{fluid}}} \qquad \text{(A.I.3)}$$

Equation A.I.3 was applied to a range of current speeds from 0 – 60 cm/s and compared with WIW_{Esw} for each of the four dislodged individuals. This is plotted in Figure A.I.2 with the 95% confidence intervals. Values of U_C that meet the value of WIW_{Esw} from Equation A.I.3 represent the minimum current necessary for a given individual to gain lift. Figure A.I.2 shows the results for each individual.

Part I: Tables and Figures

Table A.I.1: Variables for each dislodged individual used to calculate arm solidity to determine the coefficient of lift, CL. The number of pinnules per arm was averaged across all arms and rounded up. SA_{Arm} is the total planer surface area of an arm, SA_R is the rectangular area that SA_{Arm} would have without gaps between the pinnules, and Solidity is SA_{Arm}/SA_R.

	Arm Length (cm)	Number of Pinnules	SA_{Arm} (cm^2)	SA_R (cm^2)	Arm Solidity (SA_{Arm}/SA_R,)
D1	3.11	25	1.12 ± 0.03	3.53 ± 0.05	0.31 ± 0.01
D2	5.13	41	1.82 ± 0.04	5.81 ± 0.08	0.31 ± 0.01
D3	5.75	46	2.07 ± 0.05	6.52 ± 0.09	0.31 ± 0.01
D4	4.2	34	1.52 ± 0.04	4.76 ± 0.06	0.31 ± 0.01

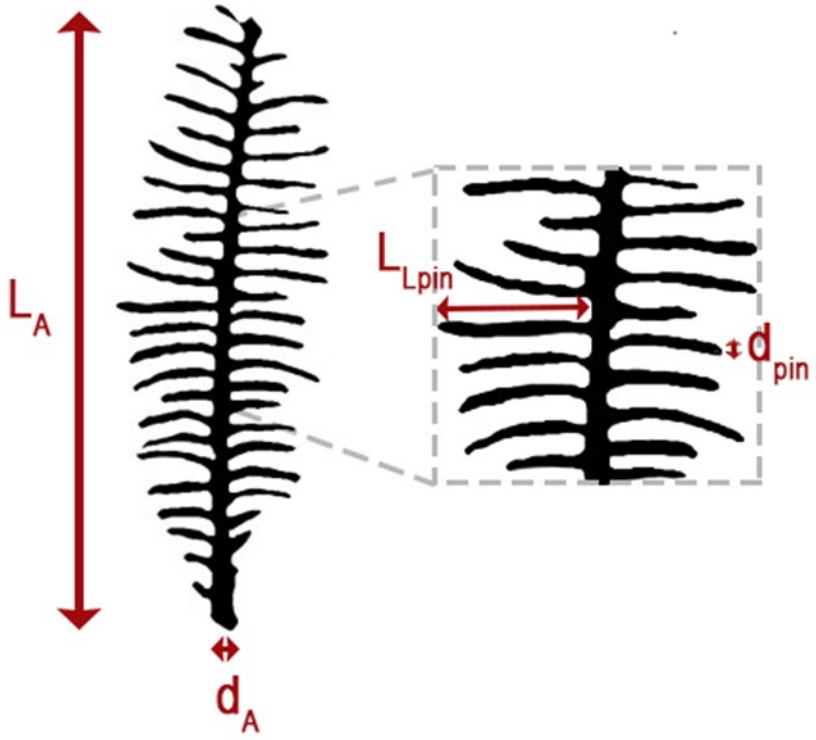

Figure A.I.1: Arm measurements used to calculate SA_{Arm} and SA_R. L_A= arm length, d_A = diameter of the arm, L_{pin} = length of a pinnule, d_{pin} = the diameter of a pinnule.

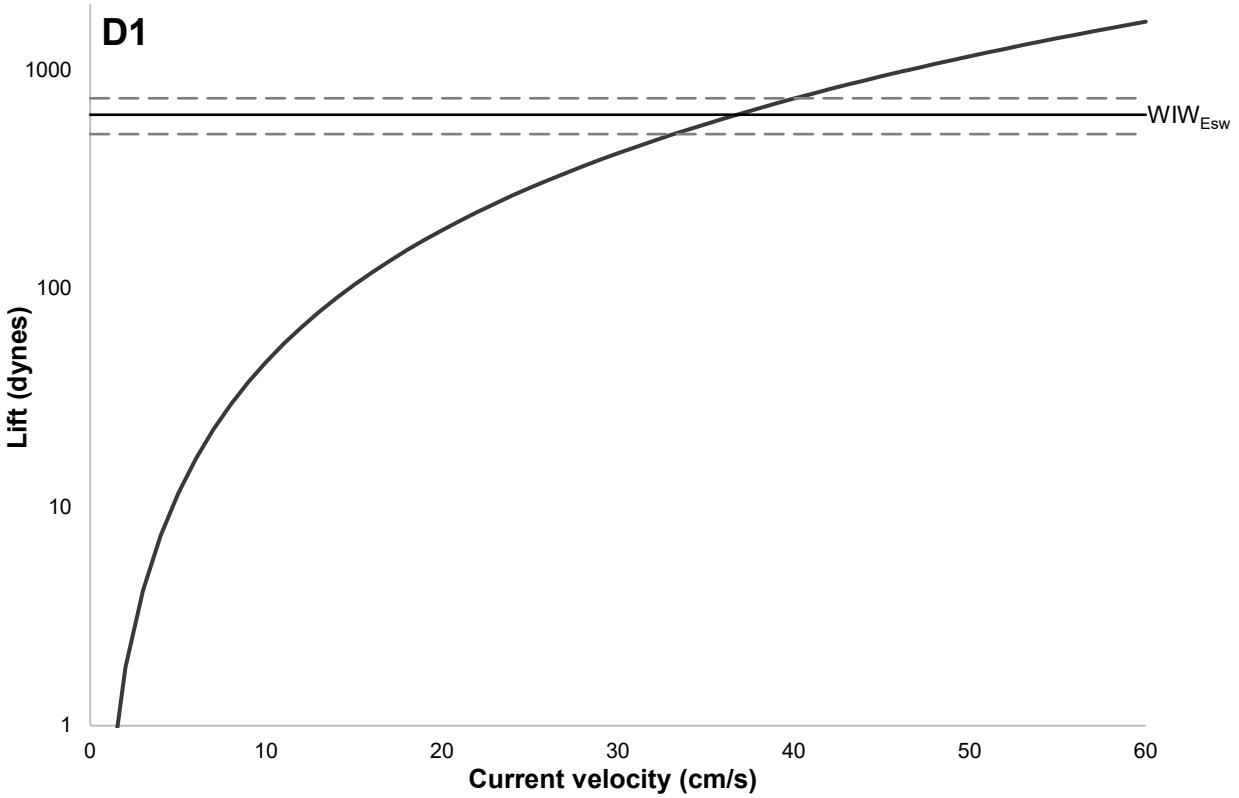
D1
1000
100
10
1
Lift (dynes)
WIW$_{Esw}$
0
10
20
30
40
50
60
Current velocity (cm/s)

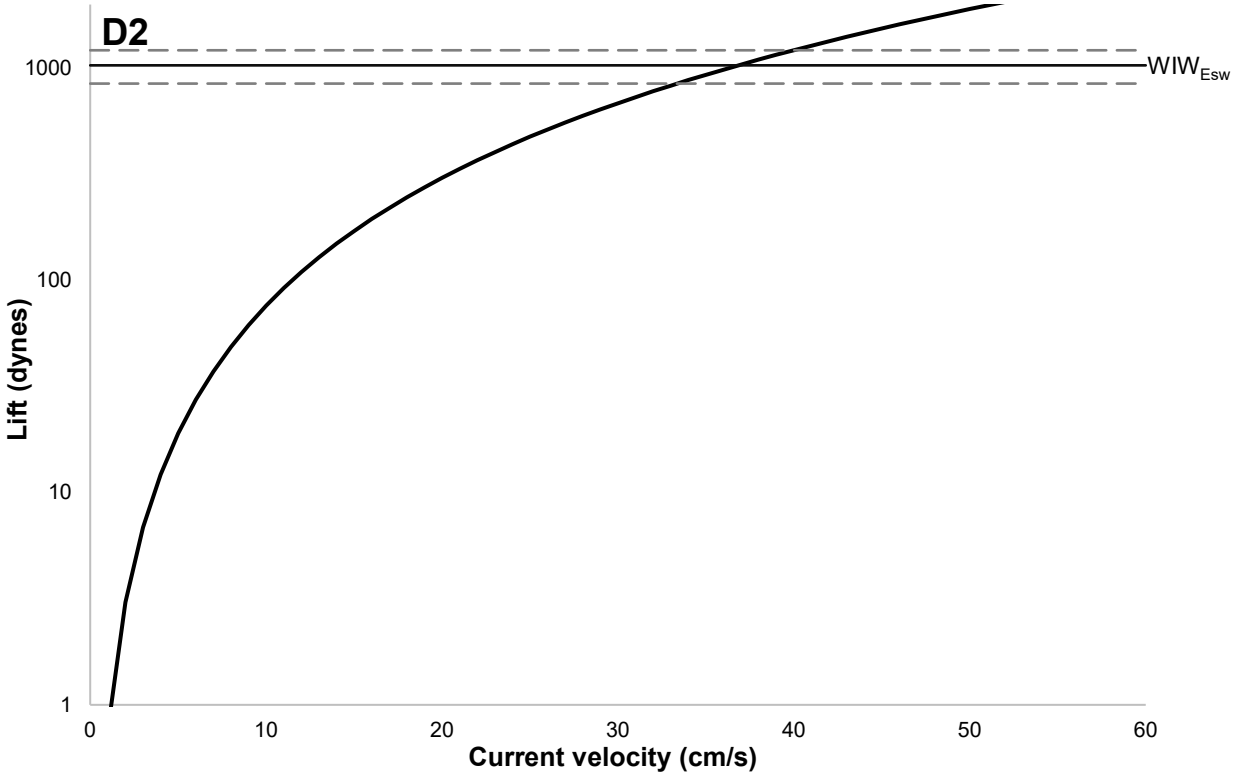
D2
1000
100
10
1
Lift (dynes)
WIW$_{Esw}$
0
10
20
30
40
50
60
Current velocity (cm/s)

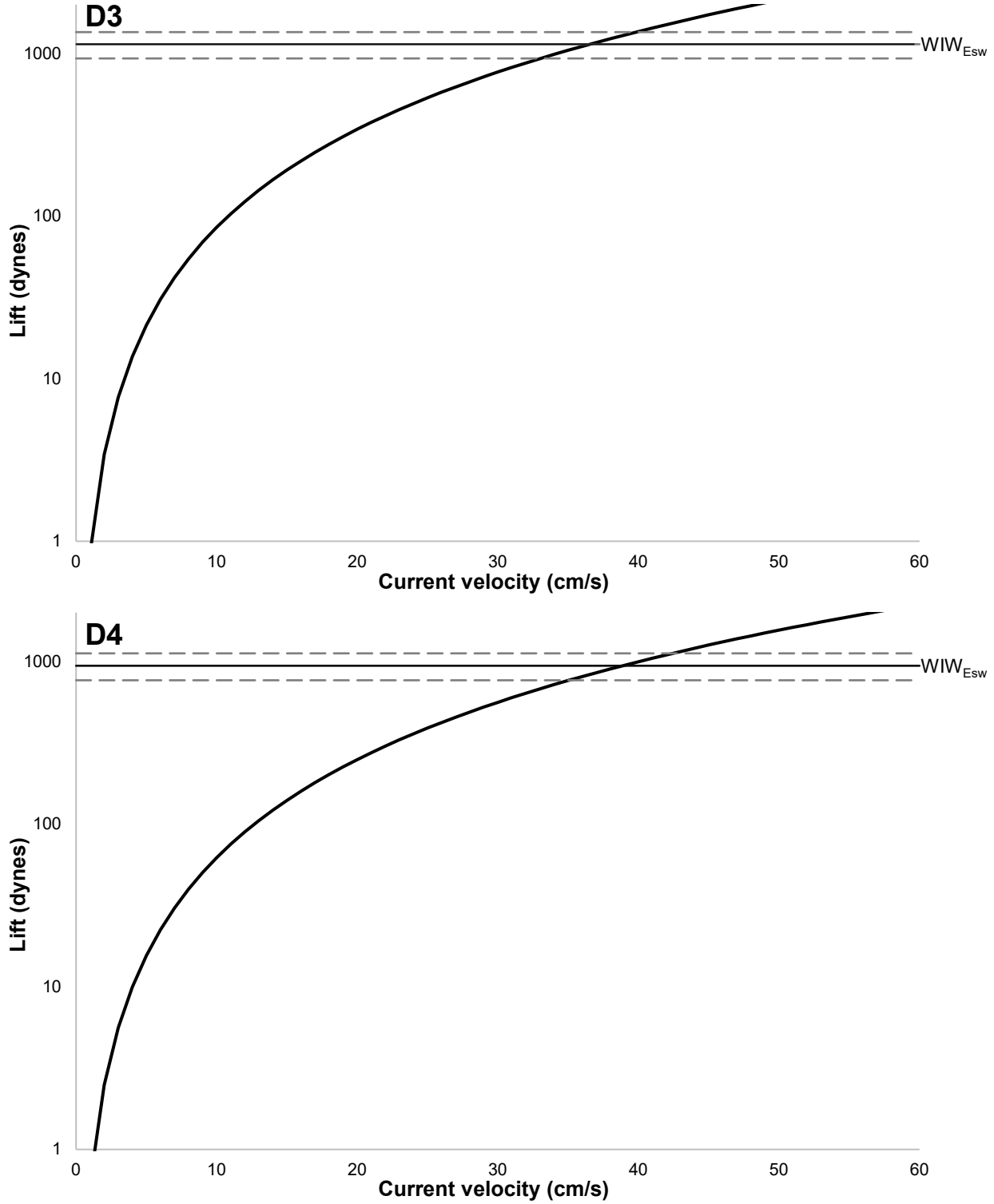

Figure A.I.2: Lift force generated for a range of current velocities, from U_C = 0 to 60 cm/s, with SA_{Arm} based upon the dimensions of each individual, D1, D2, D3, and D4 (ordered top to bottom, respectively). Each graph shows the value of WIW_{Esw} (thin black horizontal line) and its 95% CI (light grey dashed lines). F_L must be greater than the WIW_{Esw} of the individual to achieve lift. Current velocities in excess of 30 cm/s would be necessary to produce sufficient lift for any individual. Lift is plotted as log.

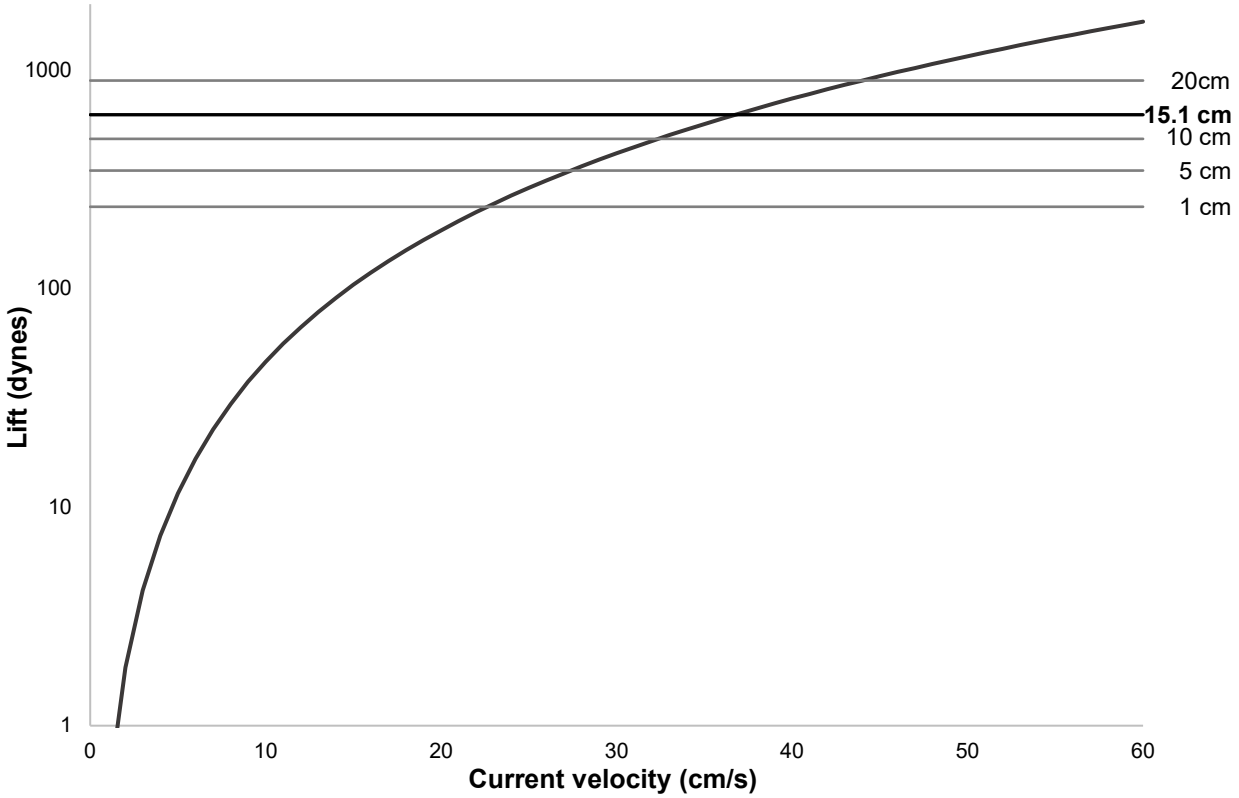

Figure A.I.3: Lift force generated for a range of current velocities, from U_C = 0 to 60 cm/s, with SA_{Arm} based upon the dimensions of D1. The WIW_{Esw} necessary to lift 1, 5, 10, and 20 cm of stalk are shown as horizontal gray lines. The WIW_{Esw} necessary to lift 15.1 cm of stalk. The length of stalk D1 had lifted by the return visit. Current velocities in excess of 30 cm/s would be necessary to produce sufficient lift for any stalk length over 5 cm, and in excess of 20 cm/s for even 1 cm of stalk. Lift is plotted as log.

Part II: Hydrodynamic Drag, the Swimming Model

The swimming model for crinoids (Janevski and Baumiller 2010) calculates vertical thrust during a crinoid's downward arm stroke. The model used empirically–derived parameters based upon the swimming behavior and morphology of *F. serratissima* (Shaw and Fontaine 1990) and a standard equation for hydrodynamic drag (Vogel 1994). Here we use a simplified version of this swimming model to maximize the potential upward thrust in a *Democrinus* sp.'s arm stroke. For example, we only consider the force associated with the power stroke while ignoring any force acting in the opposite direction generated during the recovery stroke. Further, for *Democrinus* sp,, we assume that the entire outstretched arm generates thrust, while, in feather stars, only the proximal 3/4 portion of their arm is involved (Janevski and Baumiller 2010). These conservative assumptions compensate for the possibility of additional thrust generated by tube feet, currently excluded in the model (which, although likely very minor, would increase the solidity and, therefore, thrust generation).

A power stroke for this model begins with the fully extended arm, pinnules outstretched, and the arm's long axis at angle α from vertical (Figure III.6). The arm then rotates aborally around its hinged base through angle θ at an angular velocity ω. During the rotation, it experiences a drag force that acts perpendicular to the direction of motion. The following equation governs the drag force acting on the arm:

$$D_T = \frac{1}{2} C_D \, 5SA_{Arm} \frac{1}{3} \, \rho_{fluid} {U_L}^2 \qquad \text{(A.II.1)}$$

where C_D is the coefficient of drag, 0.22, SA_{Arm} is the area of the arm filter, calculated as in the Kite model, ρ_{fluid} is the density of the fluid (seawater, 1.024 g/cm3), and U_L is the linear velocity of the arm at the tip (Distance travel at the tip of the arm/time to complete power stroke). The above equation differs from the standard drag equation (Vogel 1994) by a factor of 1/3,

accounting for the fact that the linear velocity of the arm decreases from U_L at the tip to 0 at the hinge (see equation 3 in Janevski and Baumiller, 2010, with b0 = b1).

As D_T is perpendicular to the arm's long axis, we may resolve it into two components: vertical drag, D_V, and horizontal drag, D_H. Only D_V affects the upward thrust necessary to overcome the crinoid's WIW. The D_H generated by the radial arms around the cup cancels out. The magnitude of D_V changes as an arm rotates (Figure III.6). To find the average instantaneous upward thrust, $\overline{D_V}$, equation III.4 is used:

$$\overline{D_V} = \frac{D_T}{t_p}\left(\frac{1}{\omega}\right)(\cos(\alpha) - \cos(\alpha + \theta)) \qquad \text{(III.4)}$$

where ω is the angular velocity of the arm (radians/sec), α = 30º and θ = 80º, representing the maximum observed distance for *Democrinus* sp. arm movements, t_p is the period of the stroke, and all other variables are as before (the derivation of equation 3.4 is in Janevski and Baumiller 2010). Two variables drive both D_V and D_T: (1) arm length and (2) time to complete a power stroke. Thus, we calculated $\overline{D_V}$ twice: first, for a range of arm lengths assuming max observed time (1.1 s) (Figure A.II.1), and secondly, for a range of times (Figure A.II.2). These two ranges were plotted along with the WIW_{Esw} for the dislodged *Democrinus* sp. specimens D1 – D4.

Part II: Figures

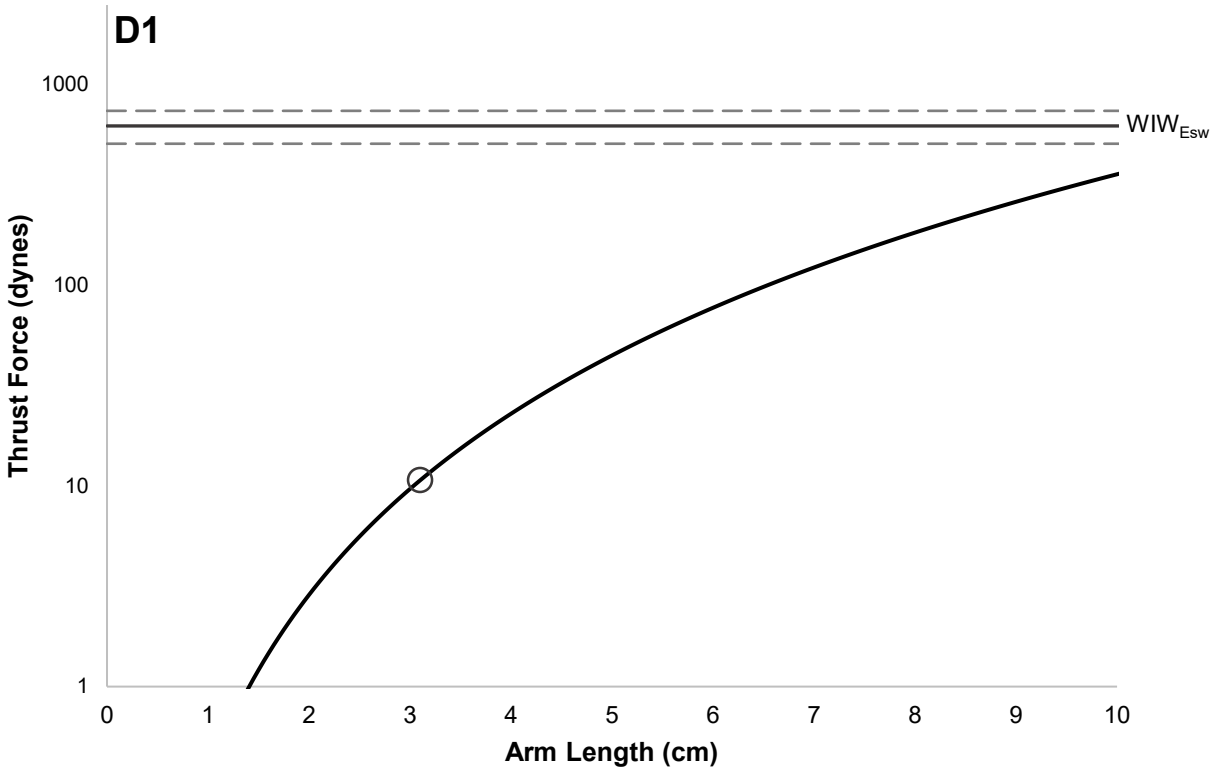

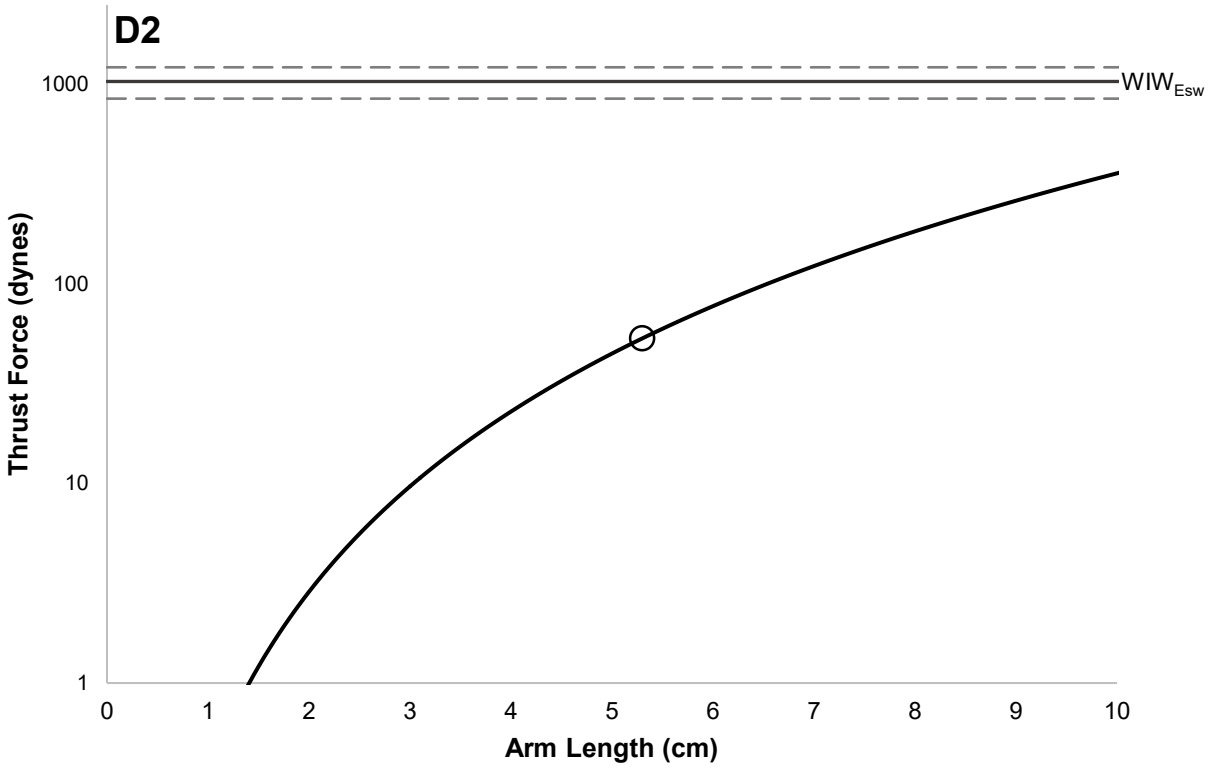

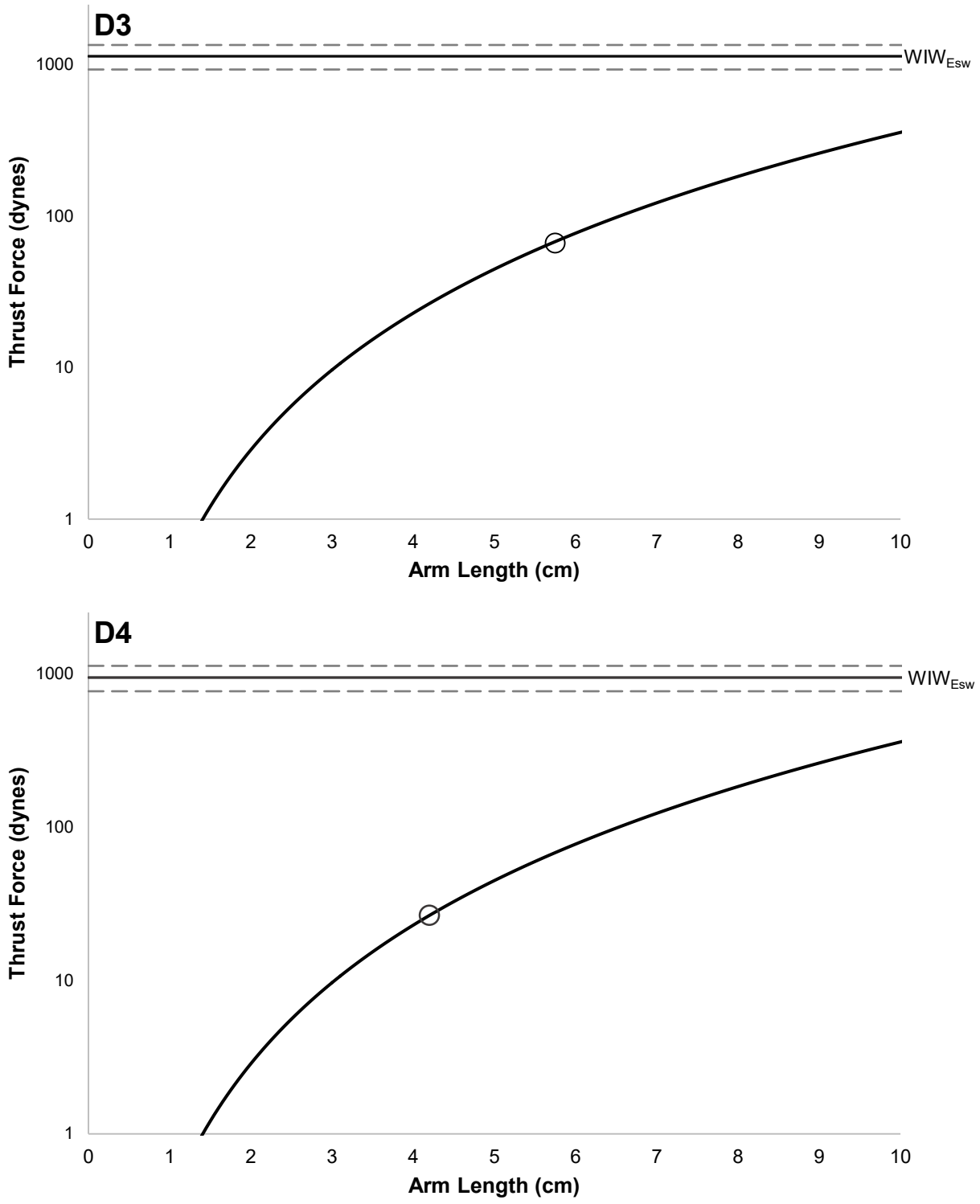

Figure A.II.1: Thrust force plotted against arm length for dislodged individuals D1, D2, D3 and D4 (ordered top to bottom, respectively) A circle denotes the arm length measured for the given individual where it falls on F_T. The thrust produced by the arm of observed length is far below that necessary for the crinoid to achieve an upright posture. Note that no *Democrinus* sp. has been measured with an arm length greater than 8 cm.

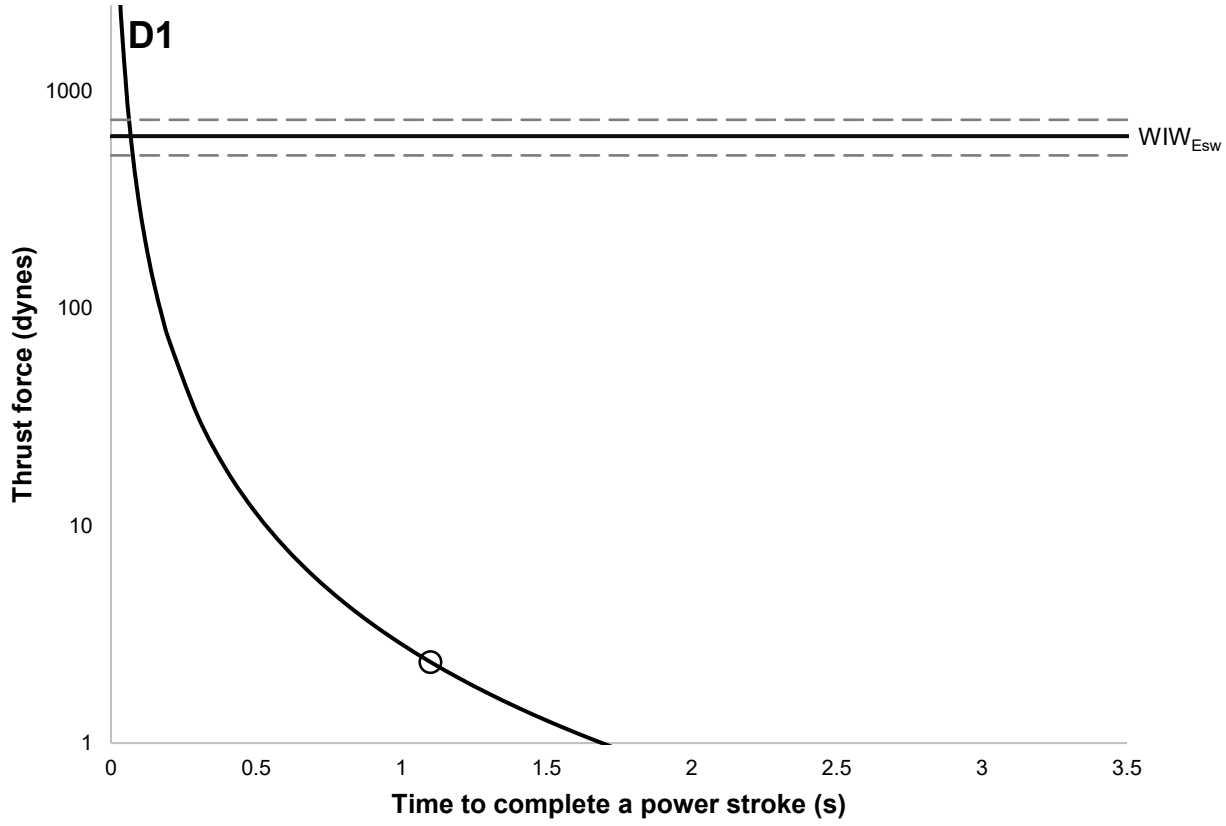
D1
1000
100
10
1
Thrust force (dynes)
WIW$_{Esw}$
0
0.5
1
1.5
2
2.5
3
3.5
Time to complete a power stroke (s)

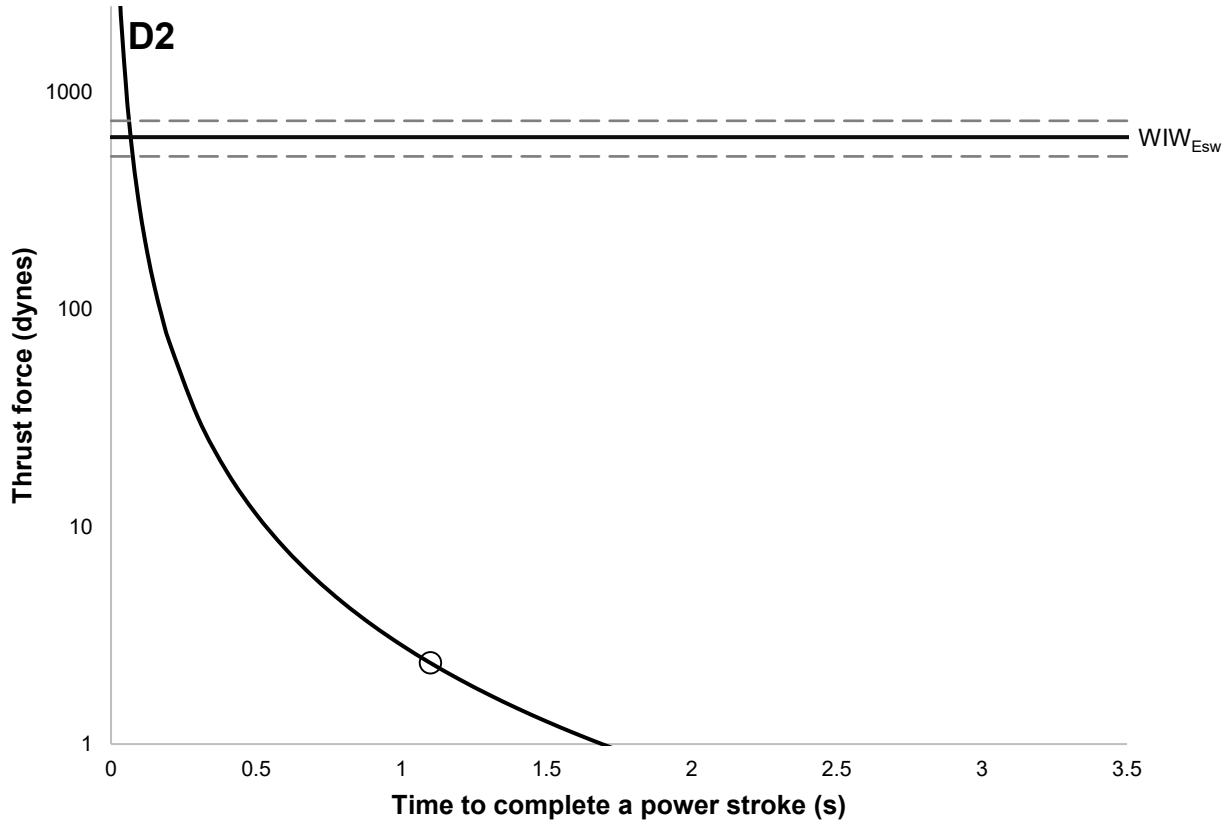
D2
1000
100
10
1
Thrust force (dynes)
WIW$_{Esw}$
0
0.5
1
1.5
2
2.5
3
3.5
Time to complete a power stroke (s)

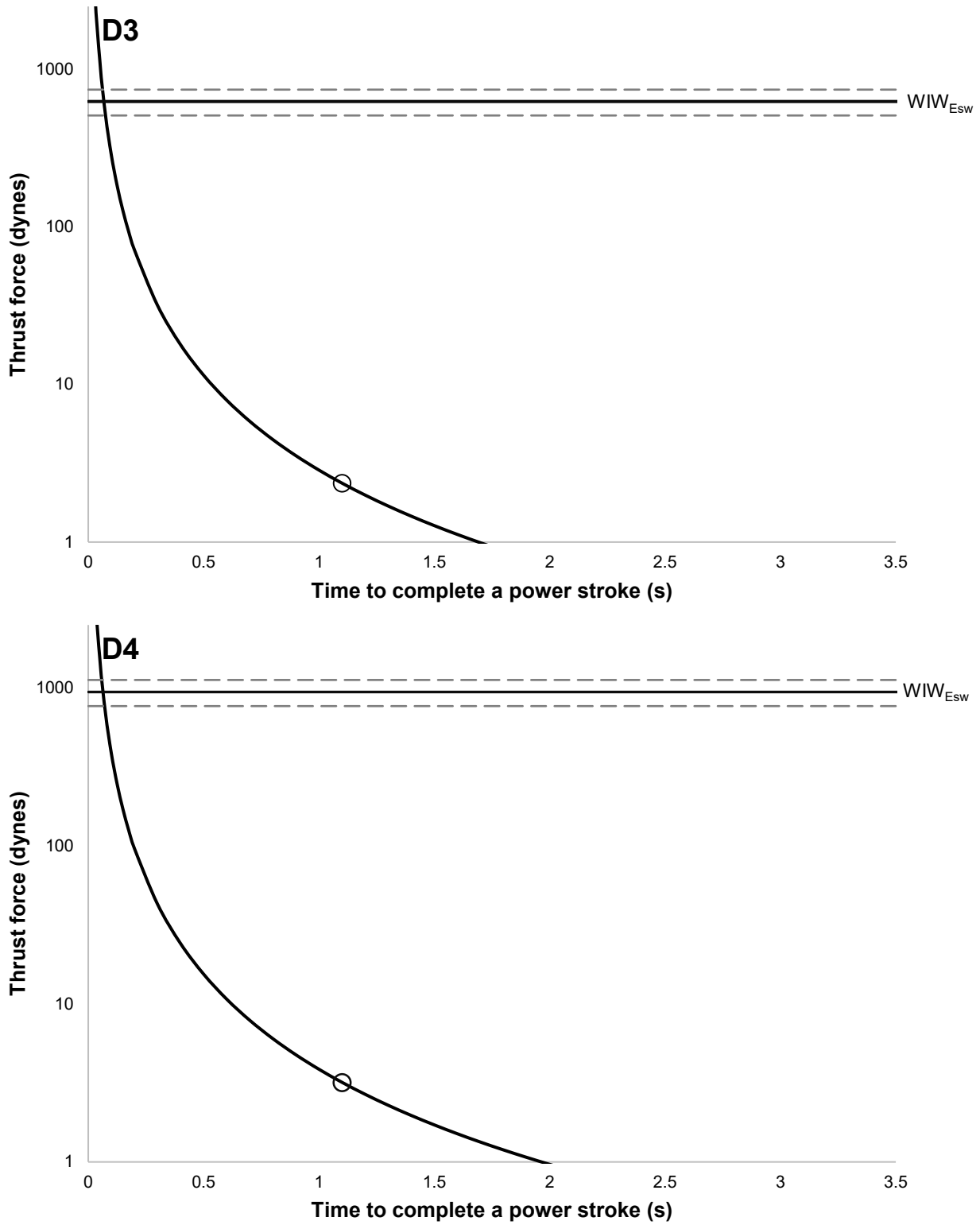

Figure A.II.2: Thrust force for dislodged individuals D1, D2, D3 and D4 (ordered top to bottom, respectively) plotted for a range of arm speeds. Arm speed (time to complete a power stroke) varied from 0.001 to 5 seconds. A circle denotes fastest power stroke seen in the field, t_p= 1.1 s, and where it falls on the F_T curve. The thrust produced at any reasonable speed (>0.1 s) is less than that necessary for the crinoid to achieve an upright posture.

Part III: List of abbreviations used in Chapter III

Table A.III.1: List of abbreviations used in Chapter III

Variable	Abbreviation (unit)	Value
Stalk diameter (avg)	d_S (cm)	0.09 ± 0.0003 cm
Stalk length	L_{Stalk} (cm)	Varies
Arm diameter (avg)	d_A (cm)	0.08 ± 0.001 cm
Arm length	L_{Arm} (cm)	Varies
Pinnule length (avg)	L_{pin} (cm)	0.50 ± 0.002 cm
Pinnule diameter (avg)	d_{pin} (cm)	0.05 ± 0.001 cm
Number of pinnules per arm	P_{num}	Varies
Mass of water	M_w (g)	Varies
Density of water	ρ_w (g/cm^3)	1.024 (g/cm^3)
Volume of a specimen	V (cm^3)	Varies
Density of a specimen	ρ (g/cm^3)	Varies
Weight in air	WIA (dyn)	Varies
Weight in water	WIW (dyn)	Varies
Weight in salt water	WIW_{sw} (dyn)	Varies
Difference between WIA and WIW	ΔW (dyn)	Varies
WIW_{sw} stalk per 1 cm	WIW_{Stalk} (dyn/cm)	27.47 ± 3.62 dyn/cm
WIW_{sw} arm per 1 cm	WIW_{Arm} (dyn/cm)	13.45 ± 0.12 dyn/cm
Estimated WIW_{sw}	WIW_{Esw} (dyn)	Varies
Lift force	F_L (dyn)	Varies
Arm as solid rectangle surface area	SA_R (cm^2)	Varies
Arm surface area	SA_{Arm} (cm^2)	Varies
Coefficient of lift	C_L	0.05
Solidity	S	0.31
Current velocity	U_C (cm/s)	0 – 60 cm/s
Drag force	D_T (dyn)	Varies
Period of a power stroke	t_p (s)	Varies, max observed = 1.1 s
Vertical component of drag force	D_V (dyn)	Varies
Coefficient of drag	C_D	0.22
Linear velocity	U_L(cm/s)	Varies
Angular velocity	ω (deg/s)	Varies
Angle an arm rotates through during a power stroke	θ (deg)	80°
Starting angle of arm from vertical	α (deg)	30°

APPENDIX B Specimen Information for Specimens Used in Chapter IV

Table B.1: Specimen Information for Specimens Used in Chapter IV

	Specimen Information					Collection Information				
	Specimen location	Catalog number	Number of specimens	Type status	Material examined	Year, collected by	Location	Depth (m)	Method	Additional notes
D. aoteanus	NIWA	511	1	Holotype	Written description, p. 208-209 and Figure 3 from McKnight 1973	1964, McKnight	Lat: -40.099 Long: 171.266	688	Trawl	Figure 3 in McKnight 1973 is in black and white.
	NIWA	92465	3		Photograph (Stacking microscope)	1980, Bohn	Tasman Basin Lat: -40.5517 Long: 170.955	570	Sled, epibenthic	Labeled 1 – 3 for this study
	NIWA	35075	10		Photograph (Stacking microscope)					Labeled 1 – 10 for this study
	NIWA	71320	6		Photograph (Stacking microscope)	1964, McKnight	Lat: - 41.1667 Long: 170.233	770	Trawl, Menzies	Labeled 1 – 6 for this study
	NIWA	71321	2		Photograph (Stacking microscope)	1964, McKnight	Lat: -38.1667 Long: 170.350	861	Trawl,	Labeled 1 – 2 for this study
	NIWA	89599	1		Photograph (Stacking microscope)	2013, Anderson	Lat: -41.1465 Long: 170.606	583	Trawl, fish, bottom	

D. aoteanus	NIWA	92465	3		Photograph (Stacking microscope)	1980, Bohn	Tasman Basin, Lat: - 40.5517 Long: 170.955	570	Sled, epibenthic	Labeled 1 – 3 for this study
	NIWA	35080	1		Photograph (Stacking microscope)	2007, Anderson	Lat: -39.8088 Long: 167.964	915-920	Sled, epibenthic	
D. brevis	BMNH	84.6.20.8	1	Holotype	Photograph (Canon: Rebel T3i); Written description, p. 675 from Clark 1909	UNK, Capt. E. Cole; cataloged in 1884	Off Colon	~549	Dredged; cable steamer *Investigator*	Specimen is still listed at BMNH as *Rhizocrinus rawsoni*; AH Clark 1909 moved it to *brevis* and designated this specimen as the holotype; AM Clark (1977) confirmed this move
	BMNH	84.6.20.9	1	Paratype	Written description, p. 675 from Clark 1909 Figure 19 B, Diagram, from Carpenter 1884	UNK, Capt. E. Cole; cataloged in 1884	Off Colon	~549	Dredged; cable steamer *Investigator*	Specimen is still listed at BMNH as *Rhizocrinus rawsoni*; AH Clark 1909 moved it to *brevis* and designated this specimen as the paratype; AM Clark (1977) confirmed this move
	NSU-CGM	CRI-538	31		Physical specimens	1985, Messing	N. Gulf of Mexico, station E2C Lat: 28.226 Long: 6.111	620-616	Trawl	Labeled A – Z, A1 – E1 for this study
	NSU-CGM	CRI-539	4		Physical specimens	1985, Messing	N. Gulf of Mexico, station WC6 Lat: 27.712 Long: 91.549	543-783	Trawl	Labeled 1 – 4 for this study Extremely delicate.

D. brevis	NSU-CGM	CRI-547	48		Physical specimens	1985, Messing	N. Gulf of Mexico, station E2D Lat: 28.127 Long: 85.860	624-631	Trawl	Labeled 1 – 48 for this study
	NSU-CGM	CRI-548	14		Physical specimens	1985, Messing	N. Gulf of Mexico, station E2A Lat: 28.584 Long: 86.762	625-625	Trawl	Labeled A – N for this study Specimen N has regen arms
	NSU-CGM	CRI-549	33		Physical specimens	1985, Messing	N. Gulf of Mexico, station E2 Lat: 28.268 Long: 86.201	613-618	Trawl	Labeled A – Z, A1 – G1 for this study Specimen H has regenerated arms
	NSU-CGM	CRI-552	5		Physical specimens	1985, Messing	N. Gulf of Mexico, station E3 Lat: 28.160 Long: 86.399	871-871	Trawl	Labeled 1–5 for this study
	NSU-CGM	CRI-553	11		Physical specimens	1984, Messing	N. Gulf of Mexico, station E2 Lat: 28.176 Long: 86.148	603-640	Trawl	Labeled A–K for this study
	NSU-CGM	CRI-557	28		Physical specimens	UNK, Messing				Labeled 1–28 for this study
	NSU-CGM	CRI-589	1		Physical specimens	1985, Messing	N. Gulf of Mexico, station E1		Trawl	
	NSU-CGM	Bellows	36			UNK, Messing				Labeled Bellows: A – Z, J1 – E1 for this study

D. cabiochi	MNHN	IE-2013-10100	1	Holotype	Photograph[1]; Written description from Roux 1976	1967	Station T453 Lat: 47.950 Long: -7.85	344-354	Trawl; Ship *Thalassa*	
D. chuni	USNM	35998	1	Syntype	Written description; Plate 1 Figure 5, Plate 6 Figure 6 from Döderlein 1907	1899, Siboga expedition		1668		
	MZC	CRI-738	1		Physical specimen	<1920	Off Cape Colony, South Africa	1647-1830		From historical Collection
			12		Written descriptions; Figures 3a, 5 - 7; Plate 3 Figures 1-7, Plate 4 Figures 1 - 6, Plate 5 Figures 2-4, Plate 6 Figures 1 - 6, Plate 7 Figures 1-5, Plate 8 Figures 1 - 10. from Döderlein 1912	1898-1899, Deutsche Tiefsee-Expedition	Near the East African Coast Station #250 Lat: -1.78 Long: -41.9667 Near the Somali Coast Station #257 Lat: 1.8 Long: -45.8	Station #250: 1668 Station #257: 1644	Trawl; SS *Valdivia*	The specimens are from two different locations, but Döderlein 1912 does not match specimens to locals. Station #250 is listed as having a 4.6°C bottom soil temperature, and globigerine mud/blue clay. Station #257 has 3.8°C bottom soil temperature 6 specimens were originally listed as *Bythocrinus baueri*; Gislén (1938) synonymized the species with *D. chuni*
	NHM	1972.8.21.123-132	2		Written description; Figure 17 A; Table 15 from Clark 1972	1964, N.I.O.	Off Durban, Station #389E Lat: -30.15 Long: 31.6167	930	Trawl; Research vessel *Anton Bruun*	NHM 1972.8.21.123-132 says it has 9 specimens (NHM 2014). Clark 1977 does not label figured specimens
			3		Written description; Plate 2 figure 8 Gislén 1938b	1929, Mortensen *Dana* Expedition	Off Durban, South Africa	411		From Mortensen (1929) Station 25

D. conifer	USNM	22679	1	Holotype	Photograph (Canon: Rebel T3i) Written description, p. 674 from Clark 1909	1887, U.S. Fish Comm.	South Atlantic Ocean, Brazil, Ceara Fortaleza Lat: -3.3667 Long: -37.8167	763	Trawl Small Beam	bottom temperature, 4.72° C (Clark 1909)
	USNM	22680	1	Holotype for *Rhizocrinus robustus*	Written description, p. 675-676 from Clark 1909	1885, U.S. Fish Comm.	Albatross station #2401; North Atlantic Ocean, Gulf of Mexico, United States, Florida, "Panama City, South of" Lat: 28.6417 Long: -85.875	260	Trawl Large Beam	Bottom conditions: green mud and broken shells (Clark 1909) *Rhizocrinus robustus* was synonymized with *D. conifer* by Gislén 1938
	NSU-CGM	CRI-528	22		Physical specimens	UNK, Messing				Labeled A-V for this study Reassessed *D. brevis* during this study
	MCZ	CRI-136	1		Physical specimens	1879, Agassiz with the U.S. Fish Comm.	off Canouan, station #238 Lat: 12.769 Long: -61.774	127	Dredged: USCSS *Blake*	
	MCZ	CRI-137	2		Physical specimens	1877 –1878 , Agassiz with the U.S. Fish Commission	North West of Tortugas, Station #44 Lat: 25.55 Long: -84.583	539	Dredged: USCSS *Blake*	Labeled A, B for this study Reassessed as likely *D. brevis* during this study
	MCZ	CRI-138	1		Physical specimens	1878, Agassiz with the U.S. Fish Commission	West of Tortugas, Station #29 Lat: 29.41, Long: -84.083	955	Dredged: USCSS *Blake*	

D. conifer	MCZ	CRI-140	3		Physical specimens	1879, Agassiz with the U.S. Fish Commission	Milligen Key, station #259 Lat: 12.0542 Long: -61.7736	159	Dredged: USCSS *Blake*	Labeled A – C for this study Reassessed as likely *D. brevis* during this study
	MCZ	CRI-1083	1		Physical specimens	1938, Schroeder	Nicholas Channel, off Puerto Sagua la Grande Station #2989 Lat: 23.2 Long: -80.067	360 - 415	Dredged via 14 Ft Blake Trawl, Research Vessel *Atlantis*	Reassessed as likely *D. brevis* during this study
D. globularis	ZMCD[5]		1	Holotype	Written description and Figures 19-21, 22 #3 from Gislén 1914	1922, Mortensen with the Danish Expedition	Off Kei islands[3] Lat: 5.483 Long: 132.617	290	Dredged	Collection site bottom was mud.
D. newnamus		Dec2017	4		Physical Specimens	2017, Veitch	Roatán, Honduras		Suction via Submerible	4 cups attached to stalks; 1 detached crown; Labeled A-D for this study
		May2014	2		Physical Specimens	2014, Baumiller and Messing	Roatán, Honduras		Suction via Submerible	2 cups attached to stalks; 2 detached crown; Labeled A, B for this study
		May2016	2		Physical Specimens	2016, Baumiller and Veitch	Roatán, Honduras		Suction via Submerible	2 cups attached to stalks; Labeled A, B for this study
		Nov2015	1		Physical Specimen	2015, Baumiller	Roatán, Honduras		Suction via Submerible	Cup with 2 arms (broken at ~12th brachial) attached to stalks

D. japonicus	ZMCD	77791	1	Holotype	Witten description; figures 47 (drawn) from Gislén 1927	1914, Mortensen with the Danish Expedition	Off Kyushu[2], Japan Station #9	162-207	Not listed	
	ZMCD [4]		23		Witten description; figures 48-80, 85-89 (drawn) from Gislén 1927	1914, Mortensen with the Danish Expedition	Off Kyushu, Japan Station #9		Not listed	Full cup characters and measurements were obtained for 8 specimens; the rest had only partial character information
	MCZ	CRI-774	2		Physical specimens	1914, Mortensen with the Danish Expedition	Southwest of Fukue Island[2]	165	Not specified. Scraper or trawl.	2 cups and partial stalks attached, one cup has regenerating arms. 1 stalk fragment ~ 2 cm long Labeled A, B for this study
D. nodipes	NBC	ZMA.CRUS.P.2621[7]	1	Holotype of *Bathycrinus minimus*	Written description; Figure 1; Plate 2 Figure 1 a-f; Plate 6, figure 5 from Döderlein 1907	1899, Siboga expedition	West of Celebes, Makassar strait Station #88 Lat: 0.5683 Long: 119.134	1301	Not specified.	Collection site bottom was fine, grey mud. *Bathycrinus minimus* was synonymized with *D. nodipes* by Gislén 1938
	NBC	ZMA.ECH.CR.2094	2	Syntype	Written description; Figure 2a; Plate 1, figure 3; Plate 6, figure 1; Plate 4, figure 5 from Döderlein 1907	1899, Siboga expedition	West of Celebes, Indonesia, Makassar strait Station #88 Lat: 0.5683 Long: 119.134	1301	Not specified.	Bottom was fine, grey mud
	NBC	ZMA-ECH.CR.2093	1	Syntype	Figure 2 b-d Plate 1, figure 4; Plate 4 a-e, g-h, Figure 3,4; Plate 6, figure 2,3	1899, Siboga expedition	North of Banda Islands, Station #241, Lat: -4.4008 Long: 129.817	1570	Not specified.	Bottom was dark sand with stones

D. parfaiti	MCZ	CRI-142	1		Physical specimens	1878	Off Havana, Station #72	175		Reassessed as likely *D. brevis* during this study
			2		Written description; Figure 7; Plate 9 Figure 2 from Döderlein 1912	1898-1899, Deutsche Tiefsee-Expedition	Canary Islands Station #33 Lat: 24.583 Long: -17.083	2500	Trawl; SS *Valdivia*	Döderlein originally assigned this specimen to *D. rawsonii*, reassigned by AM Clark 1977
	NHM	1976.1.12.10-22	1		Written description; Figure 3 A from Clark 1977		Station #175 Lat: 36.335 Long:-12.884	2210-3010	*Shackleton*	Rocky and muddy bottom
D. rawsonii	MCZ	CRI-147	4	Syntypes	4 physical specimens; Written description, p. 27-31, plate 5 from Pourtalès 1874	1871, Pourtalès and Agassiz	Off Barbados, Lat: 13.152 Long: -59.669	146-220	Dredged; expedition ship *Hessler*	1 set fragmented arms (5–8 brachials); one arm with Br1. 4 cups with ~2-3 cm of stalk, 1 attachment structure. Labeled A–D for this study. A is likely the specimen figured in Pourtalès 1844 based on measurements.
			1		Figure 133 of one individual from Clark 1915	1871, Pourtalès and Agassiz	Off Barbados, Lat: 13.152 Long: -59.669	146-220	Dredged; expedition ship *Hessler*	Based on measurements of stalk width listed in Pourtalès 1874 this specimen would be ~6.1 mm in height (Clark 1977 estimated 6 mm). Neither match any of the specimens from MCZ CRI-147
	USNM	22700	1	Holotype for *Rhizocrinus sabae*	Written description, p. 675 from Clark 1909	UNK, Capt. E. Cole	Caribbean Sea, Saba Island	366	Dredged; cable steamer *Investigator*	*Rhizocrinus sabae* was synonymized with *D. rawsonii* by Gislén 1938
	MCZ	CRI-119	2		Physical specimens		Leeward Islands, off Saba	200		Labeled A, B for this study
	MCZ	CRI-148	3		Physical specimens	1879, Agassiz with the U.S. Fish Commission	Montserrat Station #155 Lat: 16.689 Long: -62.223	161	Dredged: USCSS *Blake*	3 cups with attached stalks Labeled A – C for this study

D. rawsonii	MCZ	CRI-149	3		Physical specimens	1879, Agassiz with the U.S. Fish Commission	Off Barbados, Station #297 Lat: 13.043 Long: -59.629	225	Dredged: USCSS *Blake*	1 whole animal. 2 cups with partial stalk. 1 stalk fragment. 1 partial stalk with attachment structure Labeled A–C for this study
	MCZ	CRI-150	3		Physical specimens	1877, Agassiz with the U.S. Fish Commission	Gulf of Mexico Lat: 28.708 Long: -88.675		Dredged: USCSS *Blake*	Labeled A – C for this study
	MCZ	CRI-152	2		Physical specimens	1879, Agassiz with the U.S. Fish Commission	Off Barbados, Station #295 Lat: 13.238 Long: -59.688	329	Dredged: USCSS *Blake*	2 cups with partial attached stalks. 1 set of arms broken off cup, from second brachial onward Notes on MCZ record: 3 specimens, 1 of each Type A, B, intermediate] but only two cups were in lot. Labeled A–C for this study
	MCZ	CRI-154	1		Physical specimens	1909, Capt E. Cole	Leeward Islands off Saba	366		Reassessed as likely *D. brevis* during this study
	NSU-CGM	CRI-523	1		Physical specimens	1993, Messing	West of Grand Bahama Island Lat: 26.633 Long: -78.967	235-240	Submersible JSL 1 dive 3635	Habitat notes: Sloping veneered hardground.
	NSU-CGM	CRI-524	1		Physical specimens	1993, Messing	West of Grand Bahama Island Lat: 26.632 Long: 78.992	423.6	Submersible Johnson Sea-Link I dive 2493)	Reassessed as likely *D. brevis* during this study

D. rawsonii	NSU-CGM	CRI-529	1		Physical specimens	1984, Messing	Lat: 27.550 Long: *Johnson Sea-Link II* 79.283	350-400	R/V Cape Florida	
	NSU-CGM	JSL D3684	1		Physical specimens	2009, Messing	Lat: 27.0825 Long: -79.39278	604-630	Submersible	Reassessed as likely *D. brevis* during this study
D. weberi	NBC	ZMA.ECH.CR.2033	1	Syntype	Written description; Plate 8, figure 1 from Döderlein 1907	1900, Siboga expedition	SE of Timor Station #297 Lat: -10.65 Long: 123.6667	520		Bottom was soft, grey mud
	NBC	ZMA.ECH.CR.2031	2	Syntypes	Written description; Plate 6, figure 11 Plate 8, figures 2,3; from Döderlein 1907	1900, Siboga expedition	South of Timor-Leste Station #284 Lat: -8.7169 Long: 127.2686	828		Bottom was fine, grey mud.
	NBC	ZMA.ECH.CR.2032	2	Syntypes	Written description; Plate 7, figures 1,2 from Döderlein 1907	1899, Siboga expedition	Ceram Sea Station #173[6] Lat: -3.45 Long: 131.0014	567		Bottom was fine, yellow-green mud.
	NBC	ZMA.ECH.CR.2080	1	Syntype	Written description; Plate 7, figure 3 from Döderlein 1907	1900, Siboga expedition	SE of Timor Station #295 Lat: -10.585 Long: 124.1853	2050		Bottom was fine, grey mud
	NBC	ZMA.ECH.CR.2079	2	Syntypes	Written description; Plate 6, figure 7-10 from Döderlein 1907	1900, Siboga expedition	South of Timor-Leste, East of Timor, Station #289 Lat: -9.0025 Long: 126.4014	112		Bottom was muddy and sandy with shells

[1] Muséum national d'Histoire naturelle, Paris (France), Collection: Echinoderms (IE), Specimen MNHN-IE-2013-10100. http://coldb.mnhn.fr/catalognumber/mnhn/ie/2013-10100; Accessed July 2020.

[2] The specimen lot lists Fukaye Shima. Gislén (1927) stated that all Democrinus japonicus specimens are from Kiu Shiu, station #9. Kiu Shiu is an early (1800s- early 1900s) Europeanization of Kyūshū. However, Gislén (1927) also states station #9 is equivalent to station #12 in Gislén 1914. Station #12 list location as Gotō Islands, Kiu Shiu, Japan. Fukue island is the largest of the Gotō islands, and Fukaye Shima is likely a more obscure early Europeanization of Fukue Island (records show early sailing charts listed the island as Fukae-shima, Fukae-shima, and Fukaye Jima as alternative names; Jima itself is an alternative Europeanization of Shima, which means island in Japanese). As Gislén only lists Kiu Shui for a location in 1927, it is not completely certain if the two stations are exactly the same, or simply nearby. No latitude and longitude is listed for either station.

[3] Gislén 1925 listed the collection location as Station #56 (Lat: -5.5; Long: 132.85) near Kei islands. He later (1938) corrected the site to Station #58 (Lat: 5.483; Long: 132.617) many miles from the Kei islands. However at that same time he also still stated it was off the Kei islands, suggesting the actual location is Lat: -5.483; Long: 132.617, which is right off the Kei islands

[4] Gislén states the 96 specimens collected were sent to ZMCD. Currently ZMCD only has type specimens in their digital records. Further, it is clear some specimens were later sent elsewhere, such as MCZ (CRI-774). No obvious record of which (if any) of the specimens Gislén detailed end up outside ZMCD. ZMCD = Zoological Museum (Copenhagen, Denmark)

[5] Gislén states the specimen is at the ZMCD, but their online records do not list it, despite having a digital collection of type specimens.

[6] Station 173 is listed at Lat: 3.45 Long: 131.0014, in the Ceram sea. However, Lat: 3.45 is not in the Ceram Sea. As -3.45 is in the Ceram Sea, the original Lat listed is likely a typo

[7] Somehow incorrectly in the crustacea collection at ZMA. Naturalis Biodiversity Center